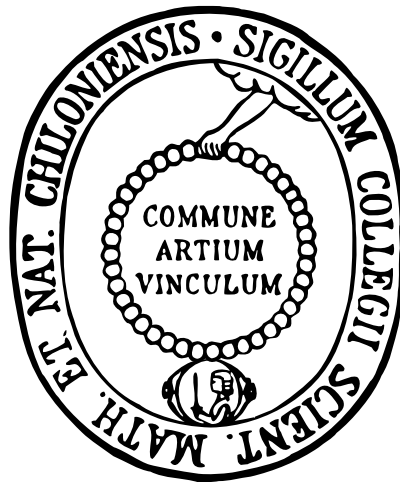


Hypoplastic Models for Soil-Structure Interfaces – Modelling and Implementation



DISSERTATION

in fulfilment of the requirements for the degree
“Dr.-Ing.”

of the Faculty of Mathematics and Natural Sciences
at Kiel University

submitted by
Hans Henning Stutz

Kiel, 2016

Schriftenreihe des Lehrstuhls Geomechanik und Geotechnik
Christian-Albrechts-Universität zu Kiel
Heft 2

ISSN 2365-7162

Herausgeber:

Lehrstuhl für Geomechanik und Geotechnik

Christian-Albrechts-Universität zu Kiel

Prof. Dr.-Ing. habil. Frank Wuttke

Ludewig-Meyn-Straße 10

24118 Kiel

Telefon: ++49 – (0)431 – 880 2857

Telefax: ++49 – (0)431 – 880 7606

Internet: www.geotechnics.ifg.uni-kiel.de

Bezugsadresse:

Christian-Albrechts-Universität zu Kiel

Lehrstuhl für Geomechanik und Geotechnik

© Lehrstuhl für Geomechanik und Geotechnik, Christian-Albrechts-Universität zu Kiel, 2016

Das Werk ist urheberrechtlich geschützt. Jede Verwendung oder Vervielfältigung ist ohne die Zustimmung des Herausgebers außerhalb der Grenzen des Urheberrechtes und der Literatur- bzw. Quellenangabe ist unzulässig und strafbar. Das gilt neben den Vervielfältigungen auch für Übersetzungen oder Nutzung in digitalen und fotografischen Systemen.

Gutachter:

1. Prof. Dr.-Ing. habil Frank Wuttke
Kiel University
2. Prof. Dr.-Ing. habil Ivo Herle
Technical University Dresden

Tag der mündlichen Prüfung: 04.11.2016

Zum Druck genehmigt: 05.12.2016

Der Dekan

Vorwort des Herausgebers

Die vorliegende Promotionsschrift von Herrn Dr.-Ing. Hans Henning Stutz ist dem Forschungs- und Arbeitsgebiet "Bodenmechanik" und der "Materialmodellierung" zuzuordnen. Die untersuchte Problemstellung ergab sich aus den bisherigen offenen Fragen zur Boden-Bauwerk-Interaktion an der Professur Geomechanik und Geotechnik bzw. an dem DFG Graduiertenkolleg 1462 "Qualität gekoppelter numerischer und experimenteller Modelle" und wurde konsequent entsprechend der eigenen Sichtweise analysiert und weiterentwickelt. Die Zielstellung der Arbeit bezieht sich dabei auf die aktuellen Fragestellungen von Grenzflächen- und der Kontaktprobleme in der Geotechnik. Um das komplexe Verhalten hinsichtlich Scher- und volumetrischen Verhalten an den Kontaktzonen korrekt zu beschreiben, muss ein geeignetes Modell verwendet werden. Jedoch sind einfach zu implementierende und korrekt beschreibende Kontaktmodelle bislang nicht vorhanden. Die Arbeit beinhaltet originäre Lösungen bezüglich der Interaktions- bzw. Grenzflächenproblematik von eingebetteten Bauwerksstrukturen bzw. Konstruktionsteilen und dem Geomaterial.

Diese Fragestellungen treten für nahezu alle eingebetteten Bauwerksstrukturen oder deren Strukturidentifikation von statischen und dynamischen Belastungen auf und sind von elementarer Bedeutung für das Design, Analysen oder Entwicklung dieser Interaktionen. In der Arbeit wurden vorhandene Kontaktmodelle analysiert sowie bewertet. Basierend auf dieser Grundlage erfolgte eine kontinuumsmechanisch konsistente Beschreibung der Kontaktfläche durch reduzierte Spannungs- und Dehnungstensoren. Die so verbesserte Modellierung der Scherspannungsmobilisierung und des volumetrischen Materialverhaltens wurde, basierend auf hypoplastischen Grundmodellen zur Materialbeschreibung für granulare Geomaterialien erweitert und für feinkörnige Materialien neu entwickelt.

Die neuen Kontaktmodelle wurden erfolgreich verifiziert und entsprechend in Finite-Elemente Software implementiert. Anhand unterschiedlicher numerischer und experimenteller Beispiele konnte die deutlich verbesserte Qualität in der Simulation von Kontaktproblemen nachgewiesen werden. Mit dem vorliegenden Beitrag kann nunmehr das Kontaktproblem realitätsnah und effektiv in numerischen Simulationen berücksichtigt werden.

Kiel, im November 2016

Frank Wuttke

Acknowledgement

The present Ph.D. thesis has been written working at Training Research Group 1492, Bauhaus University Weimar and Kiel University. Many people have contributed to this thesis directly or indirectly, I want to express my acknowledgements to them.

First and foremost, I would like to express my gratitude to my supervisor Professor Frank Wuttke. His valuable knowledge and scientific guidance was important to finish this thesis.

I would like to acknowledge Professor Ivo Herle as a member of the committee and for his valuable remarks and comments.

In addition, I would like to express my gratitude to Dr. David Mašín who gave me important insights into the hypoplastic theory and constitutive modelling. I would like to thank Professor Thomas Benz for the fruitful discussions and the opportunity to join the geotechnical group at NTNU in Trondheim, Norway. The opportunity for inspiring discussions together with Dr. Jean-Michel Perreira in Paris, is highly appreciated.

Furthermore, I would like to thank the following researchers for advice and useful discussions, Professor Gustav Grimstad, Professor Gudmund Eiksund, Professor Steinar Nordal, Dr. Ali Lashkari, Dr. David Morin, and Dr. Giuseppe Mortara.

I would like to say thank you to the geotechnical group at NTNU for the enjoyable and kind time in Norway. In particular, I say thank you to Ivan, Stian, Xenia, Priscilla, Anteneh, and Hilde.

Also, I would like to thank my former colleagues at Bauhaus-University Weimar, Frank, Holger, Bastian, Dmitrii, and all others, and my current colleagues at Kiel University, that I discussed and worked with at the Institute of Geo-Science.

Special thanks go to my parents and my family for their support during my education, studies and finally receiving my Ph.D.

Finally, I want to thank my wife Carina and my son Lennard for being patient. Thank you, for all the support you both gave me in the last years, without this the thesis would not have been completed!

Hans Henning Stutz

Abstract

The consideration of interfaces is an important issue when modelling the holistic global structural behaviour of geotechnical engineering structures. The most prominent example is the shaft friction of axial loaded piles and anchors.

This thesis reviews the behaviour of soil-structure interfaces as well as the constitutive models that can be used for their simulation. The modelling of interfaces is a difficult issue with respect to volumetric and shear behaviour, because commitment to an appropriate interface model can be challenging. Advanced models with simplified methods for implementation were previously non-existent.

It can be difficult to determine an appropriate interface model. If the interfaces are properly considered in the analysis of soil-structure interaction, the results are improved substantially.

In this thesis, a stochastic assessment scheme was proposed and applied. This scheme was modified to take into account the special considerations for the assessment of interface models. Based on the assessment and a state-of-the-art review, theoretical considerations were used and a novel scheme was developed. This scheme uses reformulated mathematical operators as well as reduced stress and strain rate tensors, based on existing constitutive equations, to model interfaces. Shear stress mobilization and the volumetric behaviour are predicted more accurately, and the bearing behaviour of frictional contacts can be modelled in a better way.

By using the novel scheme, an older hypoplastic interface model for granular interfaces was enhanced, and three different hypoplastic clay interface models were proposed. These models were verified and validated with experimental data.

In addition to the theoretical constitutive model formulation, an implementation method was developed. This allowed a user-friendly implementation of advanced constitutive models as interface models using the capabilities of a commercial finite element software package. This concept was exemplarily applied to various 3D boundary value problems and the benefits of such advanced hypoplastic interface model are discussed.

The theoretical developments as well as the development of the user-friendly implementation scheme will increase the accessibility of advanced interface models to practical engineers. The modelling and experimental observations can thus be brought into a better framework of reliable modelling results.

Zusammenfassung

Das Kontaktverhalten von geotechnischen Strukturen ist wichtig zur Berechnung des ganzheitlichen Strukturverhaltens bei der Berücksichtigung von Boden-Bauwerks-Interaktion. Bekannte Beispiele dafür sind axial belastete Pfähle und Anker.

Diese Arbeit fasst den Stand der Forschung zum Boden-Bauwerkkontakt-Verhalten und die relevanten Modelle zu deren Simulation zusammen. Die Modellierung des Volumenverhaltens und des Scherverhaltens ist schwierig, weil oft unklar ist, welches Modell das Verhalten der Kontaktflächen bestmöglich beschreibt. Einfach zu implementierende zukunftsweisende Modelle sind bis hierher nicht vorhanden bzw. bekannt.

Es ist meist schwierig, ein geeignetes Kontaktflächenmodell zu wählen, wobei aber die korrekte Berücksichtigung von Kontaktflächen bei der Analyse des Boden-Bauwerkkontaktes die Ergebnisse der Modellierung signifikant verbessert. In dieser Arbeit wurden verschiedene existierende Modelle zur Modellierung von Boden-Bauwerks-Kontakten mit Hilfe eines stochastischen Ansatzes untersucht und bewertet. Anhand dieser Bewertung und dem Stand der Forschung wurde basierend auf theoretischen Überlegungen ein Methode entwickelt. Diese erlaubt es, die Kontaktflächen mittels modifizierter mathematischer Operatoren und reduzierten Spannungs- und Dehnungstensoren, basierend auf existierenden Kontinuums-Modelle zu berechnen. Dies führt zu verbesserter Modellierung der Scherspannungs-Mobilisierung und des volumetrischen Verhaltens der Kontaktzone.

Basierend auf dem neuen Konzept wurde ein existierendes, hypoplastisches Modell für granulare Kontaktreibung verbessert und drei unterschiedliche hypoplastische Modelle für das Kontaktverhalten von feinkörnigen Böden entwickelt. Alle Modelle wurden verifiziert und mit experimentellen Daten validiert.

Zusätzlich zur Formulierung der theoretischen Modelle wurde ein Konzept erarbeitet, mit dem die entwickelten Modelle in eine Finite-Elemente Software implementiert werden konnten. Hierzu werden existierende Boden-Kontinuumsmodelle benutzt. Die Implementierung dieser Modelle wurde mittels unterschiedlicher Randwertprobleme erfolgreich validiert und die Vorteile der Modelle sowie des Implementierungskonzeptes diskutiert. Die theoretischen Überlegungen und das benutzerfreundliche Implementierungsschema wird die Zugänglichkeit dieser zukunftsweisenden Modelle für Ingenieure verbessern. Hierdurch können die Ergebnisse der Modellierungen und die experimentelle Beobachtungen angeglichen werden, was die Aussagefähigkeit von Finite-Elemente Analysen weiter verbessern wird.

Contents

List of Figures	XVI
List of Tables	XXII
1 Introduction	1
1.1 Background and motivation	1
1.2 Scope	3
1.3 Outline	3
2 Experimental modelling for soil-structure interfaces	5
2.1 Introduction	5
2.2 Testing methodologies for interface shear tests	5
2.3 Boundary conditions for soil-structure interfaces	8
2.4 Key aspects of interface behaviour	11
2.5 Summary of Chapter 2	22
3 Existing numerical modelling for soil-structure interfaces	23
3.1 Introduction	23
3.2 Numerical modelling of soil-structure interfaces	23
3.2.1 Zero-Thickness Interface element	24
3.2.2 Thin-Layer interface element	27
3.2.3 Surface-to-surface modelling approach	29
3.3 Constitutive modelling of soil-structure interfaces	32
3.3.1 Mohr-Coulomb model	34
3.3.2 Hyperbolic non-linear elastic model of Clough and Duncan (1971)	36
3.3.3 Elastoplastic model of Mortara (2003)	38
3.3.4 Hypoplastic model of Gutjahr (2003)	41
3.3.5 Elasto-plastic model by Lashkari (2013)	43
3.4 Summary of Chapter 3	45
4 Model assessment of existing constitutive soil-structure interface models	47
4.1 Introduction	47

4.2	Stochastic model properties	48
4.2.1	Uncertainty	48
4.2.2	Model sensitivity	50
4.3	Quality assessment of the constitutive interface models	52
4.3.1	Sensitivity study of the interface models	54
4.3.2	Uncertainty analysis for shear behaviour	57
4.4	Summary of Chapter 4	62
4.4.1	Implications for the extension and improvements for soil -structure interface models	63
5	Enhancement of granular soil-structure hypoplastic constitutive interface model	65
5.1	Introduction	65
5.2	Theoretical considerations	65
5.3	Hypoplasticity and Hypoplastic interface modelling	69
5.3.1	Hypoplasticity	69
5.3.2	Hypoplastic interface model by Arnold and Herle (2006)	71
5.4	Novel method for reformulation of 3D constitutive models to interface models	73
5.5	Enhanced hypoplastic granular-structure model	75
5.5.1	Enhancement of the hypoplastic granular interface model	76
5.5.2	Surface roughness modelling for granular soil-structure interfaces	76
5.6	Enhanced intergranular strain concept for interface modelling	78
5.7	Validation of the enhanced hypoplastic granular -structure interface model	79
5.7.1	Model verification	80
5.7.2	Testing the general enhanced model behaviour	81
5.7.3	Comparison of surface roughness modelling approaches	84
5.7.4	Comparison of simulated with experimental interface behaviour	85
5.7.5	Modelling granular interface using the enhanced inter-granular strain concept	88
5.8	Summary of Chapter 5	91
6	New hypoplastic models for fine-grained soil-structure interfaces	93
6.1	Introduction	93
6.2	New fine-grained hypoplastic interface constitutive model	93
6.2.1	Reference hypoplastic formulation for clay	94
6.2.2	Hypoplastic Cam clay model for interface behaviour	94
6.2.3	Clay hypoplasticity interface model with advanced asymptotic state boundary surface	96
6.2.4	Extension of the interface model for surface roughness	98
6.3	Thermo-hypoplastic interface model for partially saturated soils	99

6.4	Validation of the new hypoplastic clay-structure interface models	102
6.4.1	Model verification	102
6.4.2	Testing the clay interface models behaviour	103
6.4.3	Comparison of surface roughness modelling approaches for fine-grained interfaces	105
6.4.4	Comparison of simulated with experimental interface behaviour	107
6.4.5	Modelling fine grained interface using inter-granular strain concept . . .	110
6.5	Validation of the hypoplastic thermo-mechanical interface model for partially saturated soils	111
6.5.1	Temperature dependent modelling of fine-grained interfaces	111
6.5.2	Parameter variation for the thermo-mechanical interface modelling	113
6.5.3	Suction-dependent modelling of fine-grained soil-structure interfaces . .	115
6.6	Summary of Chapter 6	116
7	Innovative approach for modelling interfaces using existing soil constitutive models	117
7.1	Implementation algorithm of interface models using 3-D constitutive models . .	117
7.2	Verification of the implementation	121
7.2.1	Description of the numerical direct shear interface test	121
7.2.2	Mesh sensitivity analysis	122
7.2.3	Verification of coarse-grained soil-structure interfaces	123
7.2.4	Verification of fine-grained soils-solid interfaces	125
7.2.5	Comparison of Mohr-Coulomb and hypoplastic constitutive interface model	126
7.3	Boundary values problems	127
7.3.1	Modelling large shear device	128
7.3.2	Offshore geotechnical: Toroid penetrometer simulation	132
7.4	Summary of Chapter 7	139
8	Beyond hypoplasticity constitutive interface models	141
8.1	Introduction	141
8.2	Barodesy model for clay	141
8.3	Modified Cam-clay model	143
8.4	Constant Volume simulation with Cam clay, Barodesy, and HCE model	144
8.5	Summary of Chapter 8	146
9	Summary, conclusions and outlook	147
9.1	Summary	147
9.2	Conclusion	148
9.3	Outlook	150
A	Statistical parameter distribution for the interface models	173

B Results of uncertainty analysis for the model assessment	175
C Solution for mixed problem of hypoplastic constitutive equation	177

List of Figures

2.1	Comparison of direct to simple shear measurements (Uesugi and Kishida 1986)	8
2.2	Boundary conditions in the direction normal to the interface: (a) constant normal stress, (b) constant volume, (c) constant normal stiffness (from Evgin and Fakharian (1996))	9
2.3	Hypothetic model by Wernick (1978) for the aggregate interlocking at the interface	9
2.4	Influence of the different boundary conditions revealed by numerical interface simulations from Costa D Aguiar et al. (2011)	11
2.5	Interface behaviour and important factors for volumetric interface behaviour (Nakayama 2006)	12
2.6	Idealized classification of interface shearing into three failure modes by Tsubakihara et al. (1993)	14
2.7	Definition of the maximum and average roughness compared to different coarse soils by Uesugi et al. (1988)	15
2.8	Comparison of monotonic and cyclic loading paths from Uesugi et al. (1989)	17
2.9	Hypothesis for a particle movements under a) axial and b) torsional shearing (Martinez et al. 2015)	18
2.10	Examples of a post-testing zone with on top interface shear test from Ho et al. (2011) highlighting the zones with and without breakage	21
3.1	Zero-thickness interface element after Goodman et al. (1968)	24
3.2	Thin-layer interface element from Sharma and Desai (1992)	27
3.3	Reference and current configuration for Master and Slave concept based on Haraldsson (2004)	30
3.4	Contact coordinates from Haraldsson (2004)	31
3.5	Visualisation of the fitting parameter a and b for shear test data, based on Clough and Duncan (1971)	37
3.6	Idealized flow rule from elastoplastic model modified from Mortara (2003)	39
4.1	Different sources of uncertainty within a model formulation (Phoon 2008)	48
4.2	Proposed quantification methodology for interface models	53
4.3	Results of parameter uncertainty analysis for the different constitutive interface models	58

4.4	Model uncertainty simulations for dense ((a)-(c)) and loose ((d)-(e)) Hostun sand (Shahrour and Rezaie 1997)	60
4.5	Model uncertainty simulations for Toyura sand ((a)-(b)) (Mortara 2003) and ((c)-(e)) air dried quartz sand (Evgin and Fakharian 1996)	61
4.6	Comparison of model, parameter and global uncertainty for the five different models	62
5.1	Schematic overview of the direct shear interface testing as idealization of simple shear conditions: Rough and smooth surfaces behaviour of interfaces	67
5.2	Schematic representation of the interface zone showing the relation between shear strain and shear deformation modified from Gutjahr (2003)	68
5.3	Relation between e_d , e_c , e_i , and p from Herle and Gudehus (1999)	71
5.4	Contact plane and coordinate system proposed by Arnold and Herle (2006)	72
5.5	Verification of the MATLAB implementation compared to TRIAX	81
5.6	Results for the comparison of different models under CV conditions with 100, 300, and 500 kPa	82
5.7	Results for the comparison of different models under CNS with $\sigma_0 = 50, 100,$ and 150 kPa	82
5.8	Results for the comparison of different models under CNL conditions with $\sigma_0 = 50, 100,$ and 150 kPa	83
5.9	Comparison of σ_n and the in-plane σ_p normal stress at the interface for the different models	84
5.10	CNL simulation of the two different surface roughness modelling schemes at 100 kPa	85
5.11	Shear displacement u_x versus friction coefficient τ_x/σ_n plot for different surface roughness under CNL conditions with $\sigma_0 = 78$ kPa	86
5.12	Comparison of models of CNL test under an applied normal stress of 300 kPa using the experimental data of Shahrour and Rezaie (1997)	86
5.13	Comparison of AH and HvWE models with the experimental data of a staged shear test under CNL conditions (102-274 kPa)	87
5.14	Comparison of shear displacement u_x versus shear stress τ_x and normal stress σ_n using experimental data with $K = 100$ kPa from Porcino et al. (2003)	87
5.15	Constant volume condition simulation using the HvWE model with intergranular strain	89
5.16	Constant Normal Load condition simulation using the HvWE model with intergranular strain	90
5.17	Comparison of cyclic test results for Homo-gravel (Zhang and Zhang 2006) and simulations using HvWE intergranular at $\sigma_0 = 700$ kPa	90
6.1	Definition of N , κ^* , λ^* , p_e^* , and p_{cr} from Mašín (2005)	95

6.2	Verification of the MATLAB implementation compared to TRIAX	103
6.3	Stress path for Constant Volume boundary conditions for the Hypoplastic Cam clay (HCC) and extended clay Hypoplastic model (HCE) interface models for fine-grained soils	103
6.4	Stress path for Constant Volume boundary conditions: shear stress τ_x versus normal stress σ_t for the Hypoplastic Cam clay (HCC) and extended clay Hypoplastic model (HCE) interface models for fine-grained soils	104
6.5	Constant Normal Load conditions for the Hypoplastic Cam clay (HCC) and extended clay Hypoplastic model (HCE) interface models for fine-grained soils .	105
6.6	Constant Normal Stiffness conditions: the Hypoplastic Cam clay (HCC) and extended clay Hypoplastic model (HCE) interface models for fine-grained soils .	106
6.7	Results for the surface approach of Arnold and Herle (2006) and the proposed of Stutz and Mašín (2016)	106
6.8	Verification using the experimental data of Littleton (1976)	108
6.9	Comparison for the HCE (a) and HCC (b) model using the experimental data for Kawasaki marine clay (S0)	109
6.10	Validation of clay interface models with experimental data from Tsubakihara and Kishida (1993), Sun et al. (2003)	110
6.11	Comparison of HCE models without and with intergranular strain	111
6.12	Results for CNL simulation with different applied constant temperatures	112
6.13	Results for CV simulation with different applied constant temperatures	113
6.14	Results for CV simulation with parameter variation of n_t at 40°C	113
6.15	Results for CV simulation with parameter variation of l_t at 40°C	114
6.16	Results for CNL simulation with parameter variation of n_t at 40°C	114
6.17	Results for CNL simulation with parameter variation of l_t at 40°C	115
6.18	Results for CNL simulation with a variation of the suction stresses	116
7.1	Implementation scheme for the FRIC subroutine using the UMAT subroutine .	119
7.2	Geometry for direct shear verification simulation model adapted of (Weißenfels and Wriggers 2015b)	122
7.3	Coarse, intermediate and fine mesh size used to study the mesh sensitivity . . .	123
7.4	Shear displacement u_x to shear stress τ_x graphs for mesh sensitivity analysis for (a) sand and (b) clay	124
7.5	Verification between the Gauss point algorithm and the finite element implementation of the constitutive interface models for sand	124
7.6	Verification between the Gauss point algorithm and the finite element implementation of the constitutive interface models for clay	125
7.7	Comparison of the shear stress for the 100 kPa direct interface shear test using the Mohr-Coulomb and hypoplastic interface model	126

7.8	Shear displacement u_x versus shear stress τ_x for the comparison of Mohr-Coulomb and hypoplastic interface model	127
7.9	Side and top view of the large scale interface shear device of Vogelsang et al. (2013)	129
7.10	Illustration of the applied calculation process: Modelling the filling and shearing of the interface shear device (Vogelsang et al. 2015)	129
7.11	Vertical stress evolution σ_z [kPa] with increased filling height [m]	130
7.12	Simulation results for earth pressure distribution (a) and the shear force versus shear displacement results (b)	131
7.13	Results for the shear stress σ_{zy} after 60 mm shearing. Left side is the Mohr-Coulomb contact and on the right hand side the hypoplastic contact model . . .	132
7.14	Shallow toriodal penetrometer side-view and top-view (left) and the geometrical properties (right) modified of Yan et al. (2010)	133
7.15	Boundary value problem: Shallow penetrometer modelled considering cyclic symmetry as 10° section	134
7.16	Comparison of the different model combinations for calculated normalized load-deformation results	136
7.17	Detail in the z - x axis for the calculated sensitivity considering different model combinations (hypoplastic soil model with Mohr-Coulomb and hypoplastic interface models) at a normalized displacement of $u/D = 0.1$	138
8.1	Comparison of shear and normal stress versus shear strain for CV simulation for London clay. The models are abbreviated as: Barodesy clay model as BC and modified Cam-clay model as MCC.	145
8.2	Comparison of shear and normal stress versus shear strain for CV simulation for Kaolin-clay	146

List of Tables

2.1	Summary of interface testing apparatus (extended from Dietz (2000))	6
3.1	Model parameters and physical definitions for the Mohr-Coulomb friction model	36
3.2	Model parameters and physical definitions for Clough and Duncan (1971) model	38
3.3	Model parameters and physical definitions for Mortara (2003) model	41
3.4	Model parameters and physical definitions for Gutjahr (2003) model	43
3.5	Model parameters and physical definitions for the model by Lashkari (2013) . .	45
4.1	Techniques of sensitivity analysis, properties, and primary goal	51
4.2	Model abbreviations for model assessment	54
4.3	Total sensitivity S_{T_i} indices for the Mohr-Coulomb model (Van Langen 1991) . .	54
4.4	Total sensitivity S_{T_i} indices for the Hyperbolic model (Clough and Duncan 1971)	55
4.5	Total sensitivity S_{T_i} indices for the Elastoplastic model (Mortara 2003)	56
4.6	Total sensitivity S_{T_i} indices for the Hypoplastic model (Gutjahr 2003)	56
4.7	Total sensitivity S_{T_i} indices for the elasto-plastic model (Lashkari 2013)	57
4.8	Statistical distributions for quantifying the parameter uncertainty	58
5.1	Parameters for the hypoplastic sand interface model for verification and general behaviour	80
5.2	Parameters for the hypoplastic model (partly from Herle and Gudehus (1999)) .	84
5.3	Parameters for the hypoplastic model with intergranular strain	88
6.1	Parameters for the evaluation of HCC and HCE interface models	102
6.2	Parameters of the hypoplastic interface models used in the simulations	107
6.3	Properties of the different clays	107
6.4	Parameters for the hypoplastic clay interface model with intergranular strain . .	111
6.5	Parameters used for the hypoplastic thermo-mechanical interface model	112
7.1	Parameters for the verification of the implementation concept	121
7.2	Hypoplastic parameters for Karlsruhe sand (Herle and Gudehus 1999)	128
7.3	Parameters for toroidal penetrometer, soil and frictional constitutive model (Ragni et al. 2016)	135

8.1	Parameters for the different clays	145
A.1	Distribution of the Mohr-Coloumb interface parameter	173
A.2	Distribution of the hyperbolic model interface parameters	173
A.3	Distribution of the EP1 model Mortara et al. (2002) parameters	174
A.4	Distribution of the EP2 model (Lashkari 2013) parameters	174
A.5	Distribution of the hypoplasticity model Gutjahr (2003) parameters	174
B.1	Results for the model uncertainty, parameter uncertainty and global model un- certainty of the interface models	176

Nomenclature

Latin Symbols

Notation	Name/Definition		
$\mathbf{1}$:	Second order unity tensor	$\bar{a}_{\alpha\beta}$:	Metric coefficient
A :	Controls the relative importance of the volumetric and shear strain components	B :	strain-displacement term for zero-thickness interface element
A_0	Dilatancy constant (initial)	$\bar{b}_{\alpha\beta}$:	Coefficient of the curvature tensor
A_{1L}	Dilatancy constant (intermediate)	CV_y :	Coefficient of variation
A_1, B_1, C :	Coefficient to solve the quadratic polynomial	C_k :	Ratio of normal and shear stiffness
A_{con} :	contact area of the penetrometer	C' :	Tangent consistence matrix
A_L :	Magnitude of dilatancy	c :	Cohesion / Adhesion at the interface
\mathcal{A} :	Fourth-order tensor	$c_1, c_2, c_3, c_4, c_5, c_6$:	Material constants (Barodesy and Hypoplasticity)
\mathbf{A} :	Local coordinate at contact surface without contact	c_i :	Coefficient for the thermo-hydro mechanical hypoplastic model
a :	Scalar for the hypoplastic clay model	D :	Diameter of the spherical ring
a_f :	Scalar quantity (Clay Hypoplasticity)	D_f :	Damage function describing the critical state
a_{fm} :	Scalar for the hypoplastic clay model modified for surface roughness	\mathbf{D} :	Euler stretching tensor
a_r, b_r :	Fitting parameters	\mathbf{D}^0 :	Normalized stretching tensor
\mathbf{a} :	Local coordinate at contact surface with contact	\mathbf{D}^e :	Elastic constitutive matrix
		\mathbf{D}^{ep} :	Elasto-plastic constitutive matrix
		d_{50} :	Mean grain size diameter

d_{ij}, d_{ii}, d_{kl} :	Stretching rate tensor	f_{sR} :	Modified barotropy factor considering surface roughness
d_{max} :	Shear band thickness	f_u :	factor controlling the collapsible behaviour
d_s :	Shear zone thickness	G_0 :	Shear modulus at small strains
d_s^v :	Virtual shear zone thickness	G :	Shear modulus
$d(\dots)$:	Distance function for mortar method	g :	Plastic potential
$[d]$:	Nodal displacement vector	g_{BC} :	Scalar quantity for the Barodesy clay model
\mathbf{d} :	Asymptotic strain rate direction	g_N :	Distance function for the mortar method
\mathbf{d}^A :	Asymptotic strain rate direction function	\dot{g}_T^s :	Relative tangential velocity
E, E_i :	Young's and constrained modulus	\bar{g}_N :	Minimized effective distance
e :	Void ratio	H :	Hardening modulus (Lashkari 2013)
e_0 :	Initial void ratio	H_s :	Tensorial term for modelling saturation effects
e_c, e_d, e_i :	Critical, minimum, and maximum void ratio	H_t :	Tensorial term for modelling temperature effects
e_{c0}, e_{d0}, e_{i0} :	Critical, minimum, and maximum void ratio at zero pressure	h_0 :	Plastic hardening constant (Lashkari 2013)
\dot{e} :	Void ratio increment	h_s :	Granular hardness of the soil skeleton
F :	Stress function according to Matsuoka-Nakai	h_{sand} :	Soil sample height
F_m :	Matsuoka-Nakai factor	$[I]$:	Identity matrix
f :	Yield function	\mathbf{I}, \mathcal{I} :	Fourth-order unity tensor
f_{BC} :	Scalar quantity for the Barodesy clay model	K :	Constant normal stiffness
f_b :	Barotropy factor	K_0 :	Earth pressure at rest
f_c :	Additional coefficient	K_{BC} :	Radial stress (Barodesy)
f_d, f_e :	Pyknotropy factor	K_c :	Stress ratio at critical state
f_{dr} :	Modified pyknotropy factor considering surface roughness	K_I :	Stiffness number
f_d^A :	Limiting value of f_d at the ASBS	K_n :	Normal stiffness
f_d^{SBS} :	Pyknotropy factor f_d for states at the SBS	K_p :	Plastic hardening modulus
		K_s :	Shear stiffness

K_s^e, K_n^e :	Elastic shear and normal stiffness	\mathbf{m} :	Hypoplastic flow rule
K_{si} :	Initial shear stress stiffness	\mathbf{m}_M :	Gradient of the plastic potential
K_{sn}, K_{ns} :	Coupled shear-to-normal stiffness	N :	Controls the position of the isotropic normal compression line
k :	Rate of the structure degradation	N_i :	Interpolation/Shape function
L :	Lever arm length	\mathbf{N} :	Second order constitutive tensor
L_G :	Gauge length	n :	Exponent takes into account the pressure-sensitivity of the grain skeleton
L_M :	Measured length for normalisation of surface roughness	n^b :	Influence of interface state on peak stress ratio
L_M :	Measured length	n^d :	Influence of interface state on phase transformation (zero-dilatancy) stress ratio
\mathcal{L}, \mathcal{L} :	Fourth-Order constitutive tensor	n_{HY} :	Stiffness exponent Clough and Duncan (1971)
l :	Element length	n_s :	Defines the together with l_s the position and slope of NCl for partially saturated soil
l_s :	Defines the together with n_s the position and slope of NCl for partially saturated soil	n_t :	Defines the together with l_t the position and slope of NCl for heated soil
l_t :	Defines the together with n_t the position and slope of NCl for heated soil	\mathbf{n} :	Gradient of the plastic surface
M :	Slope of the critical state line	$\bar{\mathbf{n}}_c$:	Direction of the normal to the contact surface
M_L :	Critical stress ratio	p :	Mean effective stress
\mathcal{M} :	Fourth-order tangent stiffness material tensor	\dot{p} :	Rate of the mean effective stress
m_{BC} :	Strain increment ratio	p_a :	Atmospheric stress
m_R :	Ratio of the maximum shear modulus to the elastic shear modulus	p_n :	Applied normal stress
m_T :	Ratio of the shear modulus during 90° change of loading direction to the elastic shear modulus		

p_{ref}, p_r :	Reference pressure	T_0 :	Reference temperature
p_e :	Equivalent pressure	T_l :	Torsional load
p_e^* :	Hvorslev equivalent pressure	\dot{T} :	Temperature rate
q :	Node displacement for thin-layer element	\mathbf{T} :	Objective stress tensor
R :	Maximum constant value of the intergranular strain	$\dot{\mathbf{T}}$:	Objective stress rate tensor
R_f :	Failure ratio	$\hat{\mathbf{T}}, \mathbf{T}^*, \hat{\mathbf{T}}^*$:	Deviator stress tensor
R_{max} :	Maximum roughness at a surface	t :	Thickness of the interface element
R_n :	Normalized roughness coefficient	t_i :	Time
R_P :	Radius of the pile	t_{i0} :	Initial time
R_s^L :	Shear plastic velocity vector	$\dot{\mathbf{t}}$:	Objective rate of traction
R_n^L :	Normal plastic velocity vector	U :	Strain energy for zero-thickness interface element
\mathbf{R}^L :	Direction of the plastic velocity vector	u :	Relative interface displacement
\mathbf{R} :	Stress like tensor (Barodesy)	u_1, u_2, u_3, u_4 :	Nodal displacements
r :	Variable for the shear stiffness in clay hypoplasticity	u_a :	Pore air pressure
r_r :	Reduced shear stiffness considering surface roughness	u_i :	Interface displacement
S :	Sensitivity of a soil	u_{low}, u_{upp} :	Horizontal nodal displacement
S_i :	First order sensitivity index	u_n :	Displacement increment normal to the interface
S_{T_i} :	Total sensitivity index	u_p :	Plastic component of the velocity vector
s_e :	Hypoplastic model parameter for the position of the water retention curve	u_s :	Interface shear displacement
s_{ini} :	Initial soil sensitivity	u_t :	Shear displacement
s_f :	Final soil sensitivity	u_w :	Pore water pressure
s :	Matrix suction	\dot{u}_n :	Displacement increment in the normal direction
s_u :	Undrained shear strength	\dot{u}_n^p :	Normal plastic relative interface displacement
\dot{s} :	Rate of matrix suction	\dot{u}_s^p :	Shear plastic relative interface displacement
T :	Transformation matrix	$\dot{\mathbf{u}}$:	Total interface displacement

$\dot{\mathbf{u}}^p$:	Total plastic interface displacement
V :	Vertical load
V_E :	Element volume
v_1, v_2, v_3, v_4 :	Vertical nodal displacements
v_{low}, v_{upp} :	Vertical nodal displacement
\mathbf{v}^s :	Tangential relative contact movement at slave surface
$\bar{\mathbf{v}}^m$:	Tangential relative contact movement at master surface
W :	Spin tensor
w :	Embedment
$\mathbf{X}^*, \hat{\mathbf{X}}^*, \hat{\mathbf{X}}$:	Deviator stresses
\mathbf{X}^m :	Surface coordinate
x :	Coordinate
x_0 :	Initial guess for Newton-Raphson iteration
x_i^α :	Gaussian surface parameters
x_n :	Updated value in Newton-Raphson iteration
\mathbf{x} :	Surface coordinate
Y :	Scalar of degree of non-linearity
\hat{Y}_i :	Deterministic model response
\hat{Y}_{ref} :	Reference model response

Greek Symbols

Notation	Name/Definition
α :	Parameter controlling the relative density to peak friction dependency
α_{BC} :	Scalar quantity for \mathbf{R} -function
α_c :	Critical hardening value
α_f :	Parameter controlling the irreversible deformation inside ASBS
α_M :	Current value of the hardening rule
α_p :	Maximum value of the hardening rule
α_s :	Thermal expansion coefficient
β :	Parameter controlling the relative density to the soil stiffness
β_{BC} :	Scalar quantity of f_{BC} and g_{BC}
β_M :	Exponent of plastic functions
β_r :	Intergranular strain parameter controls the decay of the intergranular strain
δ :	Interface friction angle
$\boldsymbol{\delta}$:	Intergranular strain tensor
$\dot{\boldsymbol{\delta}}$:	Objective rate of the intergranular strain tensor
$\hat{\boldsymbol{\delta}}$:	Rate of the intergranular strain tensor
γ :	Soil weight
γ_i :	Shear strain in direction i
γ_w :	Unit weight of water
γ_x :	Shear strain

γ_{xy} :	Shear strain at the interface	λ^* :	Slope of the isotropic compression line
$\dot{\gamma}$:	Shear strain rate	μ :	MC friction parameter
ε :	Strain	μ_M :	d_{max} parameter (Mortara et al. 2002)
ε_n :	Strain normal to the interface	μ_s :	Mean derivation
ε_p :	In-plane strain	ν :	Parameter for control of the proportion of shear to bulk stiffness
ε_x :	Strain in x direction	ν_d :	d_{max} Parameter
ε_y :	Strain in y direction	ν_p :	Poissons ratio
$\dot{\varepsilon}_n$:	Strain normal to the interface	ξ :	Trajectory of the plastic shear strains
$\dot{\varepsilon}_{vol}, \dot{\varepsilon}_q$:	Volumetric and deviatoric strain rate	ξ_M :	w_p parameter
$\dot{\varepsilon}$:	Strain rate tensor / Euler stretching rate tensor	ξ^α :	Parameter set
$\dot{\varepsilon}^{TE}$:	Reversible component of the thermally induced strain rate	$\bar{\xi}^\alpha$:	Parameter set providing the minimal distance of master and slave surface
ϵ :	Measure of dilatancy	ξ^β :	Parameter set
ζ :	w_p parameter	π :	Circle constant
η :	Stress ratio	ρ :	Normalized magnitude of the intergranular strain
θ :	Lode angle	ρ_M :	Ratio between the stress ratios for $d = 0$ for hardening or softening condition
κ_{MCC} :	Unloading slope of the normal compression line (MCC)	ρ_s :	Density
κ_r :	Roughness coefficient	σ :	Stress
κ^* :	Unloading slope of the normal compression line	σ_c :	Critical normal stress
Λ :	Plastic multiplier	σ_n :	Stress normal to the interface
Λ_{BC} :	Scalar quantity for Barodesy	σ_{n0} :	Initial normal stress to the interface
Λ_L :	Loading index of Dafalias (1986)	σ_p :	Mean in-plane stress
λ_L :	Critical state line location in e - $\ln\sigma_n$ plane	σ_s :	Standard variation
λ_{MCC} :	Slope of the isotropic compression line (MCC)	σ_z :	Vertical stress
		$\boldsymbol{\sigma}$:	Effective stress tensor
		$\dot{\boldsymbol{\sigma}}$:	Effective stress rate tensor

$\boldsymbol{\sigma}^{net}$:	Net stress tensor
$\boldsymbol{\sigma}^{tot}$:	Total stress tensor
$\boldsymbol{\sigma}_{FRIC}$:	Stress tensor in Voigt notation in the FRIC routine
$\boldsymbol{\sigma}_{UMAT}$:	Stress tensor in Voigt notation in the UMAT routine
$\dot{\boldsymbol{\sigma}}$:	Stress rate
$\dot{\boldsymbol{\sigma}}_n$:	Stress rate normal to the interface
$\dot{\boldsymbol{\sigma}}$:	Stress rate tensor
$\hat{\boldsymbol{\sigma}}_{ij}, \hat{\boldsymbol{\sigma}}_{kl}$:	Stress tensor Gutjahr (2003)
$\hat{\boldsymbol{\sigma}}, \boldsymbol{\sigma}^*, \hat{\boldsymbol{\sigma}}^*$:	Deviator stress tensor
$\boldsymbol{\sigma}_{BC}^*$:	Reference stress (Barodesy)
τ :	Shear stress
τ_c :	Critical shear stress
τ_f, τ_p :	Peak shear stress
τ_s :	Shear stress
τ_{ult} :	Ultimate failure shear stress
τ_x :	Shear stress in x direction
$\dot{\tau}$:	Shear stress rate
φ_c :	Critical state friction angle
φ_i :	Friction angle at the interface
ϕ :	Ratio between the stress ratios for $d = 0$ for hardening or softening conditions
χ :	Controls the non-linearity of the intergranular strain stiffness
χ_s :	Effective stress factor
ψ :	Hardening rule parameters
ψ_I :	Interface dilation angle
ω :	Hardening rule parameter
ω_h :	Exponent for clay hypoplasticity

ω_r : Modified exponent for clay hypoplasticity considering surface roughness

Operators

Notation	Name/Definition
T	Transpose matrix
$(x)_\alpha$	Partial derivative of (x) to the natural coordinates
\cdot	Inner product
$:$	Double inner product
\otimes	Outer product
$[\dots]$	Matrix / Vector
$\ \dots\ $	Euclidean norm
$\langle \rangle$	Macauley bracket
$\det()$	Determinate
tr	Trace of matrix, tensor
$f()$:	UMAT function call for Newton-Raphson method
$f()'$:	First derivative of the function call

Abbreviations

Notation	Name/Definition
AH :	Hypoplastic interface model of Arnold (2004)
AHE :	Hypoplastic interface model of Arnold (2004) extended
ASBS :	Asymptotic state boundary surface
BC :	Bardoesy clay model
cf. :	conferre
CNL :	Constant normal load
CNS :	Constant normal stiffness
CNV :	Constant normal height

COV :	Coefficient of variance	PM :	Parameter mapping
CPT :	Cone penetration test	PP :	Parameter prioritization
CV :	Constant volume	PTE :	Earth pressure transducers
e.g. :	For example	RI :	Relatively intact state
<i>EP1</i> :	Elasto-plastic model after Mortara (2003)	SBS :	State Boundary Surface
<i>EP2</i> :	Elasto-plastic model after Lashkari (2013)	TOL. :	Tolerance
err. :	Error	TR-HC :	Combination of Tresca soil model with hypoplastic fine-grained model
FA :	Fully adjusted state	TR-MC :	Combination of Tresca soil model with Mohr-Coulomb interface model
FRIC :	User defined frictional subroutine	UMAT :	User defined material model subroutine
HCC :	Hypoplastic interface Cam clay	UA ^{Global} :	Global model uncertainty
HCE :	Hypoplastic clay interface model extended	UA ^{Model} :	Model uncertainty
HP :	Hypoplastic interface model	UA ^{Par} :	Parameter uncertainty
HvWE :	Enhanced granular interface model Model		
HY :	Hyberbolic model		
HY-HC :	Combination of hypoplastic model with extension for sensitivity and hypoplastic fine-grained interface model		
HY-MC :	Combination of hypoplastic model with extension for sensitivity and Mohr-Coulomb interface model		
i.e. :	id est		
ini. :	Initial		
max. :	Maximal		
MC :	Mohr-Coulomb model		
MCC :	Modified Cam-Clay model		
NCL :	Normal Compression Line		
PF :	Parameter fixing		
PIV :	Particle image velocity		

Chapter 1

Introduction

1.1 Background and motivation

The soil in contact to structural elements (anchors, piles, tunnel-lining and retaining walls) is the interface zone. This interface consists of a small soil volume attached to a structural element. This thin-layer representing the interface is of interest because of existing discontinuities in material properties i.e. the soil, which is an arrangement of different discrete particles (fine or coarse grained) and the structural element (steel, concrete, wood). Under a relative displacement, the localisation at the interface influence the structural behaviour. The interface properties and phenomena that can occur in this narrow zone are manifold. The first experimental evidence was given by Potyondy (1961). Based on his results, many different researchers started to contribute to the field of the soil-structure interface. Major early contributions were made by Coyle and Sulaiman (1967), Wernick (1978), Uesugi and Kishida (1986), Bosscher and Ortiz (1987), and Uesugi et al. (1988) (for sands) as well as Littleton (1976) and Tsubakihara and Kishida (1993) (clays). These experimental studies demonstrate that a soil volume several magnitudes of order smaller than the structure greatly influences soil-structure interaction behaviour. The effort put into research and development in this field is therefore understandable. Based on the assumptions of Wernick (1978), the importance of developing a new experimental methodology to investigate the in-situ stress and strain state of such interfaces has yet to be demonstrated. Before the research conducted by Wernick (1978), all researchers used modified direct shear tests, but could not conduct the necessary constant-normal stiffness tests. This new type of experimental methodology opened the way for the necessary experimental insights into the fundamental aspects of dilation or contraction at interfaces. This innovation was needed to explain the high values of friction were measured in site tests on model piles and anchors (Wernick 1978).

As indicated by De Gennaro and Lerat (1999), Fioravante et al. (1999), Dietz (2000), Porcino et al. (2003), DeJong et al. (2006), Hamid and Miller (2009), Hossain and Yin (2014a), and Chen et al. (2015), the interface and different phenomena have not been fully studied. A short summary of the importance of interfaces is given in Martinez et al. (2015). All this different

research indicates the importance of understanding the soil-structure interface. The interface can considerably influence the global performance of geotechnical engineering structures (e.g. Clough and Duncan (1971), Griffiths (1985), Gens et al. (1988), Griffiths (1988), Day and Potts (1998), Nakai et al. (1999), Lim and Lehane (2015), Yu et al. (2015)).

In addition to the experimental research, the first attempts to model the interface zones in rock mechanics were made by Goodman et al. (1968), who introduced a zero-thickness interface element to account for relative displacements in finite element analysis. This pioneering work of modelling interfaces into finite element analysis was followed by many varying ways of modelling such interfaces (e.g. Ghaboussi et al. (1973), Katona (1983), Beer (1985), Griffiths (1988), Hohberg (1992)).

Nowadays, numerical methods are widely used in geotechnical engineering for design. The consideration of interfaces into numerical analysis is often done by simplified Mohr-Coloumb friction laws, which are mostly empirical based. Furthermore, the interface zone can be modelled by standard finite elements (Griffiths 1985; 1988, Kim et al. 2007, Rebstock 2011, Tehrani et al. 2016). This simplification or neglecting of the experimental evidence of the important interfaces in soil-structure-interaction analysis can lead to an non-economic or over-conservative design as well as to misleading predictions in geotechnical engineering design (Day and Potts 1998, Gutjahr 2003). For example, Gutjahr (2003) points out that the wall friction under the translational point for a retaining wall is higher using a soil-structure interface model that is more realistic than a simpler Mohr-Coulomb interface model.

Besides, neglecting the interface behaviour or assuming it fully rough, a large number of different constitutive interface models were proposed (e.g. Mortara et al. (2002), Gómez et al. (2003), Liu et al. (2006), Nakayama (2006), Lashkari (2013), Cheng et al. (2013)). All of these interface models require specialised parametrisation, whereas the model of Arnold and Herle (2006) uses the model parameters from the 3D soil continuum. Considering one unique set of parameters is highly advantageous. In addition, 3D interface models have been rarely considered in recent research (Arnold and Herle 2006, Arnold 2008, Liu et al. 2014).

In light of the large number of different interface models, it is difficult to determine the most appropriate model. These models were not quantified and implemented into one numerical code for a comparative assessment.

Advanced constitutive interface models have also not been used in engineering practice. This may be due to a lack of suitable and user-friendly interface models. User-friendly does not mean simple or models with large simplifications but rather models that do not depend heavily on a special parametrization and interface tests. In particular, for clay structure interfaces, the lack of consistent modelling approaches is obvious.

In addition to the model development and theoretical considerations, it is important to supplement possibilities implementing the models. A straightforward approach for implementing such models into different numerical formulations is lacking.

1.2 Scope

The objectives of this thesis are to:

- Review the important experimental phenomena at soil structure interfaces
- Develop a simple and user-friendly quantification methodology choosing adequate constitutive interface models that incorporates the aleatory and epistemic uncertainty of constitutive interface models.
- Develop an innovative concept for transforming existing continuum 3D soil models into 2D interface constitutive models, applied to hypoplastic constitutive models
- Use this novel framework to develop and enhance various different kind of interface constitutive models for clay and sand considering only a few additional parameters
- Propose an simple and robust implementation scheme to transfer the theoretical developments of constitutive modelling into numerical simulations

In order to contribute to the use and enhancement of soil-structure interface modelling. These points will outlined below.

1.3 Outline

The thesis has nine Chapters. In **Chapter 2**, the interface problem is analysed by reviewing the state of research in geotechnical engineering. This emphasizes the experimental research contributions of several different authors. In addition to the experimental motivation, an overview of different existing numerical discretization techniques and constitutive models for modelling the interface zone is given in **Chapter 3**.

Chapter 4 presents a model assessment methodology, which can be used to quantify various constitutive soil-structure interface models. The model assessment uses model properties (sensitivity and uncertainty), which are combined in a unique framework considering multi-point objective function measures. The chapter presents the results of this assessment and gives the implications for future developments.

Motivated by the quantification of the constitutive models and the literature review, some new interface models are developed in **Chapter 5**. An existing hypoplastic interface model is adapted and modified by the in-plane stresses. Using the constitutive framework, fine-grained hypoplastic interface models are proposed (**Chapter 6**). The newly developed models are validated against each other as well as experimental data from previous research. This validation is performed using various test conditions that can be found in the literature (Littleton 1976, Tsubakihara and Kishida 1993, Sun et al. 2003).

The application of the new proposed models is shown in **Chapter 7**. This chapter describes

the implementation method and utilization of the new interface models. The validated and tested ABAQUS friction subroutine is used in boundary value problems such as direct shear simulations, large scale interface shear device by Vogelsang et al. (2013), and the simulation of a novel shallow penetrometer for characterizing the seabed for gas/oil pipelines. The importance for the advanced modelling of interface behaviour is highlighted by this application.

In addition to reformulated hypoplastic models, the novel method presented in Chapter 5.4 can be used for other modelling frameworks such as Barodesy and elasto-plastic modelling approaches. This is highlighted in **Chapter 8**.

A summary, conclusions, and an outlook for future work is given in **Chapter 9**.

Chapter 2

Experimental modelling for soil-structure interfaces

2.1 Introduction

The aim of this chapter is to review the major phenomena for different types of soil-structure interfaces, introduce and highlight the experimental observations, and address the importance of the different phenomena of the soil-structure interface.

These phenomena can be manifold. In particular, fine- (clays and silts) and coarse- (sands and gravel) grained soils are reviewed. Both soils exhibit dilation and/or contraction under continuous shear displacement at the interface. The properties and the inter-relation between the structural surface and the soil is an important issue.

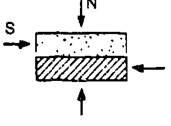
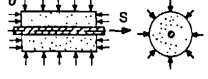
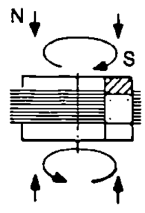
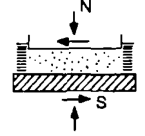
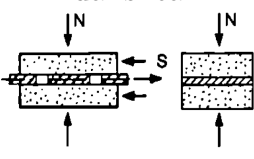
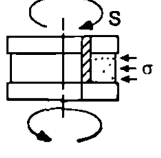
In the following sections, the experimental observations are discussed, and an overview of the existing literature is given. First, the different testing methodologies are explained (Section 2.3). This is followed by Section 2.4, which classifies the different soil-structure interface phenomena and shows the relations between these. The chapter ends with a summary.

2.2 Testing methodologies for interface shear tests

There are different test set-ups for soil structure interfaces. Dietz (2000) describes the limitations and advantages of the different testing equipment and set-ups available.

The mostly commonly used interface apparatus is the direct shear apparatus, which is modified by introducing an structural interface into the lower or top part of the direct shear device. The pioneering works of Potyondy (1961), Littleton (1976), and Wernick (1978) were conducted by using direct shear test devices. For soil-soil direct shear tests, Potts et al. (1987) studied the stress field inside a direct shear apparatus because of doubts concerning the uniformity of the stress and strain in the soil specimen. Nevertheless, the simple modification from a conventional to a modified direct shear test was an important development. Another important issue is the well known testing procedure described for direct shear tests, which can be adapted for interface

Table 2.1: Summary of interface testing apparatus (extended from Dietz (2000))

Type	Advantages	Complications	Reference
Direct shear 	Simple system failure characteristics thought to comply with apparatus kinematics, can be adapted from standard apparatus	Doubts concerning the uniformity of stress and strain, loss of material during testing through opening between surface and apparatus	Potyondy (1961), Rowe (1962), Littleton (1976), Y B et al. (1982), Tatsuoka and Haibara (1985), Bosscher and Ortiz (1987), Boulon and Nova (1990), O'Rourke et al. (1990), Al-Douri and Poulos (1992), Dove et al. (1997), Frost and Han (1999), Dietz (2000), Rao et al. (2000), De Jong et al. (2003), Hamid and Miller (2006), DeJong et al. (2006), Miller and Hamid (2007), DeJong and Westgate (2009), Taha and Fall (2014), Hossain and Yin (2014b), Zhao et al. (2014), Hossain and Yin (2014a), Feligha and Hammoud (2015), Yavari et al. (2016)
Axial-symmetric loading 	Similar to skin friction of piles, adaptable from standard apparatus	Normal stress on interface unknown, stress concentration at ends	Coyle and Sulaiman (1967), Brumund and Leonards (1973), Brumund and Leonards (1987), Hebel et al. (2015), Martinez et al. (2015)
Ring shear 	Endless interface, adapted from ring-shear	Gradient of displacement across the interface, friction of side walls and annulus + soil	Yoshimi and Kishida (1981), Neguessey et al. (1988), Tika-Vassilikos (1991), Lehane (1992), Evans and Fennick (1995), Vaughan et al. (1996), Lemos and Vaughan (2000), Ho et al. (2011), Eid et al. (2014), Chen et al. (2015)
Simple shear 	Soil deformation measured separately from interface surface slip, adapted from standard apparatus	End effects, boundary conditions promote the globalization of sample strains	Uesugi and Kishida (1986), Kishida and Uesugi (1987), Uesugi et al. (1988), Uesugi et al. (1989), Tsubakihara et al. (1993), Tsubakihara and Kishida (1993), Uesugi et al. (1989), Evgin and Fakharian (1996), Oumarou and Evgin (2005), Ao et al. (2014)
Dual shear 	Interface friction is measured on central third of interface	Instrumentation is difficult, sand over steel and steel over sand behaviour is measured	Paikowsky et al. (1995)
Ring simple-shear 	No end effects, endless interface	Interaction between particles and horizontal boundaries	De Gennaro and Lerat (1999), Corfdir et al. (2004), Dumitrescu et al. (2009), Koval et al. (2011)

shear tests.

In addition to direct shear testing, many researchers use modified simple shear interface test devices. As for the direct shear, the simple shear device can be adapted easily from the standard simple shear device to interface simple shear. The first use of this testing device was reported by Uesugi and Kishida (1986). The results of direct shear test device and simple shear test device are compared by Uesugi and Kishida (1986) (Figure 2.1). These studies indicated that in a direct shear test, the response is softer than the interface simple shear. Most researchers who used this kind of device highlighted the possibility of measuring the interface shear strain separately from the global soil specimen behaviour (Uesugi and Kishida 1986). A special kind of interface simple shear device was developed by Corfdir et al. (2004) and Koval et al. (2011). In this type of interface shear test, the stress is applied via an annular confining cell.

The last major class of modified devices is the ring-shear test devices. Two different kinds are differentiated. In the normal ring shear test, the bottom or top cap is replaced by an certain interface disk e.g. Yoshimi and Kishida (1981), Tika-Vassilikos (1991), and Ho et al. (2011). De Gennaro and Lerat (1999) developed a constant volume ring shear device. Both types of devices can apply "infinite" shearing conditions to the soil-structure interface. Because the sample is round, there are no inhomogeneities from corners or edges. A major disadvantage is that the friction values are influenced by the side walls of the horizontal boundaries. Handling the specimens (either coarse or fine-grained soils) is a challenging task.

The aforementioned types of interface shear test devices are common. More specialized devices have also been constructed. For example, the axi-symmetric loading device by Coyle and Sulaiman (1967), which similarly estimates skin friction for piles and anchors. Another test set-up is the dual-shear test device used by Paikowsky et al. (1995). The data, construction details, and the testing procedures are complicated with respect to the test results.

Interface shear testing is currently an important aspect in offshore geotechnical engineering. Recent research has focused on the shear behaviour of marine sediments and clays at low normal stress levels. Testing devices for this kind include the tilt table test (Najjar et al. 2007). This testing methodology was developed to test the interface friction at geosynthetic-soil interfaces. Najjar et al. (2007) adapted these technique for measuring the pipeline-soil interface friction. More recently, the Cam-Tor device (Kuo et al. 2015) was developed. In this testing device, a defined low shear stress can be applied by a top cap equipped with an interface, which is pushed into the soil. The shear testing then is applied by a torsional force.

Hebeler et al. (2015) and Martinez et al. (2015) used a axial-symmetric shear test for torsional and axial-symmetric shear conditions with textured defined rods. The study was performed with a soil mixture of 1% powdered phenolic resin and 99 % soil. After the interface test, the sample was heated, and the soil sample was conserved by the phenolic reaction. Using this procedure, it was possible to measure the shear characteristics and the shear band thickness of the soil specimens.

Other interface tests were conducted under temperature boundary conditions (Zhao et al. 2014,

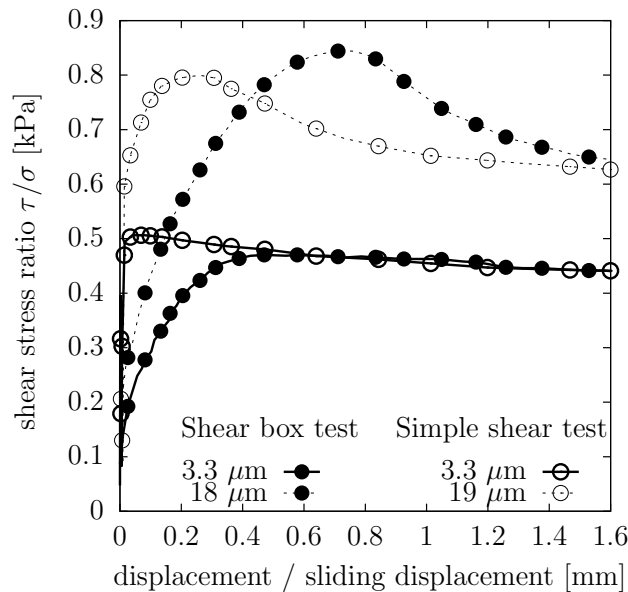


Figure 2.1: Comparison of direct to simple shear measurements (Uesugi and Kishida 1986)

Di Donna et al. 2015) and Yavari et al. (2016) or unsaturated interfaces (Hamid and Miller 2009, Hossain and Yin 2014a). Some studies revealed that chemical reactions influenced the anchor-soil interfaces (Hof 2003, Hof et al. 2004).

A large-scale interface testing device was recently presented by Vogelsang et al. (2013). This large scale interface testing device is used for the in-situ characterisation of the interface response for monotonic and cyclic shearing into a granular material.

In addition, the device is of major importance for conducting tests taking into consideration the adequate boundary condition.

2.3 Boundary conditions for soil-structure interfaces

The most important test conditions are the **Constant-Normal-Load**, **Constant-Normal-Stiffness**, and the **Constant-Volume** (which is also described as **Constant-Normal-Height** by Di Donna et al. (2015); Figure 2.2). More detailed information about the different conditions is given in the following.

Constant-Normal-Load (CNL)

The most frequently used boundary condition for studying the interface behaviour (Potyondy 1961, Littleton 1976, Uesugi and Kishida 1986, Uesugi et al. 1988) is the **Constant-Normal-Load (CNL)** condition. The constant normal load condition is characterized by a constant normal stress acting normal to the interface ($\dot{\sigma}_n = 0$). This common boundary condition is adapted from the direct shear test methodology. In conventional direct shear tests, the soil acts as a constraint to the soil-soil shear failure plane. The displacement in the normal direction of the interface is $\dot{u}_n \neq 0$. The boundary condition is shown in Figure 2.2a.

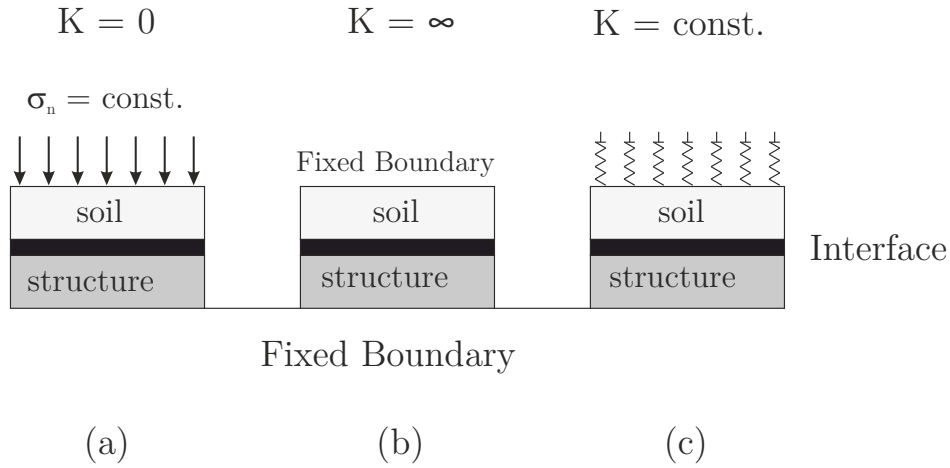


Figure 2.2: Boundary conditions in the direction normal to the interface: (a) constant normal stress, (b) constant volume, (c) constant normal stiffness (from Evgin and Fakharian (1996))

Constant-Normal-Stiffness (CNS)

Wernick (1978) studied the constant normal stiffness condition by investigating the discrepancy between the high load that can be applied to anchors and the lower overburden pressure. This boundary condition is important, especially for anchors and piles. The usage of this boundary condition revealed the differences between observational data from field tests and data from laboratory and small scale tests of anchors in sand. Wernick (1978) therefore introduced the constant normal stiffness condition. Figure 2.3 illustrates the hypothesis with the shear band thickness d_s and the axial displacement at the interface u_x .

The constant normal stiffness leads to a stress normal to the interface, which is :

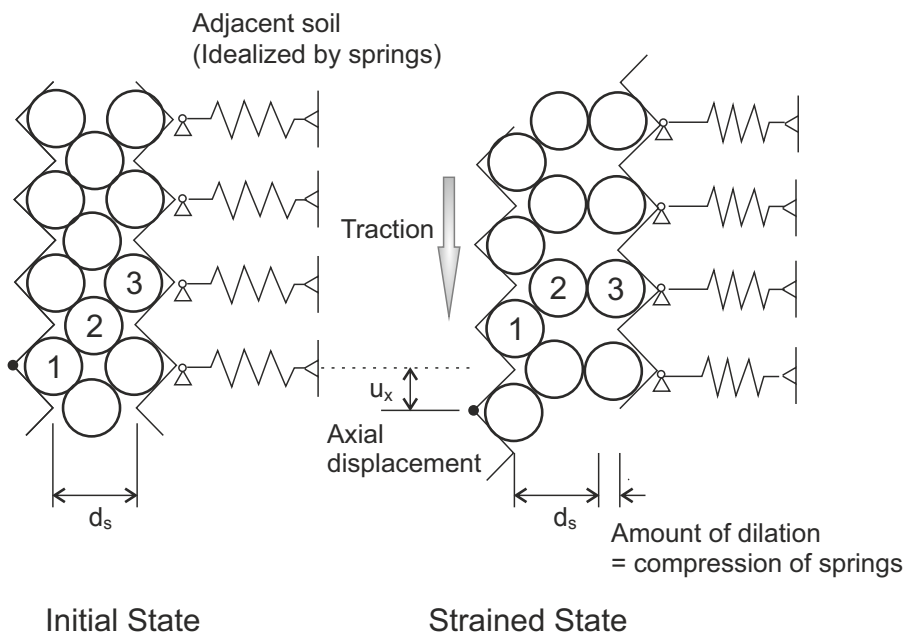


Figure 2.3: Hypothetic model by Wernick (1978) for the aggregate interlocking at the interface

$$\sigma_n = \sigma_{n0} - K\dot{\varepsilon}_n, \quad (2.1)$$

where σ_n and σ_{n0} are the current and the initially applied stress normal to the interface, K is the constraint stiffness, and ε_n is the strain normal to the interface. Wernick (1978) used the cylindrical cavity expansion theory to deduce the stiffness K from the equilibrium condition as:

$$K = \frac{2G_0}{R_P}, \quad (2.2)$$

where G_0 is the shear modulus at small strains and R_P is the radius of the pile or anchor. The stiffness K can vary from $K = 0$ to ∞ .

Fioravante et al. (1999) named this behaviour ‘‘confined dilatancy’’. Others researchers (Tabucanon et al. 1995, Fioravante et al. 1999, Fioravante 2002, DeJong et al. 2006), showed that the CNS condition is the most appropriate test boundary modelling the in-situ interface conditions. Using a spring analogy, the soil acts as a confining medium. The spring stiffness itself is $K = \text{constant}$. The rate of the normal stress and displacements are $\dot{\sigma}_n \neq 0$ and $\dot{u}_n \neq 0$. Further, Tabucanon et al. (1995) discussed that a good prediction of the frictional behaviour of geo-structures depends on the effect of dilatancy. Ghionna and Mortara (2002) stated that dilatancy is the governing phenomena for interface soil-structure behaviour. The only possibility to apply the accurate in-situ condition is the CNS boundary condition (Figure 2.2b).

Constant-Volume / Constant-Normal-Height (CV / CNH)

The constant volume condition has a stiffness of $K = \infty$, and the displacements are $\dot{u}_n = 0$. Because of the restraint of the displacement, the stress at the interface in the normal direction is $\dot{\sigma}_n \neq 0$. This boundary condition is difficult to fulfil. As a result of the shearing motion, the soil adheres to the upper and lower edges, thereby reducing the volume. Because this problem occurs most of testing devices, it is better to refer to this condition as **Constant-Normal-Height** (Di Donna et al. 2015). De Gennaro and Lerat (1999) developed a simple shear ring test in which the constant volume condition is fulfilled. This test condition can be applied if the behaviour of the soil-structure interface will be considered without any volumetric changes in the normal interface direction (e.g. pile installation considering large deformations). The boundary condition is shown in Figure 2.2c.

As mentioned above, the most frequently used condition was the CNL condition. Nowadays, the CNS condition is used because the behaviour of interfaces is tested under conditions similar to the in-situ conditions.

Costa D Aguiar et al. (2011) presented an overview of the consequences of these boundary conditions. Figure 2.4 shows the stress paths of a simulation using varying boundary conditions. It can be seen that the CV condition gives the highest shear stress τ_x and normal stress σ_n , whereas the CNL condition gives the lowest shear stress τ_x and a constant normal stress σ_n . The CV condition is often referred as the upper limit, and the CNL condition as the lower limit with respect to CNS condition, which can vary in between (Costa D Aguiar et al. 2011).

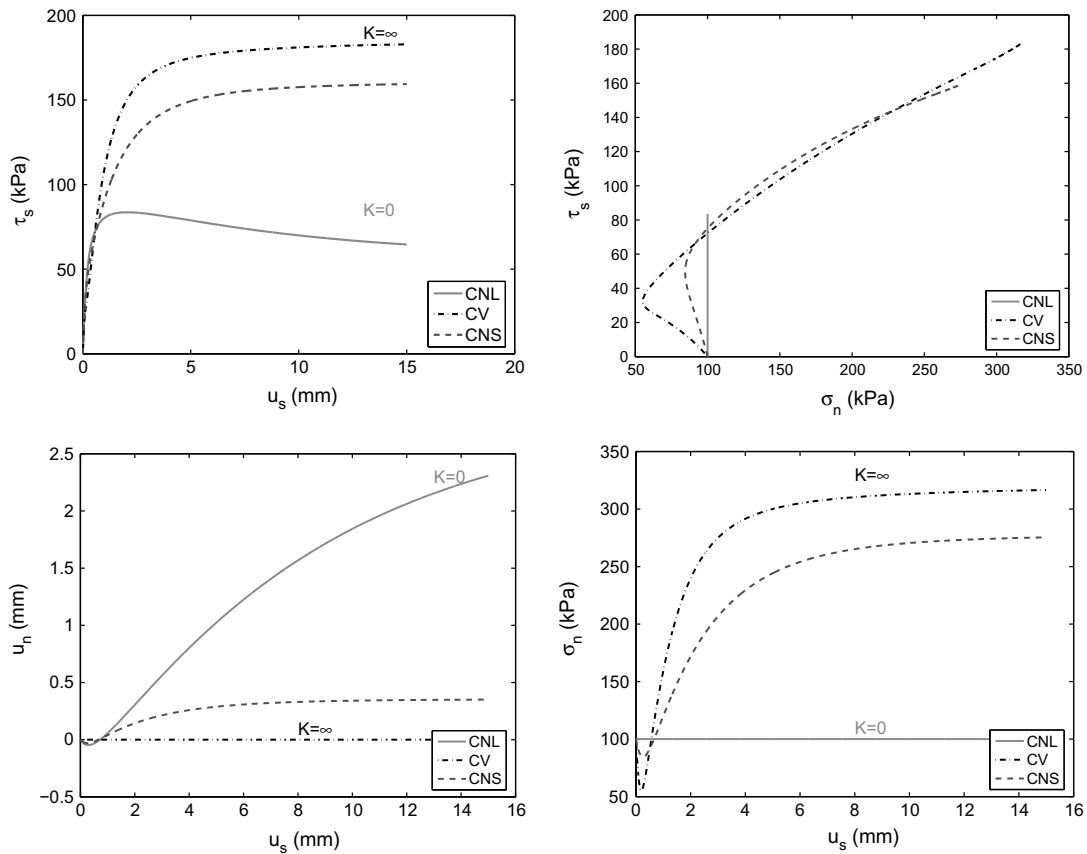


Figure 2.4: Influence of the different boundary conditions revealed by numerical interface simulations from Costa D Aguiar et al. (2011)

Beside the test conditions, the major influences is related to the relative soil density. The shear mobilisation and the tendency of contraction or dilation is proportional to the elastic confining stiffness K . The CNS condition can be stated as the intermediate case (Boulon and Nova 1990, Costa D Aguiar et al. 2011).

Understanding these different boundary conditions is important for the verifying and validating of the new proposed models in Chapters 5 and 6.

2.4 Key aspects of interface behaviour

The previous sections briefly introduce the testing devices/set-up that were developed as well as the possible boundary conditions for interface shear testing. The aim of this section is to provide a brief and comprehensive overview of the different phenomena that are important for characterizing and modelling of fine- and coarse grained interfaces.

Potyondy (1961) concluded that interface behaviour is dominated by the following factors:

- Various construction materials: wood, steel, and concrete
- Different surface conditions: rough and smooth

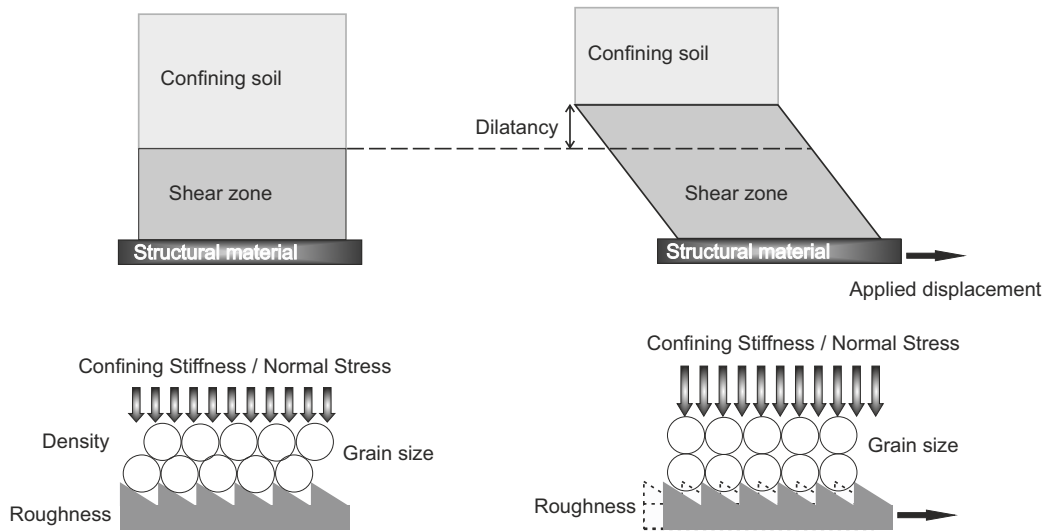


Figure 2.5: Interface behaviour and important factors for volumetric interface behaviour (Nakayama 2006)

- Various types of soils: sand, clay, and cohesive granular materials
- Variation of the normal load between the soil-interface of the friction surfaces

Fioravante et al. (1999) summarized the following important influences of the soil-structure interface behaviour in granular soils:

- Roughness of the surface
- Grain size
- Soil breakage
- Relative density of soil
- Constant normal stiffness K

The important influences for the soil-structure interface are visualised in Figure 2.5.

Surface roughness

Surface roughness has an evident role in the characterisation and the behaviour of soil-structure interfaces. Potyondy (1961) stated that surface roughness influences the skin friction coefficient of piles and anchors.

The surface roughness R_{max} as introduced by Uesugi and Kishida (1986) is the maximum roughness of a measured length L_M . With respect to soil type and soil mineralogy, it is important to normalize the surface roughness using the mean grain size d_{50} . This approach was introduced by Kishida and Uesugi (1987). Normalized roughness is defined as:

$$R_n = \frac{R_{max}(L_G = d_{50})}{d_{50}} \quad (2.3)$$

where d_{50} is the mean grain size diameter and R_{max} is the maximum roughness at the surface roughness over the gauge length of $L_G = d_{50}$. A high value of the normalized roughness R_n indicate a rough surface, Uesugi and Kishida (1986) showed for example R_n values of 130.

Porcino et al. (2003) stated that the roughness of a surface is the most important factor for the volumetric behaviour (contractive or dilative). DeJong and Westgate (2009) recently confirm the results of previous researchers (Potyondy 1961, Kishida and Uesugi 1987) that the surface roughness influences the peak stress as well as the distinctive post peak softening behaviour in granular soils. This finding supports the hypothesis that the failure will take place inside the soil mass if it has a rough surface. Hence, smooth surfaces encourage a failure directly at the interface plane (for experimental evidence, see Tejchman and Wu (1995) and Hu and Pu (2004)).

The effect of the local response was studied by DeJong and Westgate (2009). The local response near to the structural interface shows that the magnitude of the overall strain is substantially influenced by the surface roughness. For smooth interfaces, the shear and volumetric strain is concentrated close to the interface. Strains develop within the first 0.5 mm of tangential relative interface displacement (DeJong and Westgate 2009). In addition, it have to mentioned that the strain mobilisation dependent at the mean grain size diameter d_{50} . In contrast to this behaviour, the soil particles at a rough interface lock and force the strain to evolve inside the soil mass. Yasufuku et al. (2003) stated that the surface roughness is a good indicator of the deformation at the interface from yielding until the residual state. The volumetric behaviour is closely linked to the roughness of the surface. Uesugi et al. (1988) and De Jong et al. (2003) show in microscopic and particle image velocity (PIV) measurements that the particles behave in two different patterns: rolling and sliding. Smooth surfaces cause only sliding of the particles along the surface, whereas rough surfaces cause both sliding and rolling of the particles. This sliding and rolling with rough surfaces increases the peak behaviour of the soil-structure interface, which is coupled to the dilation behaviour of the geo-structural interface.

Tehrani et al. (2016) conducted tests in a half-circular pile chamber to verify the effect of surface roughness for model piles. They investigated the roughness of various sands and model piles. Density and surface roughness considerably influence to the behaviour of non-displacement model piles.

With respect to surface roughness, the major physical difference between fine and coarse grained soils is that cohesive and frictional forces contribute to the shear and strength behaviour of the interface. Littleton (1976) discussed that the influence from roughness asperities can be observed with respect to the change of surface before and after the shear test. The clay particles become clogged between the steel's surface asperities. Littleton (1976) concluded that 10% of the clay is clogged and that the shearing is governed by 90% of the steel's surface. Lupini et al. (1981) demonstrated that smooth surfaces lead to a sliding behaviour of the clay particle. This behaviour is referred to as sliding shear failure. Tsubakihara et al. (1993) classified three different modes of interface sliding. The first mode is shear failure, which occurs inside the soil.

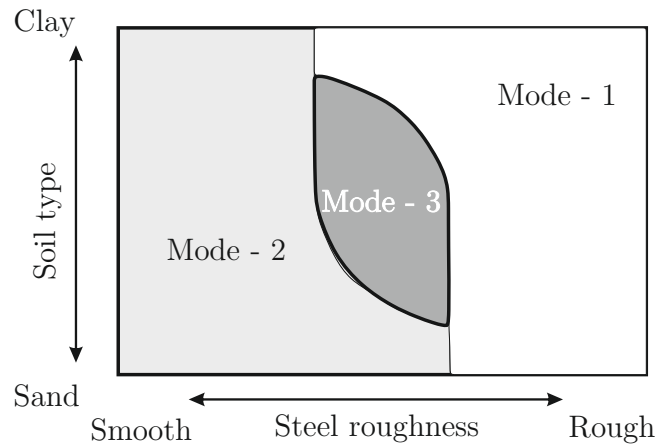


Figure 2.6: Idealized classification of interface shearing into three failure modes by Tsubakihara et al. (1993)

The second consists of full sliding and shear failure at the interface, and third consists of a mixture of mode 1 and 2 (Figure 2.6). The three modes are dependent on the critical surface roughness in sand- and clay-steel friction. Tsubakihara et al. (1993) stated that the critical surface steel roughness is $10 \mu m$. For clays with a high clay content, the residual shear strength is mainly independent of the surface roughness (Lemos and Vaughan 2000). However, for smooth surfaces, the interface shear strength resistance can be lower than the soil-soil residual strength. Lemos and Vaughan (2000) highlighted that such smooth surfaces are unlikely to occur in practical applications and that in clays with lower clay content, the presence of an interface promotes sliding, which depends on the surface roughness in the same manner as sand-structure interface shear. Rao et al. (2000) demonstrated that interfacial behaviour is more pronounced by the surface roughness. In addition, Rao et al. (2000) showed that if the critical surface roughness is reached, the interfacial friction angle is equal to the soil-soil (internal) friction angle (Uesugi et al. 1988). The experimental studies by Rao et al. (2000) demonstrate that the ratio between the interfacial and soil friction angles is independent of the over-consolidation ratio.

Feligha and Hammoud (2015) performed direct shear interface tests with different textures of the surfaces in shear direction and material surfaces. They reported that the materials have no influence on the shear behaviour but rather on the surface roughness at the interface. The effect of red-clay concrete friction was recently studied by Chen et al. (2015). For smooth interfaces, the failure occurs on the soil-structure surface. Obviously, for extremely rough surfaces, the failure takes place inside the soil mass. Furthermore, Chen et al. (2015) observed increased dilation at lower normal stress with rough interfaces. This effect is caused by a highly compressed clay matrix in the asperities at the surface. These contribute to the peak strength behaviour. In addition, Chen et al. (2015) pointed out that the asymptotic shear strength behaviour is not strongly influenced.

From these definitions, it can be seen that the mean grain size and the surface roughness are connected.

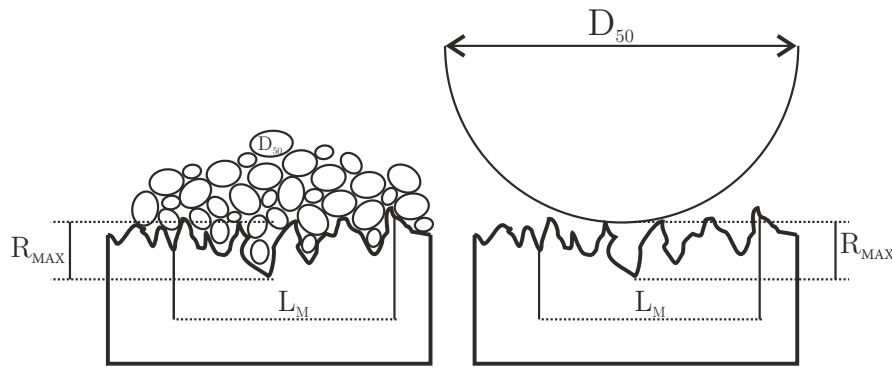


Figure 2.7: Definition of the maximum and average roughness compared to different coarse soils by Uesugi et al. (1988)

Mean particle size

The mean grain size has an important influence with respect to the interface behaviour. Uesugi et al. (1988) highlighted that the particle size and surface roughness are particularly important. This dependence was validated by Fioranvante (2002) (Figure 2.7). The mean diameter d_{50} plays an essential role for the shear band thickness. Potyondy (1961) and Kishida and Uesugi (1987) verified these findings. The particle size is the important factor behind softening and hardening behaviour in granular materials.

Soil relative density

Soil density is important for the volumetric behaviour of the interface. Yasufuku et al. (2003) showed that increased density increases the interface friction angle. Uesugi et al. (1989) explained that the upper limit of the friction coefficient of the maximum shear stress ratio depends on the relative soil density. Moreover, the volumetric behaviour of the interface is coupled with the void ratios with respect to the initial, intermediate, and residual states. DeJong et al. (2006) and DeJong and Westgate (2009) demonstrated the influence of the void ratio on stress development in the surrounding soil, especially if cyclic loading is applied at the interface.

In general, it is apparent that density is a key factor predicting the deformation of the soil in the interface zone. The influence of density is as important for interfaces as it is for soils.

In fine-grained soils the relative density does not have to be considered. The overconsolidation ratio (OCR) is more important and must be considered instead of the relative density as in granular soils.

Confining normal stress and stiffness

The stress and stiffness, which is confined to the interface, influences the behaviour of interfaces. Hansen (1961) showed that vertical deformation in a shear box tests depends on the stress ratio applied. The same hypothesis is true for interface shear tests. From the physics of the problem, it is clear that the pressure that acts in the normal direction to the interface influences the deformation.

The differences between the testing of CNL and CNS conditions was noted by Wernick (1978).

Uesugi and Kishida (1986) mentioned that the relation between the applied normal stress and the total plastic work is exhibited at the interface. Uesugi et al. (1988) reported that the total plastic work increases by the same amount of shear deformation under higher normal stresses. Evgin and Fakharian (1996) showed that the peak stress depends on the magnitude of the normal stress. Dietz (2000) reported that with an increasing normal stress, the peak stress ratio will decrease for a rough surface.

For fine-grained soils, there are similar relations between the confining stress and stiffness for the shear behaviour of interfaces. Littleton (1976) showed that the peak behaviour in the CNL tests he conducted depends on the mean effective stress that is applied. This was observed for drained and undrained shear tests. In CV and CNL tests, Tsubakihara and Kishida (1993) demonstrated that the peak and softening behaviour is influenced by normal stress. The overconsolidation ratio influences the shear stress evolution (Rao et al. 2000). However, overconsolidation ratio itself does not influence the interfacial friction angle.

There is therefore a relation between the normal stress applied and the pre- and post peak behaviour.

Structural material

The structural material may have some influence with respect to the anisotropy of the surface. Potyondy (1961) demonstrated that wood structural materials have an inherent anisotropy, which depends on the shearing direction. Similar trends were observed by Zhang et al. (2010) in gravel soil-structure shear tests. Zhang et al. (2010) illustrated the anisotropy and the influence of the granulometric properties of coarse grained soils. In addition, Zhang et al. (2010) demonstrated that the identical behaviour exists in geotextile-soil interface shear. Zhang and Zhang (2009) introduced the term “aeolotropy” for the anisotropic behaviour of interfaces. Feligha and Hammoud (2015) pointed out that shearing of the interfaces in only one shear direction does not influence the shear strength. However, shearing of the interface in two different shearing positions influences the stress-deformation behaviour of interfaces.

Monotonic or cyclic loading paths

The stress path characteristic is an important issue for interfaces subjected to repeated loads. Desai et al. (1985) stated that the amplitude of the cyclic displacement has only a small influence on the interfacial behaviour. Evgin and Fakharian (1996) carried out simple shear tests on dense silica crushed sand. These tests demonstrated that under increased cyclic loading there is substantial degradation at the interface. Evgin and Fakharian (1996) and De Jong et al. (2003) highlighted that the rate of this degradation is especially large in the first few cycles. By using particle image velocity measurement De Jong et al. (2003) observed that the interface shear zone contracts and dilates with shear reversals. In these tests, a compacted interface zone was measured under cyclic loads.

Uesugi et al. (1989) showed that for the interface friction under cyclic loading at soil-concrete interfaces, the same frictional envelope evolves as does under monotonic loading (Figure 2.8).

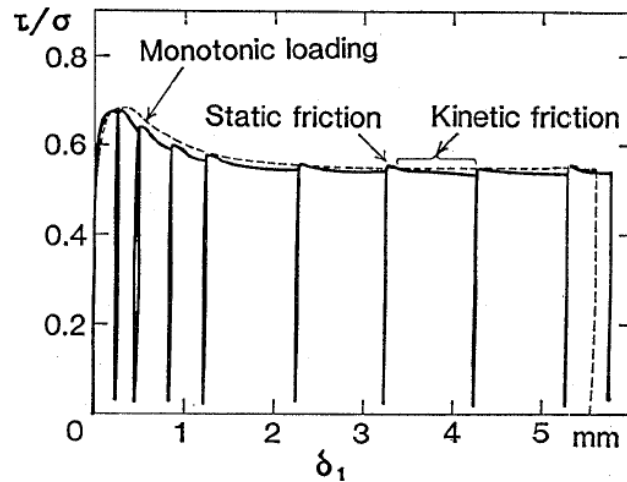


Figure 2.8: Comparison of monotonic and cyclic loading paths from Uesugi et al. (1989)

Vogelsang et al. (2013) also illustrated this behaviour for large-scale interface tests. In addition, Uesugi et al. (1989) stated that for sand-steel friction, the residual coefficient of friction does not depend on the applied stress path. These experiments showed that in the first cycle the interfacial friction angle is different than interface sliding conditions. The interface friction angle tends to the asymptotic interface friction angle in the forthcoming cycles. Mortara et al. (2007) studied the cyclic stress path behaviour at sand-structure interfaces. Post-cyclic behaviour was also investigated. The results indicated that for smooth surfaces, the shear stress will decrease in the cyclic loading phase and does not recover in the post-cyclic phase. Mortara et al. (2007) also stated that with increasing roughness, the cyclic degradation decreases, while the post cyclic degradation increases.

For fine-grained soils, less attention has been paid to cyclic interface tests. Ovando-Shelley (1995) carried out cyclic and monotonic interface tests on remoulded and natural clay samples. By using a cyclic stress amplitude $\tau_{cyc}/\tau_{st} \geq 1$, they observed that a dynamic over-strengthening lead to failure within the first cycle. This is contrary to the observation made in cyclic triaxial testing with the same clay.

Desai and Rigby (1997) carried out marine clay-steel interface tests. These tests indicated that under cyclic displacement amplitude, the interface shows high shear deformations near the interface. Under cyclic shearing conditions, the influence to the soil appear to decrease with increasing cycle number. In a very small thin-layer interface zone, the localization concentrated is attached to the structural surface (De Jong et al. 2003).

Shear band thickness at interfaces

The importance of the shear band thickness at the interface is not yet fully understood. The importance of shear band thickness is related to the importance of the modelling approach that takes into account the shear band thickness at interfaces. The shear band thickness is also as a zone of intensive shearing defined by DeJong and Westgate (2009).

The initial results indicated the thickness of the shear band indicated by Yoshimi and Kishida

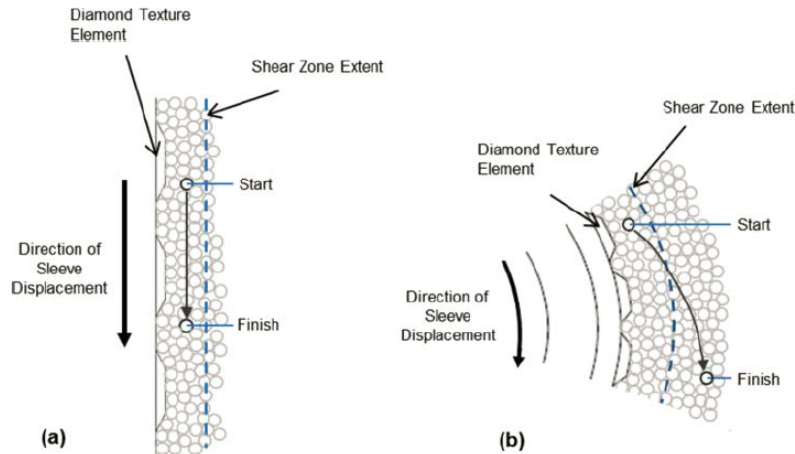


Figure 2.9: Hypothesis for a particle movements under a) axial and b) torsional shearing (Martinez et al. 2015)

(1981) was nine times the mean grain size diameter d_{50} . Tejchman and Wu (1995) conducted tests using a plane strain shear device and concluded that the shear thickness is $6 \times d_{50}$ for smooth interfaces and $40 \times d_{50}$ at the interface with a loose sand. The thickness of the interface at rough interfaces in dense sands has a range of $30 - 40 \times d_{50}$, Fioravante et al. (1999) used a range of $2 - 10 \times d_{50}$ as the interface thickness. More recent results from DeJong et al. (2006) obtained by investigating the shear zone thickness in sands indicate a shear zone thickness of $5 - 7 \times$ particle diameter adjacent to the interface measured by particle image velocity measurements. The shear band formation inside cemented specimens is more diffuse than in silica sands. It can be hypothesized that the brittle behaviour and grain crushing in carbonate sands have a major influence.

DeJong and Westgate (2009) conducted interface tests and divided the behaviour into two different zones based on their observations. Regarding these findings, the global behaviour outside the shear zone is not considerably affected by the shearing and exhibits no volumetric changes, whereas the local response and the thickness of the interface zone near to structural element increase with increasing particle angularity, surface roughness, and relative density. A reduction of the shear zone thickness is observed for decreasing particle hardness, normal stress, and stiffness. This leads to the conclusion that the particle hardness and the crushability of soils are important factors (DeJong and Westgate 2009). DeJong and Westgate (2009) observed a shear zone with a thickness of $0.1 \sim 9 \times d_{50}$ and a dilation zone with a thickness of $1 - 12 \times d_{50}$. Ho et al. (2011) conducted large deformation interface tests in different configurations. The interfaces underwent deformations up to 8 mm. In these tests, the soil tended to crush, and the crushed material concentrated in the shear zone; these ranged from $4 - 13 \times d_{50}$. The total upper limit of the shear zones was 5 mm.

Hebeler et al. (2015) and Martinez et al. (2015) used axial symmetric and torsional shear devices to quantify of the influencing factors and verify some earlier assumptions. They tested three different sands with respect of their particle angularity. The thickness of the shear band

was influenced by the roughness. The critical roughness was not exceeded in these tests. These findings are in contrast to internal shear zones. Hebler et al. (2015) compared the soil-soil shear band thickness with the interface shear band thickness and confirmed the hypothesis that the thickness at the interface shear band is one half of that at the soil-soil shear band (Frost et al. 2004). The particle angularity and the interface shear band thickness do not effect each other. Martinez et al. (2015) used the same techniques to gain additional insights into the shear zone thickness and the shear zone interface behaviour and concluded that the shear zone thickness is fully developed at very small displacements. They also carried out tests in torsional and axial shear, under torsional shear, the zone influenced was 2 – 3 times larger than in purely axial shearing. The shear zone thickness in torsional shear is $\sim 6 \times d_{50}$. The mirco-mechanical hypothesis proposed by Martinez et al. (2015) is illustrated in Figure 2.9. The thickness of the interface zone formed by the particle in axial shearing migrates along the interface, whereas in rotational shearing, the particle migrate away from the interface. The mechanical hypothesis confirms the particle behaviour in axial and torsional shearing reported by DeJong et al. (2006). Tehrani et al. (2016) stated that the shear band thickness along non-displacement rough model piles ($R_n = 0.26$ and $R_n = 1.14$) embedded in dense to medium dense sands was $3.9 - 5.2 \times d_{50}$, while the average shear band thickness was $3.2 - 4.2 \times d_{50}$. In their tests, shear zone or shear band thickness could not be observed for smooth piles ($R_n = 0.03$).

For clay-concrete interfaces, the maximum thickness of the shear band is $d_{max} = (7 \sim 8) d_{50}$ (Chen et al. 2015).

Fully and partially saturation at interfaces

Desai et al. (1985) and Desai and Rigby (1997) performed soil-structure interface tests under fully saturated conditions using fine-grained soil the behaviour of a fully saturated soil differed from the fully dry case.

Hamid and Miller (2009) discussed results for unsaturated interfaces. Unsaturated interfaces are defined as interfaces adjacent to unsaturated soils. Hamid and Miller (2009) concluded that at unsaturated interfaces, the post-peak shear strength is largely unaffected. As expected from conventional unsaturated soil mechanics, the peak shear resistance is influenced by the mean net stress and the applied suction values. Hamid and Miller (2009) also found out that the adhesion intercepts were smaller than the cohesion intercept. The values for rough interfaces were less than those for smooth interfaces. Hamid and Miller (2009) hypothesized that these difference can be attributed to volume change behaviour and physical-chemical reactions at the failure plane near by the structural surface.

Hossain and Yin (2012; 2014a) conducted tests with unsaturated soil-cement grout interfaces. Coarse grained soil was tested under various different suction conditions. In contrast to Hamid and Miller (2006; 2009), and Hossain and Yin (2014a) observed that the applied suction tend to influence the post and pre-peak interface shear behaviour. This observation is reasonable because particle movements destroy the water menisci between the grains. The loss of shear strength will lead to the same post peak behaviour as for normally saturated soils. As already

known from soil testing under higher suction values, the stiffness increases, and the soil-structure interface can bear more load. The behaviours from these two studies differed because these were not classical soil-structure interface test with respect to the cement grout that was poured into the load cell.

With respect to hydraulic hysteresis (suction loading and unloading) at the soil-structure interface, Houry and Miller (2012) reported that the shear strength after wetting and drying cycles is higher than after drying of the soil-structure interface at the same normal net stress and matric suction.

Considering a fast loading rate and low permeability at the interface under fully saturated conditions will lead to an undrained interface response (Cathie et al. 2005). This behaviour can be tested for example using a Constant-Volume boundary test condition.

Temperature effects

The temperature effects at soil-structure interfaces is a newer field of research. Nevertheless, because of an increasing need for renewable energy, these effects must be studied in detail. Examples of the temperature influences of geotechnical structures are axial shaft capacity for the design of energy-piles as well as thermo-mechanical problems such as nuclear-waste disposal, high-voltage cables, or gas and oil-pipelines.

Xiao et al. (2014) conducted interface shear tests with a silty soil. These tests were compared to soil-soil shear tests. They concluded that the shear behaviour in soil-soil friction as well as in soil-structure tends to increasing shear strength under increasing temperature.

Zhao et al. (2014) carried out tests with frozen silty soil-structure interfaces. The tests were conducted with a special shear box equipped with different thermal sensors. Zhao et al. (2014) demonstrated that under decreasing temperature, the shear strength increases followed by an degeneration of the interface friction angle in the forthcoming load cycles.

Di Donna et al. (2015) carried out sand-concrete and clay-concrete shear tests. In the sand-concrete shear tests, no effects of ambient temperature changes could be observed. In contrast, clay-concrete tests resulted in an increased shear strength with increasing temperature. As well as decreasing contraction behaviour with increasing temperature in addition to the monotonic tests, Di Donna et al. (2015) conducted cyclic interface tests under 20°C and 50°C, in these tests an increasing adhesion can be observed with increasing temperature.

Hanson et al. (2015) tested isothermal soil-interface to measure the surface profile changes after the test. But did not observe an effect of the soil-structure interface friction angle.

Yavari et al. (2016) conducted tests with intermediate heated soils (5 – 40°C), which are typical for thermo-active geotechnical structures. In contrast to the tests by Di Donna et al. (2015), the Kaolin clay samples were heated prior to the test, thereby eliminating the thermal consolidation effect. Yavari et al. (2016) observed negligible influences of the interface shear strength parameters. But reported a softening behaviour for clay-concrete interfaces; this was not observed in clay-clay direct shear tests.

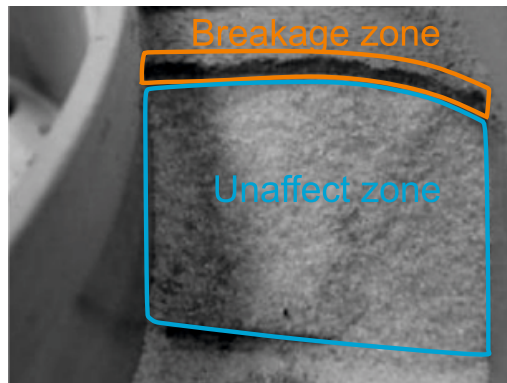


Figure 2.10: Examples of a post-testing zone with on top interface shear test from Ho et al. (2011) highlighting the zones with and without breakage

Grain breakage

Grain breakage and crushing take place at soil-structure interfaces (e.g. Uesugi et al. (1988), Al-Douri and Poulos (1992)). Uesugi and Kishida (1986) pointed out that the amount of grain breakage is proportional to the sliding distance of the interface. Uesugi et al. (1989) also noted that the particle crushing is responsible for the shear zone formation. De Jong et al. (2003) confirmed particle breakage in interface tests, especially carbonate soils tend to grain breakage. Ho et al. (2011) emphasised the importance of grain crushing with respect to the shear zone at interface as well as the influence of changes in roughness of the interface. The interface friction angle developed under large-shear displacement is notably different than that from conventional direct-shear interface tests. Ho et al. (2011) reported that the configuration (i.e. whether the interface is on top or at the bottom) does not influence the thickness and amount of particle breakage in interface shear conditions. Figure 2.10 shows an exemplary result of such a post-peak test with the different zones in the granular soil.

Lim and Lehane (2015) found that the structural damage for rough surfaces sheared in compressible sands results in radial and shear stresses at the pile shaft under shearing. This phenomena is explained by the fabric change of the sand under shearing.

Rate effects

Shear rate effects are especially important for fine-grained soils. Tsubakihara and Kishida (1993) considered a small shear rate to avoid pore-water overpressure into the sample because of the low permeability in fine-grained soils. Lemos and Vaughan (2000) conducted tests with an initial slow shear rate followed by a fast interface shearing. By this test procedure it could be observed that the ratio between fast peak shear resistance and slow residual strength increased with clay content. Lemos and Vaughan (2000) discussed that the presence of an increasing percentage of rotund particles helps to disorder the particle skeleton during fast shearing. In addition, Lemos and Vaughan (2000) studied that the loss of strength under increasing shearing rate was not accompanied with the generation of excess pore water pressure at the interface. In their study (Lemos and Vaughan 2000), a sudden increase after the stop of a fast stage of

interface shearing was observed. Lemos and Vaughan (2000) mentioned that the higher void ratio and water content at the shear zone are accompanied by contractions after stopping the fast shearing.

Ganesan et al. (2014) highlight the importance for the rate of shearing for pipeline-soil interfaces, which can be considered as undrained or drained shearing.

2.5 Summary of Chapter 2

The chapter reviewed the major experimental observations starting with the pioneering work of Potyondy (1961) and went on to discuss the special boundary conditions, which are important for the verification and validation as well as general interface behaviour. The importance of surface roughness, normal stress acting on the interface, particle angularity, relative density, void ratio, grain breakage, and stress history on interface behaviour was demonstrated by experimental studies.

It is obvious that clay-structure interfaces have been studied in less detail than sand-structure interfaces. Because the behaviour of fine-grained soil-structure interfaces is more complex than the behaviour of granular interfaces, scientific work has mainly focussed on sand-structure interfaces.

Chapter 3 presents numerical formulations and constitutive models for soil-structure interaction.

Chapter 3

Existing numerical modelling for soil-structure interfaces

3.1 Introduction

Chapter 2 reviewed and compiled the important aspects of experimental interface behaviour. These phenomena must be modelled in order to achieve a realistic and holistic modelling of interfaces. The numerical and constitutive models needed to model the interface behaviour have therefore been reviewed. The most important numerical modelling techniques, namely zero-thickness, thin-layer element, and the surface-to-surface methodology are reviewed and briefly introduced. An overview of existing constitutive interface models is given in Section 3.3. In addition, five different constitutive interface models and formulations are introduced. These five models are considered with respect to their practical use, advanced modelling approach, and different formulation. The models are used for the model assessment in Chapter 4.

3.2 Numerical modelling of soil–structure interfaces

In geotechnical engineering, the modelling of contact surfaces involves using finite element simulations that have been developed in the last four decades. The modelling of interfaces can be split into two main categories. The first part (Section 3.2) introduced the numerical techniques and in the second part (Section 3.3), constitutive modelling of interface behaviour is introduced. Desai et al. (1984) state that the general problem of modelling interfaces can be viewed in the wider context of classical contact mechanics. Nevertheless, soil-structure interface modelling has been established as a separate field of contact mechanics. As mentioned before, only the most important contributions are presented.

The first subsection will start with an overview and classification of different numerical techniques that can be used in finite element analysis. Griffiths (1985; 1988) highlighted the importance of accurate numerical solving procedure in modelling the adequate bearing behaviour of geo-structures. Other numerical techniques that also require contact mechanics (e.g. the dis-

crete element method, the material point method, extended finite elements, and others) will not be discussed.

3.2.1 Zero-Thickness Interface element

The first development of an often used modelling method was the pioneering interface element for modelling rock joints by Goodman et al. (1968). The “zero-thickness” interface element can be used in finite element analysis. The idea is that the interface itself has a zero thickness at the beginning of the analysis. After initialization, both bodies in contact can move independently but are constrained over the zero-thickness interface element. The element referred to as either called a joint element or an interface element. Goodman et al. (1968) proposed an element with four nodal points and zero-thickness. By using the relative displacement between the both nodes and an application of a joint stiffness matrix, the zero-thickness interface element is applied. The formulation of the 2D zero-thickness interface element (Figure 3.1) with four nodes is briefly introduced. The formulation of Goodman et al. (1968) can be extended to 3D as shown by Beer (1985).

Considering the C_0 -compatibility, the linear shape functions N_1 and N_2 are given as:

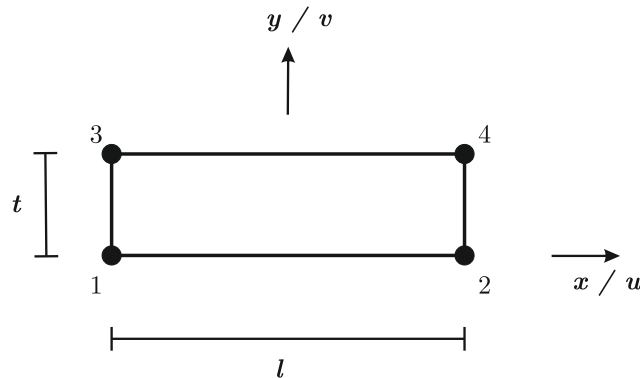


Figure 3.1: Zero-thickness interface element after Goodman et al. (1968)

$$N_1 = \frac{1}{2} - \frac{x}{l} \quad ; \quad N_2 = \frac{1}{2} + \frac{x}{l}, \quad (3.1)$$

where l is the length of the element and x is the horizontal coordinate. The horizontal nodal displacements are defined as:

$$u_{low} = N_1 u_1 + N_2 u_2 \quad ; \quad u_{upp} = N_1 u_4 + N_2 u_3 \quad (3.2)$$

The vertical nodal displacements are given as:

$$v_{low} = N_1 v_1 + N_2 v_2 \quad ; \quad v_{upp} = N_1 v_4 + N_2 v_3, \quad (3.3)$$

Assuming a constant thickness of the interface, the strain is computed from the lower and upper relative displacements as:

$$\varepsilon = \begin{bmatrix} \varepsilon_n \\ \gamma_x \end{bmatrix} = \begin{bmatrix} \frac{v_{upp} - v_{low}}{t} \\ \frac{u_{upp} - u_{low}}{t} \end{bmatrix}, \quad (3.4)$$

where t is the thickness of the interface. This thickness is initially zero or has a virtual thickness, which is introduced as a parameter. ε_n is the strain normal to the interface, and γ_x is the shear strain. The assumption of Goodman et al. (1968) is a continuous displacement field that leads to a continuous strain field through the length l . Using an arbitrary constitutive model, the stress is obtained as:

$$\begin{bmatrix} \sigma \\ \tau_x \end{bmatrix} = \begin{bmatrix} \sigma_n \\ \tau_x \end{bmatrix} = [D^e] \begin{bmatrix} \varepsilon \end{bmatrix}, \quad (3.5)$$

where D^e is the elastic constitutive matrix. Reformulating and combining Eq. 3.2, 3.3, and 3.4, the strains can be written as:

$$\begin{bmatrix} \varepsilon \end{bmatrix} = [B] \begin{bmatrix} d \end{bmatrix}, \quad (3.6)$$

where $\begin{bmatrix} d \end{bmatrix}$ and $[B]$ are the nodal displacement vector and the strain-displacement matrix. The B matrix is defined as:

$$[B] = \frac{1}{t} \begin{bmatrix} -N_1 [I] & -N_2 [I] & N_1 [I] & N_2 [I] \end{bmatrix}, \quad (3.7)$$

where $[I]$ is a two-by-two identity matrix. d is defined as

$$\begin{bmatrix} d \end{bmatrix} = \begin{bmatrix} u_1 v_1 u_2 v_2 u_3 v_3 u_4 v_4 \end{bmatrix} \quad (3.8)$$

The strain energy U can be calculated as:

$$U = \frac{1}{2} \begin{bmatrix} d \end{bmatrix}^T \int_{-l/2}^{l/2} [B]^T [D^e] [I] [B] dx \quad (3.9)$$

Equation 3.9 provides the stiffness matrix $[K]$ as:

$$[K] = \int_0^l [B]^T [D^e] [I] [D^e] dx \quad (3.10)$$

A further development based on the joint element proposed by Goodman et al. (1968) is the isoparametric interface element proposed by Beer (1985), which is a simple joint/interface element for 2D and 3D finite element analysis. This can be used between shell, solid, or mixtures of both finite element types. Beer (1985) explained that using a zero-thickness is advantageous, especially for modelling joints in rocks and rock fractures.

In addition to these studies, another problem was in the focus. This motivated some different developments of the zero-thickness interface element. The numerical integration of the zero-thickness interface element is an important issue. Pande and Sharma (1979) investigated isoparametric zero-thickness interface elements and elements proposed of Ghaboussi et al. (1973). The interface element by Ghaboussi et al. (1973) is an extension of the classical Goodman element formulation. Ghaboussi et al. (1973) used relative displacement as independent degrees of freedom. Pande and Sharma (1979) investigated these different formulations and found reasonable problems in the sense of ill-conditioning. Pande and Sharma (1979) concluded that the effort required to implement the relative displacement as an independent degree of freedom was not worth it.

The problem of the ill-conditioning of the stiffness matrix was reported by Gens et al. (1988). The behaviour of interface elements, which was studied by eigenvalue analysis of the stiffness matrix with different integration schemes, indicated that the use of a Newton quadrature scheme is beneficial for simulations using zero-thickness interface elements (Gens et al. 1988). Schellekens and de Borst (1993) studied numerical integration in great detail and discussed the ill-conditioning of zero-thickness interface elements. Gauss, Newton-Cotes, and Lobatto linear and quadratic integration schemes were studied by Schellekens and de Borst (1993). They found that the ill-conditioning resulted from large off-diagonal terms or small diagonal terms (Schellekens and de Borst 1993). In most cases, the Newton-cotes quadrature scheme is recommended.

Many different extended versions of the zero-thickness interface element have been introduced. These included:

- A new joint element for the non-linear dynamic calculation of arch dams (Hohberg 1992)
- A friction element for the simulation of arch dams (Swoboda and Lei 1994)
- A new interface element to overcome major deficiencies in the Goodman interface model (Kaliakin and Li 1995)
- An extension of the Goodman interface element with Biots consolidation theory to model interfaces and rock joints, especially when water pressure is a important factor (Ng and Small 1997)
- An extension of the zero-thickness interface element for the extended modelling of the interface soil-pile normal contact (Stutz et al. 2014)
- A 3D zero-thickness interface element for the coupled analysis of the hydro-mechanical modelling of interfaces for offshore-applications (Cerfontaine et al. 2015)

3.2.2 Thin-Layer interface element

Desai et al. (1984) criticized the approach of Goodman et al. (1968) as being unrealistic and misleading because of the soil-structure interfaces have a experimentally-proven certain thickness. Desai et al. (1984) therefore proposed the thin-layer element formulation. This element has a certain thickness.

The thin-layer interface was described in a formulation of the global coordinate system (Figure 3.2). The formulation used is given by Sharma and Desai (1992). The displacements are defined

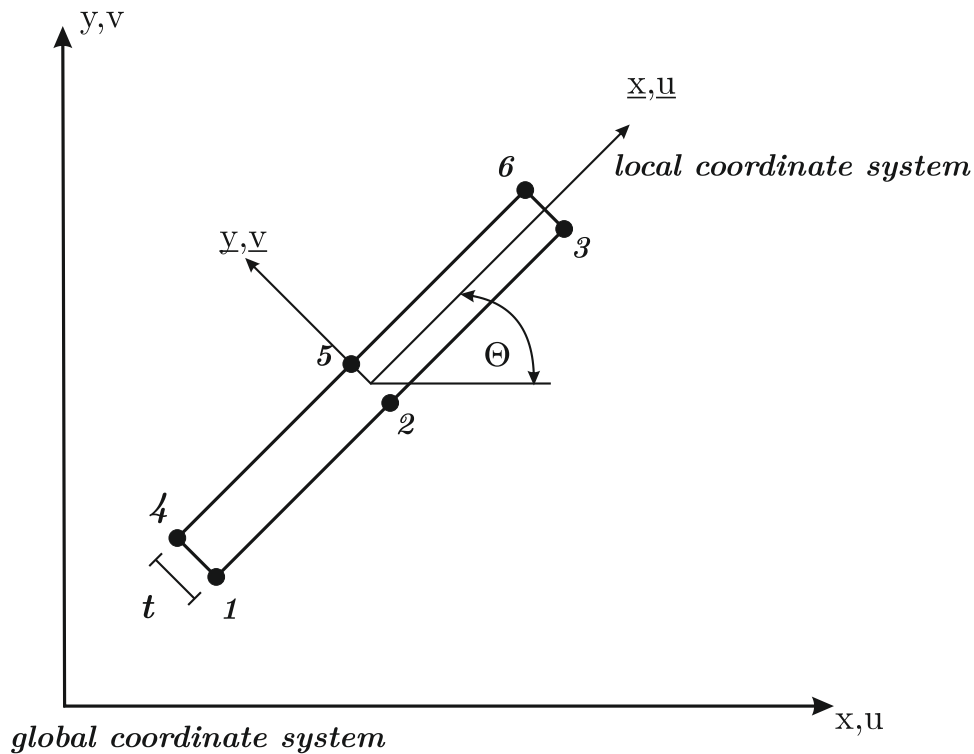


Figure 3.2: Thin-layer interface element from Sharma and Desai (1992)

as:

$$\begin{bmatrix} u \\ v \end{bmatrix} = \begin{bmatrix} N_1 & 0 & N_2 & 0 & N_3 & 0 & N_4 & 0 & N_5 & 0 & N_6 & 0 \\ 0 & N_1 & 0 & N_2 & 0 & N_3 & 0 & N_4 & 0 & N_5 & 0 & N_6 \end{bmatrix} \begin{bmatrix} q \end{bmatrix}, \quad (3.11)$$

where N_i with $i = 1 \dots 6$ are the interpolation functions, which can be either quadratic or linear. $[q^T] = (u_1 v_1 u_2 v_2 \dots u_6 v_6)$ in which u_i and v_i ($i = 1, 2, \dots, 6$) are the displacements of the i th node in x - and y - direction. Strains are related to the displacements as:

$$\begin{bmatrix} \varepsilon_x \\ \varepsilon_y \\ \gamma_{xy} \end{bmatrix} = \begin{bmatrix} \frac{\partial u}{\partial x} \\ \frac{\partial v}{\partial y} \\ \frac{\partial u}{\partial y} + \frac{\partial v}{\partial x} \end{bmatrix}. \quad (3.12)$$

Or in a shorter notation:

$$[\varepsilon] = [B] [q], \quad (3.13)$$

where ε_x , ε_y , and γ_{xy} are the in-plane, normal, and shear strain at the interface. B is the strain-displacement matrix. The global strains are calculated using the transformation matrix T :

$$\begin{bmatrix} \varepsilon \end{bmatrix} = \begin{bmatrix} T^\varepsilon \end{bmatrix} \begin{bmatrix} \varepsilon_{local} \end{bmatrix}, \quad (3.14)$$

where ε_{local} is given by equation 3.12. The transformation matrix $\begin{bmatrix} T^\varepsilon \end{bmatrix}$ is defined as:

$$\begin{bmatrix} T^\varepsilon \end{bmatrix} = \begin{bmatrix} (\sin \Theta)^2 & (\cos \Theta)^2 & -\cos \Theta \sin \Theta \\ -2 \cos \Theta \sin \Theta & 2 \cos \Theta \sin \Theta & (\cos \Theta)^2 - (\sin \Theta)^2 \end{bmatrix}. \quad (3.15)$$

The transformation matrices for stress and strains are differ from each other. The stress transformation matrix $\begin{bmatrix} T^\sigma \end{bmatrix}$ is calculated as:

$$\begin{bmatrix} T^\sigma \end{bmatrix} = \begin{bmatrix} (\sin \Theta)^2 & (\cos \Theta)^2 & -\cos \Theta \sin \Theta \\ -\cos \Theta \sin \Theta & \cos \Theta \sin \Theta & (\cos \Theta)^2 - (\sin \Theta)^2 \end{bmatrix}. \quad (3.16)$$

By using transformation matrix T^σ , the stress in global coordinates can be calculated as:

$$\begin{bmatrix} \sigma \end{bmatrix} = \begin{bmatrix} T^\sigma \end{bmatrix} \begin{bmatrix} \sigma_{local} \end{bmatrix}. \quad (3.17)$$

σ_{local} is defined as:

$$\begin{bmatrix} \sigma_{local} \end{bmatrix} = \begin{bmatrix} d\sigma_n \\ d\tau \end{bmatrix} = \begin{bmatrix} tK_n & tK_{ns} \\ tK_{sn} & tK_s \end{bmatrix} \begin{bmatrix} d\varepsilon_n \\ d\gamma \end{bmatrix}, \quad (3.18)$$

where K_n and K_s are the normal and shear stiffness and K_{ns} and K_{sn} are the coupling terms, which were ignored in Desai et al. (1984) and Sharma and Desai (1992). t is the thickness of the interface. The (tangent) consistence matrix C' is expressed as:

$$C' = \begin{bmatrix} tK_n & tK_{ns} \\ tk_{sn} & tK_s \end{bmatrix}. \quad (3.19)$$

The global increment stress-strain relation is defined as:

$$d\sigma = T^T C' T d\varepsilon = C d\varepsilon, \quad (3.20)$$

where $C = T^T C' T$. The element stiffness matrix K is given as:

$$K = \int_V B^T C B dV_E. \quad (3.21)$$

The parameter V is defined as the element volume.

To prevent penetration of the both surfaces, Desai et al. (1984) proposed an algorithm that can be used to detect the overlapping and which uses a penalty approach to prevent overlaps. The major advantage highlighted by Desai et al. (1984) is the avoidance of an unrealistic high

normal stiffness in the interface normal direction because it is done with zero-thickness interface elements. Advantages and disadvantages of the various interface elements were discussed e.g. Hohberg (1990), Desai and Nagaraj (1990), Hohberg and Schweiger (1992), Stutz et al. (2013), and Qian et al. (2013).

The thin-layer element by Desai et al. (1984) handled the interface modelling as constitutive problem rather than a numerical problem as in the zero-thickness interface elements.

An overview of the early approaches of modelling contacts with zero-thickness and thin-layer interface elements was given by Hohberg (1992).

3.2.3 Surface-to-surface modelling approach

The master- and slave concept of Hallquist (1979) also influenced the geotechnical community. This concept and some extensions are used for geotechnical simulations (Sheng et al. 2005, Nazem et al. 2006, Sheng et al. 2009, Nazem et al. 2012, Wriggers et al. 2013, Sabetamal et al. 2014, Weißenfels and Wriggers 2015a;b, Nazem 2016). Contact formulations used for pipeline-soil interaction problems were introduced by Sabetamal et al. (2015). Penetration simulations for CPT and piles were used by Huang et al. (2004) and Fischer et al. (2007). The advanced modelling approach enables the simulation of large deformation problems including the interaction of the soil and the structures. The general principals of the contact kinematics are presented in Figure 3.3. Two bodies are introduced. B_0^m is the body onto which the master surface is applied. The master surface will be called $\Gamma_{0c}^m \subset \Gamma_0^m$ and $\Gamma_c^m \subset \Gamma^m$ in the current configuration. The slave body B_0^s has the same set of contact surfaces as $\Gamma_{0c}^s \subset \Gamma_0^s$ and $\Gamma_c^s \subset \Gamma^s$. The master and slave contacts must be defined at the initial configuration. These are states for which an active or inactive contact and/or the bodies are not in contact (Figure 3.3). The master surface Γ_c^m acts as a reference for the slave surface Γ_c^s , which depends on the master surface. These surfaces should be given with Gaussian surface parameters x_i^α and must be continuously differentiable. Arbitrary points at the actual and initial reference configuration are identified with the coordinates $\mathbf{X}^m(x_i^\alpha)$ or $\mathbf{x}(x_i^\alpha)$. The local coordinate can be derived with the surface coordinates (Figure 3.4)

$$\mathbf{A}_\alpha = \mathbf{X}_\alpha^m(\xi^\alpha, t_i0) \quad ; \quad \mathbf{a} = \mathbf{x}_\alpha^m(\xi^\alpha, t_i), \quad (3.22)$$

where \mathbf{x}_α is defined as $\frac{\partial \mathbf{x}}{\partial \xi^\alpha}$. The movement of master and slave bodies can be calculated using a projection formula. This formula ensures the computation of the slave point \mathbf{x}^s at Γ_c^s to the master point \mathbf{x}^m at Γ_c^m . The coordinate $\mathbf{x}_m(\bar{\xi}^\alpha, t_i)$ must be calculated for each slave point at surface area Γ_c^m , which minimizes the distance function $d(\xi^\alpha, t_i)$:

$$d(\xi^\alpha, t_i) = \|\mathbf{x}^s - \mathbf{x}^m(\xi^\alpha, t_i)\| \rightarrow \text{MIN} \quad (3.23)$$

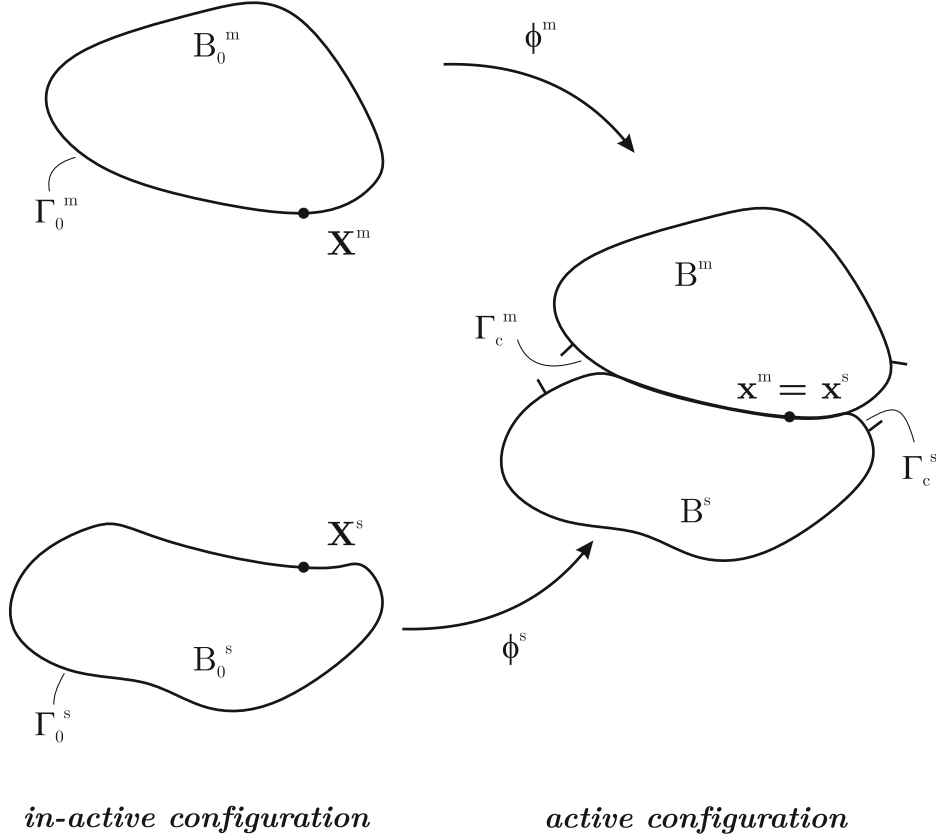


Figure 3.3: Reference and current configuration for Master and Slave concept based on Haraldsson (2004)

$\bar{\xi}^\alpha$ is the parameter set that provides the minimal distance between master and slave surface. Wriggers and Miehe (1994) proposed the following equation to calculate $\bar{\xi}^\alpha$:

$$\frac{d}{d\xi^\alpha} d(\xi^\beta, t_i) = - \frac{\mathbf{x}^s - \mathbf{x}^m(\xi^\beta, t_i)}{\|\mathbf{x}^s - \mathbf{x}^m(\xi^\beta, t_i)\|} \mathbf{x}_\alpha^m(\xi^\beta, t_i) = 0. \quad (3.24)$$

All variables with a bar are calculated with the minimized points from $\bar{\xi}^\alpha$. The tangent vector \bar{a}_α is equivalent to $\mathbf{x}_\alpha^m(\xi^\beta, t_i)$. This tangent vector can be used to calculate the distance \mathbf{x}^s to $\mathbf{x}^m(\xi^\beta, t_i)$ in the direction of the normal of the contact surface $\bar{\mathbf{n}}_c^m$. Using the relation between the master and slave surfaces by the projection points enables the definition of a distance function g as:

$$g_N = [\mathbf{x}^s - \bar{\mathbf{x}}^m] \bar{\mathbf{n}}_c^m. \quad (3.25)$$

The distance function g_N is divided into following behaviour.

$$g_N = \begin{cases} < 0 & \text{penetration} \\ = 0 & \text{contact} \\ > 0 & \text{separation} \end{cases}. \quad (3.26)$$

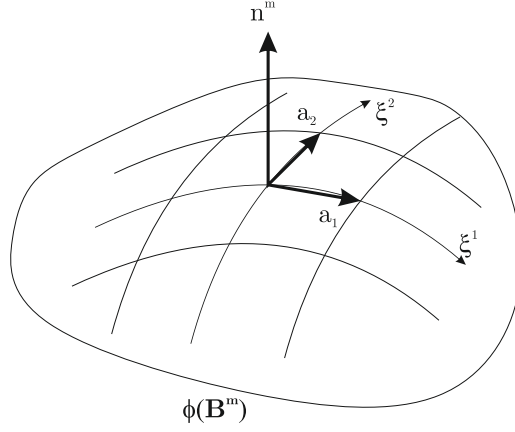


Figure 3.4: Contact coordinates from Haraldsson (2004)

A purely geometrical contact description prevents penetration of the slave surface into the master surface. This constraint is fulfilled if the following condition is true:

$$g_N \geq 0. \quad (3.27)$$

The penetration formula with a penalty approach is:

$$\bar{g}_N = \begin{cases} g_N & \text{for } g_N < 0 \\ 0 & \end{cases}. \quad (3.28)$$

According to the definition of the normal contact, the next component is the tangential contact movement. The change of the tangential displacement is associated with the change in $\bar{\xi}^\alpha = \bar{\xi}^\alpha(t_i)$. By taking the derivative of Equation 3.24 over the time t_i , $\bar{\xi}^\alpha$ can be calculated (Wriggers and Miehe 1994). With $\bar{\mathbf{x}}^m = \mathbf{x}^m(\bar{\xi}^\alpha(t_i), t_i)$ and $\bar{\mathbf{v}}^m = \frac{\partial \mathbf{x}^m(\bar{\xi}^\alpha(t_i), t_i)}{\partial t_i}$ the following equation is reformulated as:

$$\left(\mathbf{v}^s - \bar{\mathbf{v}}^m - \bar{\mathbf{x}}_\beta^m \dot{\bar{\xi}}^\beta \right) \bar{\mathbf{a}}_\alpha + (\mathbf{x}^s - \bar{\mathbf{x}}^m) \left(\bar{\mathbf{v}}_\alpha + \bar{\mathbf{x}}_{\alpha\beta}^m \dot{\bar{\xi}}^\beta \right) = 0. \quad (3.29)$$

The equation 3.29 can be modified by replacing the difference vector $(\mathbf{x}^s - \bar{\mathbf{x}}^m)$ with $g_N \bar{\mathbf{n}}_c$. The metric coefficient $\bar{a}_{\alpha\beta} = \bar{\mathbf{a}}_\alpha \bar{\mathbf{a}}_\beta$ at ∂B_c^m in point $\bar{\xi}^\alpha$ using the coefficient of the curvature tensor $\bar{b}_{\alpha\beta} = \bar{\mathbf{x}}_{\alpha\beta}^m \bar{\mathbf{n}}_c$ that gives the solution of the following equation as:

$$(\bar{a}_{\alpha\beta} - g_N \bar{b}_{\alpha\beta}) \dot{\bar{\xi}}^\beta = (\mathbf{v}^s - \bar{\mathbf{v}}^m) \bar{\mathbf{a}}_\alpha + g_N \bar{\mathbf{n}}_c \bar{\mathbf{v}}_\alpha^m \quad (3.30)$$

If the distance function is $g_N = 0$, which is the identifier for an existing contact, the equation will be degenerated to:

$$(\mathbf{v}^s - \bar{\mathbf{v}}^m) = \dot{\bar{\xi}}^\alpha \bar{\mathbf{a}}_\alpha, \quad (3.31)$$

where $\mathbf{v}^s - \bar{\mathbf{v}}^m$ is the tangential relative contact movement. The relative tangential velocity is calculated with:

$$\dot{g}_T^s = \mathbf{v}^s - \bar{\mathbf{v}}^m. \quad (3.32)$$

This serves as a local kinematic variable for the tangential shear stress. This shear stress can be calculated with different constitutive models. For a more detailed description of the discretization process as well as the formulation of the weak form, refer to Wriggers (2007) and Haraldsson (2004). The mostly used contact constitutive model in the master-slave algorithm is the classical Mohr-Coulomb friction model. Haraldsson (2004) shows that an advanced constitutive model in the contact description positively influences the modelling of soil-structure interaction problems. Dziewiecki et al. (2015) implemented a hypoplastic constitutive model into a projection scheme with a mortar method.

If the contact is established, different constitutive interface models can be applied. Some of these different constitutive models are described in Section 3.3.

3.3 Constitutive modelling of soil-structure interfaces

Some different models are briefly introduced in this section. In Sections 3.3.1–3.3.5, selected models are described in more detail. The models presented are used in Chapter 4 to assess the model quality.

The general form (stress-strain relation) of a constitutive interface model can be expressed as:

$$\dot{\boldsymbol{\sigma}} = f(\dot{\boldsymbol{\epsilon}}). \quad (3.33)$$

Most of the interface models are based on the elasto-plasticity framework. The following are needed to calculate $\dot{\boldsymbol{\sigma}}$:

1. a yield criterion to distinguish between elastic and plastic behaviour. For interface models, the yield criterion is used to estimate stick behaviour.
2. a plastic potential to describe the evolution of the yield surface
3. a hardening and/or softening rule
4. a compliance tensor, which governs the adhesion behaviour

The Mohr-Coulomb friction (Coulomb 1821) is most frequently adopted in the different elasto-plasticity interface models. The model is described in detail in section 3.3.1.

Clough and Duncan (1971) introduced a constitutive shear model that uses a hyperbolic non-linear elastic model to model interfaces. Clough and Duncan (1971) derived the model from the hyperbolic soil model of Duncan and Chang (1970). This model was extended for unloading and reloading as well as more advanced stress paths (Gómez et al. 2003). The hyperbolic model of Clough and Duncan (1971) is described extensively in section 3.3.2.

Desai and Nagaraj (1988) developed a model that takes also cyclic shearing and cyclic normal contact into account. They adapted a Ramberg-Osberg model for unloading/reloading behaviour. However, this model does not consider the coupling of the normal and shear behaviour, which is essential for the volumetric interface behaviour.

Gens et al. (1988) proposed a model for soil-reinforcement, which uses adapted analytical integration schemes. These integration schemes demonstrate a good robustness during non-linear calculations. Gens et al. (1988) also studied the pull-out behaviour of sand-geotextile interfaces with this new constitutive model.

Boulon (1989) and Boulon and Nova (1990) developed a constitutive interface model in which two different approaches were compared with each other. An elasto-plastic and a rate-type interface model were compared.

Shahrour and Rezaie (1997) developed an elasto-plastic interface model with a two surface bounding surface formulation to model cyclic interface behaviour.

Herle and Nübel (1999) described a hypoplastic constitutive interface model. Wu and Bauer (1994) and Gudehus (1996) developed a model that does not split the elastic and plastic strain. This model assumption was used by Herle and Nübel (1999) to develop a 1D constitutive model and later by Gutjahr (2003). A 3D hypoplastic model using reduced stress and strain tensors was introduced by Arnold and Herle (2006).

Fakharian and Evgin (2000) applied the model developed by Navayogarahaj et al. (1992) to calculate the three dimensional stress path interface tests. Fakharian and Evgin (2000) therefore extended the model to a fully 3D constitutive interface model. The basic model of Navayogarahaj et al. (1992) adopts a hierarchical single surface formulation that takes associative, non-associative, and strain-softening behaviour into account during monotonic and cyclic loading.

Gennaro and Frank (2002) developed a model based on the Mohr-Coulomb friction law. This models deviatoric hardening and softening, taking into account the phase transformation during compaction or dilation of the interface as well as the ultimate state conditions.

Ghionna and Mortara (2002) and Mortara (2003) developed a sand-structure elasto-plastic model in which the parameter calibration is done with CNL tests because this is the common laboratory procedure for simulating CNL and CNS conditions. Mortara et al. (2002) and Boulon et al. (2003) extended the model to account for cyclic loading conditions. Mortara et al. (2010) simplified an earlier model (Mortara 2003) to account for cyclic loaded smooth sand-steel interfaces.

The damage model of Hu and Pu (2003) uses elasto-plasticity in conjunction with a damage function:

$$D_f = 1 - \exp(-a\xi^b), \quad (3.34)$$

where a and b are material parameters and ξ is the trajectory of the plastic shear strains. At the start of the deformation, the damage function $D_f = 0$ and $D_f = 1$ describes the critical state of the interface. This unique framework uses a disturbance function, which describes the

continuous transformation from a relatively intact state (RI) to a fully adjusted state (FA). The model thus takes into account external excitations from thermal or mechanical forces acting on to the interface.

Liu et al. (2006) and Liu and Ling (2008) developed an interface constitutive model that uses the critical state concept for sands (Been and Jeffries 1985) and the generalized plasticity approach of Pastor et al. (1990). The general plasticity approach does not explicitly define a flow rule and a yield function. Instead, vectors for the elasto-plastic D^{ep} matrix are used. The model was extended to a 3D constitutive interface model by Liu et al. (2014). The idea to use a critical state parameter was also applied by Lashkari (2013). The interface model of Nakayama (2006) also uses the critical state parameter for the elasto-plastic modelling of interfaces.

Zhang and Zhang (2009) and Zhang et al. (2010) also developed a model for gravel interface and gravel geosynthetic behaviour. This involves a bounding surface approach coupled with a damage model invented by Hu and Pu (2003).

Samtani et al. (1996) described a model for modelling visco-plastic effects, which uses the concepts of Perzyna's theory of viscoplasticity and the hierarchical single surface concept.

Shao and Desai (2000) developed a model for clay-steel interfaces using the disturbance state concept with a damage function defined in Equation 3.34.

To model the progressive failure of landslides in quick clay, Jostad and Andresen (2004) used a constitutive model for clay and interface elements that are formulated on the basis of shell elements.

Shakir and Zhu (2009) developed a model for compacted clay-interfaces to take into account the behaviour of different water contents at the interface.

Cheng et al. (2013) developed a model that takes into account the normal stress history. This uses the accumulated energy as a hardening parameter. The shearing process is idealized as an energy dissipation process. Based on these assumptions Cheng et al. (2013), proposed a model for clay-concrete interfaces.

Although there are many of different interface models, several factors are not fully governed by the different models or are still under development. Examples include the cyclic accumulation behaviour of interface models (Burlon et al. 2014), the modelling of unsaturated and/or non-isothermal interface conditions Hamid and Miller (2008) and Lashkari and Kadivar (2015).

In the following sections, five different interface models are described in greater detail. These models are frequently used but differ with respect to their framework.

3.3.1 Mohr-Coulomb model

The Mohr-Coulomb friction law (Coulomb 1821, Van Langen 1991) is the most widely used interface constitutive model. This bilinear plasticity model combines linear elastic behaviour with perfect plastic behaviour. The constitutive equation is based on the following expression:

$$\dot{\mathbf{t}} = \mathbf{D}^e \dot{\mathbf{u}}^e = \mathbf{D}^e (\dot{\mathbf{u}} - \dot{\mathbf{u}}^p), \quad (3.35)$$

where $\dot{\mathbf{t}}$ is the objective rate of traction. The elastic constitutive matrix \mathbf{D}^e is defined as:

$$\mathbf{D}^e = \begin{bmatrix} G & 0 \\ 0 & E_i \end{bmatrix}. \quad (3.36)$$

The shear modulus G and the constrained modulus E_i are expressed as:

$$G = \frac{E_i}{2(1 + \nu_p)} \quad ; \quad E_i = 2G \frac{1 - \nu_p}{1 - 2\nu_p}. \quad (3.37)$$

The constitutive equation for the interface yield function of the model is given as:

$$f = \tau + \tan \varphi_i \sigma_n - c, \quad (3.38)$$

where f is the yield function, τ is the shear stress, φ_i is the friction angle at the interface, σ_n is the normal stress acting on the interface and c the adhesion at the interface. The Mohr-Coulomb model is a classical elasto-plastic model, which is typically used in finite element calculations. The interface becomes plastic if the following condition is fulfilled (Van Langen 1991):

$$f = 0 \quad \text{and} \quad \frac{\partial f^T}{\partial t} \mathbf{D}_c^e \delta u \geq 0. \quad (3.39)$$

The direction of the plastic slip rate is defined by the plastic potential g :

$$g = \tau + \sigma_n \tan \psi_I, \quad (3.40)$$

where ψ_I is the interface dilation angle. Using a non-associated flow rule ($\psi_I \leq \varphi_I$) prevents the over-prediction of plastic dilation (Vermeer and de Borst 1984). The plastic components of the interface relative displacements are defined as (Van Langen 1991):

$$\dot{u}_n^p = \Lambda \frac{\partial g}{\partial \sigma_n} \quad ; \quad \dot{u}_x^p = \Lambda \frac{\partial g}{\partial \tau}. \quad (3.41)$$

The plastic multiplier Λ is defined with a consistency condition. In this particular case, the condition is expressed as:

$$f = \sigma_n \frac{\partial f^T}{\partial \sigma_n} = 0. \quad (3.42)$$

The consistency condition is transformed to:

$$\Lambda = \frac{1}{d} \frac{\partial f^T}{\partial \sigma_n} \mathbf{D}^e u_n, \quad (3.43)$$

where d is defined as:

$$d = \frac{\partial f^T}{\partial \sigma_n} \mathbf{D}^e \frac{\partial g}{\partial \sigma_n} \quad (3.44)$$

The elasto-plastic constitutive matrix \mathbf{D}^{ep} is therefore derived as:

$$\mathbf{D}^{ep} = \mathbf{D}^e - \frac{\alpha}{d} \mathbf{D}^e \frac{\partial g}{\partial \sigma_n} \frac{\partial f}{\partial \sigma_n}^T \mathbf{D}^e, \quad (3.45)$$

where α is an indicator for plastic ($\alpha = 1$) or elastic conditions ($\alpha = 0$). The parameters for the Mohr-Coulomb model are given in Table 3.1.

Table 3.1: Model parameters and physical definitions for the Mohr-Coulomb friction model

Parameters	Physical definition	Unit
E	Young's modulus	[MPa]
ν_p	Poisson ratio	[-]
φ	Friction angle	[°]
ψ	Dilatancy angle	[°]
c	Cohesion	[MPa]

3.3.2 Hyperbolic non-linear elastic model of Clough and Duncan (1971)

The empirical hyperbolic model developed by Clough and Duncan (1971) is based on the continuum soil model developed by Duncan and Chang (1970). In this interface model, a hyperbola is used to approximate empirical the experimental data from interface tests. The model was developed for the realistic simulation of retaining walls. The empirical equation for the interface behaviour is:

$$\tau = \frac{u_s}{a_r + b_r \cdot u_s}, \quad (3.46)$$

where a_r and b_r are fitting parameters used to evaluate the goodness of fit for the hyperbola from experimental observations. The model is based on empirical assumptions. u_s is the interface shear displacement, and τ is the interface shear stress. The Equation 3.46 is modified as:

$$\frac{u_s}{\tau} = a_r + b_r \cdot u_s \quad (3.47)$$

The motivation to transpose Equation 3.46 is the determination of the fitting coefficients a_r and b_r . After linearising Equation 3.47, the plot becomes a straight line, where a_r is the intercept and b_r is the slope (Figure 3.5). This is valid if the stress varies hyperbolically with the relative displacement. The coefficient a_r is equivalent to the initial shear stiffness K_{si} . b_r is the reciprocal of the ultimate shear stress τ_{ult} . It is convenient to express the peak shear stress τ_f by using τ_{ult} :

$$\tau_f = R_f \tau_{ult}, \quad (3.48)$$

where R_f is the failure ratio and varies from 0.82 to 0.95 (Clough and Duncan 1971). Gómez et al. (2003) defined a range from 0.40 to 0.95. The hyperbolic interface model uses the equation

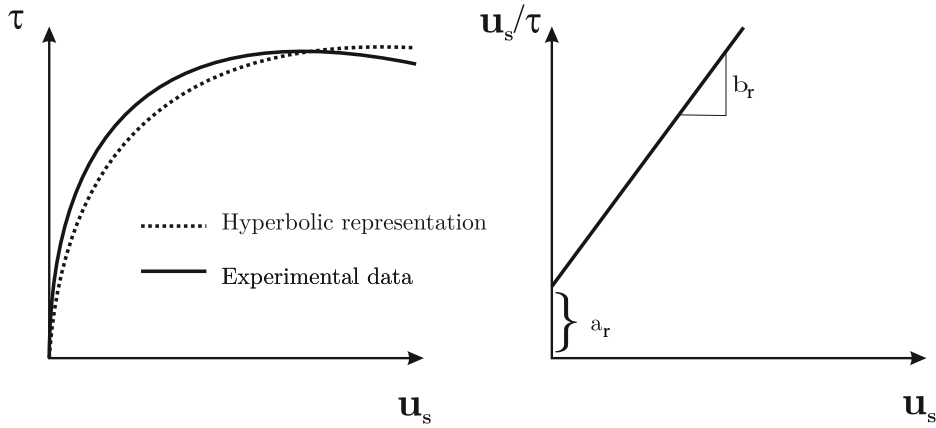


Figure 3.5: Visualisation of the fitting parameter a and b for shear test data, based on Clough and Duncan (1971)

of Janbu (1963) to take into account the normal and shear stiffness dependence in relation to the normal pressure. The initial shear stiffness K_{si} is given as:

$$K_{si} = K_I \gamma_w \left(\frac{\sigma_n}{p_a} \right)^{n_{HY}}, \quad (3.49)$$

where K_I is a dimensionless stiffness number, γ_w is the unit weight of water, and n_{HY} is a stiffness exponent. Identical to the interface model of Coulomb, the shear stress is proportional to the normal stress and is expressed as:

$$\tau_f = \sigma_n \tan \varphi_i, \quad (3.50)$$

where φ_i is the friction angle for soil-structure interface shearing. Clough and Duncan (1971) substituted Equations 3.48, 3.49, and 3.50 to calculate the shear stress variation.

$$\tau = \frac{u_s}{\frac{1}{K_I \gamma_w \left(\frac{\sigma_n}{p_a} \right)^{n_{HY}} + \frac{R_f u_s}{\sigma_n \tan \varphi_c}}}. \quad (3.51)$$

In a non-linear finite element analyses with interface elements according to Goodman et al. (1968), the tangent stiffness of the model is derived by differentiating $\tau = \frac{\partial \tau}{\partial u_s}$ and eliminating u_s to yield the following equation:

$$K_s = K_I \gamma_w \left(\frac{\sigma_n^{n_{HY}}}{p_a} \right) \left(1 - \frac{R_f \tau}{\sigma_n \tan \varphi_i} \right)^2. \quad (3.52)$$

The hyperbolic model is called a non-linear elasticity model. The stress-displacement relationship is thus:

$$\begin{bmatrix} \tau \\ \sigma_n \end{bmatrix} = \begin{bmatrix} u_s \\ u_n \end{bmatrix} \begin{bmatrix} K_s & 0 \\ 0 & K_n \end{bmatrix}, \quad (3.53)$$

where u_n is the deformation normal to the interface and K_n is the stiffness in normal direction. To prevent overlapping in the zero-thickness interface elements, the normal stiffness is typically high. The model cannot simulate any coupled volumetric behaviour. The model for-

Table 3.2: Model parameters and physical definitions for Clough and Duncan (1971) model

Parameters	Physical definitions	Unit
γ_w	Unit weight of water	[MPa]
K_I	Dimensionless stiffness number	[-]
n_{HY}	Stiffness exponent	[-]
R_f	Failure ratio	[-]
δ	Interface friction angle	[-]

mulation of the hyperbolic model proposed by Clough and Duncan (1971). Gómez et al. (2003) improves the model but does not incorporate a better formulation for the volumetric interface behaviour. Therefore, only a linear relationship is implemented into the model for the normal stress formulation. In addition to the Mohr-Coulomb and hyperbolic model, the more advanced models presented in the following sections are able to model the important volumetric normal behaviour of interfaces.

3.3.3 Elastoplastic model of Mortara (2003)

The elasto-plastic model proposed by Mortara (2003) is an interface constitutive model that can simulate monotonic stress paths. The extension to cyclic loading is described in Mortara et al. (2002) and Boulon et al. (2003). The strength of the model anticipates CNS tests for the parameter calibration and estimation. The model can be calibrated with CNL tests and accurately simulates both boundary conditions (CNL and CNS). The inverse constitutive elasto-plastic formulation is defined by Mortara (2003) as:

$$\dot{\sigma} = \mathbf{D}^{ep} \dot{\epsilon}, \quad (3.54)$$

where \mathbf{D}^{ep} , the elasto-plastic constitutive matrix for 2D interface conditions, is written as:

$$\dot{\sigma} = \begin{bmatrix} \dot{\tau}_n \\ \dot{\sigma}_n \end{bmatrix} \dot{\mathbf{u}} = \mathbf{D}^{ep} \begin{bmatrix} \dot{u}_x \\ \dot{u}_n \end{bmatrix} = \mathbf{D}^e - \frac{\mathbf{D}^e \mathbf{m}_M \mathbf{n}^T \mathbf{D}^e}{H + \mathbf{n}^T \mathbf{D}^e \mathbf{m}_M}, \quad (3.55)$$

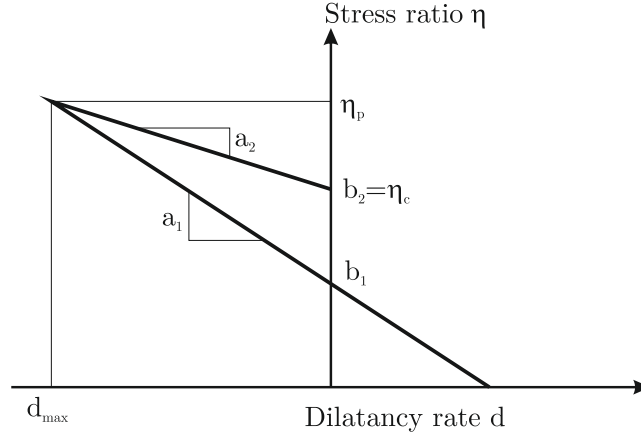


Figure 3.6: Idealized flow rule from elastoplastic model modified from Mortara (2003)

where $\dot{\sigma}_n$ is the normal stress rate, $\dot{\tau}$ is the shear stress rate, \dot{u}_n is the displacement normal to the interface, \dot{u}_x is the shear displacement, and \mathbf{D}^{ep} is the elasto-plastic matrix. The terms related to \mathbf{D}^{ep} are given as:

$$\mathbf{D}^e = \begin{bmatrix} K_s^e & 0 \\ 0 & K_n^e \end{bmatrix} \quad \mathbf{m}_M = \begin{bmatrix} \frac{\partial g}{\partial \tau} \\ \frac{\partial g}{\partial \sigma_n} \end{bmatrix} \quad \mathbf{n} = \begin{bmatrix} \frac{\partial f}{\partial \tau} \\ \frac{\partial f}{\partial \sigma_n} \end{bmatrix} \quad H = -\frac{\partial f}{\partial u_x^p}, \quad (3.56)$$

where \mathbf{D}^e is the elastic matrix, K_s^e and K_n^e are the elastic shear and normal stiffness, \mathbf{m}_M is the gradient of the plastic potential, \mathbf{n} is the gradient of the plastic surface, and H is the hardening modulus. The plastic potential g is given as:

$$g = \tau - \frac{b}{1+a} \sigma_n \left[1 + a \left(\frac{\sigma_n}{\sigma_c} \right) - \frac{1+a}{a} \right] = 0 \quad (3.57)$$

with

$a = a_1$ and $b = b_1$ for hardening conditions

$a = a_2$ and $b = b_2$ for softening conditions

where σ_c is defined as the critical normal stress. The parameters a and b are the slope and intercept of the flow rule to the stress ratio $\eta = \frac{\tau}{\sigma_n}$ plot (Figure 3.6). The model considers a double flow rule (Mortara 2003). The existence of the double flow rule for interface shearing is under discussion. Mortara (2003) argued that the double flow rule is appropriate, whereas Dietz (2000) pointed out that the existence of this double flow rule is based on the restrictions of a modified direct interface shear box testing.

The plastic function, which is also referred to as the yield function in 3D continuum soil models, is written as:

$$f = \tau - \alpha_M \sigma_n^{\beta_M} = 0, \quad (3.58)$$

where α_M is the current value of the hardening rule. The elastic behaviour of the model is defined in the following relationship.

$$\begin{bmatrix} \dot{\tau} \\ \dot{\sigma}_n \end{bmatrix} = \begin{bmatrix} K_s^e & 0 \\ 0 & K_n^e \end{bmatrix} \begin{bmatrix} \dot{u}_x^e \\ \dot{u}_n^e \end{bmatrix}, \quad (3.59)$$

where the elastic shear stiffness K_s^e is proportional to the elastic normal stiffness K_n^e with:

$$K_s^e = C_k K_n^e. \quad (3.60)$$

Ghionna and Mortara (2002) noted that the choice of the elastic constants does not significantly influence the model behaviour. The function of $\alpha(u_n)$ represents the hardening law of the interface model. This is an interpolation function between different α_M values.

$$\alpha(u_n) = \alpha_c \left[(\omega u_n + 1)^\psi - 2 \right] \exp[-L u_n^M] + \alpha_c, \quad (3.61)$$

where α_c is the critical hardening value, and ω and ψ are hardening rule parameters. The terms L and M are functions of these. The yield surface equations can be characterised for peak failure and critical state conditions as follows:

$$\tau_p = \alpha_p \sigma_n^{\beta M} \quad (3.62)$$

and

$$\tau_c = \alpha_c \sigma_n^{\beta M}, \quad (3.63)$$

where α_p and α_c are the maximum (peak) and the critical values of the hardening rule. The different terms of L and M can be derived from:

$$\alpha_M|_{u_n=1} = \alpha_p \quad (3.64)$$

and

$$\frac{d\alpha_M}{du_n}|_{u_n=1} = 0. \quad (3.65)$$

These equations lead to the constants of L :

$$L = \ln \left(\frac{\alpha_c}{\alpha_p - \alpha_c} \left[(\omega + 1)^\psi - 2 \right] \right) \quad (3.66)$$

and the constant M :

$$M = \frac{\alpha_c}{\alpha_p - \alpha_c} \frac{\omega^\psi}{L \exp(L)} (\omega + 1)^{\psi-1} \quad (3.67)$$

The required parameters can be calibrated using of CNL tests. The model parameter identification is explained in detail in Ghionna and Mortara (2002) and Mortara (2003).

The model is capable of reproducing the CNS interface behaviour if the parameters are cali-

brated with CNL tests. The model does not, however, incorporate the critical state and void-ratio dependence. The model must therefore be calibrated for each different void ratio and surface roughness expected in order to use the model according to the description given by Mortara (2003).

Table 3.3: Model parameters and physical definitions for Mortara (2003) model

Parameters	Physical definitions	Unit
K_n^e	Elastic normal stiffness	[Pa/m]
C_k	Ratio between normal and shear stiffness	[-]
α_p	Maximum value of the hardening function	[PA ^{1-β_M}]
α_c	Asymptotic value of the hardening function	[PA ^{1-β_M}]
ξ_M	w_p parameter	[PA ⁻¹]
ζ	w_p parameter	[m]
μ_M	d_{max} parameter	[PA ⁻¹]
ν_d	d_{max} parameter	[-]
ρ_M	Ratio between the stress ratios for $d = 0$ for hardening or softening condition	[-]
β_M	Exponent of plastic functions	[-]
ω	Hardening law parameter	[-]
ψ	Hardening law parameter	[-]

3.3.4 Hypoplastic model of Gutjahr (2003)

The hypoplastic interface model is based on the hypoplastic model of von Wolffersdorff (1996). Gutjahr (2003) developed this model to calculate interfaces at retaining walls. The precursor is the model of Herle and Nübel (1999). The formulation of the model was adapted by Gutjahr (2003). The model is developed for 2D calculations and reduced to a 1D interface model. The model of von Wolffersdorff (1996) can be written in tensor index notation as:

$$\dot{\sigma}_{ij} = f_b f_e \frac{1}{\hat{\sigma}_{kl} \hat{\sigma}_{kl}} \left[F^2 d_{ij} + a^2 \hat{\sigma}_{ij} (\hat{\sigma}_{kl} d_{kl}) + f_d a F (\hat{\sigma}_{ij} + \hat{\sigma}_{ij}^*) \sqrt{d_{kl} d_{kl}} \right], \quad (3.68)$$

where σ_{ij} and d_{ij} are the stress and stretching rate tensor, F is the stress function, and a is a constitutive parameter given in Equation 3.76. The pyknotropy factor f_d and f_e are given as:

$$f_d = \left(\frac{e - e_d}{e_c - e_d} \right)^\alpha; \quad (3.69)$$

$$f_e = \left(\frac{e_c}{e} \right)^\beta, \quad (3.70)$$

where α controls the dependency of the peak friction angle φ_p on the void ratio and β influences the size of the response envelope. Both are material parameters. e_i , e_c , e_d for maximum, critical,

and minimum void ratios are calculated from the relationship proposed by Bauer (1996). The Bauer formula is defined as:

$$\frac{e_d}{e_{d0}} = \frac{e_c}{e_{c0}} = \frac{e_i}{e_{i0}} = \exp \left[- \left(\frac{tr(\sigma_{ij})}{h_s} \right)^n \right], \quad (3.71)$$

where h_s is the granular hardness of the soil skeleton with n as exponent that influences the compression behaviour. e_{i0} , e_{d0} , and e_{c0} are the maximum, minimum, and critical void ratios at zero pressure. The void ratio depends on the strain rate as:

$$\dot{e} = -\varepsilon(1 + e)d_{ii} \quad (3.72)$$

In the case of 1D shearing (plane strain 2D model), the stress function $F = 1$. Herle and Nübel (1999) used a stress tensor simplified to a stress vector with two components:

$$\sigma_i = \begin{bmatrix} \sigma_n \\ \tau \end{bmatrix}. \quad (3.73)$$

The reduced stretching tensor is:

$$d_i = \begin{bmatrix} \dot{\varepsilon}_n \\ \dot{\gamma} \end{bmatrix} \quad (3.74)$$

By simplifying of the fully hypoplastic model, the constitutive hypoplastic interface model is defined as:

$$\begin{bmatrix} \dot{\sigma}_n \\ \dot{\tau} \end{bmatrix} = \frac{f_b f_e}{1 + \tau^2 / \sigma_n^2} \left[\begin{bmatrix} \dot{\varepsilon}_n \\ \dot{\gamma} \end{bmatrix} + a^2 \begin{bmatrix} 1 \\ \frac{\tau}{\sigma_n} \end{bmatrix} \left(\dot{\varepsilon}_n + \dot{\gamma} \frac{\tau}{\sigma_n} \right) - f_d a \begin{bmatrix} 1 \\ 2 \frac{\tau}{\sigma_n} \end{bmatrix} \sqrt{\dot{\varepsilon}_n^2 + \dot{\gamma}^2} \right]. \quad (3.75)$$

The constitutive coefficient a at limit state is calculated as:

$$a = \frac{\tau}{\sigma_n} = \frac{1}{\tan \varphi_c}. \quad (3.76)$$

The barotropy factor f_b is given as:

$$f_b = \frac{h_s}{n} \left(\frac{e_{i0}}{e_{c0}} \right)^\beta \frac{1 + e_i}{e_i} \left(\frac{\sigma_n}{h_s} \right)^{1-n} \left[1 + a^2 - a \left(\frac{e_{i0} - e_{d0}}{e_{c0} - e_{d0}} \right)^\alpha \right]^{-1}. \quad (3.77)$$

The modified rate of the void ratio is given by:

$$\dot{e}_i = -n \dot{\sigma}_n \frac{e_{i0}}{h_s} \left(\frac{\sigma_n}{h_s} \right)^{n-1} \exp \left[- \left(\frac{\sigma_n}{h_s} \right)^n \right]^{-1} \quad (3.78)$$

Table 3.4: Model parameters and physical definitions for Gutjahr (2003) model

Parameters	Physical definitions	Unit
h_s	Granulate hardness	[MPa]
n	Exponent takes into account the pressure-sensitivity of the grain skeleton	[-]
α	Exponent	[-]
β	Exponent	[-]
e_{i0}	Maximum void ratio at zero pressure	[-]
e_{d0}	Minimum void ratio at zero pressure	[-]
e_{c0}	Critical void ratio at zero pressure	[-]
φ_c	Critical friction angle	[°]

3.3.5 Elasto-plastic model by Lashkari (2013)

The last model to be presented in detail was published by Lashkari (2013). The interface model is based on critical state soil mechanics using the state parameter (Been and Jeffries 1985). The model is proposed by Lashkari (2013). The stress rate vector is defined as:

$$\boldsymbol{\sigma} = \begin{bmatrix} \sigma_n \\ \tau \end{bmatrix}. \quad (3.79)$$

The relative displacement vector corresponds to the stress vector and is defined as:

$$\mathbf{u} = \begin{bmatrix} u_n \\ u_x \end{bmatrix}. \quad (3.80)$$

In accordance with the elasto-plasticity theory, the relative velocity vector is defined as:

$$\dot{\mathbf{u}} = \dot{\mathbf{u}}^e + \dot{\mathbf{u}}^p, \quad (3.81)$$

where $\dot{\mathbf{u}}^e$ is the elastic relative velocity part and $\dot{\mathbf{u}}^p$ is the plastic part of the relative velocity vector. The yield function f is formulated as:

$$f = \tau - \eta\sigma_n, \quad (3.82)$$

where η is the stress ratio, which determines the yield function size and plays a role in estimating the hardening parameter. The yield function is based on the assumption that the majority of the plastic velocity is generated as a result of a change in the stress ratio η . Lashkari (2013) used a modified state parameter described by Been and Jeffries (1985) defined as:

$$\psi = e - e_c = e - (e_0 - \lambda_L \ln(\sigma_n/p_{ref})), \quad (3.83)$$

where e_0 and λ_L are model parameters for the critical state line location in the e - $\ln \sigma_n$ plane. p_{ref} is the reference pressure, and e_c is the critical void ratio, which corresponds to the current value of normal stress defined as:

$$e_c = e_0 - \lambda_L \ln(\sigma_n/p_{ref}). \quad (3.84)$$

The elastic part of the velocity vector \mathbf{u}^e is defined as:

$$\boldsymbol{\sigma} = \frac{1}{t} \mathbf{D}^e \mathbf{u}^e, \quad (3.85)$$

where t is the definition of the shear band thickness at the interface. Lashkari (2013) recommended using values from $5 \times d_{50}$ to $10 \times d_{50}$. The elastic stiffness \mathbf{D}^e is expressed by:

$$\mathbf{D}^e = \begin{bmatrix} K_n^e & 0 \\ 0 & K_s^e \end{bmatrix} = \begin{bmatrix} K_{n0}^e \sqrt{\sigma_n/p_{ref}} & 0 \\ 0 & K_{s0}^e \sqrt{\sigma_n/p_{ref}} \end{bmatrix}, \quad (3.86)$$

where K_{s0}^e and K_{n0}^e are the shear and normal elastic stiffness. The general expression of the constitutive equation describes the relationship between stress rate and deformation rate, and is expressed as:

$$\dot{\boldsymbol{\sigma}} = \frac{1}{t} \mathbf{D}^{ep} \dot{\mathbf{u}}. \quad (3.87)$$

The generalized elasto-plastic stiffness matrix \mathbf{D}^{ep} is written as:

$$\mathbf{D}^{ep} = \mathbf{D}^e - \frac{\mathbf{D}^e \mathbf{R}^L \mathbf{n}^T \mathbf{D}^e}{K_p + \mathbf{n}^T \mathbf{D}^e \mathbf{R}^L}, \quad (3.88)$$

where K_p is the plastic hardening modulus. K_p is calculated as proposed by Li and Dafalias (2000):

$$K_p = h_0 K_s^e \left(\frac{M_L \exp(-n^b \psi)}{\eta} - 1 \right), \quad (3.89)$$

where h_0 is the plastic hardening constant and n^b is a parameter describing the influence of the interface state on the peak stress ratio. M_L is the critical stress ratio. The yield direction vector \mathbf{n} is :

$$\mathbf{n} = \begin{bmatrix} n_n \\ n_s \end{bmatrix} = \begin{bmatrix} \partial f / \partial \sigma_n \\ \partial f / \partial \tau \end{bmatrix} = \begin{bmatrix} -\eta \\ 1 \end{bmatrix}. \quad (3.90)$$

The direction of the plastic velocity vector is defined as:

$$\mathbf{R}^L = \begin{bmatrix} R_n^L \\ R_s^L \end{bmatrix} = \begin{bmatrix} d \\ 1 \end{bmatrix}. \quad (3.91)$$

Table 3.5: Model parameters and physical definitions for the model by Lashkari (2013)

Parameters	Physical definitions	Unit
K_{s0}^e	Elastic tangential stiffness constant	[MPa]
K_{n0}^e	Elastic normal stiffness constant	[MPa]
A_0	Dilatancy constant (initial)	[-]
A_{1L}	Dilatancy constant (intermediate)	[-]
h_0	Plastic hardening modulus constant	[-]
M_L	Critical stress ratio	[-]
e_0	Initial void ratio	[-]
λ_L	Critical state line location in $e - \ln \sigma_n$ plane	[-]
n^b	Influence of interface state on peak stress ratio	[-]
n^d	Influence of interface state on phase transformation (zero dilatancy) stress ratio	[-]

The plastic component of the velocity vector is calculated as:

$$u^p = \begin{bmatrix} \dot{u}_n \\ \dot{u}_x \end{bmatrix} = \Lambda_L t \mathbf{R} = \Lambda_L t \begin{bmatrix} d \\ 1 \end{bmatrix}. \quad (3.92)$$

The loading index Λ_L is defined according to Dafalias (1986) as:

$$\Lambda_L = \frac{1}{K_p} \mathbf{n}^T \dot{\boldsymbol{\sigma}} = \frac{\dot{\tau} - \eta \dot{\sigma}_n}{K_p}. \quad (3.93)$$

The dilatancy function is applied in the following form:

$$d = A_L (M_L \exp(n^d \psi) - \psi), \quad (3.94)$$

where n^d is a model parameter, which has an important role in simulating the transformation from contraction to dilation. For modelling a double flow rule as suggested by Mortara (2003), the following definition is used:

$$A_L = A_0 \sqrt{\frac{p_{ref}}{\sigma_n}} + \left(A_{1L} - A_0 \sqrt{\frac{p_{ref}}{\sigma_n}} \right) \left(\frac{\eta}{M_L \exp(-n^b \psi)} \right), \quad (3.95)$$

where A_0 and A_{1L} are parameters for simulating the magnitude of dilatancy under an increased shear displacement. The model parameters are listed in Table 3.5.

3.4 Summary of Chapter 3

In this Chapter, three different modelling techniques frequently used in the geotechnical community were introduced. The zero-thickness interface element, the thin-layer interface, and the contact kinematics for the master and slave concept were introduced.

A review of the existing constitutive models was also given. The quantity of the different mod-

elling approaches was also demonstrated. In summary, nearly every constitutive model framework used for modelling interfaces was adapted from 3D constitutive modelling. Furthermore, most models were developed for sand-structure interfaces. Reviewing the state of the art, two different important aspects could be identified: the lack of models formulated for 3D conditions and models for clay-structure interfaces.

Chapter 4

Model assessment of existing constitutive soil-structure interface models

4.1 Introduction

In Chapter 3, many different models were described. This makes it difficult for users to determine, which model should be used for a particular application. Griffiths (1985; 1988) demonstrated that the correct modelling choice for the interface positively influences the performance of a geotechnical structure.

Kim et al. (2007) studied the importance of interface modelling in calculating loads that could be feasibly carried by sand-anchors. Said et al. (2009) studied the influence of neglecting interface models using an adjusted Mohr-Coulomb model and a highly sophisticated plasticity constitutive interface model. In particular, the volumetric interface behaviour has a large influence for the realistic modelling of the pile-soil contact (Said et al. 2009).

Keitel et al. (2013; 2014) reported on the influence of the soil-structure interaction on the global structural performance taking into account different soil-structure interaction models. Keitel et al. (2014) developed a methodology to quantify the proportional influence of each model contributing to the global performance. This combines a graph theory scheme with a global sensitivity analysis.

With respect to global structural performance, it is important to assess soil-structure interface models. It is important to select the model that will yield the best prediction. For example, Ling and Liu (2009) compared a simplified and sophisticated finite element model. They observed that especially in the construction phase of a reinforced soil wall, a simple model leads to approximately the same results as the advanced soil model.

The aim of this chapter is to present a methodology for assessing the interface models presented in Chapter 3. The proposed approach is comparable to the methodology by Most (2011), Jung et al. (2012), Stutz et al. (2015), and Motra et al. (2016).

The models and modelling techniques are normally compared in a deterministic manner to estimate the best model fit. The drawback of a fully deterministic approach is the tendency to use highly sophisticated models, which are flexible and can be over-fitted to the experimental data. The stochastic model properties are thus introduced in Section 4.2 before these properties are presented and combined to derive the model assessment method. The proposed method differs from the previous methodology through the use of a multi-point objective measures instead of a single objective value.

4.2 Stochastic model properties

The stochastic model properties of uncertainty and sensitivity will be introduced and explained in this chapter. In the following, the most important model properties (Huber and Stutz 2013) are introduced. These properties are used to assess the different interface models.

4.2.1 Uncertainty

Uncertainty describes the incomplete knowledge of the models, parameters, constants, and data (Helton 1997). The model uncertainty describes the lack of knowledge of the model. Several factors contribute to this uncertainty (Figure 4.1). The uncertainties that arise from applying a model can be categorized as:

Model framework uncertainty

The model framework itself is normally uncertain. It is a result of incomplete knowledge or data for example, a model based on assumptions and incomplete validation data will be uncertain (clay anisotropy).

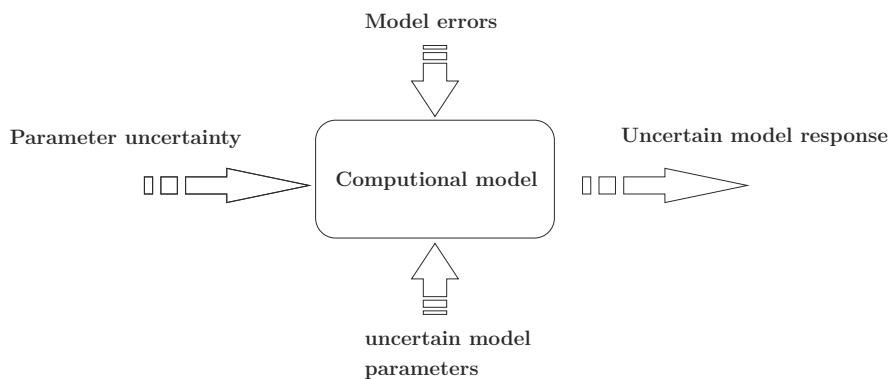


Figure 4.1: Different sources of uncertainty within a model formulation (Phoon 2008)

Model niche uncertainty

This kind of uncertainty occurs if a model is used outside the range of reproducibility. For example the use of a clay model for sand.

Model input uncertainty

The model input uncertainty results from measurement uncertainties, errors, and incongruities between measured data and those needed for the model. This kind of uncertainty is different from measurement uncertainty and variability of the data because of natural and inherent randomness. The consideration of measurement uncertainty in particular is relatively new in civil engineering, e.g. Motra and Hildebrand (2013).

All these kinds of uncertainty can influence the modelling approach. Mašín (2015) demonstrated that experimental and sampling uncertainty may negatively affect the prediction quality of numerical analysis.

In Helton (1997), two different terms are used to define uncertainty in models. These can be categorized as *aleatoric* and *epistemic* uncertainty. The word aleatoric is derived from the Latin word “alea”, which means dice. An aleatoric uncertainty can thus arise from an intrinsic uncertainty of the phenomena. The word epistemic is derived from the Greek word “episteme”, which means knowledge. This work presents an approach that uses model (aleatoric) uncertainty and parameter (epistemic) uncertainty to quantify the total uncertainty of a model.

The parameter or input uncertainty is estimated by the generation of a statistical fluctuating uses Latin hypercube sampling (McKay et al. 1979). Using the samples generated, the model response \hat{Y} is computed, and the coefficient of variation CV_Y is calculated as:

$$CV_Y = \frac{\sigma_s}{\mu_s}, \quad (4.1)$$

where σ_s is the standard derivation and μ_s the mean. The mean μ_s is calculated as:

$$\mu_s = \sum xP(x). \quad (4.2)$$

The mean is defined as each possible value of x and the probability $P(x)$. By summation of all these products the mean μ_s can be calculated.

The parameter uncertainty itself is a stochastic property of the model. The model uncertainty must also be calculated. The model uncertainty describes the uncertainty that is related to the intrinsic properties of a model (e.g. mathematical formulation, constitutive assumptions). This model uncertainty is a point of controversy (Dithinde et al. 2011). The model uncertainty is hard to determine because it depends on a reference. For example, the reference solution can be another type of model (more complex numerical, experimental data, or analytical expression).

Reference models can be manifold, and experimental data is often utilised. Assuming a reference model, the model uncertainty can be calculated using a deterministic formula such:

$$UA_i^{\text{Model}} = \frac{|\hat{Y}_i - \hat{Y}_{ref}|}{1.645 \cdot \hat{Y}_{ref}}, \quad (4.3)$$

where \hat{Y}_i is the deterministic model response from the i th model, \hat{Y}_{ref} is the response of the reference model. 1.645 is the 95% quantile. This represents a small fluctuation of the input to the reference model itself (Jung 2015). After defining the model and parameter uncertainty, the total model uncertainty can be calculated as:

$$UA_i^{\text{Global}} = \sqrt{UA_i^{\text{Model}} + UA_i^{\text{Par}}}. \quad (4.4)$$

In order to discuss the approach, the following statements have to be pointed out. The model assessment has the underlying assumptions:

- A model must consist of different assumptions; these assumptions are parametrized.
- The total behaviour of a reference model is dependent on the uncertainty of the model input for the reference solution.

The above statements describe the problem of addressing an indicator to assess models. The assessment assumes that in the case of parameter uncertainty, the model does not have any defects in the model derivation. However, upon closer inspection, no model can be assumed to be perfect. Conversely, for assessing the model, the parameters are assumed to be in good agreement with the data studies. Based on these assumptions, it is possible to estimate the global model uncertainty of a model within the given framework. The quantification of models always has an underlying subjective approach. This is logical because of a model cannot be formulated without any parameters.

The combination of the model and parameter uncertainty is described in Section 4.3. The next subsection discusses sensitivity as property of models.

4.2.2 Model sensitivity

The sensitivity of a model describes how the model input parameters influence the model response. Different kinds of sensitivity analysis can be performed. The outcome of a sensitivity analysis for a model can be used to draw various conclusions regarding the model itself. According to (Satelli et al. 2008), the general kinds are:

- Parameter fixing (PF): Model parameters with a low sensitivity can be considered as deterministic for further investigations, thereby reducing the complexity of the model
- Parameter prioritization (PP): identifying important parameters that can reduce the variance of these parameters, thereby decreasing uncertainty

- Parameter mapping (PM): identifying the parameter combination that can lead to a certain parameter limit

Table 4.1 lists the most common techniques and their primary goal (further details see Satelli et al. (2008) and Satelli et al. (2004)). For the before mentioned sensitivity analysis, only

Table 4.1: Techniques of sensitivity analysis, properties, and primary goal

Technique	Consideration of parameter interaction	primary goal
partial derivative	–	PP
elementary effects	✓	PF
scatter plots	✓	PM
regression based	✓	PP/PM
variance based method, first order	–	PP
variance based method, second order	✓	PF

uncorrelated input quantities can be considered. Improvements for variance-based sensitivity analysis have been proposed by Xu and Gertner (2008), Most (2012), and Mara and Tarantola (2012). The aim of the sensitivity analysis used in this thesis is parameter fixing (PF). Therefore, variance based sensitivity analysis is used and briefly introduced.

In the first step, the first order sensitivity indices are described taking into consideration the model with conditional variances:

$$Y = f(X_1, X_2, X_3, \dots, X_n), \quad (4.5)$$

where X_i is a generic parameter of model Y . We can use X_i as a measure of the importance of X_i .

$$V_{X \sim i}(Y|X_i = x_i^*). \quad (4.6)$$

If $V_{X \sim i}(Y|X_i = x_i^*)$ decreases, the influence of X_i increases. This introduces a measure of importance. Nevertheless, this is dependent on the choice of x_i^* . To remove this dependence, the average of this measure can be used as:

$$E_{x_i}(V_{X \sim i}(Y|X_i)). \quad (4.7)$$

This is the expected result that should be removed from the total output variance in order to quantify the real influence of X_i on the model output. Decomposing $V(Y)$ yields:

$$V(Y) = +V_{X_i}(E_{X \sim i}(Y|X_i)), \quad (4.8)$$

where a large $+V_{X_i}(E_{X \sim i}(Y|X_i))$ or a small $E_{x_i}(V_{X \sim i}(Y|X_i))$ implies that X_i is important for the model output response. The first order sensitivity index is then calculated as:

$$S_i = \frac{V_{X_i}(E_{X \sim i}(Y|X_i))}{V(Y)}. \quad (4.9)$$

The first order index is referred to as the “main effect index” (Satelli et al. 2004). For clarification, the first order sensitivity index describes the contribution of X_i to the output variance. It is only a measure for the variation of X_i . The variations of the other input parameters are averaged over the whole output results. To investigate the high-order effects of the models, the expression for S_i must be extended. Assuming two generic parameters X_i and X_j , the following equation is true:

$$V(E(Y|X_i, X_j)) = V_i + V_j + V_{ij} \quad (4.10)$$

with

$$V_i = V(E(Y|X_i)); \quad (4.11)$$

$$V_j = V(E(Y|X_j)); \quad (4.12)$$

$$V_{ij} = V(E(Y|X_i, X_j)) - V_i - V_j, \quad (4.13)$$

where V_{ij} is the interaction term between the parameters X_i and X_j . It detects the effect that cannot be calculated by separately superimposing the effects. Considering all possible combinations, the total sensitivity index is defined as:

$$S_{T_i} = 1 - \frac{V(E(Y|X_{\sim X_i}))}{V(Y)}. \quad (4.14)$$

First and total order sensitivity analyses were conducted to identify the major influencing parameters for the models investigated. More details are described in Satelli et al. (2004) and Satelli et al. (2008).

4.3 Quality assessment of the constitutive interface models

The models used for the quantification were described in Sections 3.3.1–3.3.5. For the quantification, the model properties described above were used to assess the constitutive interface models. As mentioned by Keitel et al. (2014) for assessing the model sensitivity itself is not suitable to assess a model. Hence, the model sensitivity was used to assess the key parameters of the different models.

The methodology is illustrated in Figure 4.2. First, the sensitivity analysis is conducted to estimate the influencing parameter of the models. The parameters that will be identified as sensitive are chosen for the following uncertainty quantification. This decreases computation effort and CPU time. It also prevents the sampling of non-converging or non-physical parameter sets. In general this must be ensured by the sampling. However, in this case, the effect and thus the effort to ensure physical samples is minimized. The Latin hypercube samples are used to calculate the mean and the covariance of the different models. The parameter uncertainty is

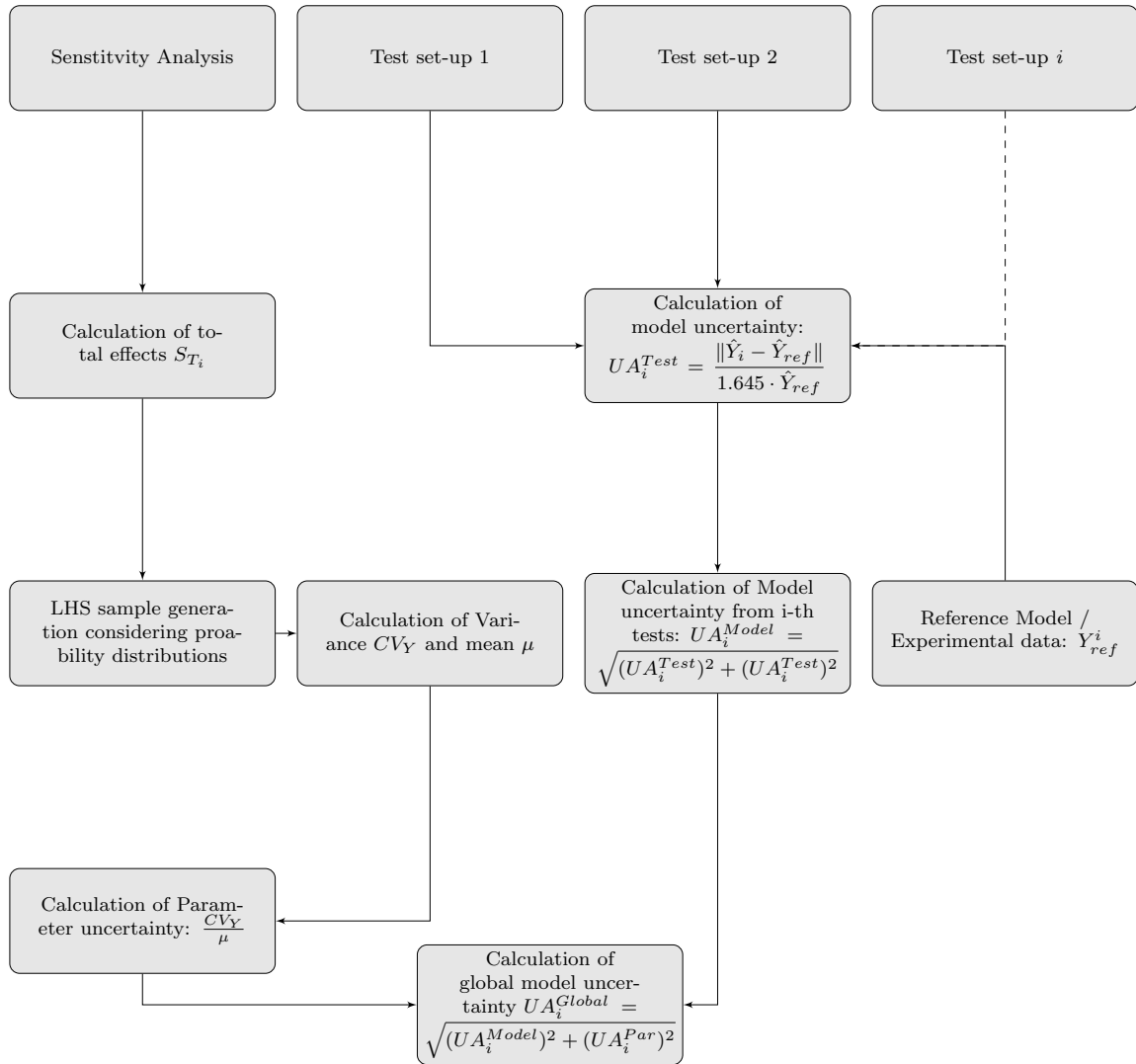


Figure 4.2: Proposed quantification methodology for interface models

calculated with Equation 4.1.

The second path in the methodology is used to calculate the model uncertainty as described in Section 4.2.1. By modelling different tests, a deterministic result is compared to a reference model. The reference models are different experimental results from published literature (Shahrour and Rezaie 1997, Fakharian and Evgin 2000, Mortara 2003). The global model uncertainty is then calculated using Equation 4.4.

The calculation of the parameter uncertainty is related to an appropriate choice of the parameter distribution. The real parameter distributions could not be determined using the limited available test data. Normal distribution was thus assumed for most of the parameters.

The following abbreviations are used for the models:

Table 4.2: Model abbreviations for model assessment

Model	Abbreviation of the model
Mohr-Coulomb model	MC
Hyperbolic model (Clough and Duncan 1971)	HY
Elasto-plastic model (Ghionna and Mortara 2002)	EP1
Elasto-plastic model (Lashkari 2013)	EP2
Hypoplastic model (Gutjahr 2003)	HP

4.3.1 Sensitivity study of the interface models

The results of the sensitivity analysis for each of the different models are presented. All sensitivity studies were conducted with 20000 samples created by a Latin hypercube sampling. The objective measure was the shear stress under a given deformation value, which is a value in the asymptotic response of the model.

For all different models, a granular soil-structure interface was assumed because the used models were mainly built for granular soil-structure interfaces.

Mohr-Coulomb model

The results of the sensitivity analysis are presented in Table 4.3. The total effect sensitivity indices were calculated with two different values for the coefficient of variance. This was done to demonstrate the effect of the coefficient of variance (COV) on the parameter sensitivity. The

Table 4.3: Total sensitivity S_{T_i} indices for the Mohr-Coulomb model (Van Langen 1991)

Parameter	Mean value	S_{T_i}	
		$COV = 0.05$	$COV = 0.1$
Friction angle φ	[°] 35	0.51	0.66
Dilatancy angle ψ	[°] 5	0.03	0.01
Poisson's ratio ν_p	[-] 0.33	0.42	0.48
Young's modulus E	[kPa] 60000	0.05	0.08
Cohesion c	[kPa] 1	0.04	0.0

results indicate the major importance of the friction angle with respect to the overall global shear behaviour, this is not surprising. Based on the constitutive description of the model because the yield function given in Equation 3.38 mainly depends on the friction angle. In addition to the friction angle φ , another important parameter is the Young's modulus E . In contrast to all the parameters, which is very low.

For the analysis, a non-cohesive soil (sand) was assumed. The material parameter for the adhesive behaviour was therefore neglected. As can be seen from the yield function, modelling a fine-grained soil with a reasonable cohesion will increase the sensitivity index of the cohesion parameter.

Hyperbolic model by Clough and Duncan (1971)

Table 4.4: Total sensitivity S_{T_i} indices for the Hyperbolic model (Clough and Duncan 1971)

Parameter	Mean value	S_{T_i}	
		$COV = 0.05$	$COV = 0.1$
Dimensionless stiffness number K_I	[-] 37500	0.01	0.01
Stiffness exponent n_{HY}	[-] 0.35	0.00	0.00
Failure ratio R_f	[-] 0.875	0.40	0.41
Interface friction angle δ	[°] 32	0.59	0.60

The mean values of the hyperbolic interface model parameters are given by Gómez et al. (2003). Compared to the Mohr-Coulomb model, the hyperbolic model showed an equivalent trend in the sensitivity analysis. The failure ratio R_f , which describes the maximum exceeded limiting stress, and the interface friction angle δ are the major parameters contributing to the model response.

Unlike the Mohr-Coulomb model, differences in the coefficient of variance and the calculation of the total sensitivity indices influenced the model output.

Elasto-plastic model by Mortara (2003)

The first sophisticated elasto-plastic model that was studied have been proposed by Mortara (2003). During the sensitivity analysis, it was obvious that only a small number of parameters could be investigated because of the hugely sensitive parameters in the model formulation. The analysis could therefore only use a low $COV = 0.01$ for some sensitive parameters; these are marked with a star in Table 4.5.

Large constraints in the model are connected with using w_p parameter ξ_M . In addition to ξ_M , the other parameters had a small or negligible influence on the output response. The model formulation is influenced by this parameter because it describes the maximum peak behaviour and is an essential part of the hardening modulus defined in Equation 3.56.

The large constraint in the sensitivity analysis was because of the model calibration, which is closely connected to the CNS laboratory tests. It is debatable whether such a model should be applied.

Table 4.5: Total sensitivity S_{T_i} indices for the Elastoplastic model (Mortara 2003)

Parameter	Mean value	S_{T_i}		
		COV 0.05	COV 0.1	
K_n^e Elastic normal stiffness	[Pa/m]	$1 \cdot 10^{10}$	0.00	0.00
C_k Ratio between normal and shear stiffness	[-]	1.0	0.00	0.00
α_p^* Maximum value of the hardening function	[Pa $^{1-\beta}$]	2.6	0.01	0.00
α_c^* Asymptotic value of the hardening function	[Pa $^{1-\beta}$]	2.15	0.00	0.00
ξ_M w_p parameter	[Pa $^{-1}$]	0.905	0.99	0.99
ζ^* w_p parameter	[-]	220.6	0.00	0.00
μ_M d_{max} parameter	[Pa $^{-1}$]	0.158	0.00	0.00
ν_d d_{max} parameter	[-]	$3.687 \cdot 10^{-9}$	0.00	0.00
ρ_M Stress ratios for $d = 0$ for hardening or softening condition	[-]	$7.264 \cdot 10^{-4}$	0.01	0.00
β_M Exponent of plastic functions	[-]	$2.171 \cdot 10^{-7}$	0.00	0.00
ω Hardening law parameter	[-]	-0.226	0.00	0.00
ψ Hardening law parameter	[-]	0.55	0.00	0.00

Hypoplastic model by Gutjahr (2003)

After the first advanced elasto-plastic model, the hypoplastic model was studied by Gutjahr (2003). Table 4.6 shows the results of the total sensitivity analysis for the hypoplastic interface model. The model used the minimum, maximum, and critical void ratio at zero pressure as input parameter. To avoid non-physical samples and convergence problems, only the e_{c0} critical state void ratio was sampled using the LHS sampling technique. The minimum and maximum void ratios at zero pressure were obtained from empirical relations. The following relations from Herle and Gudehus (1999) and Suchomel and Mašín (2011) were used: the maximum void ratio $e_{i0} = 1.2e_{c0}$ and the minimum void ratio $e_{d0} = e_{c0}0.379$.

As indicated by the formulation of the model, the high sensitivity of the void ratios and the

Table 4.6: Total sensitivity S_{T_i} indices for the Hypoplastic model (Gutjahr 2003)

Parameter	Mean value	S_{T_i}		
		COV 0.05	COV 0.1	
Granulate hardness h_s	[MPa]	3000	0.01	0.01
Exponent for the pressure-sensitivity of the grain skeleton n	[-]	0.29	0.01	0.02
Exponent α	[-]	0.25	0.06	0.06
Exponent β	[-]	2.0	0.00	0.01
Critical void ratio at zero pressure e_{c0}	[-]	0.75	0.11	0.12
Critical friction angle φ_c	[°]	30	0.82	0.84

friction angle φ_c was not surprising. In general, all parameters contributed equally to the global behaviour with the exception of β , because at critical state, β had less of an influence than the

parameter α .

Elasto-plastic model by Lashkari (2013)

The results of the sensitivity analysis for the elasto-plastic model of Lashkari (2013) are presented in Table 4.7. The friction or interface angle of the soil is incorporated as a function of the critical stress ratio M_L . The total sensitivity indices for sensitivity analysis shows that the most

Table 4.7: Total sensitivity S_{T_i} indices for the elasto-plastic model (Lashkari 2013)

Parameter	Mean value	S_{T_i}		
		COV 0.05	COV 0.1	
Elastic tangential stiffness constant K_{s0}^e	[MPa]	3600	0.0	0.00
Elastic normal stiffness constant K_{n0}^e	[MPa]	3000	0.0	0.01
Dilatancy constant (initial) A_0	[-]	3.5	0.0	0.01
Dilatancy constant (intermediate) A_{1L}	[-]	0.45	0.0	0.00
Plastic hardening modulus constant h_0	[-]	0.6	0.0	0.01
Critical stress ratio M_L	[-]	0.64	0.45	0.47
Critical state line location in $e - \ln \sigma_n$ plane e_0	[-]	0.85	0.51	0.53
Critical state line location in $e - \ln \sigma_n$ plane λ_L	[-]	0.047	0.01	0.02
Influence state on peak stress ratio n^b	[-]	1.8	0.02	0.0
Influence state at zero dilatancy – stress ratio n^d	[-]	1.0	0.0	0.03

influential parameters were the critical stress ratio M and e_0 . This parameter incorporated the frictional angle at the interface into the model formulation. Parameter e_0 , which defines the critical state line location, had a greater sensitivity. The sensitivity indices of λ_L and n^b are several magnitudes of order smaller.

Based on the sensitivity analysis, it can be stated that PF was possible because of the total effects in the dependence of the objective function.

4.3.2 Uncertainty analysis for shear behaviour

This section describes the uncertainty analysis for interface shear behaviour. The aleatory and the epistemic uncertainty was treated separately and then combined as defined by Equation 4.4.

Parameter uncertainty

The parameter uncertainty was calculated using various input parameters. A summary of the distribution used for the sample generation is given in Table 4.8. The distributions for the Mohr-Coulomb model were based on the research of Phoon (2008). For the hypoplastic model, the parameter distributions were given in Suchomel and Mašín (2010; 2011). Because of the lack of knowledge, the distribution of the parameters for the interface models from Clough and Duncan (1971), Mortara et al. (2002), and Lashkari (2013) were assumed to be normally

Table 4.8: Statistical distributions for quantifying the parameter uncertainty (“nor.” for Gaussian distribution and “log.” for lognormal distribution)

MC	Par.	φ	ψ	E	ν_p	c							
	Dist.	log.	log.	log.	nor.	log.							
HY	Par.	K_I	n	R_f	δ								
	Dist.	nor.	nor.	nor.	log.								
EP1	Par.	K_n^e	C_k	α_p	α_c	ζ	ξ_M	μ_M	ν_d	ρ_M	β_M	ω	ψ
	Dist.	nor.	nor.	nor.	nor.	nor.	nor.	nor.	nor.	nor.	nor.	nor.	nor.
EP2	Par.	K_{s0}^e	K_{n0}^e	A_0	A_{1L}	h_0	M_L	e_0	λ_L	n^b	n^d		
	Dist.	nor.	nor.	nor.	nor.	nor.	nor.	nor.	nor.	nor.	nor.	nor.	
HP	Par.	h_s	n	α	β	e_{c0}	φ_c						
	Dist.	log.	log.	log.	nor.	nor.	log.						

distributed. Detailed information about the standard derivation and the mean values of the single parameters can be found in Appendix A.

The sample size for the parameter uncertainty analysis was 10000. Surprisingly, the model with fewer parameters also had a low model uncertainty (Figure 4.3).

The results indicate that the model of Mortara (2003) had the highest uncertainty value of all models. From the sensitivity analysis, it was expected that the model would have a great parameter uncertainty. The most interesting result of the uncertainty analysis is that the Hypoplastic model (Gutjahr 2003) and the elasto-plastic model of Lashkari (2013) had lower variances than the simpler models such as the Mohr-Coulomb and the hyperbolic model. An increasing sample size lead to comparable variances (not shown). The aim of the parameter

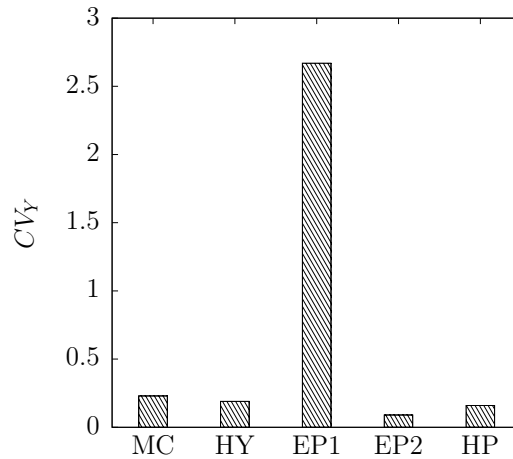


Figure 4.3: Results of parameter uncertainty analysis for the different constitutive interface models

uncertainty analysis was to obtain an indicator for the ability of the model robustness in the sense of a fluctuation in the input-output relation. The comparison of the models can only be done together by a global uncertainty measure considering the model and parameter uncertainty. Otherwise such a comparison between the different model will lack important information.

Model uncertainty

The model uncertainty was estimated with different test data that was available. The test data was regularly cited and could be seen as high quality experimental data. It was therefore chosen to estimate the model uncertainty. As discussed above, the model uncertainty is an important model property. The test data was taken from the following literature sources:

- Shahrour and Rezaie (1997) conducted CNL tests with Hostun sand in a modified interface direct shear box. The results of the deterministic model assessment are shown in Figures 4.4a–4.4c (dense Hostun sand) and Figures 4.4d–4.4e (loose Hostun sand) subjected to different normal stresses.
- Evgin and Fakharian (1996) conducted CNL tests with varying normal stress (Figures 4.5c–4.5e). The tests were conducted in a modified simple shear apparatus with air-dried medium quartz sand.
- Mortara (2003) conducted experimental tests in a modified direct shear box with a normal stiffness of $K = 800$ kPa. The results of the deterministic model comparison are shown in Figure 4.5a–4.5b. Toyura sand was used for the comparison.

The model uncertainty was calculated as the norm based on all different model evaluations found in this Section using the following formula:

$$CV_{mod_n} = \sqrt{CV_{mod_i}^1 + CV_{mod_i}^2 + CV_{mod_i}^3 \cdots CV_{mod_i}^k}. \quad (4.15)$$

Equation 4.15 was used to calculate the model uncertainty for all experimental data, and will be used as a reference.

The data set in the quantification represented the interface behaviour as loose and dense for different granular materials and different boundary conditions. In the dense sand under CNL conditions from Shahrour and Rezaie (1997) (Figures 4.4a–4.4c), all models could model the main trend of the experimental data. The Mohr-Coulomb and the hyperbolic model tended to underestimate the hardening behaviour and could not be model the softening behaviour. All models were able to model the critical state with good agreement to the experiments. For the loose sand (Figures 4.4d–4.4e), only the hardening and the critical state were used for the model assessment. For the loose sand, the same parameters used for the model of Lashkari (2013) and the hypoplastic model of Gutjahr (2003) were taken into consideration. For the model of Mortara (2003), a new parameter set had to be defined for each experimental test because of the void ratio, which is not explicitly dependent on one unique parameter set.

The CNS tests using a Toyoura sand according to Mortara (2003) (Figures 4.5a and 4.5b) need particular attention because only the model of Lashkari (2013) and Mortara (2003) were able simulate interface behaviour close to the experimental data. The model of Lashkari (2013) had a peak stress that was too large. However, the hardening response of the model was in good agreement with the experimental data. The hypoplastic model showed a peak that was

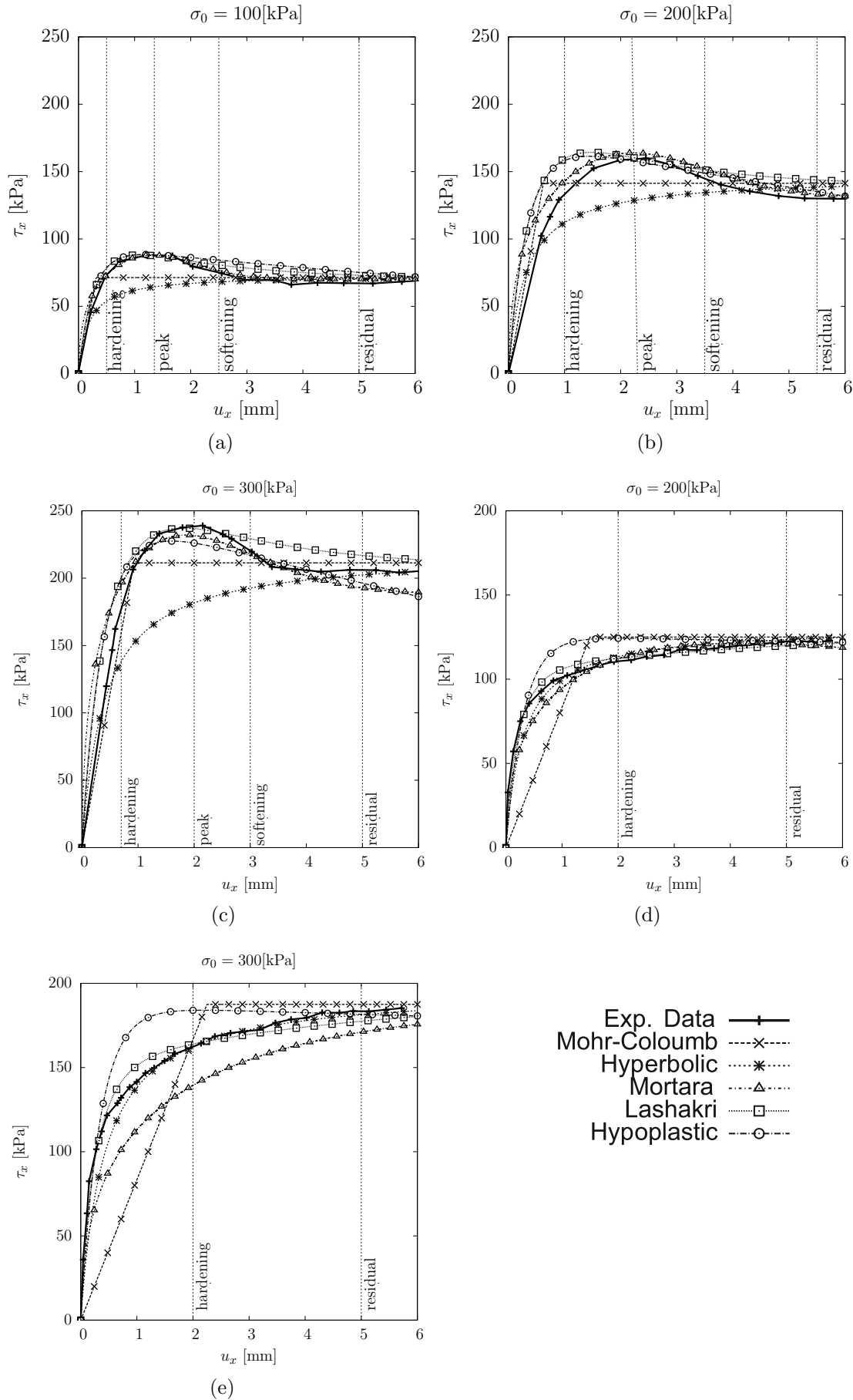


Figure 4.4: Model uncertainty simulations for dense ((a)-(c)) and loose ((d)-(e)) Hostun sand (Shahrour and Rezaie 1997)

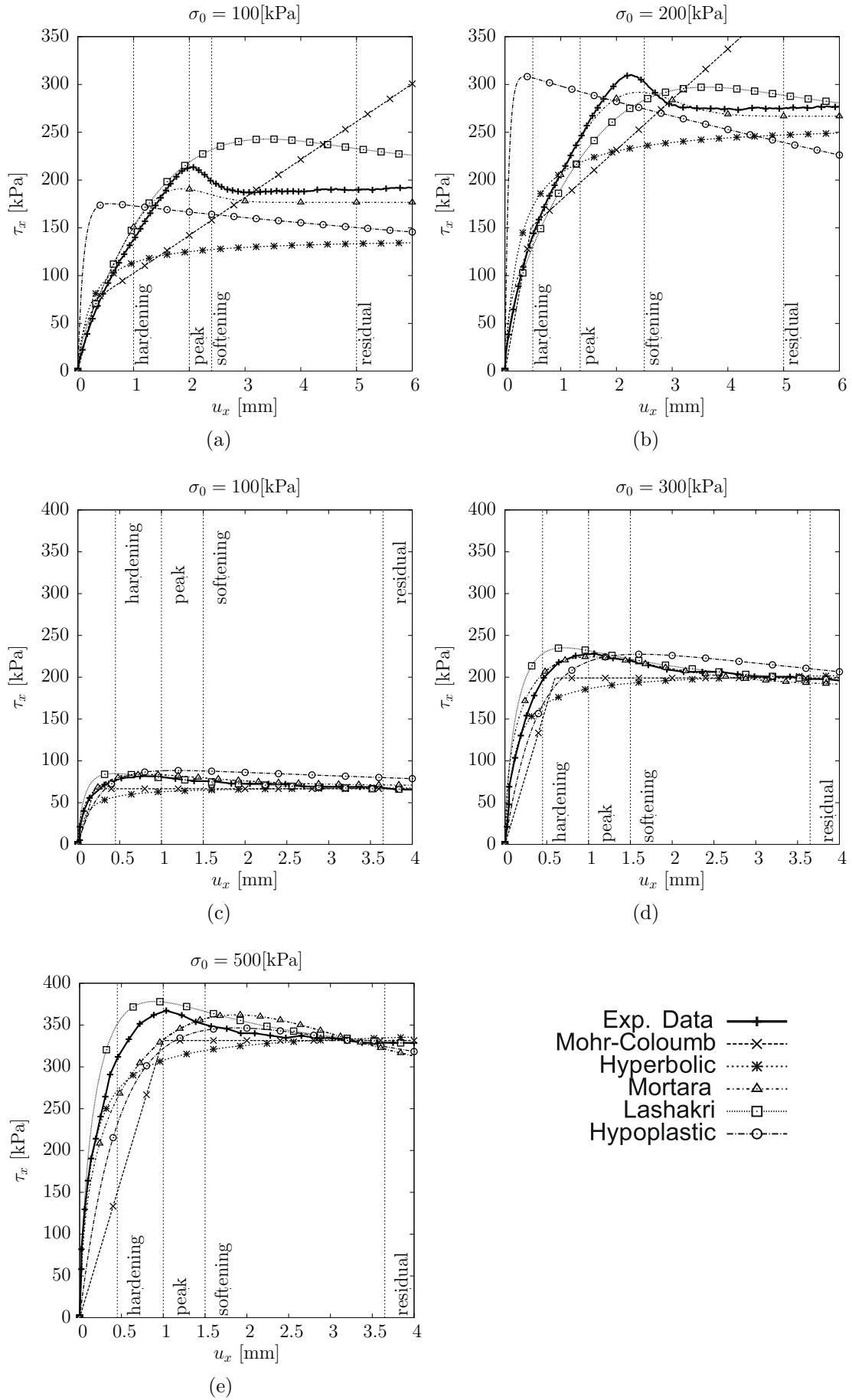


Figure 4.5: Model uncertainty simulations for Toyura sand ((a)-(b)) (Mortara 2003) and ((c)-(e)) air dried quartz sand (Evgin and Fakharian 1996)

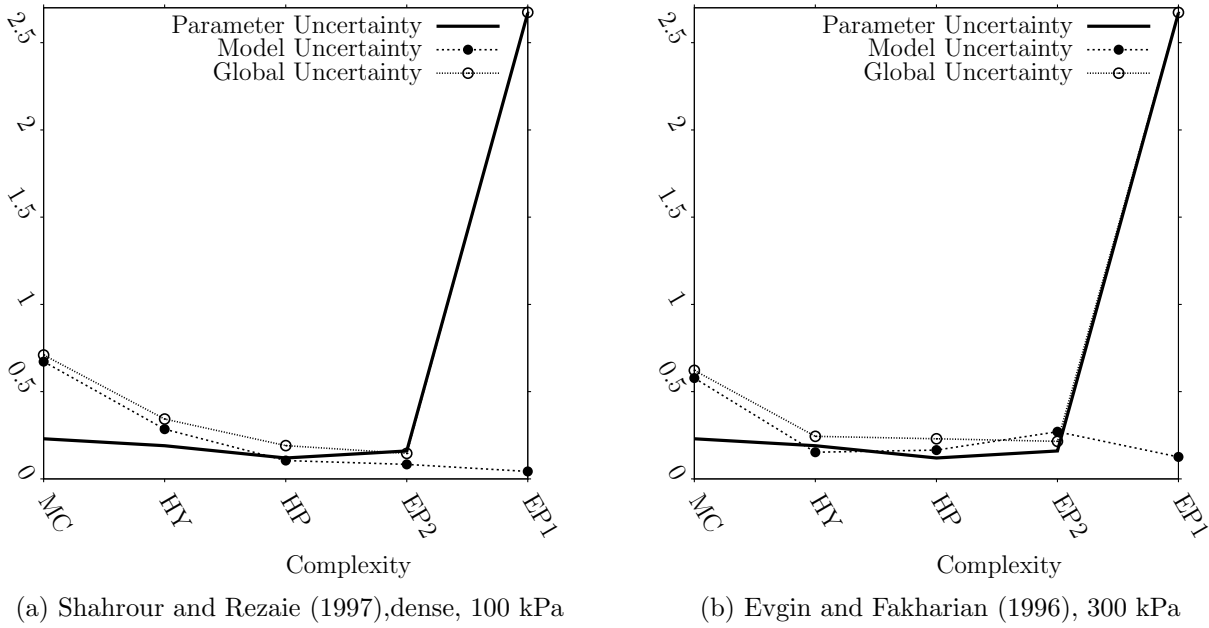


Figure 4.6: Comparison of model, parameter and global uncertainty for the five different models

too high and softening behaviour that was not representative of the experiments. The results for the model, parameter, and global uncertainty are summarized in Table B.1 in Appendix B. The results of the model assessment are highlighted in Figures 4.6a and 4.6b. The model of Mortara (2003) tended to have an excellent model uncertainty but was penalized by the parameter uncertainty. The assessment showed that the EP1 model was dominated by the parameter uncertainty. The model was therefore worse than all other models – even the simpler hyperbolic model and the Mohr-Coulomb model. As recorded in the sensitivity analysis, the model was highly flexible. However, the model is difficult to use without a proper calibration. This ultimately led to the problem that predictions (e.g. Class-A predictions (Lambe 1973)) are difficult to conduct without any previous knowledge of the soil and soil-structure interface behaviour.

The relationship between the model and parameter uncertainty was as expected (e.g. Lahmer et al. (2011), Figures 4.6a and 4.6b).

Except for the Mohr-Coulomb model, the global uncertainty of the models is comparable. The HP model had quite a low model and parameter uncertainty, which seems to be beneficial.

4.4 Summary of Chapter 4

Chapter 4 proposed a model assessment framework for the quantification of constitutive interface models. For this purpose, the model properties model sensitivity and model uncertainty were introduced. These model properties were used in a special framework to quantify existing constitutive interface models. The model sensitivity served as a preliminary property to iden-

tify the important model parameters. This was followed by the assessment of the model and parameter uncertainty. Both of these uncertainties were combined and used as model assessment measure. The definition of different objective function values enables the quantification of the model uncertainty. Different states of the interface (e.g. the consideration of hardening, softening, peak behaviour, and asymptotic states) are thereby taken into account.

The results shown in Section 4.3 indicate that the global model uncertainty can be derived on the basis of the proposed framework. In this thesis, it was done for the shear behaviour of the interface models in order to demonstrate the ability of the assessment framework. It was therefore unnecessary to use the framework twice to additionally quantify the normal interface behaviour. The adequate modelling of the shear behaviour can also be studied by considering an adequate peak and softening behaviour.

4.4.1 Implications for the extension and improvements for soil - structure interface models

The model of Mortara (2003) had a low model uncertainty but a high parameter uncertainty. The Mohr-Coulomb model and the hyperbolic model were not able to model important aspects of interface behaviour (e.g. softening and peak behaviour).

This facts led to the elasto-plastic model of Lashkari (2013) and the hypoplastic model of Gutjahr (2003). The model of Lashkari (2013) uses a void ratio dependence, which is important for giving a unique set of parameters for a given soil. The model is also able to model CNL and CNS conditions, but extending the model to 3D conditions appears to be complicated.

The hypoplastic model of Gutjahr (2003) is a reduced version of the 3D hypoplastic soil model of von Wolffersdorff (1996). The benefit of this model that a 3D interface model (Arnold 2004, Arnold and Herle 2006) exists and no additional parameters must be introduced. This model requires less parameters than the models of Mortara (2003) and Lashkari (2013), thereby extending and improving the models based on hypoplasticity theory with respect to the expected benefits.

In addition, Herle (1997) stated that the hypoplastic model after von Wolffersdorff (1996) is robust because a fluctuation into the input lead to a maximum of 10% output fluctuation.

The findings from this chapter and the review of the current modelling approaches in Chapter 3 have shown that there are only a few models for fine-grained interface models. This can be overcome by adapting the reduced tensor modelling for clay hypoplastic model (Mašín 2005). The theoretical considerations to model the interface with reduced tensors will be shown in Section 5.2. An enhanced version of the granular soil-structure constitutive interface model will be described.

Chapter 5

Enhancement of granular soil-structure hypoplastic constitutive interface model

5.1 Introduction

Chapter 4 introduced a model assessment suggests that the hypoplastic model from Gutjahr (2003) is a suitable candidate enhancing the model formulation. This is based on the model assessment itself and the fact that a 3D model formulation that can be simplified to a 2D formulation is preferable to a 2D model, which is hard to modify (Liu et al. 2014).

This chapter introduces the theory of hypoplasticity. In particular, the hypoplastic model of von Wolffersdorff (1996) is presented, and the interface model (Arnold and Herle 2006) is derived from the von Wolffersdorff (1996) hypoplastic model. The theoretical considerations for a model enhancement for interfaces are also described. The innovative concept of reformulating constitutive soil models into constitutive interface models is introduced in Section 5.4. The enhanced model that is reformulated on the proposed method is thus derived.

The enhanced model is then verified and validated with the experimental data of Uesugi and Kishida (1986), Shahrour and Rezaie (1997), Porcino et al. (2003), and Gómez et al. (2003) and compared to the old formulation of Arnold and Herle (2006).

5.2 Theoretical considerations

The effects of interface shearing and the governing mechanism are equal to the triaxial shearing of soils. Boulon (1989) and Boulon and Nova (1990) showed that triaxial and interface shear testing are analogous. In principle, the interface, which is a small soil continuum, has in the same deformation pattern as the continuum itself. The interface can therefore be treated as a soil continuum under simple shear conditions.

Feda (1976) highlighted that the direct shear testing is directly related to the *in-situ* behaviour

of interfaces. Arnold (2008) found a strong similarity between the interface and soil modelling. Weißenfels and Wriggers (2015b) and Dziewiecki et al. (2015) followed the idea that interface behaviour is similar to the full soil behaviour. Boulon (1989) introduced the concept that shear localisation occurs directly above the structural interface. This assumption led to the idea that one part of the sample acts as an oedometric part over the underlying interface zone. The interface zone itself has to bear the shear deformations and governs the soil-structure interaction behaviour. Figure 5.1 illustrates the shear behaviour in a direct interface shear test and shows the differences between smooth and a rough surfaces as well as the consequences for modelling such interfaces. As mentioned in Section 2.4, roughness is the major quantity for determining whether a failure has occurred place inside the soil specimen or in the interface. The similarities used as a hypothesis for the modelling approach: a simple-shear condition for the modelling of interfaces. The behaviour at the interface must be distinguished from the different surface roughness. Arnold and Herle (2006) first attempted to use a stress and stretching rate tensors. In contrast, the reduced stress and stretching tensors of Arnold and Herle (2006) have only three components and assume that $\sigma_{22} = \sigma_{33} = \sigma_n$. With respect to the assumption of a simple shear condition at the interface, the stress and strain definition of Arnold and Herle (2006) is incorrect compared to the 3D constitutive model consequently, under the simple shear condition, the in-plane stress differs from that applied normally to the interface (Figure 5.1). The in-plane strain ε_p is assumed to be zero. These assumptions of the stresses and strains for 3D shearing are used by Doherty and Fahey (2011) inter alia. The stress and strain tensor for interface behaviour can be defined as:

$$\boldsymbol{\sigma}^f = \begin{bmatrix} \sigma_{11} & \sigma_{12} & \sigma_{13} \\ \sigma_{21} & \sigma_{22} & \sigma_{23} \\ \sigma_{31} & \sigma_{32} & \sigma_{33} \end{bmatrix} \Rightarrow \boldsymbol{\sigma} = \begin{bmatrix} \sigma_t & \tau_x & \tau_y \\ \tau_x & \sigma_p & 0 \\ \tau_y & 0 & \sigma_p \end{bmatrix}, \quad (5.1)$$

where $\boldsymbol{\sigma}^f$ denotes the full stress tensor, and the reduced vectorial form $\boldsymbol{\sigma}$ is:

$$\boldsymbol{\sigma} = \begin{bmatrix} \sigma_t \\ \sigma_p \\ \tau_x \\ \tau_y \end{bmatrix}. \quad (5.2)$$

Simultaneously, the stretching rate tensor $\dot{\boldsymbol{\varepsilon}}$ is defined as:

$$\dot{\boldsymbol{\varepsilon}}^f = \begin{bmatrix} \dot{\varepsilon}_{11} & \dot{\varepsilon}_{12} & \dot{\varepsilon}_{13} \\ \dot{\varepsilon}_{21} & \dot{\varepsilon}_{22} & \dot{\varepsilon}_{23} \\ \dot{\varepsilon}_{31} & \dot{\varepsilon}_{32} & \dot{\varepsilon}_{33} \end{bmatrix} \Rightarrow \dot{\boldsymbol{\varepsilon}} = \begin{bmatrix} \dot{\varepsilon}_t & \frac{\dot{\gamma}_x}{2} & \frac{\dot{\gamma}_y}{2} \\ \frac{\dot{\gamma}_x}{2} & 0 & 0 \\ \frac{\dot{\gamma}_y}{2} & 0 & 0 \end{bmatrix}, \quad (5.3)$$

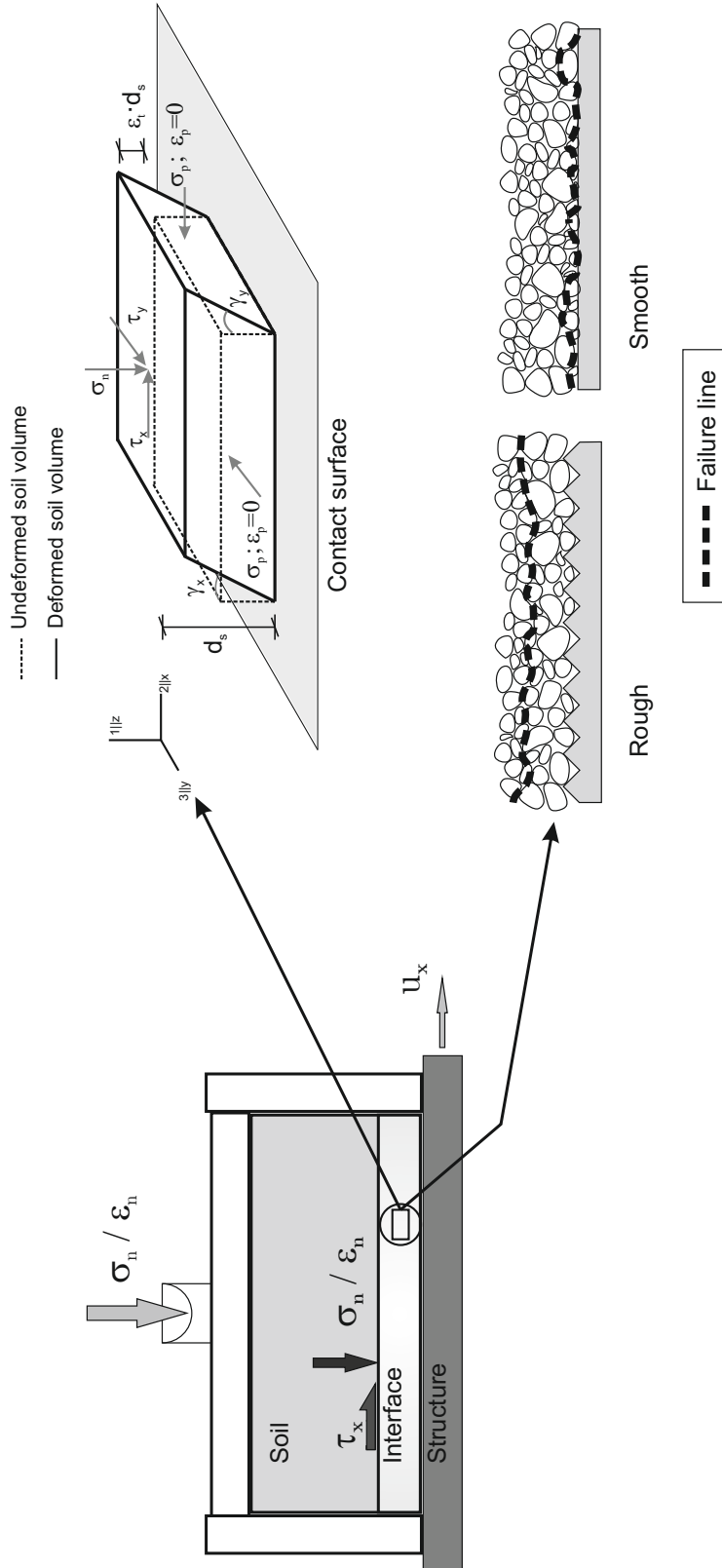


Figure 5.1: Schematic overview of the direct shear interface testing as idealization of simple shear conditions: Rough and smooth surfaces behaviour of interfaces

where $\dot{\boldsymbol{\epsilon}}^f$ denotes the full stretching tensor, and the reduced vectorial form $\dot{\boldsymbol{\epsilon}}$ is:

$$\dot{\boldsymbol{\epsilon}} = \begin{bmatrix} \dot{\epsilon}_t \\ 0 \\ \frac{\dot{\gamma}_x}{2} \\ \frac{\dot{\gamma}_y}{2} \end{bmatrix}. \quad (5.4)$$

The hypothesis is the assumption of a simple shear condition at a thin soil volume close to the structural material. From this hypothesis, it can be assumed that in general, a 3D constitutive model can be applied for interface modelling. Motivated by this hypothesis, a method using a continuum soil model as an interface constitutive model is presented in Section 5.4.

Shear zone thickness

Based on this assumption, the shear zone thickness has to be addressed with special emphasis. First, the interface constitutive models will be defined in a stress-strain space; the applied displacement must thus be calculated for a given strain and vice versa. Gutjahr (2003) and Arnold and Herle (2006) introduced the dependence of the shear zone thickness d_s on the shear strain γ_i to calculate the interface displacement u_i (Figure 5.2). Lashkari (2013) and Liu et al. (2006) used the same assumption that the interface strains can be calculated using the shear zone thickness. The shear zone thickness is correlated with the mean grain size d_{50} . An overview for the size of shear band thickness is given in Section 2.4. The shear strain γ_i is given in terms of the shear displacement:

$$\tan \gamma_i = \frac{u_i}{d_s} \quad (5.5)$$

d_s depends on the density, the mean grain size diameter d_{50} , and the surface roughness.

The exact choice of d_s is difficult to determine, although d_s can be used from back-calculations (Arnold and Herle 2006). Arnold (2008) also described a procedure to determine the shear

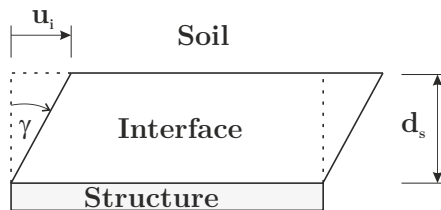


Figure 5.2: Schematic representation of the interface zone showing the relation between shear strain and shear deformation modified from Gutjahr (2003)

zone thickness, which is appropriate in a simulation. First, the $d_s = 1$ and $\kappa_r = 1$, which is a roughness coefficient (see Section 5.5.2), are used. Parameter κ_r is then modified to model the correct peak behaviour. The correct choice of d_s is then assessed because the interface thickness acts as a displacement scaling parameter (Section 7.1).

5.3 Hypoplasticity and Hypoplastic interface modelling

In this section, the hypoplastic modelling framework is introduced, and the first hypoplastic interface models developed by Herle and Nübel (1999), Gutjahr (2003), and Arnold and Herle (2006) are described. This section in particular is related to the modelling of granular soil-structure interfaces.

5.3.1 Hypoplasticity

The first hypoplasticity model was introduced by Kolymbas (1977). The model was continually developed with major contributions from Bauer (1996), Gudehus (1996), and Wu and Bauer (1994). The hypoplastic framework proposed by Gudehus (1996) was also used to simulate the contact behaviour of granular-solid interfaces. The hypoplasticity formulation proposed by Wu and Bauer (1994) was adapted from Herle and Nübel (1999) to model of an infinite simple-shear condition as a kind of 1D interface model.

The first interface model based on hypoplasticity, was developed by Gutjahr (2003). This 1D hypoplastic interface model used the hypoplasticity 3D model with a predefined limit state surface proposed by von Wolffersdorff (1996). The model of Gutjahr (2003) is also able to simulate arbitrary surface roughness conditions. Arnold and Herle (2006) extended the model and used reduced stress and strain tensors to model 2D interface conditions with the 3D hypoplastic model (von Wolffersdorff 1996).

A brief description is given for the basic hypoplasticity formulations and tensorial notations. The classical hypoplasticity theory has the major advantage of being able to model soil behaviour in the absence of various mathematical notions (yield surface, plastic potential and flow rule) which are necessary for elasto-plasticity models. In hypoplasticity, the strain does not have to be separated into reversible and irreversible parts (Kolymbas 2000).

In general, the hypoplastic equation can be described by a non-linear tensorial equation. This equation relates the objective stress rate $\dot{\mathbf{T}}$ to the Euler stretching rate \mathbf{D} . Wu and Bauer (1994) proposed an equation for practical use that is expressed as:

$$\dot{\mathbf{T}} = \mathcal{L} : \mathbf{D} + \mathbf{N} : \|\mathbf{D}\|, \quad (5.6)$$

where \mathcal{L} and \mathbf{N} are the fourth and second-order constitutive tensors. In the earlier versions of hypoplasticity, the Cauchy stress tensor was used. The hypoplastic model formulation proposed by Gudehus (1996) included pyknosity, which is the influence of density and barotropy on the modelling with respect to the stress level. The proposed hypoplastic constitutive equation is written as:

$$\dot{\mathbf{T}} = f_s (\mathcal{L} : \mathbf{D} + f_d \mathbf{N} \|\mathbf{D}\|), \quad (5.7)$$

where $\dot{\mathbf{T}}$ and \mathbf{D} are the objective stress rate and stretching rate tensor. f_s is the barotropy factor controlling the influence of the mean stress, and f_d is the pyknosity factor considering

the influence of the relative density.

von Wolffersdorff (1996) extended the basic form of the hypoplastic model incorporating the predefined limit state surface of Matsuoka and Nakai (1974). This model became a standard model for the non-linear modelling of sand behaviour (Kolymbas and Medicus 2016). The second order constitutive tensor \mathcal{L} is defined as:

$$\mathcal{L} = f_s \frac{1}{\hat{\mathbf{T}} : \hat{\mathbf{T}}} \left(F^2 \mathbf{I} + a^2 \hat{\mathbf{T}} \otimes \hat{\mathbf{T}} \right) \quad (5.8)$$

and the fourth-order constitutive tensor \mathbf{N} is given as:

$$\mathbf{N} = f_s f_d \frac{a \cdot F}{\hat{\mathbf{T}} : \hat{\mathbf{T}}} \left(\hat{\mathbf{T}} + \hat{\mathbf{T}}^* \right), \quad (5.9)$$

where $\hat{\mathbf{T}} = \mathbf{T} / \text{tr} \mathbf{T}$ and $\hat{\mathbf{T}}^* = \hat{\mathbf{T}} - \frac{1}{3} \mathbf{1}$ deviator stresses. von Wolffersdorff (1996) introduced the Matsuoka-Nakai failure condition into the model. This condition is given as:

$$F = \sqrt{\frac{1}{8} \tan^2 \psi + \frac{2 - \tan^2 \psi}{2 + \sqrt{2} \tan \psi \cos 3\theta}} - \frac{1}{2\sqrt{2}} \tan \psi, \quad (5.10)$$

where the Lode angle θ is defined as:

$$\cos 3\theta = -\sqrt{6} \frac{\text{tr} \left(\hat{\mathbf{T}}^* \cdot \hat{\mathbf{T}}^* \cdot \hat{\mathbf{T}}^* \right)}{\left[\hat{\mathbf{T}}^* : \hat{\mathbf{T}}^* \right]^{3/2}} \quad (5.11)$$

with $\tan \psi = \sqrt{3} \|\hat{\mathbf{T}}^*\|$. The barotropy factor f_s controls the influence of the mean stress and is given as:

$$f_s = \frac{h_s}{n} \left(\frac{e_i}{e} \right)^\beta \frac{1 + e_i}{e_i} \left(\frac{-\text{tr}(\mathbf{T})}{h_s} \right)^{1-n} \cdot \left[3 + a^2 - a\sqrt{3} \left(\frac{e_{i0} - e_{d0}}{e_{c0} - e_{d0}} \right)^\alpha \right]^{-1}, \quad (5.12)$$

where e_d , e_c , and e_i are the limiting void ratios. Under increasing mean pressure, the void ratio decreases until the limiting values e_{d0} , e_{c0} , and e_{i0} are reached (Figure 5.3).

$$\frac{e_d}{e_{d0}} = \frac{e_c}{e_{c0}} = \frac{e_i}{e_{i0}} = \exp \left[- \left(\frac{\text{tr}(\mathbf{T})}{h_s} \right)^n \right]. \quad (5.13)$$

The pyknotropy factor f_d controls the influence of the relative density, i.e.:

$$f_d = \left(\frac{e - e_d}{e_c - e_d} \right)^\alpha. \quad (5.14)$$

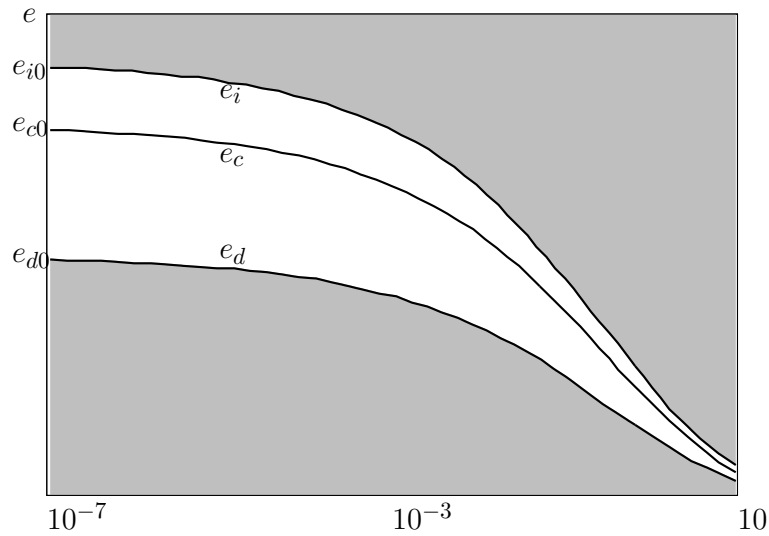


Figure 5.3: Relation between e_d , e_c , e_i , and p from Herle and Gudehus (1999)

The constitutive coefficient a is defined as:

$$a = \frac{\sqrt{3}(3 - \sin \varphi_c)}{2\sqrt{2} \sin \varphi_c}. \quad (5.15)$$

The model parameters are φ_c , the critical state friction angle, h_s , the granular hardness, and n , which controls the normal compression line and the critical state line. α controls the relative density to peak friction dependency, and β controls the relative density to the soil stiffness dependency. More details about the hypoplastic model with a predefined limit surface and the parameter determination of the model are given in von Wolffersdorff (1996) and Herle and Gudehus (1999). Additional information about the genealogy of hypoplastic models can be found in Kolymbas and Medicus (2016).

5.3.2 Hypoplastic interface model by Arnold and Herle (2006)

On the basis of the hypoplastic model from von Wolffersdorff (1996) and Arnold and Herle (2006) formulated a 2D hypoplastic interface model. By introducing reduced stress and stretching rate tensors, it is assumed that the global axis is related to the contact plane axis as $1||z, x||2$, and $y||3$ (Figure 5.4). The shear stress relations are defined as: $\sigma_{12} = \sigma_{21} = \tau_x$, $\sigma_{13} = \sigma_{31} = \tau_y$. The normal interface stress is the mean effective stress in the z -direction $\sigma_{11} = \sigma$. The other two mean stresses are assumed to be $\sigma_{22} = \sigma_{33} = \sigma_n$. The out-of-plane shear stress is assumed to be $\sigma_{23} = 0$. The stress tensor \mathbf{T} is defined as:

$$\mathbf{T}^f = \begin{bmatrix} \sigma_{11} & \sigma_{12} & \sigma_{13} \\ \sigma_{21} & \sigma_{22} & \sigma_{23} \\ \sigma_{31} & \sigma_{32} & \sigma_{33} \end{bmatrix} \Rightarrow \mathbf{T} = \begin{bmatrix} \sigma_n & \tau_x & \tau_y \\ \tau_x & \sigma_n & 0 \\ \tau_y & 0 & \sigma_n \end{bmatrix} \quad (5.16)$$

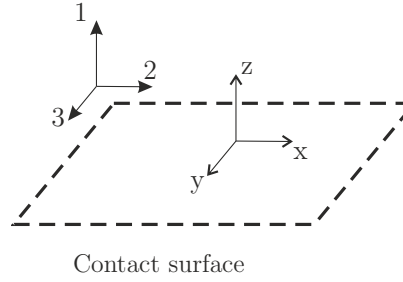


Figure 5.4: Contact plane and coordinate system proposed by Arnold and Herle (2006)

where \mathbf{T}^f denotes the full stress tensor, and \mathbf{T} denotes the reduced stress tensor. Considering the same assumptions as for the stress tensor, the strain tensor \mathbf{D}^f is defined as:

$$\mathbf{D}^f = \begin{bmatrix} \dot{\epsilon}_{11} & \dot{\epsilon}_{12} & \dot{\epsilon}_{13} \\ \dot{\epsilon}_{21} & \dot{\epsilon}_{22} & \dot{\epsilon}_{23} \\ \dot{\epsilon}_{31} & \dot{\epsilon}_{32} & \dot{\epsilon}_{33} \end{bmatrix} \Rightarrow \mathbf{D} = \begin{bmatrix} \dot{\epsilon}_n & \frac{\dot{\gamma}_x}{2} & \frac{\dot{\gamma}_y}{2} \\ \frac{\dot{\gamma}_x}{2} & \dot{\epsilon}_n & 0 \\ \frac{\dot{\gamma}_y}{2} & 0 & \dot{\epsilon}_n \end{bmatrix}. \quad (5.17)$$

Arnold and Herle (2006) used these reduced stress and stretching rate tensors to derive the interface hypoplastic model. Instead of the notation of Arnold and Herle (2006), the notation adapted here is a vectorial *Voigt* definition of the reduced stresses and stretching rates. These are given as:

$$\mathbf{T} = \begin{bmatrix} \sigma_n \\ \sigma_n \\ \tau_x \\ \tau_y \end{bmatrix} \quad (5.18)$$

where σ_n is the stress normal to the interface and τ_x, τ_y are the shear stresses. The strain rate vector is written as:

$$\mathbf{D} = \begin{bmatrix} \dot{\epsilon}_n \\ \dot{\epsilon}_n \\ \frac{\dot{\gamma}_x}{2} \\ \frac{\dot{\gamma}_y}{2} \end{bmatrix} \quad (5.19)$$

where $\dot{\epsilon}_n$ is the strain rate normal to the interface and $\frac{\dot{\gamma}_x}{2}, \frac{\dot{\gamma}_y}{2}$ are the shear strain rates in the x - and y -directions. These tensors are used within the modified tensorial operators given in Section 5.4. The modified tensorial notation is used with the standard formulation of the hypoplastic model (von Wolffersdorff 1996). This leads to the model proposed of Arnold and Herle (2006). In addition to these modifications to the original model, different terms are used in the interface model by Arnold and Herle (2006). The influence of these modifications will be

discussed in Sections 5.5.1 and 5.7. The Lode angle at critical state is assumed to be $\cos 3\theta = 0$. The Matsuoka–Nakai stress factor (Arnold and Herle 2006) is expressed as:

$$F = \sqrt{1 - \frac{9}{4} \left(\left(\frac{\tau_x}{3\sigma_n} \right)^2 + \left(\frac{\tau_y}{3\sigma_n} \right)^2 \right)} - \frac{\sqrt{3}}{2} \sqrt{\left(\frac{\tau_x}{3\sigma_n} \right)^2 + \left(\frac{\tau_y}{3\sigma_n} \right)^2}. \quad (5.20)$$

Arnold and Herle (2006) also proposed a modified scalar coefficient a based on the suggestion of Herle and Nübel (1999) i.e. that the correct behaviour of the interface zone at critical state is modelled as:

$$a = 3\sqrt{\frac{1}{2\tan^2\psi} - \frac{1}{8}} - \frac{\sqrt{3}}{2\sqrt{2}}. \quad (5.21)$$

It is assumed that under uni-axial shearing in the x-direction, the shear stress $\tau_y = \dot{\gamma}_y/2 = 0$ vanishes.

The hypoplastic interface model proposed by Arnold and Herle (2006) has several shortcomings. In particular, the in-plane stress σ_p and in-plane stretching rate ε_p are not incorporated into the model formulation.

5.4 Novel method for reformulation of 3D constitutive models to interface models

The following modelling approach was developed from the theoretical motivation given in Section 5.2 (Stutz et al. 2016). The interface behaviour can be modelled by preserving the continuum model formulation and redefining the tensorial definitions. Using this combined with reduced stress and strain vectors, the interface behaviour can be accurately modelled with the preserved continuum model.

The idea of this modelling approach can be summarized as follows: preserving the formulation of the continuum constitutive models, redefining of the tensorial operators in combination with the reduced stress and strain rate vectors of the models correctly simulates the constitutive interface behaviour. The reduced stress and stretching rate vectors are used for the tensorial notation. Based on of this tensorial notation the enhanced models are developed.

The newly defined tensorial operators use the *Voigt* notation to reduce the second order and fourth order tensors into vectors and matrices. The general definitions of the modified tensorial operators are defined by the first rank tensors \mathbf{X} and \mathbf{Y} and the second rank tensor \mathcal{S} as:

$$\mathbf{X} = \begin{bmatrix} X_1 \\ X_2 \\ X_3 \\ X_4 \end{bmatrix} \quad \mathbf{Y} = \begin{bmatrix} Y_1 \\ Y_2 \\ Y_3 \\ Y_4 \end{bmatrix} \quad \mathcal{S} = \begin{bmatrix} S_{11} & S_{12} & S_{13} & S_{14} \\ S_{21} & S_{22} & S_{23} & S_{24} \\ S_{31} & S_{32} & S_{33} & S_{34} \\ S_{41} & S_{42} & S_{43} & S_{44} \end{bmatrix}. \quad (5.22)$$

The trace of \mathbf{X} is defined as:

$$tr(\mathbf{X}) = X_1 + 2X_2. \quad (5.23)$$

The determinate of \mathbf{X} is defined as:

$$\det(\mathbf{X}) = X_1X_2^2 - X_4^2X_2 - X_3^2X_2. \quad (5.24)$$

The Euclidean norm of \mathbf{X} is written as:

$$\|\mathbf{X}\| = \sqrt{\mathbf{X} : \mathbf{X}} = \sqrt{X_1^2 + 2X_2^2 + 2X_3^2 + 2X_4^2}. \quad (5.25)$$

The second order unity tensor is:

$$\mathbf{1} = \begin{bmatrix} 1 \\ 1 \\ 0 \\ 0 \end{bmatrix}, \quad (5.26)$$

and the fourth order unity tensor is defined as:

$$\mathbf{I} = \begin{bmatrix} 1 & 0 & 0 & 0 \\ 0 & 0.5 & 0 & 0 \\ 0 & 0 & 0.5 & 0 \\ 0 & 0 & 0 & 0.5 \end{bmatrix}. \quad (5.27)$$

Three different definitions of the deviator stresses are required. The first definition is \mathbf{X}^* given as:

$$\mathbf{X}^* = \mathbf{X} + \mathbf{1} \left(\frac{-tr\mathbf{X}}{3} \right) = \begin{bmatrix} \frac{2}{3}X_1 - \frac{2}{3}X_2 \\ \frac{X_2}{3} - \frac{X_1}{3} \\ X_3 \\ X_4 \end{bmatrix}. \quad (5.28)$$

The second deviator stress $\hat{\mathbf{X}}^*$ is defined in vectorial notation:

$$\hat{\mathbf{X}}^* = \frac{\mathbf{X}}{tr\mathbf{X}} - \frac{\mathbf{1}}{3} = \begin{bmatrix} \frac{X_1}{X_1 + 2X_2} - \frac{1}{3} \\ \frac{X_2}{X_1 + 2X_2} - \frac{1}{3} \\ \frac{X_3}{X_1 + 2X_2} \\ \frac{X_4}{X_1 + 2X_2} \end{bmatrix}. \quad (5.29)$$

The third deviator stress $\hat{\mathbf{X}}$ is defined:

$$\hat{\mathbf{X}} = \frac{\mathbf{X}}{\text{tr}\mathbf{X}} = \begin{bmatrix} \frac{X_1}{X_1 + 2X_2} \\ \frac{X_1 + 2X_2}{X_2} \\ \frac{X_1 + 2X_2}{X_3} \\ \frac{X_1 + 2X_2}{X_4} \\ \frac{X_1 + 2X_2}{X_1 + 2X_2} \end{bmatrix}. \quad (5.30)$$

The inner product (\cdot) is given as:

$$\mathbf{X} \cdot \mathbf{Y} = \begin{bmatrix} X_1Y_1 + X_3Y_3 + X_4Y_4 \\ X_2Y_2 + X_3Y_3 \\ X_1Y_3 + X_3Y_2 \\ X_4Y_1 + X_2Y_4 \end{bmatrix}. \quad (5.31)$$

The double inner product $(:)$ between two first-rank tensors is defined as:

$$\mathbf{X} : \mathbf{Y} = X_1Y_1 + 2X_2Y_2 + 2X_3Y_3 + 2X_4Y_4. \quad (5.32)$$

The double inner product $(:)$ between second-rank (\mathcal{S}) and first-rank tensors (\mathbf{X}) is given as:

$$\mathcal{S} : \mathbf{X} = \begin{bmatrix} S_{11}X_1 + 2S_{12}X_2 + 2S_{13}X_3 + 2S_{14}X_4 \\ S_{21}X_1 + 2S_{22}X_2 + 2S_{23}X_3 + 2S_{24}X_4 \\ S_{31}X_1 + 2S_{32}X_2 + 2S_{33}X_3 + 2S_{34}X_4 \\ S_{41}X_1 + 2S_{42}X_2 + 2S_{43}X_3 + 2S_{44}X_4 \end{bmatrix}, \quad (5.33)$$

and the outer product (\otimes) is defined as:

$$\mathbf{X} \otimes \mathbf{Y} = \begin{bmatrix} X_1Y_1 & X_1Y_2 & X_1Y_3 & X_1Y_4 \\ X_2Y_1 & X_2Y_2 & X_2Y_3 & X_2Y_4 \\ X_3Y_1 & X_3Y_2 & X_3Y_3 & X_3Y_4 \\ X_4Y_1 & X_4Y_2 & X_4Y_3 & X_4Y_4 \end{bmatrix}. \quad (5.34)$$

These tensorial operators and the reduced stress and stretching rate tensors are used in the notation to model different advanced interface models.

5.5 Enhanced hypoplastic granular–structure model

This section presents the enhanced developed constitutive interface model, which uses the modified tensorial operators, the reduced stress, and stretching tensors to develop the model. For the sake of completeness, the model definitions that are mainly equal to the 3D continuum

models proposed by different authors to model soils by the use the hypoplasticity framework. The enhanced model by Stutz et al. (2016) is presented in Section 5.5.1. After introducing an enhanced version for granular-solid interfaces, an enhanced version of the intergranular strain for modelling interfaces will be presented.

5.5.1 Enhancement of the hypoplastic granular interface model

As outlined in Section 5.4, the hypoplastic interface model by Arnold and Herle (2006) has been enhanced. The model formulation leads to the understanding that the assumption that the stress tensor entries $\sigma_{22} = \sigma_{33}$ are equal to normal contact stress σ_n is not valid (Stutz et al. 2016). To improve the model predictions the reduced stress and strain tensor are redefined in Equations 5.2 and 5.4.

The fact that reduced tensors were used to establish the enhanced model for hypoplastic granular interfaces implies that odeometric condition was established at the interface instead of an isotropic stress state according to the model of Arnold and Herle (2006). The in-plane stress σ_p also can develop separately from the normal stress σ_n during continuous shearing.

The enhanced model formulation uses the reduced stress and stretching tensor in conjunction with the reformulated tensorial notation by using the standard continuum models. The model uses the same hypoplastic parameters described in Section 5.3.1.

5.5.2 Surface roughness modelling for granular soil-structure interfaces

The model introduced in Sections 5.3.2 and 5.5.1 assumes fully rough conditions. As indicated by various researchers (Potyondy 1961, Uesugi et al. 1988, DeJong and Westgate 2009), the surface roughness is particularly important for the interface shear behaviour. Gutjahr (2003) and Arnold and Herle (2006) introduced different approaches to model the surface roughness. To demonstrate their differences and equalities, the notation from the original publications Stutz et al. (2016) has been adjusted.

Surface roughness approach by Gutjahr (2003)

Gutjahr (2003) proposed the following empirical formula to estimate κ_r :

$$\kappa_r = 0.25 \log R_n + 1.05 \leq 1 \quad (5.35)$$

where κ_r is the surface roughness parameter, and R_n is the normalized roughness. R_n thus depends on the surface roughness R and the mean grain size d_{50} (Uesugi and Kishida 1986). Gutjahr (2003) also proposed another formula to determine κ_r :

$$\kappa_r = \tan \varphi_{int} / \tan \varphi_c \leq 1.0, \quad (5.36)$$

where φ_{int} is the interface friction angle. This definition describes the relationship between the soil-soil friction angle and the interface friction angle φ_{int} . Gutjahr (2003) suggested that the existing surface roughness will alter the pyknosity factor f_d and the critical state friction angle φ_c . The scalar function of a (Eq. 5.15) is also dependent on φ_c . This dependence is modelled by Gutjahr (2003), who used the constitutive scalar a :

$$a_r = \frac{\sqrt{3}(3 - \sin \varphi_c \kappa_r)}{2\sqrt{2} \sin \varphi_c \kappa_r}. \quad (5.37)$$

Based on their results, Uesugi and Kishida (1986) concluded that loose soil on rough surfaces has the same behaviour as dense soil on smooth surfaces. Gutjahr (2003) thus proposed a new pyknosity factor f_d expressed as:

$$f_{dr} = \left(\frac{e - e_d}{e_c - e_d} \right)^{\alpha \kappa_r^2}. \quad (5.38)$$

Gutjahr (2003) then defined a modified barotropy factor f_s expressed as:

$$f_{sr} = \frac{h_s}{n} \left(\frac{e_i}{e} \right)^\beta \frac{1 + e_i}{e_i} \left(\frac{-tr(\mathbf{T})}{h_s} \right)^{1-n} \cdot \left[3 + a_r^2 - a_r \sqrt{3} \left(\frac{e_{i0} - e_{d0}}{e_{c0} - e_{d0}} \right)^{\alpha \kappa_r^2} \right]^{-1}. \quad (5.39)$$

These modifications are used in the formulation of the \mathcal{L} Tensor and the \mathbf{N} Tensor by replacing a , f_d , and f_s by a_r , f_{dr} , and f_{sr} .

Surface roughness approach by Arnold and Herle (2006)

Arnold and Herle (2006) proposed a scheme that differs from the one proposed by Gutjahr (2003) to model various surface roughnesses. The scalar value a is modified identically to the approach by Gutjahr (2003). However, Arnold and Herle (2006) adjusted the mobilisation of the shear stress by introducing the additional coefficient f_c , which is expressed as:

$$f_c = \frac{1}{\kappa_r}. \quad (5.40)$$

Arnold and Herle (2006) found that this modification leads to better predictions when simulations are compared with experimental results. The additional coefficient f_c is a modification of the barotropy factor and is implemented into the general form of the hypoplastic equation (Eq. 6.2):

$$\dot{\mathbf{T}} = f_s f_c (\mathcal{L} : \mathbf{D} + f_d \mathbf{N} \|\mathbf{D}\|) \quad (5.41)$$

5.6 Enhanced intergranular strain concept for interface modelling

Niemunis and Herle (1997) proposed the intergranular strain concept as an extension of the hypoplastic model according to von Wolffersdorff (1996). This concept prevents the use of excessive ratcheting upon cyclic loading. This is achieved by an additional state variable that represents the interlayer deformation between the different grains. The model behaviour in the small-strain region is improved by this extension of the hypoplastic model. The intergranular strain concept was then adapted to model fine-grained soils (Mašín 2005; 2013). The enhanced formulation of the hypoplastic models can be written as:

$$\dot{\mathbf{T}} = \mathcal{M} : \mathbf{D}, \quad (5.42)$$

where \mathcal{M} is a fourth-order tangent stiffness material tensor. In this formulation, an additional state variable δ is needed. This is a symmetric second order tensor called the intergranular strain. It is a result of the intergranular interface layer deformation and the rearrangement of the soil skeleton. The normalized magnitude of the intergranular strain δ is written as:

$$\rho = \frac{\|\delta\|}{R}, \quad (5.43)$$

where R is the maximum constant value of the intergranular strain. The direction for intergranular strain is given as:

$$\hat{\delta} = \begin{cases} \delta / \|\delta\|, & \text{for } \delta \neq 0; \\ \mathbf{0}, & \text{for } \delta = 0. \end{cases} \quad (5.44)$$

The fourth-order tensor \mathcal{M} is calculated from the hypoplastic tensors \mathcal{L} and \mathbf{N} using the following interpolation function:

$$\mathcal{M} = [\rho^\chi m_T + (1 - \rho^\chi) m_R] f_s \mathcal{L} + \begin{cases} \rho^\chi (1 - m_T) f_s \mathcal{L} : \hat{\delta} \otimes \hat{\delta} + \rho^\chi f_s f_d \mathbf{N} \hat{\delta}, & \text{for } \hat{\delta} : \mathbf{D} > 0; \\ \rho^\chi (m_R - m_T) f_s \mathcal{L} : \hat{\delta} \otimes \hat{\delta}, & \text{for } \hat{\delta} : \mathbf{D} \leq 0 \end{cases}, \quad (5.45)$$

where m_R is defined by the ratio of the maximum shear modulus to the elastic shear modulus, m_T is the ratio of the shear modulus during 90° change of loading direction to the elastic shear modulus, and χ controls the non-linearity of the stiffness on the intergranular strain. The evolution of the intergranular strain tensor δ is given as:

$$\dot{\delta} = \begin{cases} (\mathcal{I} - \hat{\delta} \otimes \hat{\delta} \rho^{\beta_r}) : \mathbf{D}, & \text{for } \hat{\delta} : \mathbf{D} > 0; \\ \mathbf{D}, & \text{for } \hat{\delta} : \mathbf{D} \leq 0 \end{cases}, \quad (5.46)$$

where $\hat{\boldsymbol{\delta}}$ is the objective rate of the intergranular strain tensor and β_r is an additional material parameter. β_r controls the rate of decay of the intergranular strain.

Arnold (2008) used the intergranular strain concept to enhance the hypoplastic granular-structure interface model. This was investigated under the same assumption of the reduced stress and strain rate tensors for the intergranular strain tensor. The intergranular strain tensor proposed by Arnold (2008) was modified to the following enhanced intergranular strain tensor for interfaces:

$$\boldsymbol{\delta}^f = \begin{bmatrix} \delta_{11} & \delta_{12} & \delta_{13} \\ \delta_{21} & \delta_{22} & \delta_{23} \\ \delta_{31} & \delta_{32} & \delta_{33} \end{bmatrix} \Rightarrow \boldsymbol{\delta} = \begin{bmatrix} \delta_n & \delta_x & \delta_y \\ \delta_x & \delta_p & 0 \\ \delta_y & 0 & \delta_p \end{bmatrix}. \quad (5.47)$$

The in-plane intergranular strain is $\delta_p = 0$. Based on this assumption, the intergranular strain tensor is reduced to a vector in *Voigt* notation:

$$\boldsymbol{\delta} = \begin{bmatrix} \delta_n \\ \delta_p \\ \delta_x \\ \delta_y \end{bmatrix} \Rightarrow \begin{bmatrix} \delta_n \\ 0 \\ \delta_x \\ \delta_y \end{bmatrix} \quad (5.48)$$

Arnold (2008) noticed that after oedometric loading of the interface the correct initialisation of the model should be initialized by $\delta_n = 0$, $\delta_x = \frac{R}{\sqrt{3}}$, and $\delta_y = \frac{R}{\sqrt{3}}$

5.7 Validation of the enhanced hypoplastic granular -structure interface model

In the following, different models are compared. Two different model formulations without the enhanced reduced stress and strain rate tensors are used. The enhanced model uses the following differences compared to the model of Arnold and Herle (2006):

- The Lode angle assumption in the model of Arnold and Herle (2006) is corrected, i.e. $\cos 3\theta \neq 0$
- The standard definition of the coefficient a (Equation 5.15) is used
- The Matsuoka-Nakai stress factor F from the original constitutive model of von Wolffersdorff (1996) is used (Equation 6.40)

Understanding these differences helps to understand the model responses. The enhanced granular interface models proposed by Stutz et al. (2016) are also used. The three different models are abbreviated as:

1. Model proposed by Arnold and Herle (2006): **AH**

2. Model based on the definition of Arnold and Herle (2006) enhanced by using the original formulations of $\cos 3\theta$, a , and F from the 3D continuum model: **AHE**
3. Enhanced model with $\kappa_r = 1.0$ proposed in this paper: **HvWE**

Evgin and Fakharian (1996) defined the following interface testing boundary conditions as follows:

- Constant volume (CV): $K = \infty$; $\dot{\sigma} \neq 0$; $\dot{\varepsilon} = 0$
- Constant normal load (CNL): $K = 0$; $\dot{\sigma} = 0$; $\dot{\varepsilon} \neq 0$
- Constant normal stiffness (CNS): $K = \text{constant}$; $\dot{\sigma} \neq 0$; $\dot{\varepsilon} \neq 0$

The definition of validation and verification used in the following will be introduced and is based on the ideas of Schwer (2001). Verification is the analysis of the implemented code from this thesis with external software i.e. TRIAX (Mašín 2016).

Validation is the comparison of experimental data to simulation results and can also be called comparison. It also describes the calibration and determination of material parameters for a material model.

The constitutive equation for the model verification and validation is solved by a simple Euler's forward scheme at constant normal stress $\dot{\sigma}_n = 0$, the shear stress and volumetric strains change (CNL or CNS), and this becomes a mixed control problem. The solution of the constitutive equation with the mixed control problem is exemplified in Appendix C.

5.7.1 Model verification

The implementation of the models for the calculations based on Gauss-point integration are examined and compared with the element-test software TRIAX (Mašín 2016). To develop of the different models and testing purposes, the interface constitutive models were implemented with the interpreter language MATLAB in order to verify the implementation of the enhanced granular-structure interface model. The parameters used in the verification and in Section 5.7.2 are given in Table 5.1. Figure 5.5 shows the results of this verification. The initial void ratio of $e_0 = 0.60$ and constant normal loads of 100 and 200 kPa are used. The stress strain curves from the implementation into MATLAB perfectly match those from the implementation into the TRIAX software with the HvWE model.

Table 5.1: Parameters for the hypoplastic sand interface model for verification and general behaviour

	φ_c (°)	h_s (MPa)	n	e_{d0}	e_{c0}	e_{i0}	α	β
Evaluation	28	2000	0.29	0.61	0.96	1.09	0.13	2

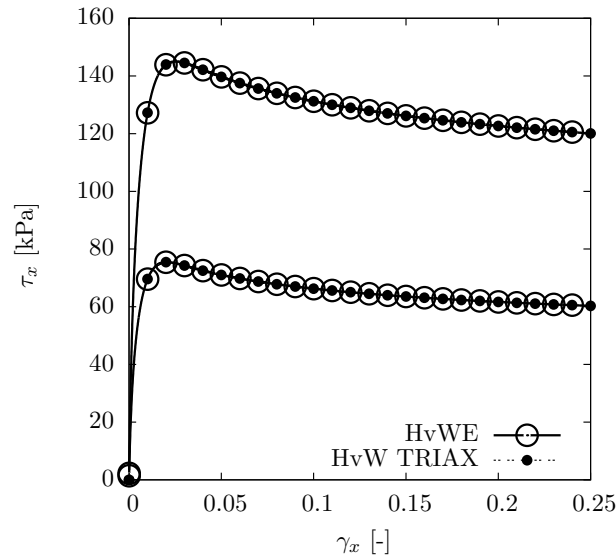


Figure 5.5: Verification of the MATLAB implementation compared to TRIAX

As mentioned in Section 5.2, the interface constitutive models and the 3D continuum models deliver the same results under the assumption of a simple shear condition in the interface.

5.7.2 Testing the general enhanced model behaviour

The stress paths for the CV tests are shown in Figures 5.6a and 5.6b. In all CV simulations, the initial void ratio was defined as $e_0 = 0.8$. The model proposed (HvWE) gave the lowest shear stress τ_x at different normal stress levels. The model response showed the same trend, but the shear stress varies. The original model (AH) produced the highest shear stresses. The AHE and HvWE models show a small difference in their response. At a higher normal stress, the model responses show increased differences.

Similar results were observed for τ_x versus σ_n results (Figure 5.6b). The difference between the HvWE and AHE model was small compared with the AH model. The predicted normal stresses were higher for the AH than for the AHE model. This difference was caused by the different Lode angle formulation used in the AH, AHE, and HvWE model.

The results of the constant volume condition using all three models show that this boundary condition is not suitable to justify whether the models are correct (Figures 5.7b and 5.7a). This is because of the normal strain, which is zero. The applied constant normal stiffness was 1000 kPa. The initial void ratio applied in the CNS and CNL simulations was $e_0 = 0.85$. The normal stress varied from 50 to 150 kPa. The shear behaviour was similar in all models (Figure 5.7b). However, the HvWE model showed the largest shear stress at all different normal stress levels. Figure 5.7a shows the behaviour in the σ_n versus τ_x plane. The normal stress in the HvWE model differed from the results obtained with the model of Arnold and Herle (2006). This behaviour was due to the different formulations of the stress tensor, in particular for the normal stress σ_n and the in-plane stress σ_p .

Models were then compared under a constant normal load (CNL). This condition is charac-

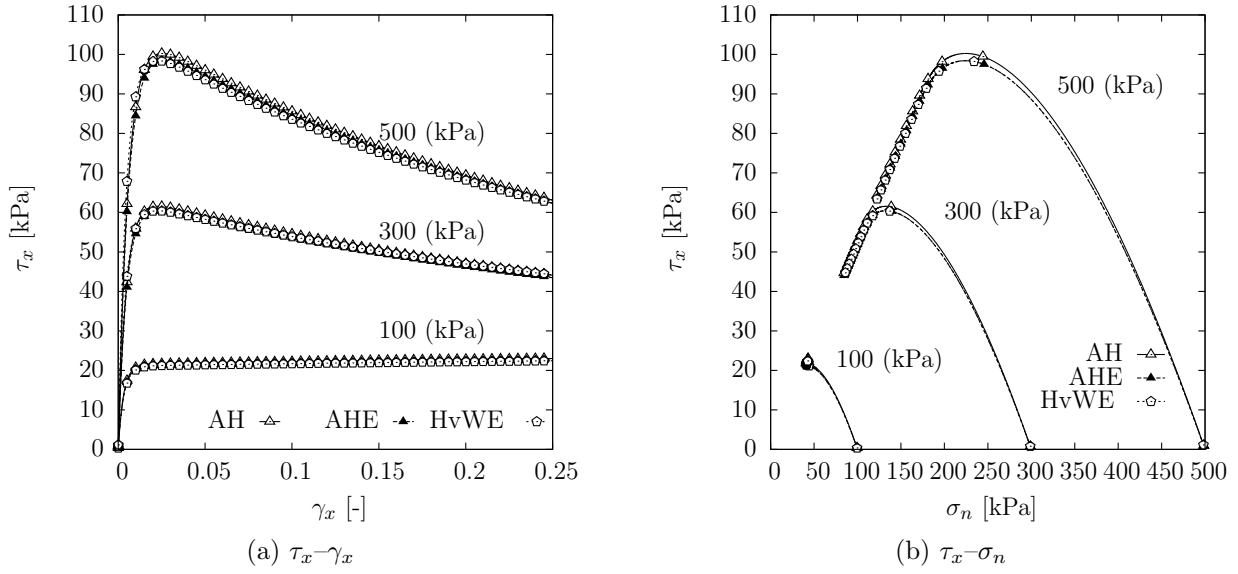


Figure 5.6: Results for the comparison of different models under CV conditions with 100, 300, and 500 kPa

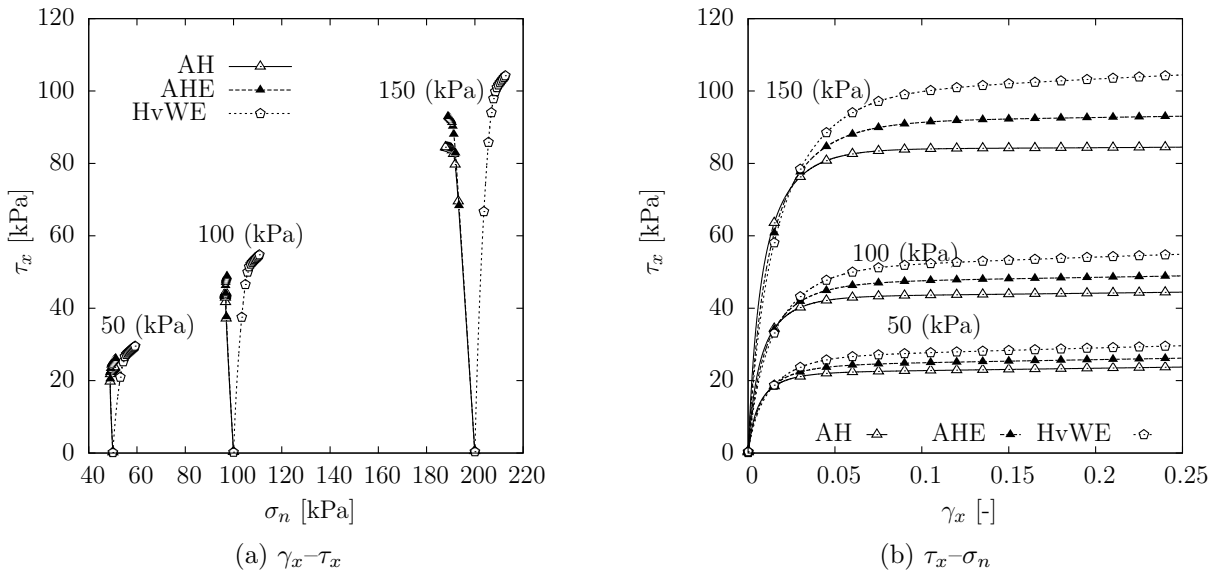


Figure 5.7: Results for the comparison of different models under CNS with $\sigma_0 = 50, 100,$ and 150 kPa

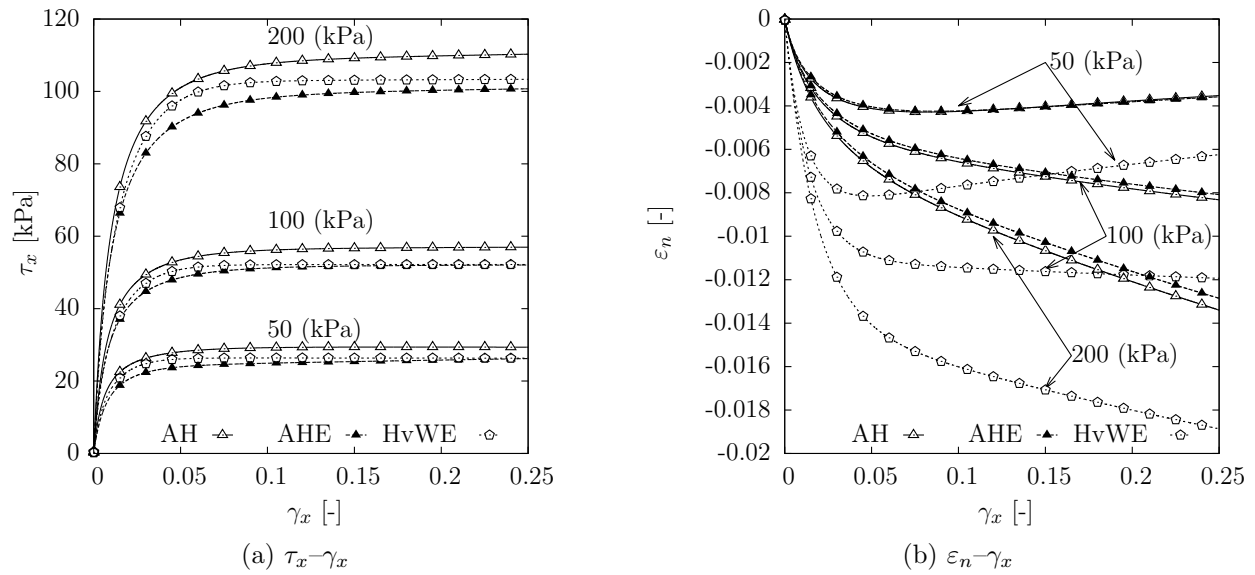


Figure 5.8: Results for the comparison of different models under CNL conditions with $\sigma_0 = 50, 100, \text{ and } 150 \text{ kPa}$

terized by $\dot{\sigma}_n = 0$ and $\dot{\varepsilon}_n \neq 0$. The results (Figure 5.8a) show different stress evolutions using the three different models. The AHE and HvWE model have comparable asymptotic stress. The original model of Arnold and Herle (2006) had a different critical stress level because of the assumption of the Matsuoka-Nakai failure criterion and the Lode-Angle of zero. All three models had small differences in their response. Compared to the CNS simulations (Figure 5.7b), lower shear stresses developed under CNL conditions. The model responses differ because of the different formulation of the reduced stress vector and the differences in $\cos 3\theta$, a , and F . In summary, all three models (AH, AHE and HvWE) yielded different responses. Reasons for the differences will be discussed below.

Discussion of model behaviour and the enhancement of the model

The behaviour of the granular soil interface models differs in several aspects. The first aspect is the proposed coefficient a , the factor of the Matsuoka-Nakai failure criterion F and the Lode angle $\cos 3\theta = 0$ of Arnold and Herle (2006) that explains the difference between the AH and AHE model. The differences between the AH, AHE, and HvWE (Stutz et al. 2016) models are associated with the in-plane stress σ_p . Figure 5.9 demonstrates the normal stress and in-plane stress development under CNS conditions for the AH and HvWE models.

Figure 5.9 highlights the significant effect of the in-plane stresses for the simulations. The in-plane and transversal stresses are highly important for modelling interfaces. The modelling of the interface is similar to model of the soil itself (Arnold 2008): neglecting the in-plane stresses in typical interface models is thus compensated by other model components. This behaviour is then explicitly implemented by special models, which are not consistent with the applied 3D continuum soil model.

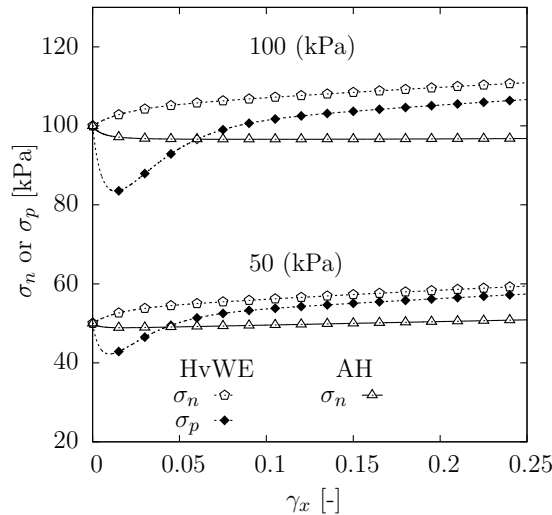


Figure 5.9: Comparison of σ_n and the in-plane σ_p normal stress at the interface for the different models

The following section introduces and compares the two different approaches for incorporating the surface roughness into the proposed enhanced interface model.

5.7.3 Comparison of surface roughness modelling approaches

In the following section, the two surface roughness approaches from Section 5.5.2 are evaluated. The parameters from Table 5.2 were used in a constant normal load simulation. Under fully rough conditions, the use both approaches led to the same results. With increasing smoothness, the results started to diverge (Figure 5.10a). This is mainly because of the modification of the barotropy factor f_c . Both schemes for modelling the surface roughness were implemented into the enhanced hypoplastic interface model (HvWE) (Section 5.5.1). The CNL simulations were done with an initial normal stress of 100 kPa. As expected for $\kappa_r = 1.0$, both schemes gave identical results. By using a lower surface roughness coefficient $\kappa_r \leq 1.0$, the approach of Arnold and Herle (2006) showed a softer response than the model of Gutjahr (2003) because of the scalar f_c , which was introduced by Arnold and Herle (2006) to improve predictions of the model response.

As described above, the model shows no differences when considering fully rough conditions (Figure 5.10b). The results demonstrate that the scheme of Arnold and Herle (2006) had less

Table 5.2: Parameters for the hypoplastic model (partly from Herle and Gudehus (1999))

	φ_c ($^\circ$)	h_s (MPa)	n	e_{d0}	e_{c0}	e_{i0}	α	β
Hostun Sand	31	1000	0.29	0.61	0.96	1.09	0.13	2
Toyura Sand	30	2600	0.27	0.61	0.98	1.10	0.25	1
Ticino Sand	31	1000	0.29	0.61	0.96	1.09	0.13	2
Density Sand	32	750	0.25	0.62	0.97	1.06	0.13	1.5

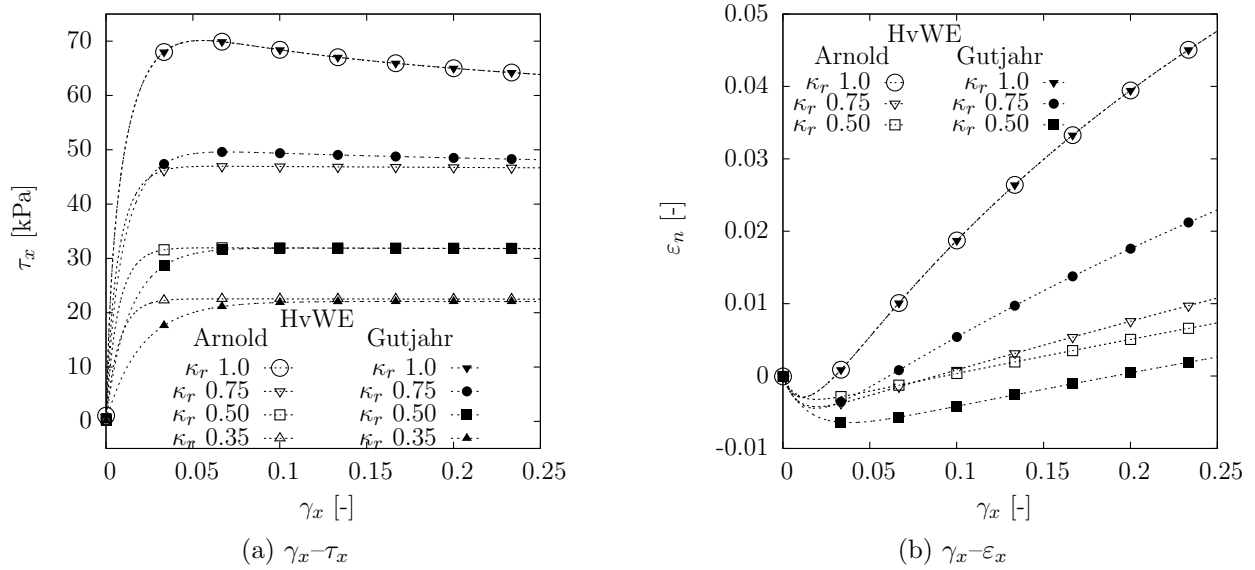


Figure 5.10: CNL simulation of the two different surface roughness modelling schemes at 100 kPa

influence on the normal behaviour, whereas the scheme of Gutjahr (2003) showed a dilative behaviour. For a smoother surface with $\kappa_r = 0.50$, the initial compaction was followed by a minor dilative behaviour. All simulations used an initial void ratio of $e_0 = 0.85$.

5.7.4 Comparison of simulated with experimental interface behaviour

The enhanced model (HvWE) was used with both surface roughness approaches. The experimental set-up was described in Uesugi and Kishida (1986) and Uesugi et al. (1988) with a modified direct shear test. The material tested was Toyoura sand with the parameters given in Table 5.2. The surfaces of the test apparatus were constructed from mild steel, and the predefined surface roughness was measured (Figure 5.11). Both schemes and the experimental data gave similar responses for smooth interface conditions ($\kappa_r = 0.35$). For intermediate surface roughness ($\kappa_r = 0.50$), the scheme of Gutjahr (2003) showed a slightly better model response than the scheme of Arnold and Herle (2006).

Considering rough surface conditions ($\kappa_r = 0.905$), the simulation and experimental results differ. However, with the approach of Gutjahr (2003), this was not the case. The surface modelling approach of Arnold and Herle (2006) simulated only small peak behaviour. After the peak stress was reached, the simulations for both approaches tended towards the same residual stress at critical state. The simulations showed a shear stress similar to the values obtained from the experiments (Figure 5.11). This difference can be explained by the scalar f_c , which reduces the barotropy factor f_s .

After experimentally comparing the two schemes it is recommended to use the scheme of Gutjahr (2003) to model surface roughness. The second validation was conducted with the experimental data of Shahrouz and Rezaie (1997) obtained with Hostun sand (parameters are given in Table

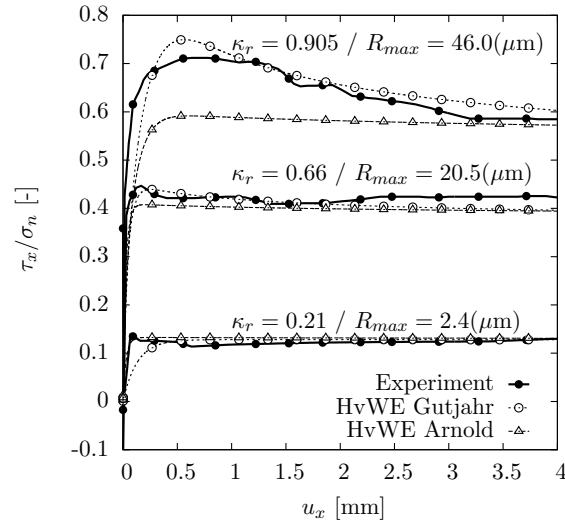


Figure 5.11: Shear displacement u_x versus friction coefficient τ_x/σ_n plot for different surface roughness under CNL conditions with $\sigma_0 = 78$ kPa

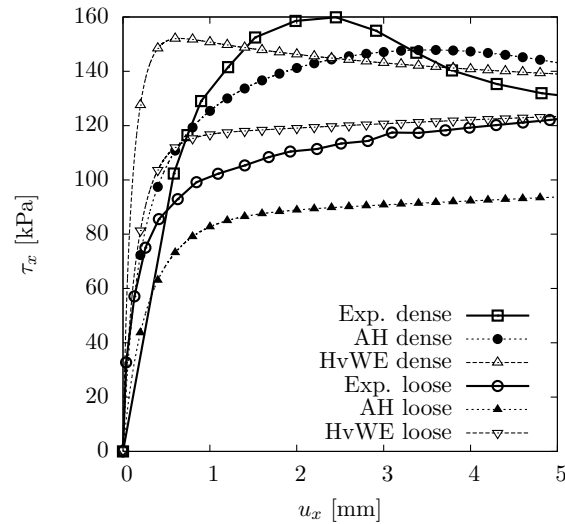


Figure 5.12: Comparison of models of CNL test under an applied normal stress of 300 kPa using the experimental data of Shahrour and Rezaie (1997)

5.2). The normal stress was 300 kPa, and the experiments were conducted on sand in both a dense ($e_0 = 0.68$) and loose ($e_0 = 0.95$) state. None of the models matched the experimental observations (Figure 5.12). Nevertheless, the HvWE model gave a more accurate prediction than the AH model.

The next model validation used staged shear stress paths, which Gómez et al. (2003) defined as stress paths with fluctuating normal stress under continuously applied shear displacement. Gómez et al. (2003) showed that such a stress path can occur at the walls of navigation locks. A staged shear test is shown in Figure 5.13. The parameters used for the comparison are given in Table 5.2. The initial void ratio ($e_0 = 0.68$) was taken from the experimental set-up of Gómez et al. (2003).

The experimental data (Gómez et al. 2003) was compared with the AH and HvWE models.

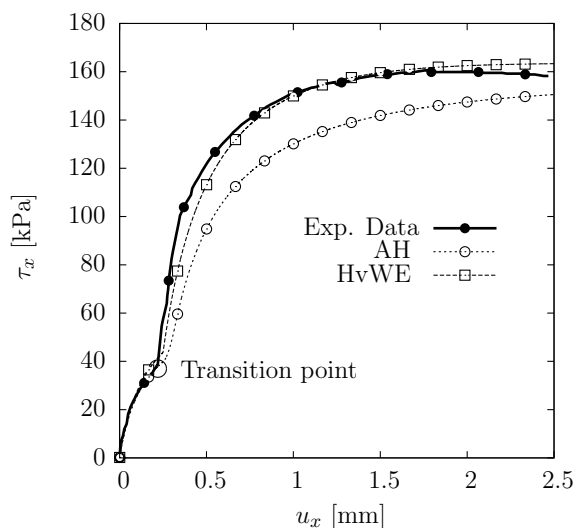


Figure 5.13: Comparison of AH and HvWE models with the experimental data of a staged shear test under CNL conditions (102-274 kPa)

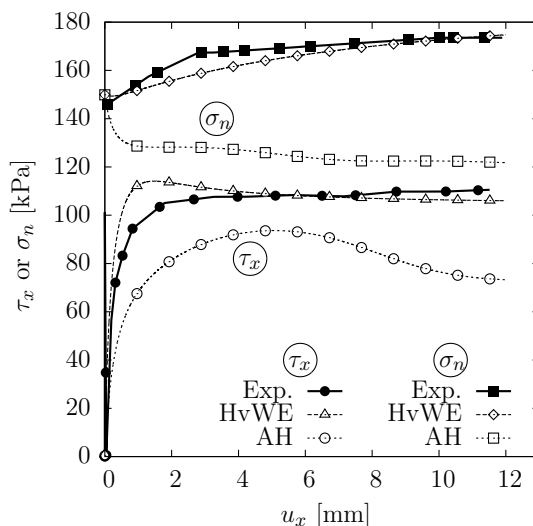


Figure 5.14: Comparison of shear displacement u_x versus shear stress τ_x and normal stress σ_n using experimental data with $K = 100$ kPa from Porcino et al. (2003)

The transition point in Figure 5.13 denotes the normal stress change in the test. A normal stress of 102 kPa was initially applied at the interface. When the shear displacement reached 0.25 mm, the normal stress increased to 274 kPa. The HvWE produced results similar to those of Gómez et al. (2003). The AH model had an identical response until the transition point. After this point, the model response did not correspond to the simulated shear stresses. This comparison highlights the enhanced predictive capability of the proposed HvWE model if the in-plane stresses σ_p are considered.

The last verification used experimental data from Porcino et al. (2003). The parameters used are shown for the Ticino sand (Table 5.2). Detailed information on the sand properties and parameters can be found in Herle and Gudehus (1999).

Porcino et al. (2003) conducted CNS tests in a modified direct-shear apparatus to investigate

Table 5.3: Parameters for the hypoplastic model with intergranular strain

Parameters	Toyorua sand (Arnold 2008)	Homo-Gravel (Zhang and Zhang 2006)
φ_c ($^\circ$)	30	44
h_s (GPa)	2.6	20
n	0.27	0.18
e_{d0}	0.61	0.26
e_{c0}	0.98	0.45
e_{i0}	1.1	0.5
α	0.18	0.10
β	1.0	2.0
R	$1 \cdot 10^{-4}$	$1 \cdot 10^{-4}$
m_R	5	7
m_T	2	2
β_r	0.12	0.12
χ	1	0.75

different types of sand under changing normal stiffness conditions and varying interface roughness. The shear behaviour of the HvWE model was similar to the experimental results (Figure 5.14). After the peak, the HvWE model displayed a softening, which could not be observed in the experiment. The AH model showed a strong softening in the model response, and the shear stress at the critical state was underestimated.

The normal behaviour of the models (Figure 5.14) showed that the AH model exhibited only a decrease of the normal stress and had a constant residual normal stress. The HvWE model simulated a small decreasing stress followed by an increase under continuous shearing. None of the models matched the experimental observation; however, the HvWE model demonstrated a better behaviour than the AH model.

The differences (Figure 5.14) were due to the Lode angle $\cos 3\theta$, which was constant in the model formulation of the AH model.

5.7.5 Modelling granular interface using the enhanced inter-granular strain concept

The intergranular strain concept of Niemunis and Herle (1997) was used in conjunction with the model proposed by Stutz et al. (2016) to simulate interfaces under cyclic loading conditions. The parameters from Table 5.3 were used. As described in Section 5.6, the intergranular strain concept was used by Arnold (2008) to model interfaces. The intergranular strain concept uses an enhanced version of the reduced stress and strain rate tensors (Section 5.6). The enhanced version can be used to model the behaviour of interfaces under non-monotonic loading. In the following, results for CV and CNL conditions are simulated by the enhanced model. Figures 5.15a and 5.15b show the results for the CV conditions. The simulation was conducted with

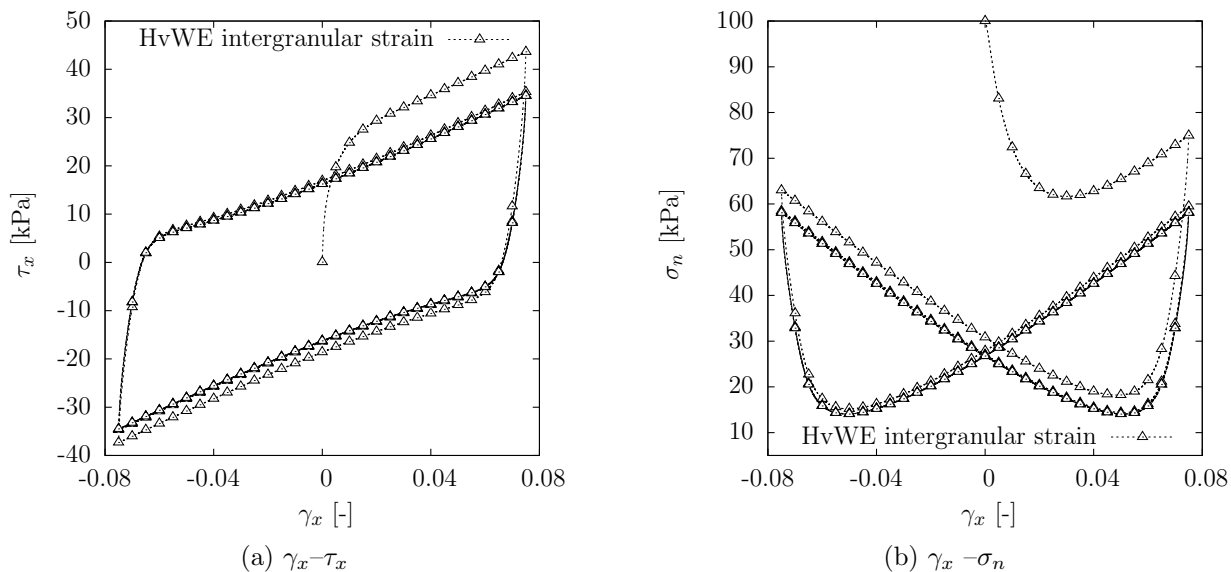


Figure 5.15: Constant volume condition simulation using the HvWE model with intergranular strain

10 cycles of an amplitude of $\gamma_x = \pm 0.075$. The initial void ratio was defined as $e_0 = 0.65$, the applied normal stress was 100 kPa, and $\kappa_r = 1.0$. The results indicated the typical behaviour of undrained cyclic simple shearing. From the first cycles, the ultimate cyclic shear stress dropped until a certain threshold. The results in Figure 5.15b indicate a cyclic stabilization behaviour that is reached after three cycles. The results for the CNL conditions are presented in Figures 5.16a and 5.16b. These were conducted with the same initial parameters; a void ratio of $e_0 = 0.65$, $\sigma_0 = 100$ kPa, and a cyclic shear strain of $\gamma_x = \pm 0.075$.

There was a small peak during the initial loading (Figure 5.16a). This decreased in all subsequent load cycles. The shear stress tended towards a lower limit of 53 kPa. The shear strain γ_x versus normal strain ε_n graph (Figure 5.16b) demonstrates the same behaviour as shown by Uesugi et al. (1989) under two way cyclic loading. The general behaviour of the enhanced hypoplastic interface model (Stutz et al. 2016) was also used with the enhanced intergranular strain concept to model the behaviour of interfaces under cyclic loading. The data from the gravel-solid interfaces tests of Zhang and Zhang (2006) were used for comparison.

Zhang and Zhang (2006) tested homogeneous gravel against a rough steel interface. The behaviour was studied with particle image velocity measurements as well as standard stress and displacement measurements. Figure 5.17a shows result of a CNL test at a normal stress of 700 kPa. The blue dots/lines indicate the first cycle, whereas the black dots/lines show cycle 60. The void ratio was $e_0 = 0.42$, and the roughness coefficient was $\kappa_r = 0.96$.

Upon comparison of the simulation and the test results of Zhang and Zhang (2006) showed a good agreement. The HvWE model with intergranular strain underestimated the stress in the first cycle but agrees reasonably well with the further extension of the stress-deformation path. Figure 5.17b depicts the results for the u_n versus u_x paths. The normal displacement u_n was overestimated, and the simulation and the experiment for cycle 60 shows a discrepancy. This

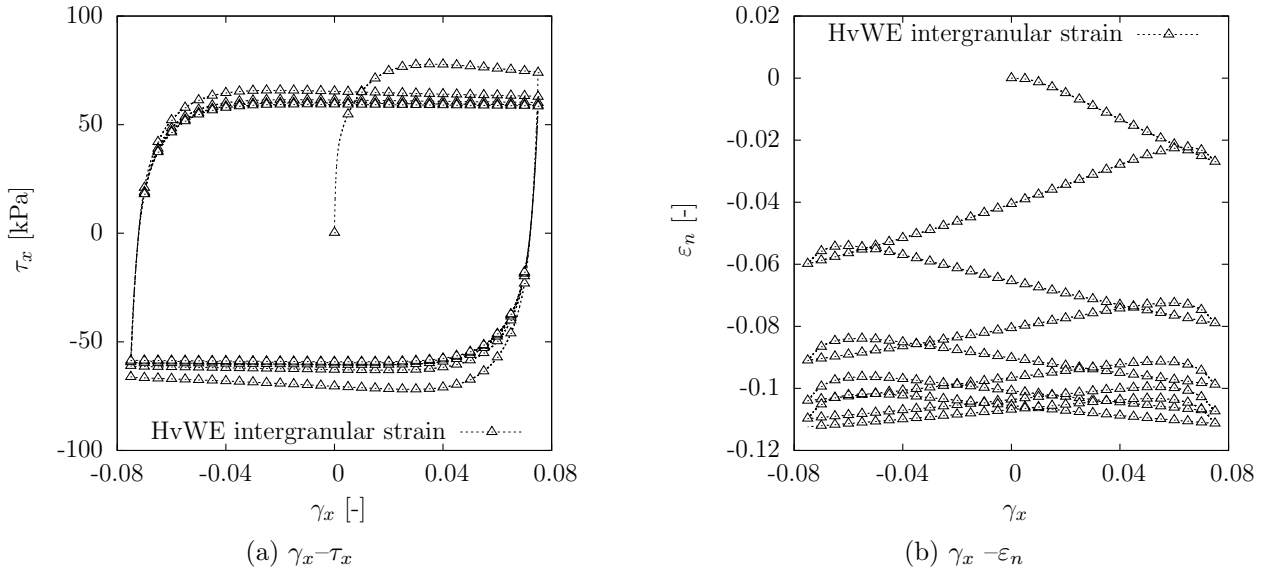


Figure 5.16: Constant Normal Load condition simulation using the HvWE model with intergranular strain

may be because of parameter calibration for the modelling of the interface behaviour. The lack of extensive softening behaviour is typical for gravelly–structure interfaces (Zhang and Zhang 2009).

The results indicated a possibility to use the enhanced intergranular strain concept in conjunction with the HvWE model. The use of the intergranular strain enabled the modelling of the small strain stiffness and cyclic behaviour of interfaces. For high-cyclic modelling of interfaces, an explicit accumulation model as proposed by Burlon et al. (2014) could be used.

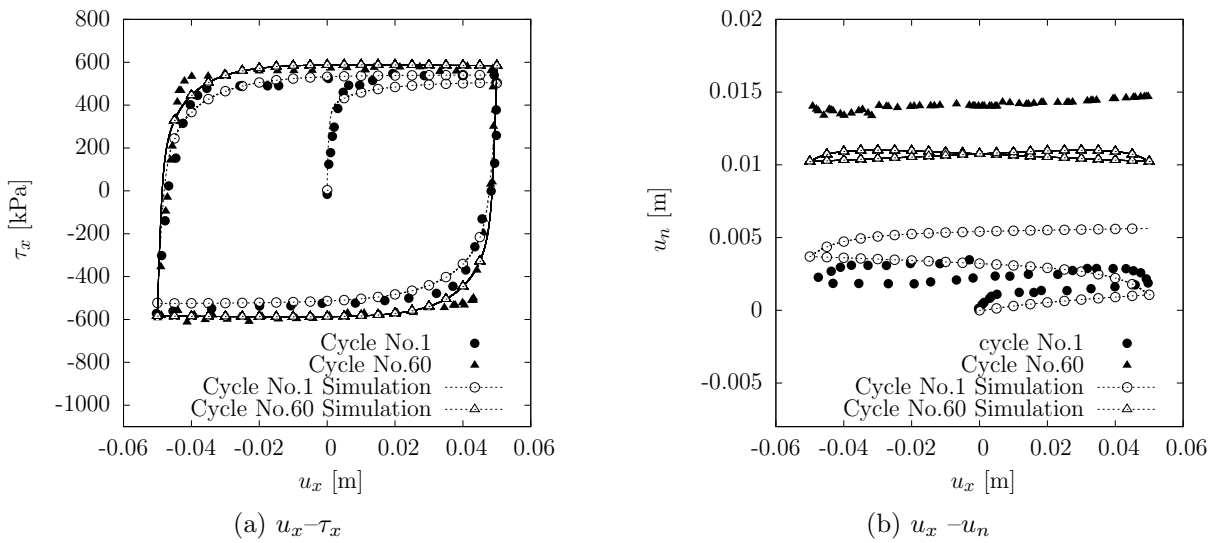


Figure 5.17: Comparison of cyclic test results for Homo-gravel (Zhang and Zhang 2006) and simulations using HvWE intergranular at $\sigma_0 = 700$ kPa

5.8 Summary of Chapter 5

Chapter 5 started with a short summary of the theoretical aspects governed by the behaviour at the soil-structure interface. From this perspective and based on the underlying assumptions it can be concluded that the shearing at the interface is a special case of the simple shear condition for a 3D continuum model. The interface behaviour can be modelled with the standard continuum model, by preserving of the standard tensorial notation with the redefined modified tensorial operators.

First the proposed enhancement of the existing model of Arnold and Herle (2006) was presented followed by an enhanced version of the intergranular strain model. These enhancements are based on the intergranular strain concept interface model of Arnold (2008).

Additional options for modelling the surface roughness are discussed (Gutjahr 2003, Arnold and Herle 2006).

Afterwards, the enhanced model and the enhanced intergranular strain concept were then successfully verified and validated. The enhanced model showed that the continuum and interface model simulated the same results under fully rough conditions the validation also showed a better fit of the models to the experimental data than the model of Arnold and Herle (2006). The proposed model can be used for static and cyclic loading, with the intergranular strain concept. The modelling of the surface roughness can be used to take into account the corrosion or ageing of the surface over the entire lifetime of the geotechnical structure. Grain breakage could be explicitly incorporated into the von Wolffersdorff (1996) hypoplasticity, and the interface models used this as a basis. For example, a first approach could be to implement the stress and history dependent void ratios as done by Engin et al. (2014).

Chapter 6

New hypoplastic models for fine-grained soil-structure interfaces

6.1 Introduction

Chapter 5 proposed an innovative method to derive interface constitutive models by reformulating 3D constitutive models in a simplified and generalized way. As mentioned in Chapter 4, only a small number of clay-interface models exist. The models of Shakir and Zhu (2009) and Cheng et al. (2013) cannot model the complex phenomena at the soil-structure interface in fine-grained soils.

Based on this, it seems necessary to develop novel clay-interface models that can handle the most important mechanical phenomena at the fine-grained soil interface. In this chapter, such interface constitutive models are proposed. The models are reformulated on a basis of the hypoplastic 3D continuum models of Mašín and Khalili (2012) and Mašín (2012; 2013) together with the innovative concept of preserving the existing constitutive description with the mathematical operators proposed in Section 5.4.

In the course of this chapter, the three different models will be examined. The possibilities and limitations will then be addressed.

6.2 New fine-grained hypoplastic interface constitutive model

With respect to the coarse-grained soil modelling, the modelling of fine-grained soils use the hypoplasticity framework was somewhat delayed (Mašín 2006). Herle and Kolymbas (2004) introduced a model with low friction angles. This model acts as basis for the development of the hypoplastic clay model of Mašín (2005). Mašín (2005) proposed a clay hypoplastic model to predict the behaviour of fine-grained soils. These models use the modified hypoplastic formulation proposed by Niemunis (2003). The fourth-order tensor \mathcal{L} , the limiting critical stress

condition, and the hypoplastic flow rule can thus be modified independently of other model components. With respect to the reformulation, the second-order tensor \mathbf{N} was expressed as:

$$\mathbf{N} = \mathcal{L} : \left(-Y \frac{\mathbf{m}}{\|\mathbf{m}\|} \right) \quad (6.1)$$

where Y is the scalar of degree for non-linearity, and \mathbf{m} is a second order tensor, which denotes the hypoplastic flow rule. The model was subsequently extended to explicitly incorporate asymptotic stress states (Mašín 2012; 2013; 2014). The hypoplastic clay models outlined in Mašín (2012) and Mašín (2013) have been adapted to model the behaviour of clay-structure interfaces.

6.2.1 Reference hypoplastic formulation for clay

As described in Section 5.3.1, the general form of the hypoplastic model formulation (Gudehus 1996) is expressed as:

$$\dot{\boldsymbol{\sigma}} = f_s (\mathcal{L} : \dot{\boldsymbol{\varepsilon}} + f_d \mathbf{N} \|\dot{\boldsymbol{\varepsilon}}\|). \quad (6.2)$$

Based on the general form of the hypoplastic constitutive formulation (Equation 6.2), Mašín (2012) developed an alternative expression for the hypoplastic model, which is expressed as:

$$\dot{\boldsymbol{\sigma}} = f_s \mathcal{L} : \dot{\boldsymbol{\varepsilon}} - \frac{f_d}{f_d^A} \mathbf{A} : \mathbf{d} \|\dot{\boldsymbol{\varepsilon}}\| \quad (6.3)$$

where f_d^A describes the value of f_d at the asymptotic state boundary surface (ASBS). \mathbf{A} is defined as:

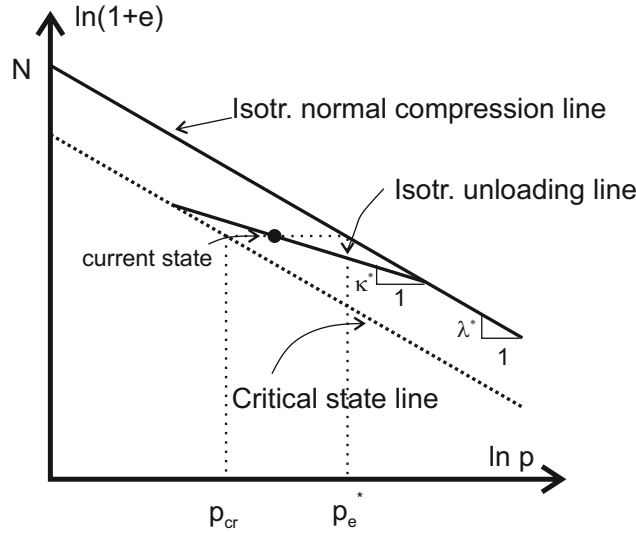
$$\mathbf{A} = f_s \mathcal{L} + \frac{\boldsymbol{\sigma}}{\lambda^*} \otimes \mathbf{1} \quad (6.4)$$

where λ^* is a model parameter. Equation 6.3 enables the use and incorporation of any appropriate arbitrary shape of the asymptotic shape boundary surface by specifying the dependence of f_d^A on the void and stress ratio (Mašín 2012). Equation 6.4 is used to further establish the hypoplastic fine-grained interface models. The general underlying assumptions of the stress and strain rate tensor given in Section 5.4 are valid.

6.2.2 Hypoplastic Cam clay model for interface behaviour

The hypoplastic Cam clay (HCC) model (Mašín 2012) is the first hypoplastic clay model that allows a reformulation to incorporate any arbitrary asymptotic state boundary surface into the model formulation.

Reduced stress (Equation 5.2) and strain tensors (Equation 5.4) with redefined mathematical operators were used to reformulate the HCC (Section 5.5.1). The model, which is briefly intro-


 Figure 6.1: Definition of N , κ^* , λ^* , p_e^* , and p_{cr} from Mašín (2005)

duced, is used as reference model for the hypoplastic interface Cam clay model. The constitutive model equation is written as:

$$\dot{\boldsymbol{\sigma}} = f_s \mathcal{L} : \dot{\boldsymbol{\varepsilon}} - \left(\frac{p}{p_e^*} \right) \frac{M^2 + \eta^2}{M^2} \left(f_s \mathcal{L} + \frac{\boldsymbol{\sigma}}{\lambda^*} \otimes \mathbf{1} \right) : \mathbf{d} \|\dot{\boldsymbol{\varepsilon}}\| \quad (6.5)$$

where \mathbf{d} is defined as the asymptotic strain rate direction, and the fourth order constitutive tensor \mathcal{L} represents isotropic elasticity. \mathcal{L} is expressed as:

$$\mathcal{L} = \mathbf{I} + \frac{\nu}{1 - 2\nu} \mathbf{1} \otimes \mathbf{1} \quad (6.6)$$

where the parameter ν controls the proportion of the shear and bulk stiffness. The Hvorslev equivalent pressure p_e^* is defined in Equation 6.7:

$$p_e^* = p_r \exp \left[\frac{N - \ln(1 + e)}{\lambda^*} \right] \quad (6.7)$$

where p_r is the reference stress of 1 kPa. N and λ^* are model parameters, and M is the slope of the critical state line in the p - q plane. The deviatoric invariant is defined as $q = \sqrt{\frac{3}{2}} \|\boldsymbol{\sigma}^*\|$. The stress ratio is expressed as $\eta = \frac{q}{p}$. Following the modified Cam clay formulation, the asymptotic strain rate direction \mathbf{d} is assumed to be normal to the ASBS. The asymptotic strain rate direction \mathbf{d} is expressed as:

$$\mathbf{d} = \frac{3\boldsymbol{\sigma}^* - \mathbf{1}p \frac{M^2 - \eta^2}{3}}{\|3\boldsymbol{\sigma}^* - \mathbf{1}p \frac{M^2 - \eta^2}{3}\|} \quad (6.8)$$

The barotropy factor f_s is expressed as:

$$f_s = \frac{3p}{2} \left(\frac{1}{\lambda^*} + \frac{1}{\kappa^*} \right) \frac{1 - 2\nu}{1 + \nu}. \quad (6.9)$$

The hypoplastic Cam clay model uses the same parameters as the modified Cam clay model in which the slope of the critical state line M is calculated with the critical state friction angle:

$$M = \frac{6 \sin \varphi_c}{3 - \sin \varphi_c}. \quad (6.10)$$

The parameter λ^* is the slope of the isotropic normal compression line in $\ln(1 + e)$ versus $\ln(p)$, and κ^* controls the unloading line in the same plane. N is the value of $\ln(1 + e)$ at the isotropic normal compression line for $p = p_r = 1$ kPa, and ν controls the shear stiffness. Figure 6.1 illustrates the physical meaning of the different model parameters. The void ratio e and $\boldsymbol{\sigma}$ are also used as primary state variables.

6.2.3 Clay hypoplasticity interface model with advanced asymptotic state boundary surface

As already mentioned, the hypoplastic clay model is the parent model for reformulating the model as a hypoplastic interface model. Based on the clay hypoplasticity model (Mašín 2005) with explicitly defined asymptotic states (Mašín 2013), the corresponding interface constitutive model is derived with the reduced stress and strain rate tensors. The model of Mašín (2013) corrects several shortcomings in the original model formulation (Mašín 2005). The model uses the general formulation of hypoplasticity with explicitly defined asymptotic states (Equation 6.3). There are, however some differences from the hypoplastic Cam clay model (Mašín 2012), the constitutive tensors \mathcal{L} , f_s , and \mathbf{A} are identical to the model presented in Section 6.2.2. f_d was modified by Mašín (2013) and expressed as:

$$f_d = \left(\frac{2p}{p_e} \right)^{\alpha_f}, \quad (6.11)$$

where the exponent α_f controls the irreversible deformation inside the ASBS. Alternatively, Mašín (2014) suggested α_f from the previous model (Mašín 2005), which improved the prediction of the model response. α_f can also be treated as an independent parameter (Mašín 2005) to control the non-linear response inside the ASBS.

$$\alpha_f = \frac{\ln \left(\frac{\lambda^* - \kappa^*}{\lambda^* + \kappa^*} \left(\frac{3 + a_f^2}{a_f \sqrt{3}} \right) \right)}{\ln(2)}, \quad (6.12)$$

where a_f is expressed as:

$$a_f = \frac{\sqrt{3}(3 - \sin \varphi_c)}{2\sqrt{2} \sin \varphi_c}. \quad (6.13)$$

The factor f_d^A is the limiting value of f_d at the ASBS. f_d^A is defined as:

$$f_d^A = 2^{\alpha_f} (1 - F_m)^{\alpha_f/\omega_h}, \quad (6.14)$$

where the exponent ω_h is expressed as:

$$\omega_h = -\frac{\ln(\cos^2 \varphi_c)}{\ln(2)} + a_f (F_m - \sin^2 \varphi_c). \quad (6.15)$$

The factor F_m (Matsuoka and Nakai 1974) is expressed as:

$$F_m = \frac{9I_3 + I_1I_2}{I_3 + I_1I_2} \quad (6.16)$$

To calculate the Matsuoka-Nakai factor, the following invariants are required:

$$I_1 = \text{tr} \boldsymbol{\sigma}; \quad I_2 = \frac{1}{2} [\boldsymbol{\sigma} : \boldsymbol{\sigma} - (I_1)^2]; \quad I_3 = \det \boldsymbol{\sigma} \quad (6.17)$$

with the Lode angle θ , which is defined in Equation 5.11. The asymptotic strain rate direction \mathbf{d} is expressed as:

$$\mathbf{d} = \frac{\mathbf{d}^A}{\|\mathbf{d}^A\|} \quad (6.18)$$

where \mathbf{d}^A is defined as:

$$\mathbf{d}^A = -\hat{\boldsymbol{\sigma}}^* + \mathbf{1} \left[\frac{2}{3} - \frac{1}{4} F_m^{1/4} \right] \frac{F_m^{\xi/2} - \sin^\xi \varphi_c}{1 - \sin^\xi \varphi_c}. \quad (6.19)$$

ξ controls the ratio of the volumetric strain to the shear strain. Mašín (2013) obtained this using an optimisation procedure to ensure that the stretching rate direction approximately satisfied the Jaky formula (Jaky 1948):

$$\xi = 1.7 + 3.9 \sin^2 \varphi_c \quad (6.20)$$

Using the novel reformulation method (Section 5.4) combining all components for the hypoplastic model with explicitly defined asymptotic states (Equation 6.3) led to the new hypoplastic interface model.

The model requires five parameters: φ_c the critical state friction angle, λ^* , κ^* , N , and ν (Section 6.2.2).

6.2.4 Extension of the interface model for surface roughness

The approach suggested by Arnold and Herle (2006) was used to incorporate the surface roughness into the HCC and HCE models κ_r is the friction coefficient, which can be calculated in dependence of the surface traction profile of the structural element that is in contact with the surrounding soil. If the surface condition is not completely rough, the frictional coefficient $\varphi_{interface} \leq \varphi_{soil}$ and the value of κ_r can be calculated as:

$$\kappa_r = \frac{\varphi_{interface}}{\varphi_{soil}}. \quad (6.21)$$

κ_r is introduced in the HCC model by modifying parameter M for the critical state line as follows:

$$M = \frac{6 \sin(\varphi_c \kappa_r)}{3 - \sin(\varphi_c \kappa_r)}. \quad (6.22)$$

As described in Section 5.5.2, Arnold and Herle (2006) suggested a reduction of the barotropy factor f_s of the hypoplastic model in order to decrease the predicted soil stiffness. This modelling approach was thought to alter the shear and compression stiffness.

An alternative way to model the surface roughness was proposed by Stutz and Mašín (2016). By using the hypoplastic model (Mašín 2013), the shortcoming is reducing the response in shear can be overcome. The formulation originally proposed in Herle and Kolymbas (2004) was adopted by Mašín (2005) and used to model the interface surface roughness. The shear stiffness is governed by the variable r . In clay hypoplasticity, the value of r is equal to:

$$r = \frac{4}{3} \frac{\kappa^*}{\lambda^* + \kappa^*} \frac{1 + \nu}{1 - 2\nu}. \quad (6.23)$$

The value of r for the reduced shear stiffness (denoted as r_r) is expressed as:

$$r_r = \frac{4\kappa_r}{3} \frac{\kappa^*}{\lambda^* + \kappa^*} \frac{1 + \nu}{1 - 2\nu} \quad (6.24)$$

and the value of ν_r used in the modified model in place of ν is expressed as:

$$\nu_r = \frac{3r_r (\lambda^* + \kappa^*) - 4\kappa^*}{6r_r (\lambda^* + \kappa^*) + 4\kappa^*}. \quad (6.25)$$

In the HCE model, the same equations are adapted to implement structural surface roughness. a_f is also modified as follows:

$$a_{fm} = \frac{\sqrt{3}(3 - \sin \varphi_c \kappa_r)}{2\sqrt{2} \sin \varphi_c \kappa_r}. \quad (6.26)$$

ω_h adapted for the surface roughness extension is expressed as:

$$\omega_r = -\frac{\ln(\cos^2 \varphi_c \kappa_r)}{\ln(2)} + a_{fm} (F_m - \sin^2 \varphi_c \kappa_r), \quad (6.27)$$

and the modified asymptotic strain rate direction \mathbf{d}^A is expressed as:

$$\mathbf{d}^A = -\hat{\boldsymbol{\sigma}}^* + \mathbf{1} \left[\frac{2}{3} - \frac{1}{4} F_m^{1/4} \right] \frac{F_m^{\xi/2} - \sin^\xi \varphi_c \kappa_r}{1 - \sin^\xi \varphi_c \kappa_r}. \quad (6.28)$$

In addition to fine- and coarse grained soils other advanced hypoplastic models can be used to model complex effects for the constitutive interface modelling. These will be described below.

6.3 Thermo-hypoplastic interface model for partially saturated soils

The thermo-mechanical hypoplastic model for variable saturated soils was developed by Mašín and Khalili (2012). The model is formulated on the basis of the hypoplastic model for clays (Mašín 2005) and the hypoplastic model for unsaturated fine-grained soils (Mašín and Khalili 2008). These models are able to predict unsaturated soil behaviour. The model of Mašín and Khalili (2012) can also predict the thermo-mechanical behaviour of unsaturated soil. The first version as thermo-mechanical model was proposed by Stutz et al. (2016). As mentioned in Section 2.4, temperature and variable saturation affect the behaviour of the interface in various ways. The model is therefore used to reformulate the constitutive soil model into a thermo-hydro-mechanical interface model. The stress-strain rate hypoplastic equation is given in Equation 6.2.

The thermo-mechanical model will be briefly introduced. The stress-strain rate equation for the thermo-mechanical and variably saturated soil is defined as:

$$\dot{\boldsymbol{\sigma}} = f_s (\mathcal{L} : (\dot{\boldsymbol{\epsilon}} - \dot{\boldsymbol{\epsilon}}^{TE}) + f_d \mathbf{N} \| (\dot{\boldsymbol{\epsilon}} - \dot{\boldsymbol{\epsilon}}^{TE}) \|) + f_u (H_t + H_s) \quad (6.29)$$

where $\boldsymbol{\sigma}$ and $\dot{\boldsymbol{\sigma}}$ are the effective stress and objective effective stress rate tensors. These are defined as:

$$\boldsymbol{\sigma} = \boldsymbol{\sigma}^{net} - \chi_s s \mathbf{1} \quad ; \quad \dot{\boldsymbol{\sigma}} = \dot{\boldsymbol{\sigma}}^{net} - \psi \dot{s} \mathbf{1} \quad (6.30)$$

where $\boldsymbol{\sigma}^{net} = \boldsymbol{\sigma}^{tot} + u_a \mathbf{1}$ is a net stress, $\boldsymbol{\sigma}^{tot}$ is a total stress tensor, u_a is the pore air pressure, u_w is the pore water pressure, and s is the matrix suction defined as $s = u_a - u_w$. The effective stress factor χ_s defined by Khalili and Khabbaz (1998) is expressed as:

$$\chi_s = \begin{cases} 1 & \text{for } s < s_e \\ \frac{s_e^\gamma}{s} & \text{for } s \geq s_e \end{cases}, \quad (6.31)$$

where s_e is a model parameter and $\gamma = 0.55$. The parameter ψ is defined as $\psi = (1 - \gamma)\chi_s$ or $\psi = 1$. The temperature related strain is expressed as:

$$\dot{\boldsymbol{\epsilon}}^{TE} = \frac{1}{3}\alpha_s \dot{T}, \quad (6.32)$$

where α_s is a model parameter and \dot{T} is the rate of temperature. The constitutive \mathcal{L} tensor is expressed as:

$$\mathcal{L} = 3(c_1 \mathcal{I} + c_2 a^2 \hat{\boldsymbol{\sigma}} \otimes \hat{\boldsymbol{\sigma}}), \quad (6.33)$$

where $\hat{\boldsymbol{\sigma}} = \boldsymbol{\sigma}/\text{tr}\boldsymbol{\sigma}$, the two scalars defined in Herle and Kolymbas (2004) and modified by Mašín (2005) are expressed as:

$$c_1 = \frac{2(3 + a^2 - 2^\alpha a \sqrt{3})}{9r}; \quad c_2 = 1 + (1 - c_1) \frac{3}{a^2}, \quad (6.34)$$

where r is a model parameter and a are scalars defined as:

$$a = \frac{\sqrt{3}(3 - \sin \varphi_c)}{2\sqrt{2}\varphi_c} \quad (6.35)$$

and α as:

$$\alpha = \frac{1}{\ln 2} \ln \left[\frac{\lambda^* - \kappa^*}{\lambda^* + \kappa^*} \left(\frac{3 + a^2}{a\sqrt{3}} \right) \right]. \quad (6.36)$$

The second order constitutive tensor \mathcal{N} is expressed as:

$$\mathbf{N} = \mathcal{L} : \left(-Y \frac{\mathbf{m}}{\|\mathbf{m}\|} \right) \quad (6.37)$$

where $Y = 1$ coincides with the critical stress condition of the Matsunoka–Nakai formulation. Y is defined as:

$$Y = \left(\frac{\sqrt{3a}}{3 + a^2} - 1 \right) \frac{(I_1 I_2 + 9I_3)(1 - \sin^2 \varphi_c)}{8I_3 \sin^2 \varphi_c} + \frac{\sqrt{3a}}{3 + a^2}. \quad (6.38)$$

The second order tensor \mathbf{m} is expressed as:

$$\mathbf{m} = -\frac{a}{F} \left[\hat{\boldsymbol{\sigma}} + \text{dev} \hat{\boldsymbol{\sigma}} - \frac{\hat{\boldsymbol{\sigma}}}{3} \left(\frac{6\hat{\boldsymbol{\sigma}} : \hat{\boldsymbol{\sigma}} - 1}{(F/a)^2 + \hat{\boldsymbol{\sigma}} : \hat{\boldsymbol{\sigma}}} \right) \right] \quad (6.39)$$

using the factor F , which is expressed as:

$$F = \sqrt{\frac{1}{8} \tan^2 \psi + \frac{2 - \tan^2 \psi}{2 + \sqrt{2} \tan \psi \cos 3\theta}} - \frac{1}{2\sqrt{2}} \tan \psi. \quad (6.40)$$

The barotropy factor f_s is calculated as:

$$f_s = \frac{3p}{\lambda^*(s, T)} \left(3 + a^2 - 2^\alpha a \sqrt{3} \right)^{-1} \quad (6.41)$$

and the pyknotropy factor as:

$$f_d = \left(\frac{2p}{p_e} \right)^\alpha \quad (6.42)$$

with

$$p_e = p_r \exp \left[\frac{N(s, T) - \ln(1 + e)}{\lambda^*(s, T)} \right], \quad (6.43)$$

where the reference pressure $p_r = 1$ kPa. The temperature-dependent values of $\lambda^*(s, T)$, and $N(s, T)$ are defined as:

$$\lambda^*(s, T) = \lambda^* + l_t \ln \left(\frac{T}{T_0} \right) + l_s \left\langle \ln \frac{s}{s_e} \right\rangle \quad (6.44)$$

and

$$N(s, T) = N + n_t \ln \left(\frac{T}{T_0} \right) + n_s \left\langle \ln \frac{s}{s_e} \right\rangle, \quad (6.45)$$

where N , λ^* , l_s , n_s , l_t , and n_t are model parameters. The tensorial terms H_T are expressed as:

$$H_T = -c_i \frac{\boldsymbol{\sigma}}{T \lambda^*(s, T)} \left[n_t - l_t \ln \frac{p_e}{p_r} \right] \langle \dot{T} \rangle \quad (6.46)$$

where

$$c_i = \frac{3 + a^2 - f_d a \sqrt{3}}{3 + a^2 - f_d^{SBS} a \sqrt{3}} \quad (6.47)$$

The tensorial term for the suction is defined as:

$$H_s = -c_i \frac{\boldsymbol{\sigma}}{s \lambda^*(s, T)} \left[n_s - l_s \ln \frac{p_e}{p_r} \right] \langle -\dot{s} \rangle. \quad (6.48)$$

The value of the pyknotropy factor f_d for states at the SBS was defined by Mašín and Herle (2005) as:

$$f_d^{SBS} = \|f_s \mathcal{A}^{-1} : N\|^{-1} \quad (6.49)$$

The fourth order tensor \mathcal{A} is expressed as:

$$\mathcal{A} = f_s \mathcal{L} - \frac{1}{\lambda^*(s, T)} \boldsymbol{\sigma} \otimes \mathbf{1} \quad (6.50)$$

the collapsible behaviour is controlled by f_u , which is expressed as:

$$f_u = \left(\frac{f_d}{f_d^{SBS}} \right)^{m/\alpha}. \quad (6.51)$$

Finally, the evolution of the state variable e (void ratio) expressed as:

$$\dot{e} = (1 + e) \operatorname{tr} (\dot{\boldsymbol{\epsilon}} - \dot{\boldsymbol{\epsilon}}^{TE}). \quad (6.52)$$

The model of Mašín and Khalili (2012) described above can be used as interface model using the reduced stress and strain rate vectors with the redefined mathematical operators and the surface roughness approach (Section 6.2.4).

6.4 Validation of the new hypoplastic clay-structure interface models

The models are verified and validated using constant volume, constant normal load, and constant normal stiffness test simulations. Experimental data from illitic clay (Littleton 1976), Kawasaki clay (Tsubakihara and Kishida 1993), and a Kaolin clay (Sun et al. 2003) was used to compare the models.

The two different hypoplastic fine-grained interface models were validated with the parameters given in Table 6.1. These are artificial parameters used in Mašín and Khalili (2012) and Mašín (2013). The HCC model uses parameter M calculated from Equation 6.22 for mutual comparability. It is important to note that the parameter N is the value of $\ln(1 + e)$ for $p = p_r = 1$ kPa in the following.

Table 6.1: Parameters for the evaluation of HCC and HCE interface models

Parameters	Hypoplastic Cam clay (HCC)	explicit Hypo-plastic clay model (HCE)
λ^*	0.1	0.1
κ^*	0.01	0.01
ν	0.2	0.2
M/φ_c	0.98	25
N	1.0	1.0
κ_r	1.0	1.0

6.4.1 Model verification

The model implemented in MATLAB was verified (Figure 6.2). The stress path resulting from the use of the reduced stress and strain tensor proposed by Arnold and Herle (2006) is shown in Figure 6.2.

It is obvious that the reduced stress and strain rate tensors of Arnold and Herle (2006) do not produce the same stress strain path as the enhanced version of the reduced stress and strain tensors proposed by Stutz et al. (2016).

The enhanced reduced stress and strain tensors coincide with the fully 3D formulation of the hypoplastic clay model with an explicitly defined asymptotic state. This can be explained by the use of in-plane stresses σ_p in the enhanced formulation of the model.

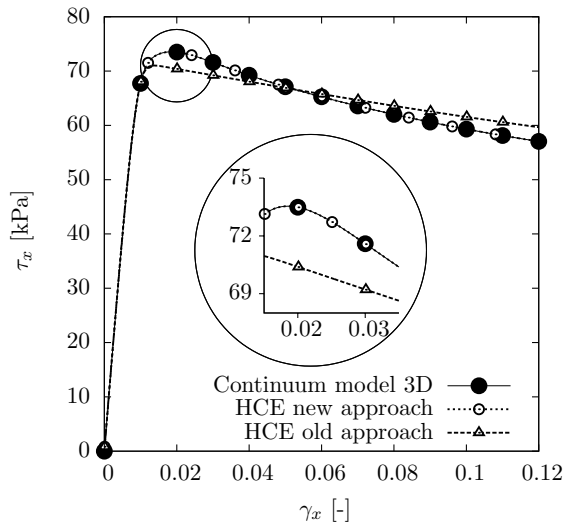


Figure 6.2: Verification of the MATLAB implementation compared to TRIAX

6.4.2 Testing the clay interface models behaviour

The model behaviour of the fine-grained hypoplastic interface models is simulated below using three boundary conditions.

Constant volume simulation

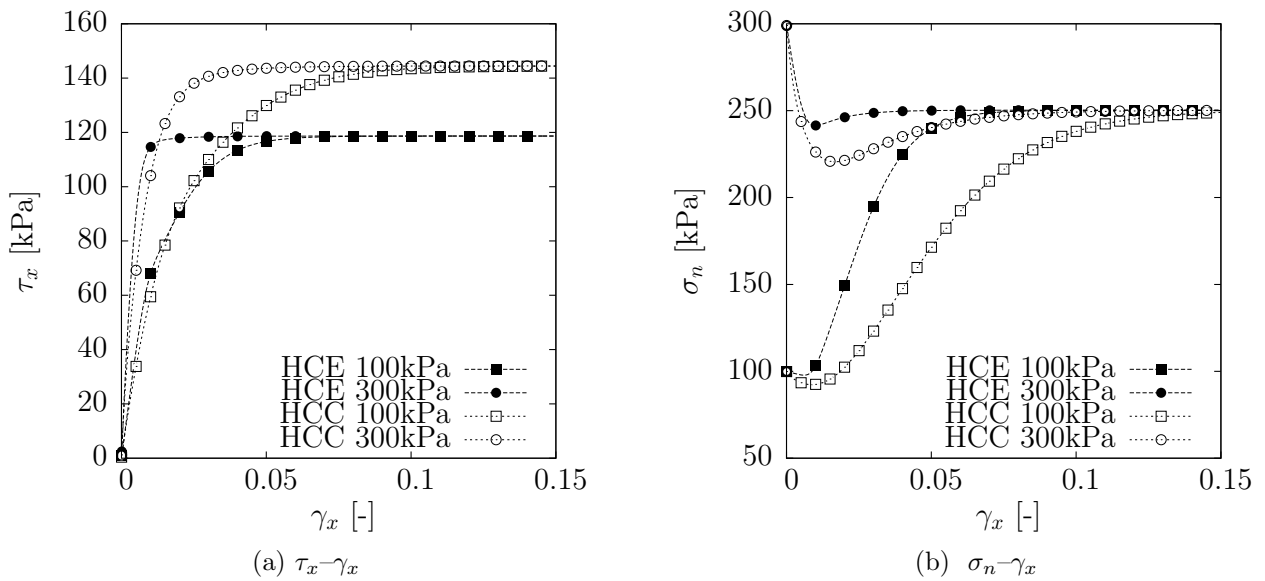


Figure 6.3: Stress path for Constant Volume boundary conditions for the Hypoplastic Cam clay (HCC) and extended clay Hypoplastic model (HCE) interface models for fine-grained soils

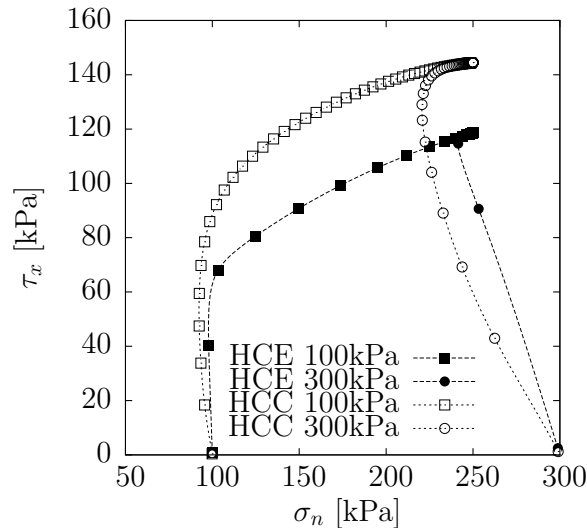


Figure 6.4: Stress path for Constant Volume boundary conditions: shear stress τ_x versus normal stress σ_t for the Hypoplastic Cam clay (HCC) and extended clay Hypoplastic model (HCE) interface models for fine-grained soils

The parameters from Table 6.1 were used to verify constitutive interface models under CV conditions. The CV test conditions are often referred as undrained behaviour ($\dot{\epsilon}_t = 0$) of the interface. $\dot{\epsilon}_t = 0$ implies a constant void ratio $\dot{e} = 0$.

The simulations for the comparison were carried out with two different applied normal stresses 100 and 300 kPa. Figure 6.3a shows the shear stress τ_x versus shear strain γ_x results, Figure 6.3b shows the normal stress σ_t versus shear strain γ_x results and Figure 6.4 shows the normal stress σ_t versus shear strain τ_x path of the interface. The HCE model clearly predicted a lower final shear stress than the HCC model, although the models were calibrated to have the same critical state friction angle. These differences arose from the more advanced shape of the ASBS in the HCE model with the Matsuoka-Nakai deviatoric cross-section. The HCE model predicts a lower critical state stress ratios because of the Lode angles in shear tests. These differed from the Lode angles associated with triaxial compression tests.

The behaviour was typically associated with undrained (Constant Volume) conditions as shown by Tsubakihara and Kishida (1993) and Sun et al. (2003).

Constant normal load simulation

The simple shear conditions were validated (Figures 6.5a and 6.5b). Figure 6.5a shows the shear deformation γ_x versus shear stress τ_x behaviour. Both models showed the same trend but differed in the critical shear stress. Both models had a similar stress path at small shear deformations.

At high pressures (300 kPa), the behaviour of the normal strain $\dot{\epsilon}_t$ to the shear strain γ_x tend to be identical (Figure 6.5b). However, the behaviour at lower pressures (100 kPa) was different for both models. The normal strain rate in the HCE model was higher than in the HCC model. As already mentioned, the differences in the Lode angle and the more advanced shape of the

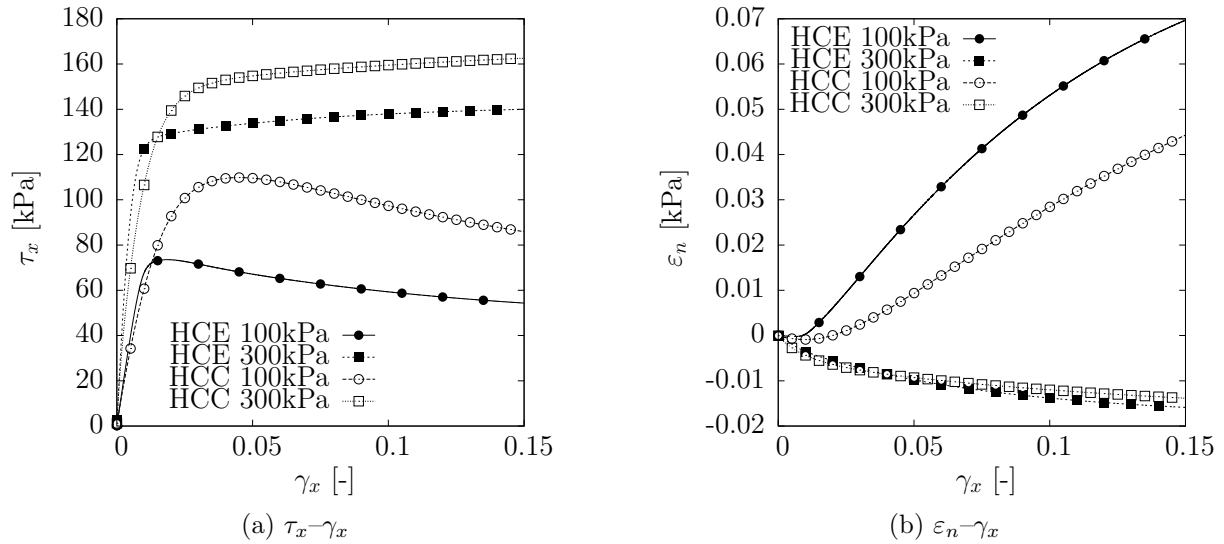


Figure 6.5: Constant Normal Load conditions for the Hypoplastic Cam clay (HCC) and extended clay Hypoplastic model (HCE) interface models for fine-grained soils

asymptotic state boundary surface (HCE) were the reason for the discrepancies between the two models.

Constant normal stiffness simulation

The first simulation was conducted with an applied stiffness K of 100 kPa and the second with 1000 kPa (Figures 6.6a and 6.6b).

As mentioned in Section 2.3, the shear stress and the normal stress evolution increased with increasing normal stiffness. Under CNS conditions, the HCE model typically showed a stiffer response than the HCC model. This was the result of the critical state parameter M . However, the models showed the expected trend for the CNS boundary condition. The differences are explained above.

6.4.3 Comparison of surface roughness modelling approaches for fine-grained interfaces

Explicit modelling of the surface roughness was introduced in Section 6.2.4. This development was compared to the approach of Arnold and Herle (2006). With $\kappa_r \leq 1$, the behaviour should tend to a softer response at the interface rather than using fully rough conditions with $\kappa_r = 1.0$. The surface roughness extension for both models was examined by using different κ_r . The evaluation parameters from Table 6.1 were used.

The three different κ_r values used were 1.0, 0.75, and 0.5. In the τ_x versus γ_x simulations, both models showed a softer response for $\kappa_r < 1.0$ (Figure 6.7a). The surface extension for the HCC and HCE models was able to incorporate the effect of surface roughness as expected. The surface roughness approach was handled differently than in the granular structure interface

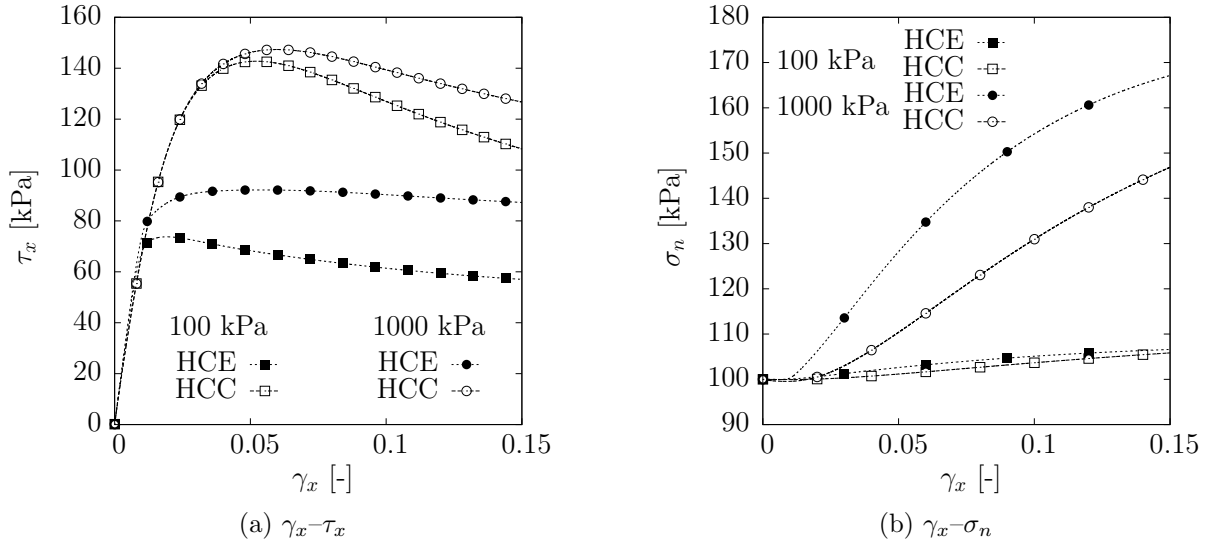
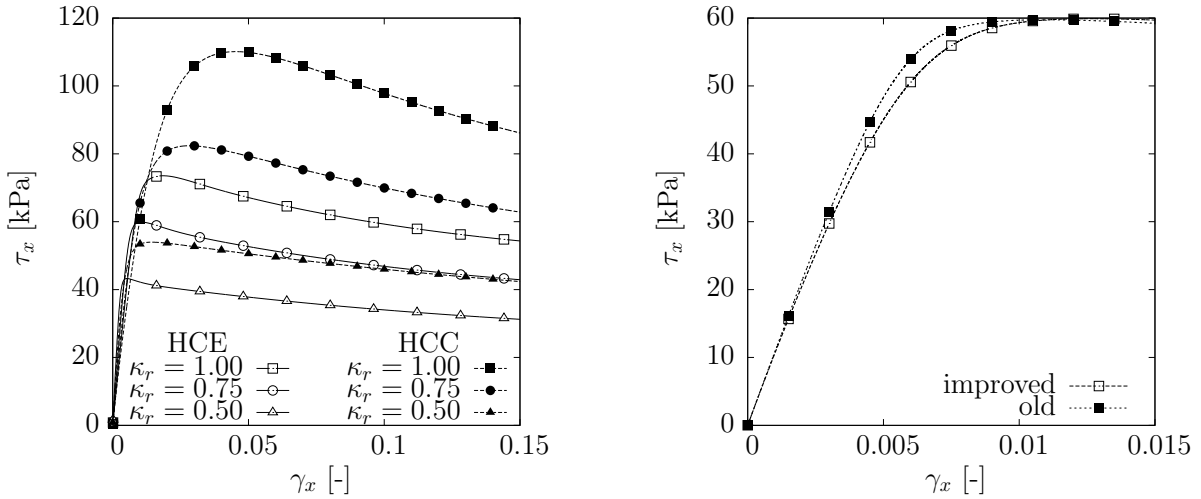


Figure 6.6: Constant Normal Stiffness conditions: the Hypoplastic Cam clay (HCC) and extended clay Hypoplastic model (HCE) interface models for fine-grained soils



(a) Comparison of Constant Normal Stress path with varying roughness factors for HCE and HCC interface models

(b) Comparison of Arnold and Herle (2006) and proposed approach by Stutz and Mašín (2016)

Figure 6.7: Results for the surface approach of Arnold and Herle (2006) and the proposed of Stutz and Mašín (2016)

Table 6.2: Parameters of the hypoplastic interface models used in the simulations

Soils	λ^*	κ^*	ν	ϕ_c	N	κ_r
Illitic clay (Littleton 1976)	0.06	0.04	0.45	20	0.8	0.79
Clay S0 (HCE) (Tsubakihara and Kishida 1993)	0.11	0.08	0.3	27.5	1.26	0.83/0.73/0.56
Clay S0 (HCC) (Tsubakihara and Kishida 1993)	0.05	0.03	0.2	27.5	0.84	0.83/0.73/0.56
Clay S4 (HCE) (Tsubakihara and Kishida 1993)	0.105	0.085	0.2	29	0.88	0.83
Clay S4 (HCC) (Tsubakihara and Kishida 1993)	0.043	0.029	0.2	29	0.8	0.83
Kaolin clay (Sun et al. 2003)	0.11	0.02	0.2	22.5	1.03	0.75

hypoplastic model (cf. Figure 6.7b) is shown. The surface roughness extension proposed by Stutz and Mašin (2016) reduced the stiffness in the small strain regime.

6.4.4 Comparison of simulated with experimental interface behaviour

The ability to model different clay-interfaces is shown for the hypoplastic Cam clay (HCC) and extended Hypoplastic (HCE) model and compared with experimental data. The data from Littleton (1976) and Tsubakihara and Kishida (1993) was used to compare the HCC and HCE models under constant normal load conditions. Data from Sun et al. (2003) was used to compare experimental to simulation results under constant volume conditions.

The parameters are given in Table 6.2, and the clay properties are summarized in Table 6.3. For the clays used in this section, the hypoplastic parameters were not available. The physical

Table 6.3: Properties of the different clays

Properties	Illitic clay Littleton (1976)	Kawasaki clay Tsubakihara and Kishida (1993)	Kaolin clay Sun et al. (2003)
Plastic limit [%]	30.0	48.1	40.3
Liquid Limit [%]	83.0	86.0	75.3
Density ρ_s [g/m^3]	2.61	2.65	2.70

properties were therefore used to estimate a best fit with experimental observations.

Simulations of the experimental data from Littleton (1976)

Littleton (1976) performed a modified direct shear test on two different clays. The lower part of the box was replaced with a solid mild steel block. The average roughness was $0.18 \mu\text{m}$ in the centre line of the block. The cut-off length was 0.84 mm. The shear box was used in a modified and conventional manner in order to find the internal (soil-soil) and external (soil-solid) frictional shear strength (Littleton 1976). Littleton (1976) used Kaolin clay and illitic

clay. The results from the illitic clay were used for verification. The illitic clay was mixed to a

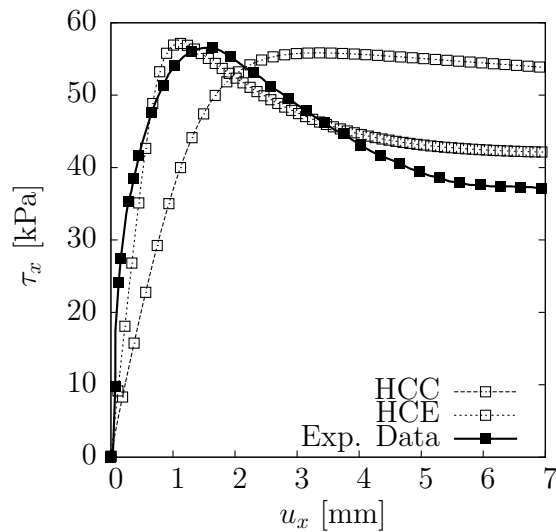


Figure 6.8: Verification using the experimental data of Littleton (1976)

moisture content of 90%. The clay was consolidated under a gradually increasing load to ensure that 95 % of the consolidation had taken place before testing. The verification parameters are listed in Table 6.2. The vertical load of the test was 626 N, which is equivalent to a vertical applied stress of 173 kPa. The illitic clay and the solid mild steel block showed typical behaviour of clay interfaces i.e. a higher peak at smaller displacements and lower residual shear strength at displacements larger than in soil–soil direct shear tests. The experimental behaviour was quantitatively simulated with both the HCC and HCE models (Figure 6.8). The HCC model showed a higher peak shear stress than the HCE model. This unexpected behaviour was unexpected because one parameter set was used for both models. It was anticipated that one hypoplastic parameter set would be satisfactory to validate both models. However, the simulations using the HCC model could clearly be improved with a different set of parameters. In summary, both the HCC and HCE models were able to simulate the interface behaviour of illitic clay after calibration.

Simulation of the experimental data from Kawasaki clay (Tsubakihara and Kishida 1993)

Tsubakihara and Kishida (1993) used simple and direct shear devices for constant normal stress tests of Kawasaki clay to study the effect of surface roughness and determine how the different test devices influence the interface frictional behaviour. The soils used were reconstituted Kawasaki marine clay (S0) and Kawasaki marine clay mixed with Toyoura sand (S4) (Table 6.3). The samples were consolidated at 294.4 kPa and 98 kPa respectively. After applying a vertical consolidation pressure, the stress was held constant (constant normal load condition). Low-carbon steel was used as construction material in the apparatus, and the surface roughness was investigated and measured. The experimental data used to compare the HCE and HCC models was taken from the simple shear testing device under CNL conditions (Tsubakihara and Kishida 1993).

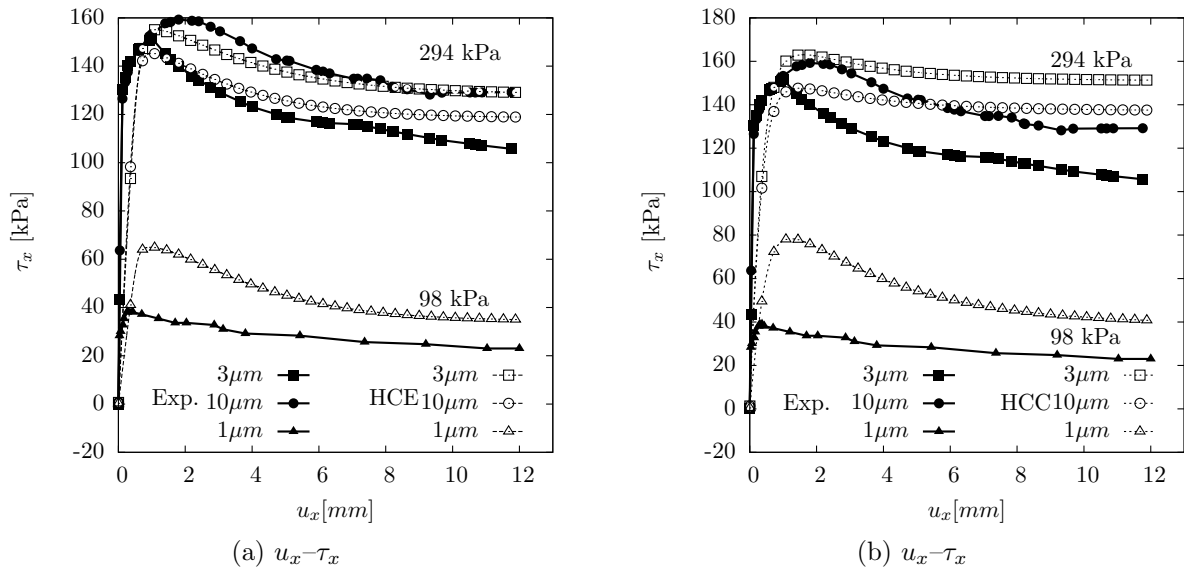


Figure 6.9: Comparison for the HCE (a) and HCC (b) model using the experimental data for Kawasaki marine clay (S0)

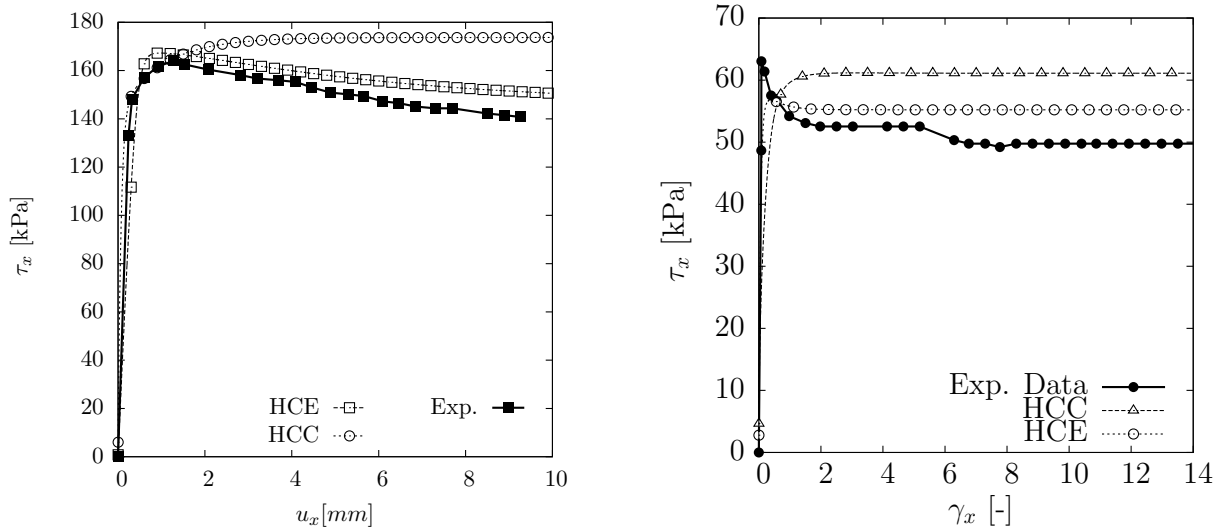
Different parameters sets in the HCE and HCC models were used to demonstrate the simulation capability. The different model parameter sets are given in Table 6.3. The roughness coefficients used in both models are $\kappa_r = 0.83$ for $10 \mu\text{m}$ and $\kappa_r = 0.73$ for $3 \mu\text{m}$ at a constant normal load of 294 kPa. For the calculation at a constant normal load of 98 kPa, κ_r was 0.65.

From the shear stress experiments of Tsubakihara and Kishida (1993), three different experimental results were compared (Figure 6.9a). All three different experiments had a stiff initial response and a peak after a small hardening behaviour. The HCE model was able to simulate the results of Tsubakihara et al. (1993). There was a good match between the experimental data and the simulation results for all normal loads and different roughness values. The results for the HCC model (Figure 6.9b) were similar. The simulations showed a small degree of overestimation compared with the experimental data. Both the HCC and HCE model were able to reproduce the behaviour of the experimental data reported by Tsubakihara and Kishida (1993) and Tsubakihara and Kishida (1993).

Both models were used to simulate the experimental results for a mixture of Kawasaki clay and Toyoura sand (S4) (Figure 6.10a). Tsubakihara and Kishida (1993) applied a constant load of 294 kPa. As already mentioned, the HCC and HCE models were able to simulate the experimental results with sufficient accordance.

Clay-Interface undrained shear tests from Sun et al. (2003)

Sun et al. (2003) conducted tests with a modified direct shear apparatus under constant volume conditions with different clay sand mixtures and varying roughness of the steel plates. The data for pure Kaolin clay was used for verification. This clay was tested under normal consolidated conditions at a consolidation pressure of 98 kPa. Low-carbon steel was used as the structural surface.



(a) Validation used the experimental data of Tsubakihara and Kishida (1993)

(b) Validation used the experimental data of Sun et al. (2003)

Figure 6.10: Validation of clay interface models with experimental data from Tsubakihara and Kishida (1993), Sun et al. (2003)

The effects of the consolidation ratio, surface roughness and, shearing rate were recorded by Sun et al. (2003). In the experimental data, the consolidation pressure was 400 kPa, and the shearing rate was 1 mm/min. This shearing rate was the lowest applied by Sun et al. (2003). The experimental results of Sun et al. (2003) were modelled (Figure 6.10b). However, the distinctive peak behaviour could not be reproduced by the HCC and HCE model. For the peak stress, there was no good match between the simulation and experimental results. The general stress path also differed at higher deformations. Nevertheless, the HCE and HCC models can be used to model the behaviour at interfaces under constant volume test conditions.

With respect to all three different validation examples, the outputs deviated because their state boundary surfaces were formulated differently. The HCE model with a more advanced state boundary surface should therefore be used (Mašín 2013).

6.4.5 Modelling fine grained interface using inter-granular strain concept

The aim of this section is to demonstrate that the fine-grained interface constitutive model HCE can be used to model the cyclic behaviour of interfaces. To this aim, the enhanced intergranular strain concept for interfaces can be used (Section 5.6). The parameters are given in Table 6.4. Figures 6.11b and 6.11a show the results with and without intergranular strain concept for an given amplitude. The model without the intergranular strain (Figure 6.11b) yielded a constant stiffness, whereas the intergranular strain yielded a more realistic modelling of the shear behaviour of the interface. The τ_x versus γ_x results illustrated that the ratcheting in the small strain region could not be modelled without the intergranular strain concept. The

Table 6.4: Parameters for the hypoplastic clay interface model with intergranular strain

Parameters	cyclic CNL
φ_c (°)	22
λ^*	0.128
κ^*	0.01
ν	0.33
N	1.51
R	$1 \cdot 10^{-4}$
m_R	5
m_T	2
β_r	0.12
χ	1

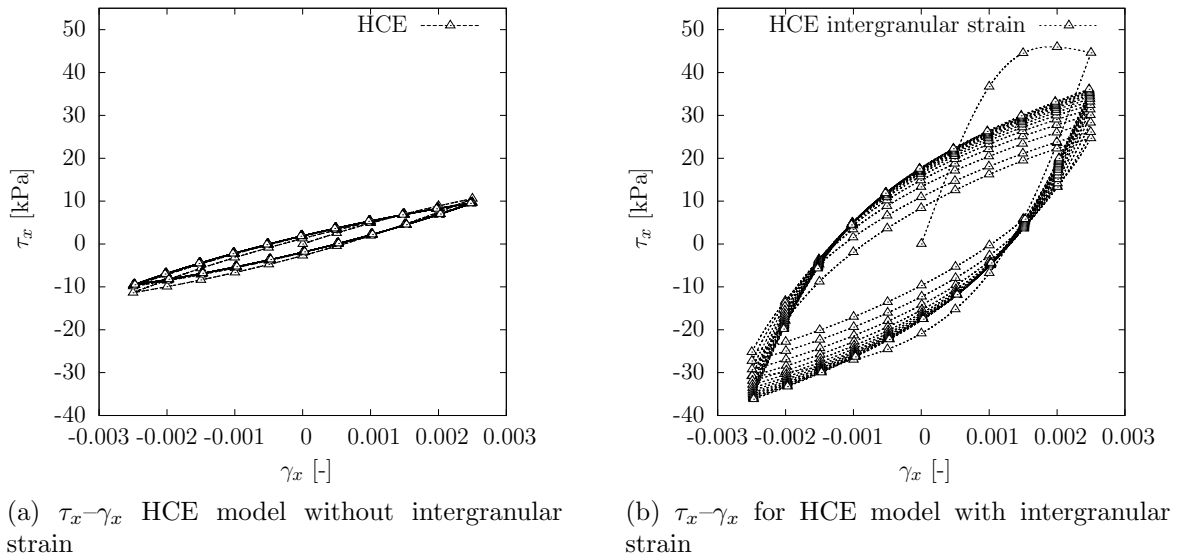


Figure 6.11: Comparison of HCE models without and with intergranular strain

initial stiffness used for the cyclic behaviour was not correct when the small strain behaviour was ignored. This interface behaviour could also be modelled for fine-grained soils using the intergranular strain concept.

6.5 Validation of the hypoplastic thermo-mechanical interface model for partially saturated soils

6.5.1 Temperature dependent modelling of fine-grained interfaces

The two boundary conditions, the constant normal load condition (CNL) and the constant volume condition (CV) were examined for temperature dependent interface modelling.

The limited experimental temperature data hindered the comparison of simulations to exper-

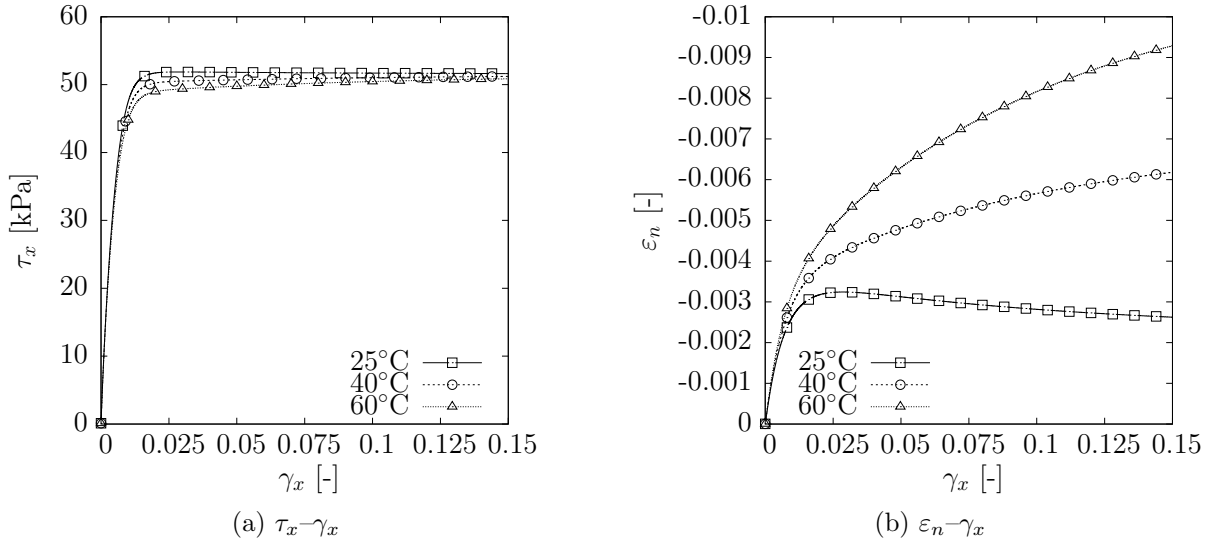


Figure 6.12: Results for CNL simulation with different applied constant temperatures

imental data. To this aim, a generic set of parameters was used (Table 6.5). These artificial parameters were used to evaluate the model response. The reference temperature was 25°C. The

Table 6.5: Parameters used for the hypoplastic thermo-mechanical interface model

Parameter	Soil 1	CV	CNL
φ_c (°)	27.5	27.5	27.5
λ^*	0.09	0.09	0.09
κ^*	0.01	0.02	0.04
N	0.88	0.82	0.82
r	0.2	0.2	0.2
α_s	$3.5 \cdot 10^{-5}$	$3.5 \cdot 10^{-5}$	$3.5 \cdot 10^{-5}$
l_t	0	var.	var.
n_t	-0.01	var.	var.
m	2.5	2.5	2.5
e_0	0.5	0.45	0.45
σ_0	300	300	100
T	var.	40	40

normal stress was $\sigma_0 = 300$ kPa. The shear stress decreased slightly under increasing temperature (Figure 6.12a). The normal strain ε_n (Figure 6.12b) increased with increasing temperature. To model a different behaviour as indicated by Di Donna et al. (2015) an another parameter set can be used (Section 6.5.2).

Increasing temperature led to decreasing shear stresses τ_x and normal stresses σ_n (Figure 6.13a and 6.13b).

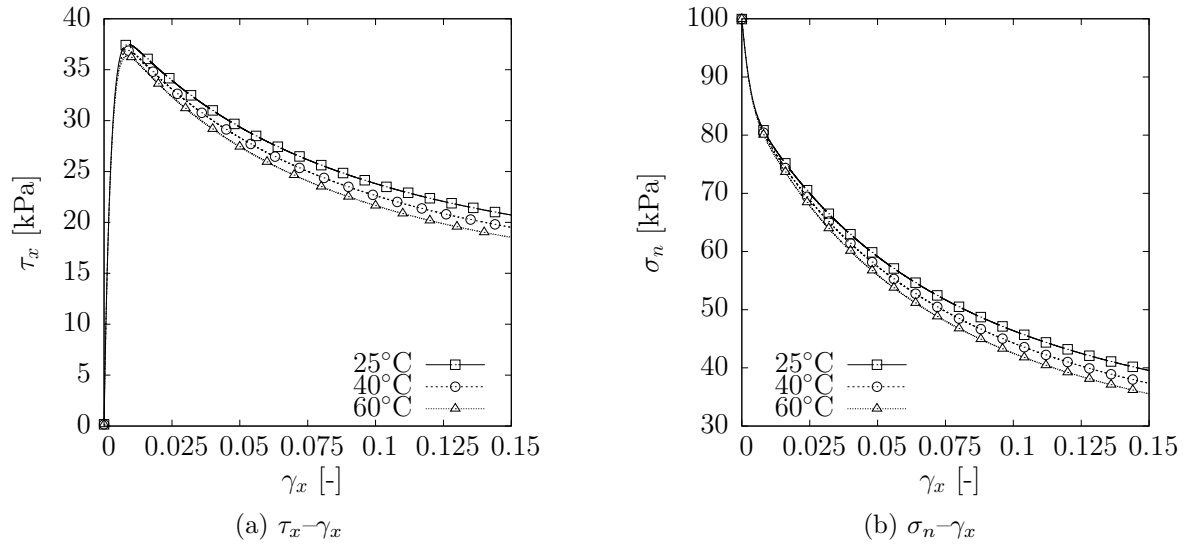


Figure 6.13: Results for CV simulation with different applied constant temperatures

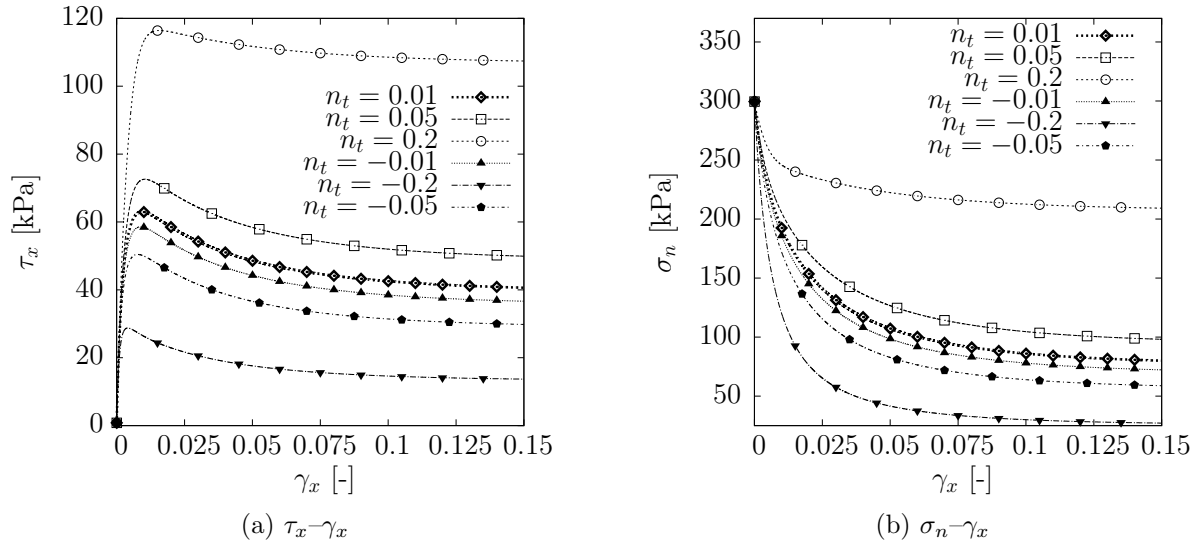


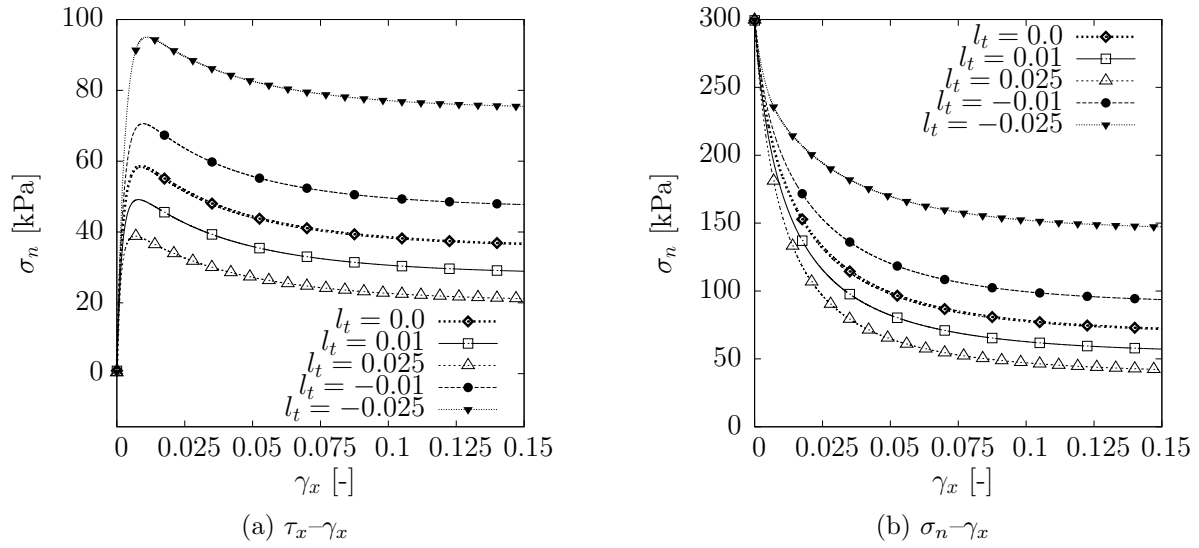
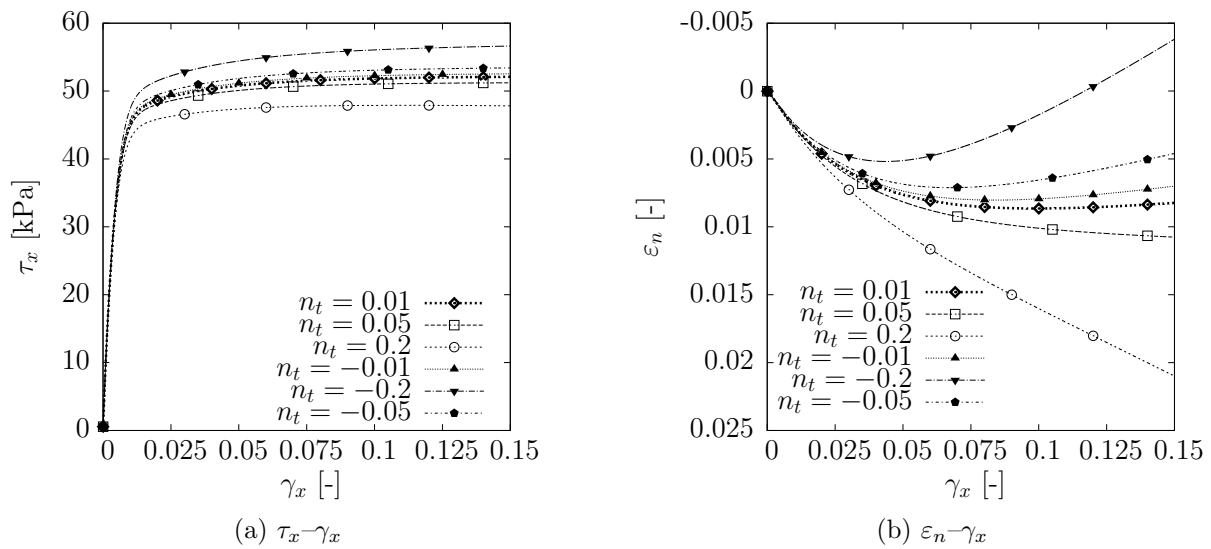
Figure 6.14: Results for CV simulation with parameter variation of n_t at 40°C

6.5.2 Parameter variation for the thermo-mechanical interface modelling

Parameters n_t and l_t control the position and slope of the Normal Compression Line (NCL) for heated soils (Figures 6.14b and 6.15b). Those two parameters are essential for modelling the thermo-mechanical interface response under constant temperature.

The parameter study was conducted under constant temperature of 40°C and a normal stress of 300 kPa. A positive algebraic sign of l_t and n_t leads to a decreased shear and normal stresses. A negative algebraic sign leads to an increased shear and normal stress (Figures 6.14b and 6.15b).

The simulated tests were conducted under 100 kPa. As indicated for the CV conditions, the


 Figure 6.15: Results for CV simulation with parameter variation of l_t at 40°C

 Figure 6.16: Results for CNL simulation with parameter variation of n_t at 40°C

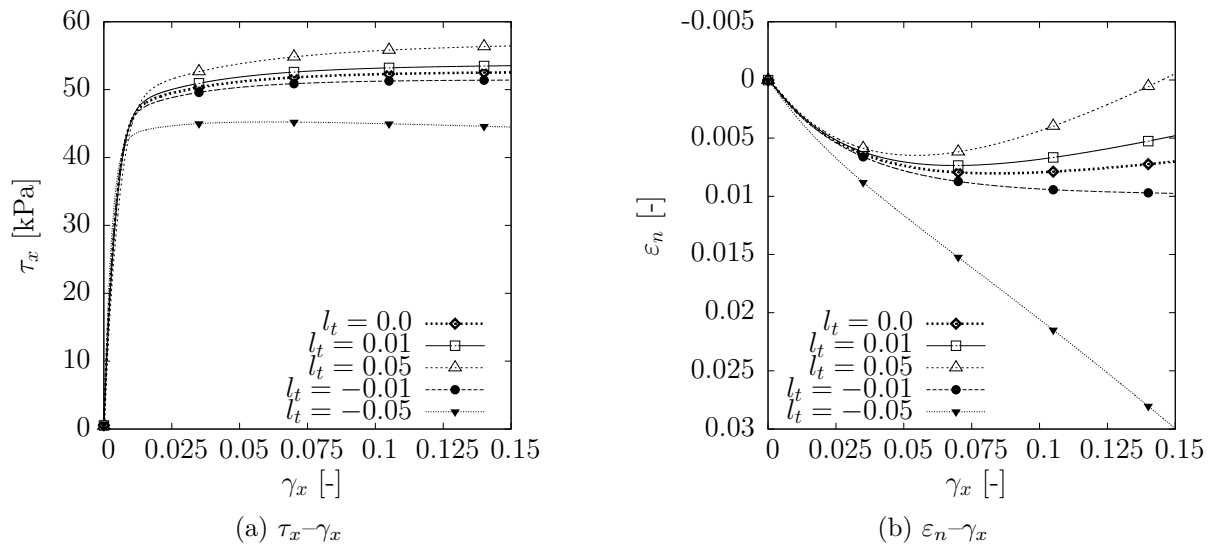


Figure 6.17: Results for CNL simulation with parameter variation of l_t at 40°C

CNL results indicated the same behaviour as in the CV results (Figures 6.16b and 6.17b). A positive algebraic sign will lead to a decreased shear stress τ and normal stress σ_n . A negative algebraic sign will invert the behaviour of the model (Figures 6.16b and 6.17b).

6.5.3 Suction-dependent modelling of fine-grained soil-structure interfaces

The model formulation described in Section 6.3 can be used to model unsaturated interfaces. The behaviour of unsaturated interfaces was introduced in Section 2.4. The last section will be used to briefly introduce the possibilities of modelling unsaturated interfaces with the hypoplastic thermo-mechanical interface model proposed in Section 6.3. The Figures 6.18a and 6.18a show the results of CNL test simulations under different applied suction values. As mentioned by Hamid and Miller (2009), the shear strength is increasing with increasing suction. This behaviour is modelled by the hypoplastic model taking into consideration temperature and hydro-mechanical coupling (Section 6.3). The newly proposed interface model is able to simulate the behaviour of different suction stresses and corresponds well with the experimental behaviour of unsaturated interfaces.

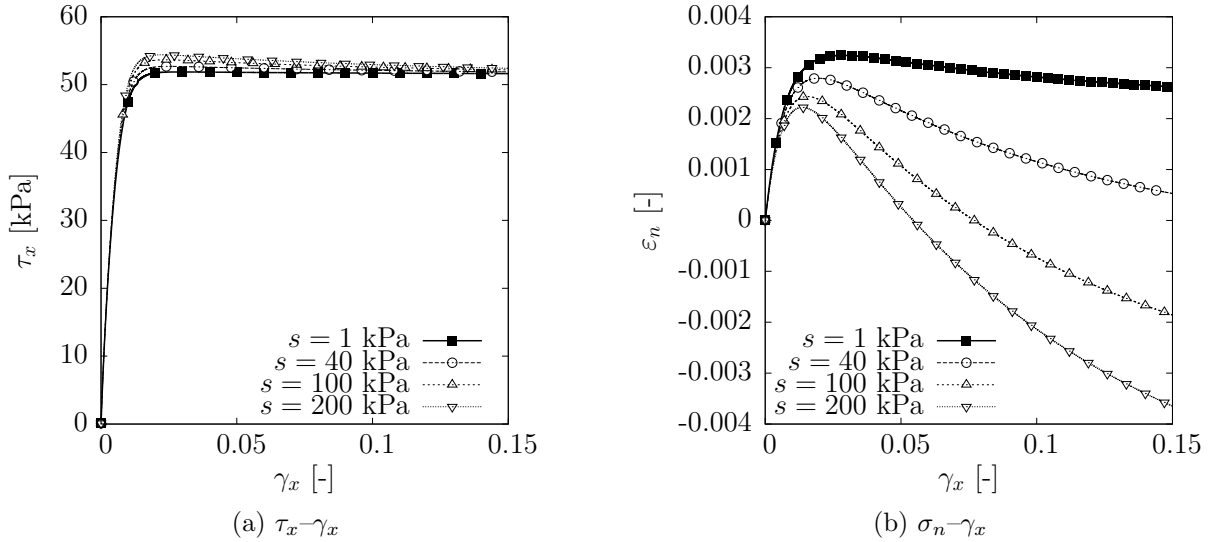


Figure 6.18: Results for CNL simulation with a variation of the suction stresses

6.6 Summary of Chapter 6

Chapter 6 presented the development of novel fine-grained constitutive interface models based on the fine-grained hypoplastic continuum soil models. The HCC and HCE hypoplastic interface models (Stutz and Mašín 2016) are suitable for modelling static and cyclic mechanical loading if extended by the intergranular strain concept. The third model based on the hypoplastic model of Mašín and Khalili (2012) can be used to model temperature and partial saturation effects at interfaces. The reformulation of the continuum model led to a novel application area for different boundary value problems in modelling important aspects of fine-grained soil-interface behaviour.

The two mechanical hypoplastic interface models were successfully validated by comparing the general model behaviour and experimental data. This accounts for the CNL, CNS, and CV test conditions. The temperature and partial saturation model were validated by addressing the opportunities for modelling suction and temperature with different parameter combinations. The proposed reformulation and introduction of novel interface constitutive models afford accurate modelling techniques and more precise simulations. This will be discussed in Chapter 7.

Chapter 7

Innovative approach for modelling interfaces using existing soil constitutive models

Chapters 5 and 6 proposed new and enhanced hypoplastic interface models, which showed potential for modelling interfaces.

Based on the theoretical considerations mentioned in Sections 5.2 and 5.4 an innovative and user-friendly concept is needed to implement these models. The aim of Chapter 7 is to describe a method for coding the new enhanced models using the software package ABAQUS FEA (Hibbit et al. 2015a). It should be noted that the methodology proposed is not limited to the specific software and can be applied to any other codes and numerical techniques (e.g. Beer (1985), Belgacem et al. (1998)).

In Section 7.1, the implementation algorithm of the hypoplastic interface model will be explained. Section 7.2.1 compares the ABAQUS simulation and the Gauss point integration simulations used in Chapters 5 and 6.

After the first verification, Section 7.3 will discuss two different boundary value problems simulated using the new constitutive interface models. The first boundary value problem is a comparison of experimental results from a large interface shear device with simulation results. The device was developed by Vogelsang et al. (2013) for the experimental modelling of granular soil interfaces. The second boundary value problem is the modelling of a novel penetrometer for the offshore mudline.

7.1 Implementation algorithm of interface models using 3-D constitutive models

The finite element software ABAQUS was chosen for the implementation because it allowed for user defined subroutines. In ABAQUS, it is possible to define a user constitutive model for

frictional behaviour. This subroutine (FRIC) is implemented by the use of a mortar method (Section 3.2.3).

For clarification, the UMAT subroutine can be used for the: “User subroutine to define a material’s mechanical behavior”. The FRIC subroutine allows the: “User subroutine to define frictional behavior for contact surfaces”. Additional information about both subroutines is provided in the ABAQUS documentation (Hibbit et al. 2015b).

Weißenfels and Wriggers (2015a) developed a projection method for integrated plasticity models in a mixed mortar formulation. This section defines a methodology that can be used for any constitutive model with the mortar method.

Typically, in the finite element method, models for interfaces are implemented with the primary state variables stress, the strain rate normal to the interface $(\sigma_t, \dot{\epsilon}_p)$, shear stress (τ_x, τ_y) , and shear strain components $(\dot{\gamma}_x, \dot{\gamma}_y)$. To incorporate the in-plane σ_p stress, it must be considered as an additional state variable together with the void ratio e . With respect to the use of a stretching tensor \mathbf{D} , the spin tensor \mathbf{W} can be neglected because only rigid body rotations occur in the mortar method.

Implementation scheme

Using the reduced tensor notation as described in Chapter 6, only the governing tensor entries will be used in the FRIC subroutine. The tensor entries are transformed and transferred to the 3D UMAT implementation available from the soilmodel.info project (Gudehus et al. 2008). The innovative approach is presented in Figure 7.1. In the current time increment, the FRIC subroutine is invoked. The input of all necessary parameters, stresses, and displacements is supplemented by the ABAQUS calculation kernel. The relative shear displacements u are transformed using the virtual shear zone thickness to shear strains $\varepsilon_x; \varepsilon_y$.

The input from the FRIC routine is formatted to match with UMAT input format and passed to the UMAT subroutine assuming a normal strain rate of $\dot{\epsilon}_n = 0$ for the first iteration. To ensure a volumetric behaviour according to the simple shear conditions, the normal contact stress rate $\dot{\sigma}_n^{Press}$ is used to find the appropriate normal strain rate $\dot{\epsilon}_n$. This is done by using a Newton-Raphson iteration scheme. The interface contact stress rate is derived according to the normal deformation, which must be chosen according to the stress contact rate $\dot{\sigma}_n^{Press}$. After the UMAT call, the relative error “*err.*” is compared to the tolerance (*TOL*). If the tolerance *TOL* is smaller than the error, a new value of the $\dot{\epsilon}_n^{n+1}$ must be approximated using the Newton-Raphson iteration formula until the condition of $err \leq TOL$ is fulfilled. The stresses σ_{UMAT} are transformed back into the stress definition used by the FRIC subroutine σ_{FRIC} . This procedure is used in each iteration loop when the FRIC routine is invoked.

The scheme can be used with any kind of 3D constitutive model. Here, the hypoplastic fine-grained and granular interface model are used. This innovative approach can be used with different constitutive models by adapting the proposed scheme. The use of the Newton-Raphson method, which is used to derive the normal strain rate and the virtual thickness approach, is defined below.

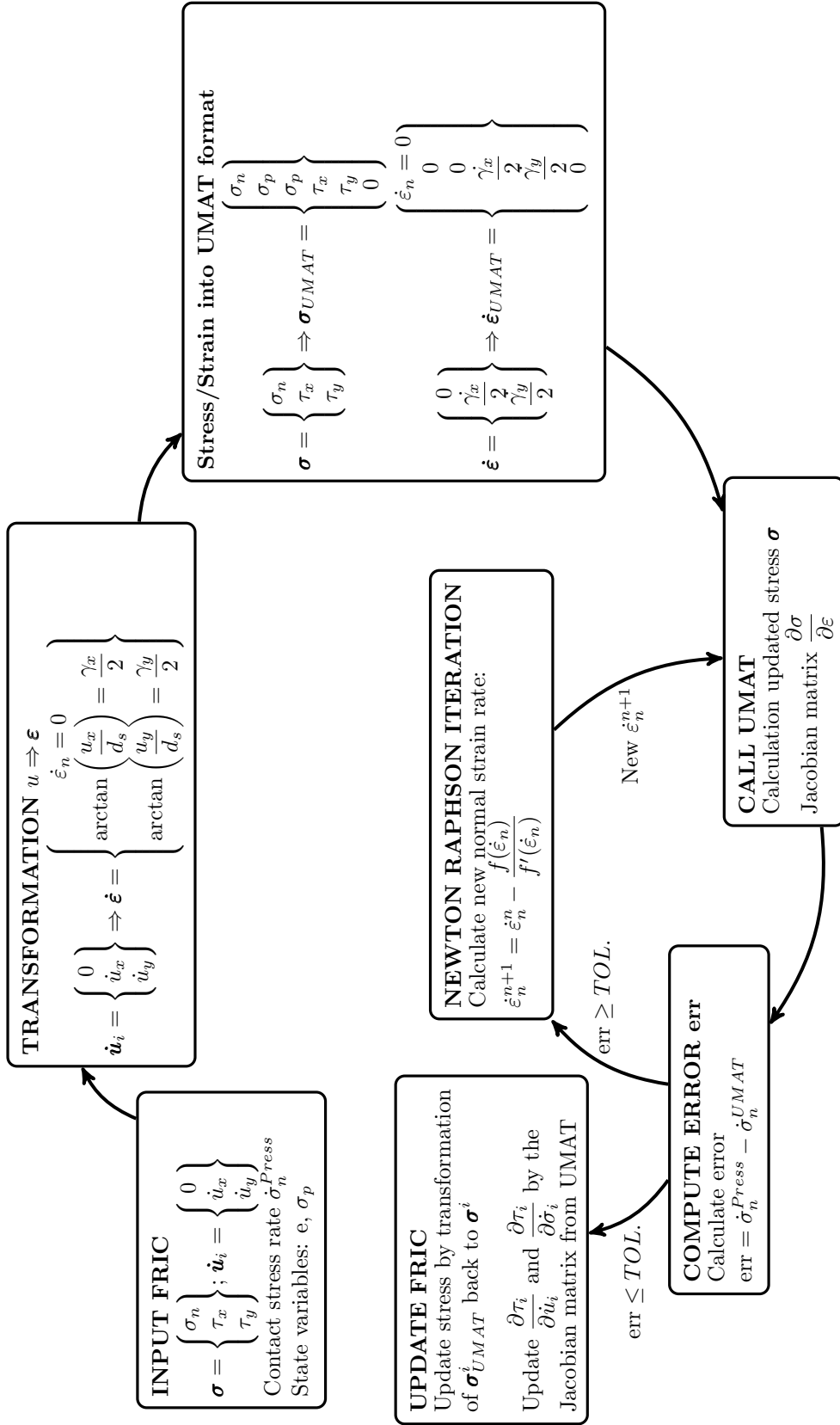


Figure 7.1: Implementation scheme for the FRIC subroutine using the UMAT subroutine

Newton-Raphson method

The Newton-Raphson method, which is named after Isaac Newton and Joseph Raphson (Figure 7.1) is used to find the necessary normal contact strain for reaching the normal stress rate, which is inserted into the FRIC user subroutine by the ABAQUS kernel. The formula for the Newton-Raphson iteration is:

$$x_1 = x_0 - \frac{f(x_0)}{f'(x_0)}, \quad (7.1)$$

where x_1 is the new value of the value sought, x_0 is the initial guess for the value to be obtained, and f is the function used with x_0 , and f' is the first derivative of the function considering x_0 for the initial guess.

This is repeated with the formula:

$$x_{n+1} = x_n - \frac{f(x_n)}{f'(x_n)}, \quad (7.2)$$

until a certain error tolerance TOL is reached. Further details of the Newton-Raphson algorithm can be found in Deuffhard (2014). The stability and efficiency of the proposed method for the given normal contact strain rate is demonstrated (Section 7.2). In the overlay implementation, the following equation is used:

$$\dot{\varepsilon}_n^{n+1} = \dot{\varepsilon}_n^n - \frac{f(\dot{\varepsilon}_n^n)}{f'(\dot{\varepsilon}_n^n)}, \quad (7.3)$$

where f is the function that calls the UMAT. In the UMAT the first derivative is defined by the Jacobian matrix $\frac{\partial \sigma_n}{\partial \varepsilon_n}$ (Figure 7.1).

Virtual thickness approach

As mentioned by Gutjahr (2003), the shear zone thickness depends on the shear strain and shear displacement. Arnold (2005) mentioned the possibility to use a virtual shear zone thickness to scale the relative displacements in the interface. By this approach, it is possible to calibrate the shear stress evolution for experimental data. Similar approaches are used in other finite element packages.

The approach mentioned by Arnold (2016) was used. The product of the specific length of the contact face (CHRENTGH) and a multiplier t_i as a virtual shear zone thickness d_s was applied.

The shear strains in the asymptotic state were defined by Gutjahr (2003), Arnold and Herle (2006), and Stutz et al. (2016) to be:

$$\tan \dot{\gamma}_i = \frac{u_i}{d_s^v}. \quad (7.4)$$

For this reason, the shear strain will be extremely high, which necessitates the use of a small time-increment size in the finite element simulations. To overcome this problem, the shear-zone thickness was introduced as a virtual shear zone thickness d_s^v , which is expressed:

$$d_s^v = t_i \cdot \text{CHRENGTH}, \quad (7.5)$$

where CHRENGTH is the ABAQUS keyword for the specific length of the contact face.

7.2 Verification of the implementation

The FRIC subroutine was verified using the concept presented in Section 7.1 and the parameter sets from Table 7.1. Different aspects are studied below:

- Comparison of explicit Gauss-forward integration to the finite element implementation for coarse and fine-grained soils
- Study of the mesh sensitivity simulations

Table 7.1: Parameters for the verification of the implementation concept

Hypoplastic Granular model		Hypoplastic Clay model	
Parameters	Value	Parameters	Value
φ_c	31	λ^*	0.095
h_s (kPa)	$1 \cdot 10^6$	κ^*	0.015
n	0.29	ν	0.1
e_{d0}	0.61	φ_c	21.9
e_{c0}	0.96	N	1.19
e_{i0}	1.09	κ_r	1.0
α	0.13		
β	2		

7.2.1 Description of the numerical direct shear interface test

The interface shear test model used for the verification was presented by Weißenfels and Wriggers (2015b). This boundary value problem was modified in this thesis. The model consists of the soil and the continuum (Figure 7.2).

The soil sample has dimensions of $25 \times 25 \times 5$ cm. The soil is applied over the structural part with dimensions of $35 \times 25 \times 5$ cm. The initial applied stress is p_n , and u_t is the shear displacement. This displacement was applied to all nodes of the structural part to model a homogeneous displacement field at the interface. The steel block was modelled as a linear elastic material using a Young's modulus of 1×10^{16} kPa and a Poisons ratio of $\nu = 0.25$. The element type used was

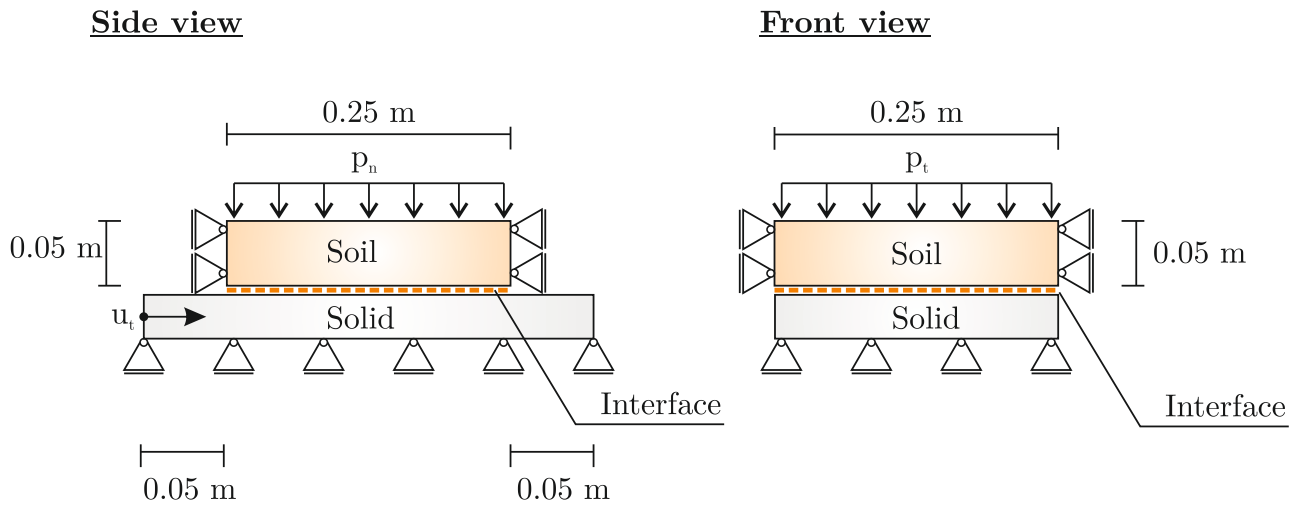


Figure 7.2: Geometry for direct shear verification simulation model adapted of (Weißenfels and Wriggers 2015b)

linear interpolation 8 noded elements (Abaqus Keyword: C3D8). The thick orange line (Figure 7.2) indicates the interface, which was modelled by a mortar method using the master–slave concept (ABAQUS documentation Hibbit et al. (2015b)). The tangential interface behaviour was modelled with the new developed hypoplastic constitutive interface models (Chapters 5 and 6) using the proposed implementation concept. These simulations were compared with the standard Mohr-Coulomb tangential contact formulation. In the normal contact direction, the augmented Lagrange approach was used to establish the contact stress in the normal direction. The simulation was done using the following steps. After applying a geostatic stress field (Step 1) and the application of a body force to activate the unit weight (Step 2) of the soil sample, the shearing was started (Step 3). A shear displacement of $u_t = 5$ cm was used.

The following subsections were organized as follows. First, the influence of the mesh size was analysed followed by the general verification between the explicit Gauss-forward integration and the finite element implementation.

7.2.2 Mesh sensitivity analysis

The three different meshes shown in Figure 7.3. These were used together with the direct interface shear test model described above. The meshes consisted out of various elements:

- coarse mesh size: 1 element
- intermediate mesh size: 128 elements
- fine mesh size: 507 elements

These different meshes were used to shown that the behaviour and the response of the model are influenced by the subroutine and that using different mesh sizes only leads to negligible differences.

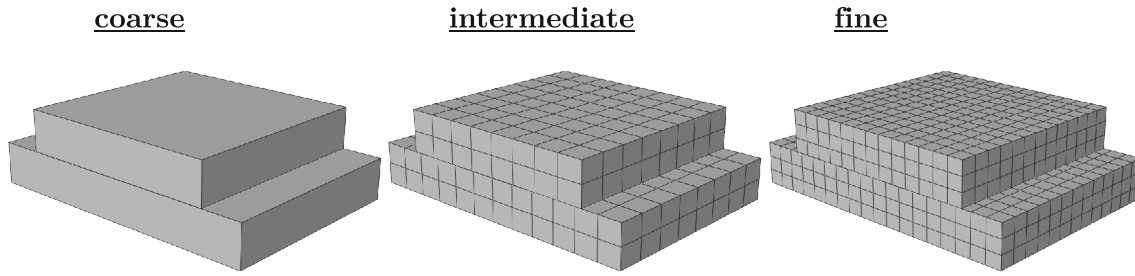


Figure 7.3: Coarse, intermediate and fine mesh size used to study the mesh sensitivity

The normal pressure p_n was 200 kPa, and the interface was assumed to be fully rough $\kappa_r = 1.0$. Figure 7.4a shows the shear stress evolution for the three different mesh sizes. For the coarse mesh with one soil element, the peak behaviour was underestimated the intermediate and fine mesh show similar results with small differences in the model response. For all different mesh sizes, the same asymptotic shear stresses were reached at the final displacement of $u_t = 5$ cm. Figure 7.4b shows the shear stress evolution for the three different mesh sizes. After 0.01 m, the shear stresses tended to reach a critical state. The clay mesh sensitivity analysis was assumed to be fully rough ($\kappa_r = 1.0$). The applied normal stress p_n was 100 kPa in all three simulations. The results were similar to those for sand. The coarse mesh simulated a slightly smaller shear stress than the other both meshes (intermediate and fine).

The two different mesh sensitivity analyses underline that the mesh size only influences the evolution of the shear stress development to a small degree. The effect may have been introduced from the different continuum of mesh sizes and did not necessarily depend on the FRIC subroutine that was used. The subsequent analysis therefore used an intermediate mesh size. In the next sections verification based on the Gauss-point code and the ABAQUS results will be discussed.

7.2.3 Verification of coarse-grained soil-structure interfaces

The shear stress and normal strain evolution were verified (Figures 7.5a and 7.5b). For the different normal stresses, p_n was either 100, 200, or 300 kPa. The intermediate mesh size was used as described in the previous section. The virtual shear zone thickness d_s^v was 1.0. For all three different stresses, the finite element implementation slightly overestimated the results from the Gauss point algorithm. The error is less tolerable because for both solutions, the numerical integration scheme was used in the finite element implementation. In the finite element model, a tolerated relative global error of 0.03% was used, whereas the Gauss-point solution can be treated as quasi-analytical solution with a tolerance of approximately 0.0%. The soil sample overlaying the steel surface was also modelled with the hypoplastic 3D constitutive model. This led to minimal vertical displacements, which can explain the small differences in the shear stress. Comparing the results for the normal strain ε_n (Figure 7.5b), the agreement

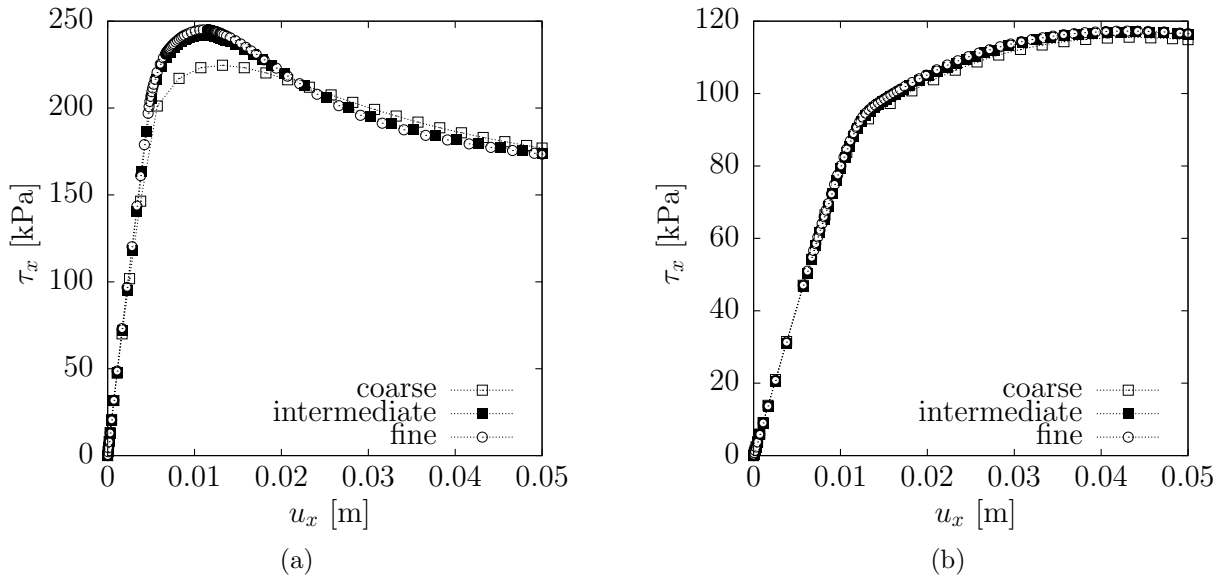


Figure 7.4: Shear displacement u_x to shear stress τ_x graphs for mesh sensitivity analysis for (a) sand and (b) clay

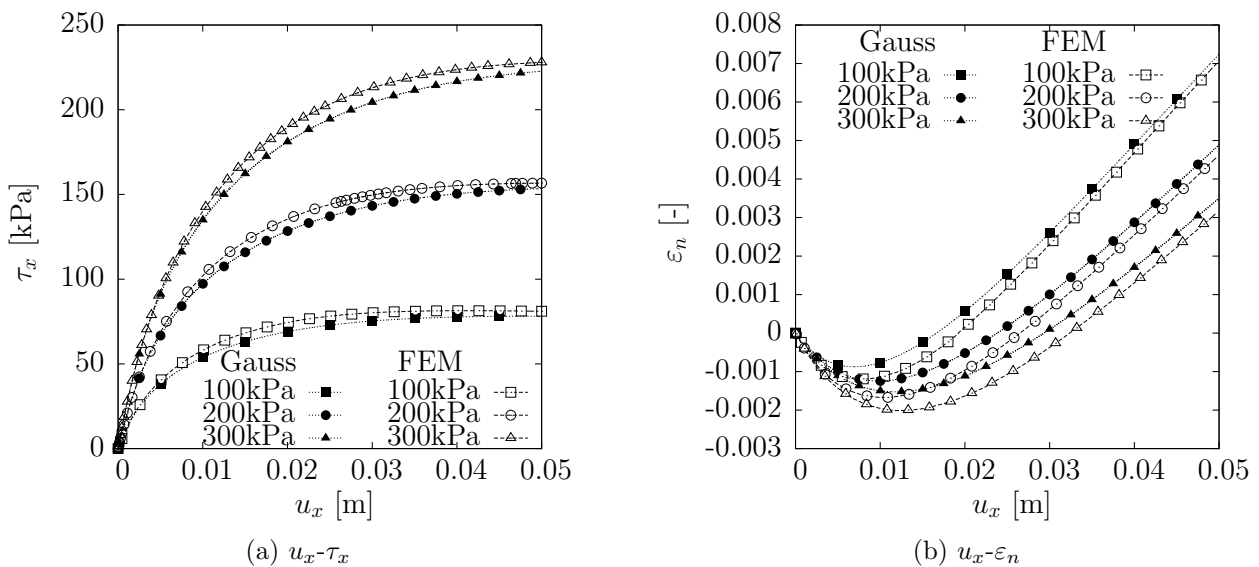


Figure 7.5: Verification between the Gauss point algorithm and the finite element implementation of the constitutive interface models for sand

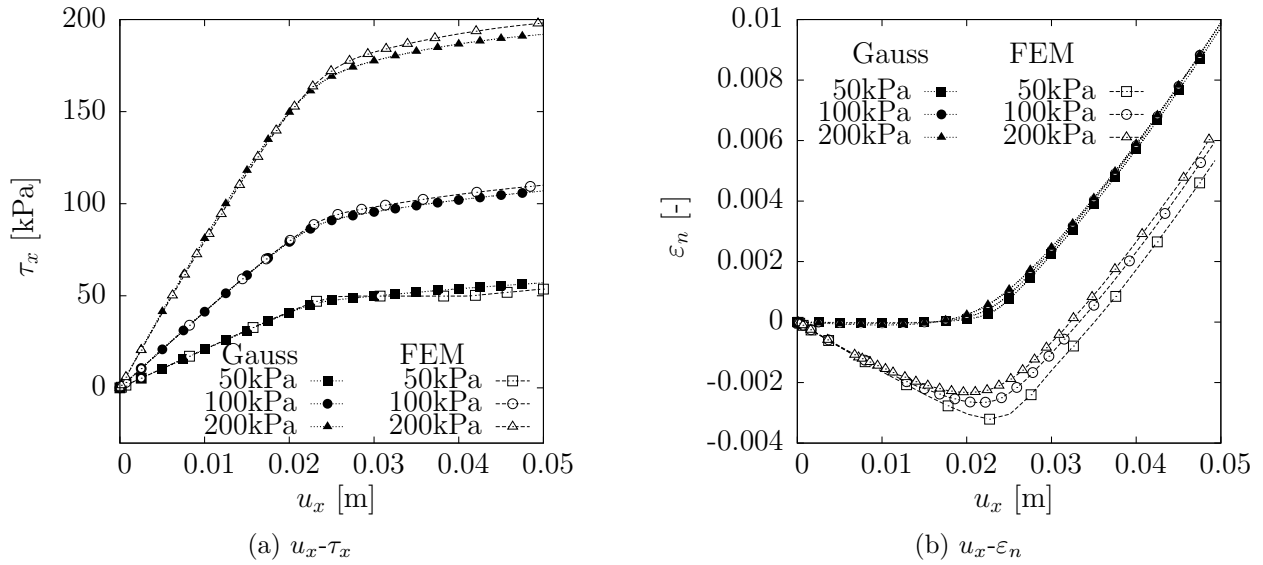


Figure 7.6: Verification between the Gauss point algorithm and the finite element implementation of the constitutive interface models for clay

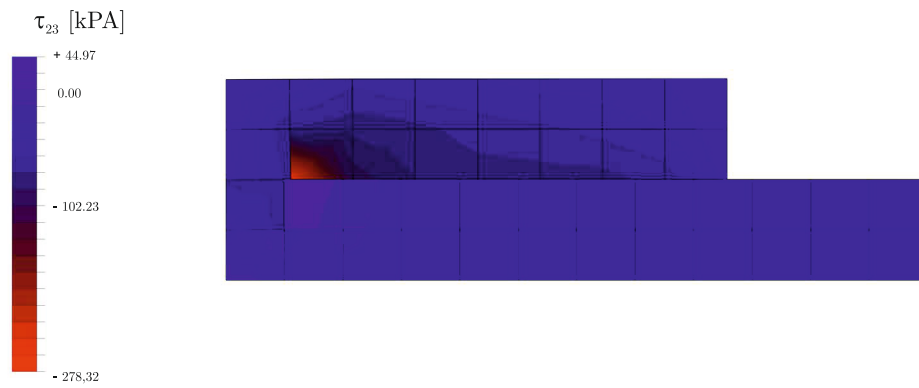
between both solutions was sufficient. The slightly smaller strain can be explained by the soil deformation.

7.2.4 Verification of fine-grained soils-solid interfaces

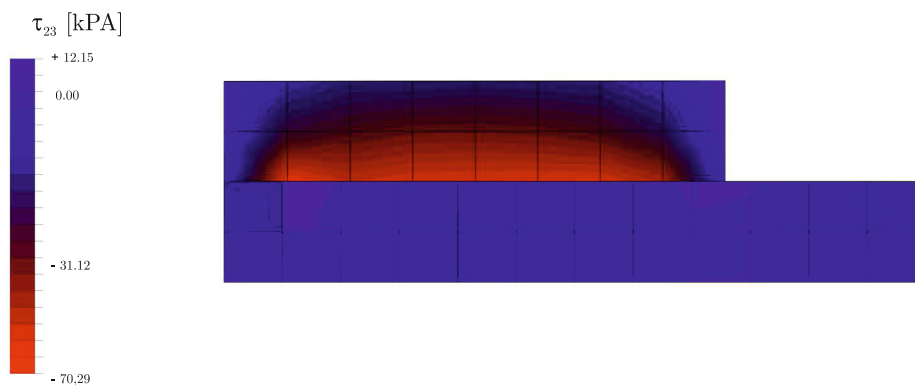
The verification was conducted by applying a normal stress p_n of 50, 100, and 200 kPa. d_s^v was 1.0 and a fully rough interface ($\kappa_r = 1.0$) was assumed.

When using the finite element implementation and the Gauss point calculations, there was a nearly perfect match between the shear stress evolution (Figure 7.6a). The results are similar to those for the granular interface model for the shear behaviour. Compared with the Gauss point algorithm there was a slight overestimation of the finite element solution. The only exception is the slight underestimation of the shear stress for the simulation using $p_n = 50$ kPa at a shear deformation of $u_t = 3$ cm. This is because of the small number of steps allowed for the Newton-Raphson iteration scheme. At $u_t = 3$ cm, the iteration scheme reaches the maximum allowable number of Newton-Raphson iterations. This led to a discrepancy between the calculated stress rate and the normal stress rate provided by the FRIC subroutine. In all different load cases, there was a slight overestimation of the direct interface shear simulation (Figure 7.6a).

When verifying the normal behaviour, there was a mismatch of the normal strains from the finite element to the Gauss point simulation (Figure 7.6b). The trend for all different models was comparable, but the simulations with the finite element method showed a more extensive contractive behaviour than in the Gauss point analysis results. As mentioned in Section 7.2.3, this was because of the soil behaviour over the interface, which was modelled by the hypoplastic fine-grained soil model.



(a) Mohr-Coulomb



(b) Hypoplastic

Figure 7.7: Comparison of the shear stress for the 100 kPa direct interface shear test using the Mohr-Coulomb and hypoplastic interface model

7.2.5 Comparison of Mohr-Coulomb and hypoplastic constitutive interface model

Three fully rough simulations demonstrated the influence of the interface model in a simple direct interface shear test (Section 7.2.1). A model not using the mortar method was also simulated. The first simulation was conducted with the Mohr-Coulomb friction model, which is a default model for simulations considering interfaces between soils and structural elements. The second model used was the enhanced hypoplastic granular interface model. The soil and the interface were modelled with the hypoplastic model of von Wolffersdorff (1996) using the parameter for Hostun sand given in Table 7.1.

The Mohr-Coulomb default model needs only the friction coefficient, which was assumed to be $\mu = 1.0$ for fully rough conditions. The comparison of shear stresses after the final deformation of 0.05 m showed for the Mohr-Coulomb a localised stress field and for the enhanced hypoplastic interface model a contentious stress field (Figure 7.7).

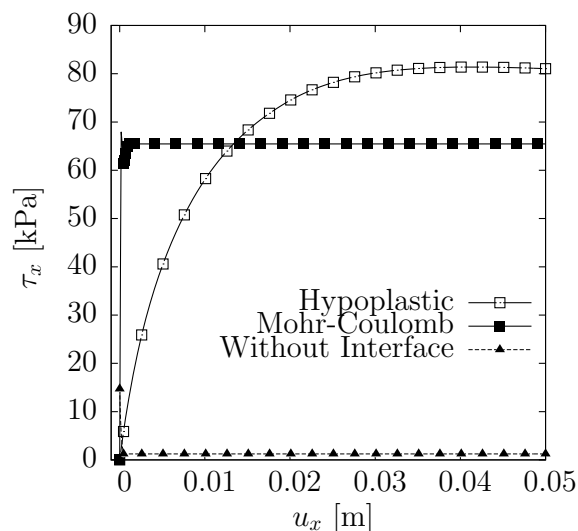


Figure 7.8: Shear displacement u_x versus shear stress τ_x for the comparison of Mohr-Coulomb and hypoplastic interface model

The shear stress that developed in the soil mass was two- to three-fold smaller for the hypoplastic interface model than for the Mohr-Coulomb model. Applying unlike the Mohr-Coulomb model, the hypoplastic model also led to a continuous shear stresses field along the interface.

This can also be interpreted from the shear displacement u_x versus shear stress τ_x plot (Figure 7.8). As shown by the results, the behaviour using the Mohr-Coulomb model is understandable because only a maximum shear stress was allowed. After this shear stress was exceeded, the additional shear stress was not considered because the yield stress limit was reached. In the Mohr-Coulomb model, the shear stress, which may have developed at the interface, was reduced to the perfect plastic formulation. The third simulation (Figure 7.8), which was performed without considering an interface, showed a short increase in the shear stress and then dropped to a value of 1.0 kPa. This behaviour can be explained by the mesh locking and the large shear stress that developed in the neighbouring elements. These findings are comparable with the results given by Griffiths (1985) and Griffiths (1988) and highlight the need for modelling techniques for soil-structure interfaces considering larger shear displacements. From the results that were compared, it is clear that the behaviour of soil masses along interface was predicted more accurately using a more sophisticated model. This is especially helpful if the model does not need any different model parameters or special parameter calibration. Rotta Loria et al. (2015) stated that higher pile-soil strength leads to higher yield stresses in the soil mass. A homogeneous stress field in the soil continuum is therefore preferable.

7.3 Boundary values problems

The section demonstrates the possibilities for using the newly developed models in boundary value problems. The previous verification showed that consistent modelling between the structure and the soil is preferable because of the simpler model calibration (Chapter 2). First, the

Table 7.2: Hypoplastic parameters for Karlsruhe sand (Herle and Gudehus 1999)

φ_c	h_s [kPa]	n	e_{d0}	e_{c0}	e_{i0}	α	β
31	$1 \cdot 10^6$	0.29	0.61	0.96	1.09	0.13	2

large interface shear device developed at the Karlsruhe Institute of Technology is described and modelled using the granular enhanced version of the interface constitutive model (Stutz et al. 2016). In addition to the shearing, the filling process of the test device was modelled for a holistic simulation.

The second boundary value problem is related to offshore geotechnics. The simulation of a novel offshore penetrometer is used to highlight the efficiency and importance of using an advanced fine-grained constitutive interface model.

7.3.1 Modelling large shear device

The large shear device developed at the Karlsruhe Institute of Technology was described in detail by Vogelsang et al. (2013) and Rebstock (2011). The main goal of the interface shear device is to designate reliable test data as benchmarks for numerical models (Vogelsang et al. 2015).

The test device has the dimensions presented in Figures 7.9a and 7.9b. The device can be used to model the installation effect for various geotechnical engineering structures. The device can therefore also be used as interface shear device for estimating tip resistance and 2D cavity expansion tests. These different problems are important when considering of holistic modelling and design in geotechnical engineering. Detailed information can be found in Vogelsang et al. (2013; 2015).

The model used the hypoplasticity model of von Wolffersdorff (1996) with the parameters summarized in Table 7.2. These parameters were given by Vogelsang et al. (2015) and differ from those parameters for Karlsruhe Sand specified by Herle and Gudehus (1999). The contact was modelled with the normal contact augmented Lagrange formulation, which tends to be more numerically stable than a penalty approach (Puso et al. 2008, Dziewiecki et al. 2015). The enhanced hypoplastic granular interface model presented in Chapter 6 was used for the comparison with the Mohr-Coulomb interface model.

The rough segment as modelled with a fully rough frictional value in the Mohr-Coulomb model $\mu = 1.0$ and a roughness value of $\kappa_r = 1.0$ for the enhanced hypoplastic model.

The stepwise modelling procedure of the filling without the shearing stage was adapted according to Vogelsang et al. (2015). The experimental results used to compare the experimental and numerical data was given in Vogelsang et al. (2015).

The test was modelled using the procedure described by Vogelsang et al. (2015) with a detailed procedure to capture the initial test set-up stress state in the device. This modelling technique

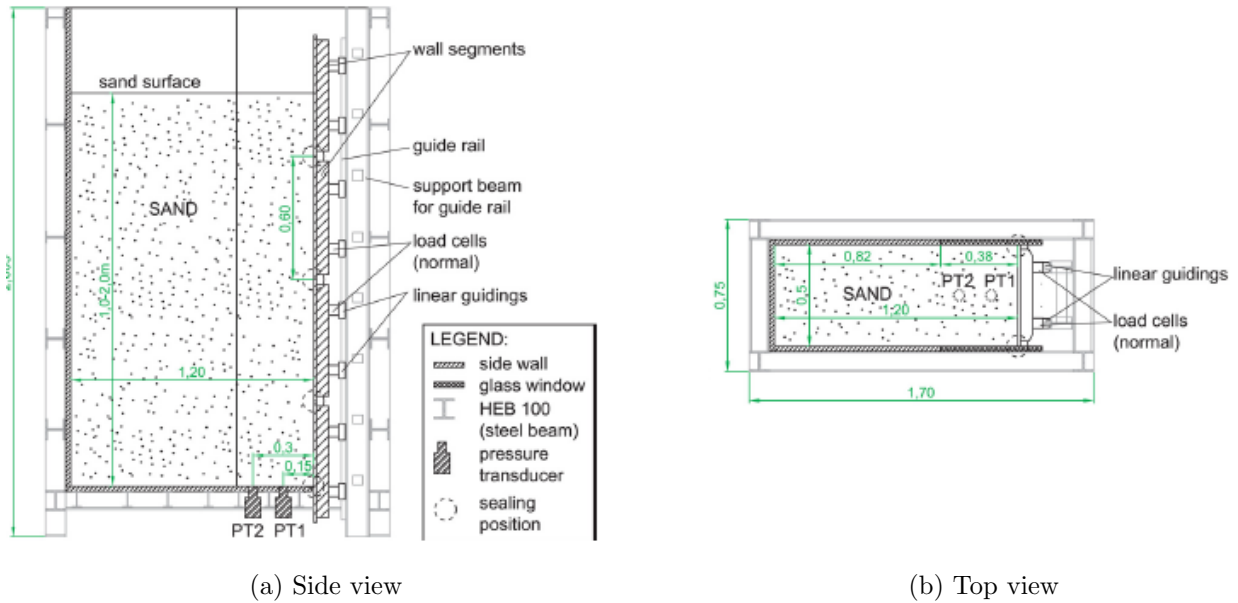


Figure 7.9: Side and top view of the large scale interface shear device of Vogelsang et al. (2013)

proved to be able to model the test device filling. The model used had a soil sample height of 1.50 m and a relative density of $I_D = 0.65$ (Vogelsang et al. 2015). Initial void ratio of $e_0 = 0.75$ was used. In the following models it was shown that the use of 10 layers is sufficient (Vogelsang et al. 2015). The procedure is shown in detail in Figure 7.10.

1. Applying a body force x -times smaller than the normal gravity to the soil sample. This step is necessary to achieve equilibrium with minimal displacements. (**Initial**)
2. Stepwise application of gravity to the model with n -layer. The filling process of the test device is thereby modelled. (**Filling**)
3. After the final layer is deposited, the displacement is applied to the wand panels. (**Shearing**)

The vertical stress distribution using the Mohr-Coulomb and enhanced hypoplastic model were compared (Figures 7.11a and 7.11b). The experimental data showed a non-linear behaviour

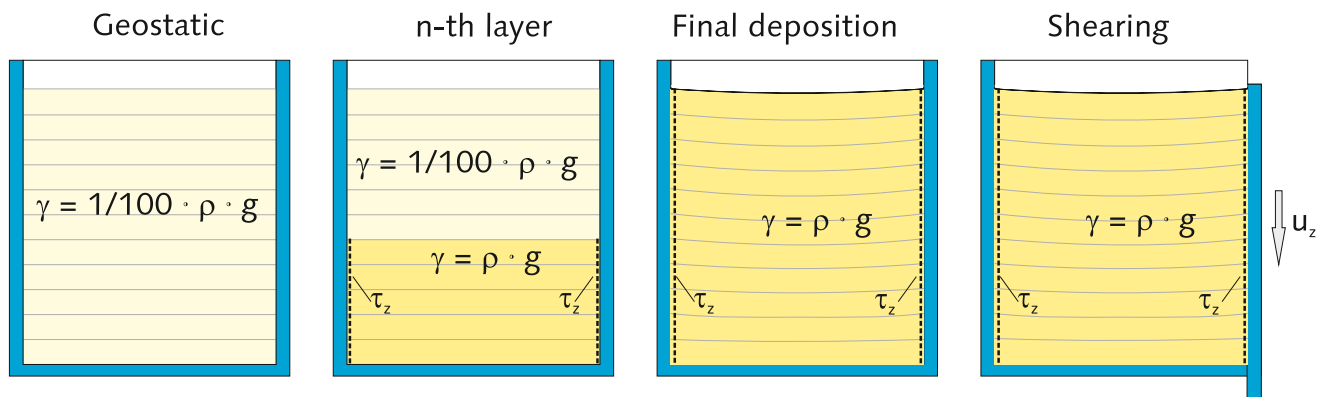


Figure 7.10: Illustration of the applied calculation process: Modelling the filling and shearing of the interface shear device (Vogelsang et al. 2015)

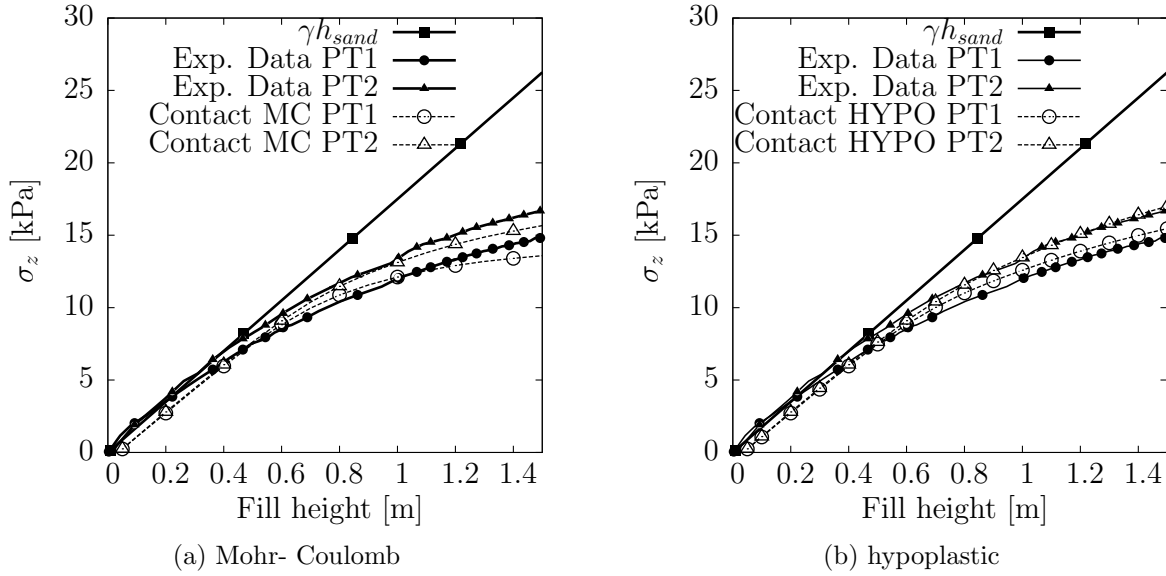
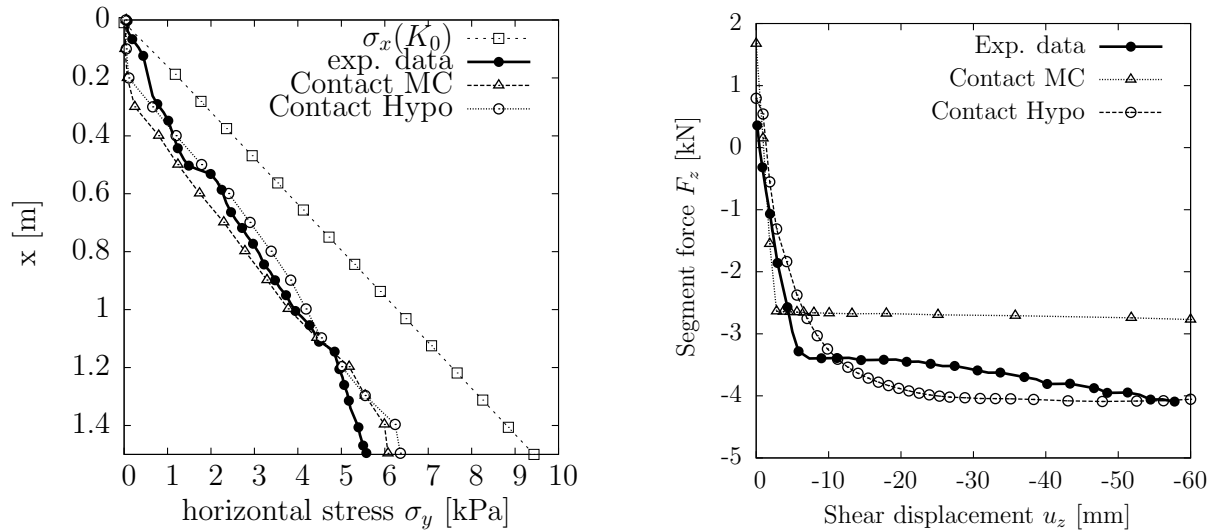


Figure 7.11: Vertical stress evolution σ_z [kPa] with increased filling height [m]

for the normal stress σ_z evolution, which was expected from experimental earth pressure measurements. The sensor positions of PTE1 and PTE2 are shown in Figure 7.9b and 7.9a. The hypoplastic contact modelling approach showed a good agreement for the evolution of the vertical stress σ_z . The Mohr-Coulomb frictional model showed a small discrepancy at the end of the filling process. In addition, in both graphs, the linear relation of the height γh_{sand} multiplied by the soil weight is shown for comparison. The evolution of horizontal stress is also given after the completed filling (Figure 7.12a). The earth pressure distribution is shown for comparison (Figure 7.12a) and was calculated with a value of $K_0 = 0.37$ according to Vogelsang et al. (2015). For the modelling the filling process, the hypoplastic contact model led to better predictions than the Mohr-Coulomb interface model. Both models slightly overestimated the horizontal stress at the bottom of the box. Vogelsang et al. (2015) mentioned that such a discrepancy may be due to the low stresses applied to the model device. This is in contrast to the higher stress used to calibrate the hypoplastic model parameters for the Karlsruhe sand (Herle and Gudehus 1999).

The experimental data showed small jumps in the horizontal stress distribution. These were because of the transition from one segment to another segment and the earth pressure measurement system (Vogelsang et al. 2015). In the finite element simulations with the Mohr-Coulomb or the enhanced hypoplastic interface constitutive model, these jumps did not exist because a smooth earth pressure distribution without jumps was expected.

After modelling the filling of the test device, the shear phase was simulated. The shear phase of the large shear device was simulated using the enhanced hypoplastic and the Mohr-Coulomb model (Figure 7.12b). The experimental data showed a small increase of the shear stress until the final deformation of 60 mm. The model with the Mohr-Coulomb interface model showed an underestimated compared with the experimental data (Vogelsang et al. 2015). The use



(a) Earth pressure distribution into the ITD device

(b) Shear force for the rough panel: Comparison of experimental data with simulations using the Mohr-Coulomb and hypoplastic interface models

Figure 7.12: Simulation results for earth pressure distribution (a) and the shear force versus shear displacement results (b)

of the hypoplastic contact model led to improved behaviour (Figure 7.12b). The asymptotic value was identical to the value in the experimental data. The general behaviour using the hypoplasticity contact routine was similar to the experimental data except for a slight difference around the small peak in the experimental data and the hypoplastic model. In the experimental data, after the peak point, a small increase of the shear force was observed. This was not the case for the hypoplastic interface model. This may have happened for various reasons e.g. the initial horizontal stress condition was higher than in the experimental recorded data (Figure 7.12a) or the parameters were not calibrated for the small stresses. However, the hypoplastic interface model resulted in better behaviour than the Mohr-Coulomb model and is therefore preferable. Under a shear displacement of 60 mm, the shear stress contour plot of σ_{zy} (Figure 7.13) demonstrated a more distinct mobilised shear stress field for the enhanced hypoplastic model than for the Mohr-Coulomb interface model. When the Mohr-Coulomb model was used, the shear stress tended to be lower (cf. Figure 7.12b). Interestingly, the Mohr-Coulomb model tended towards a higher mobilised shear stress zone than the enhanced hypoplastic interface model (Stutz et al. 2016). In summary, when modelling a large scale shear device, a more advanced constitutive model for frictional behaviour, which the volumetric response of the interface, results in improved modelling. Predictions are therefore important. This was shown by modelling the filling process of the device and later by using the enhanced hypoplastic model for the shearing simulation. As mentioned by Gutjahr (2003) and Arnold (2005), the modelling of the contacts (e.g. retaining wall calculations) led to more reliable interactions between the rigid wall and the soil body (Rotta Loria et al. 2015).

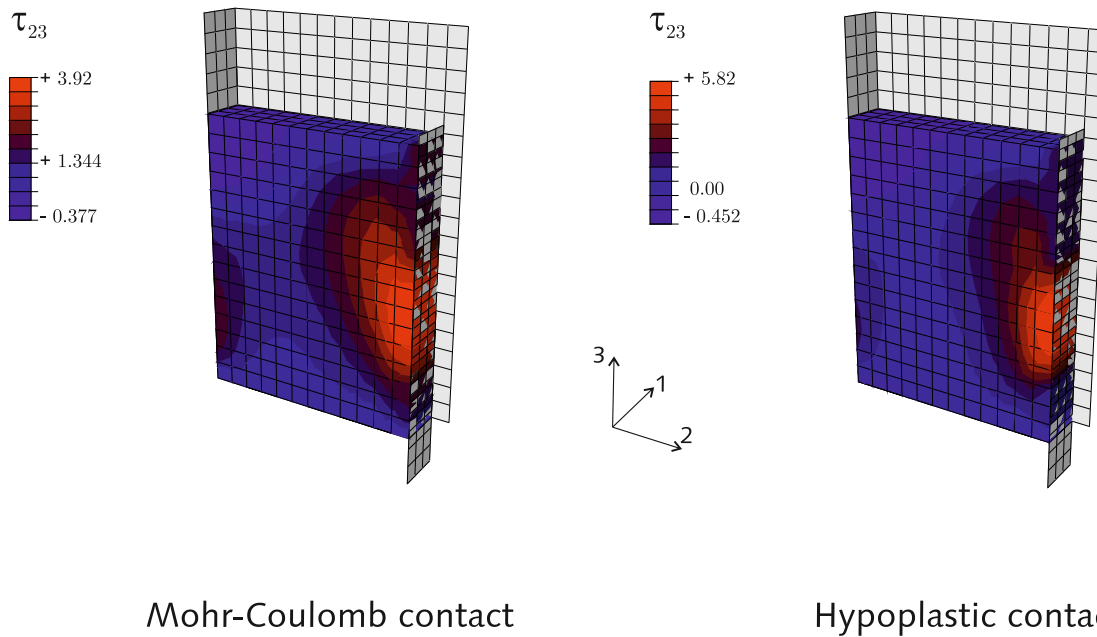


Figure 7.13: Results for the shear stress σ_{zy} after 60 mm shearing. Left side is the Mohr-Coulomb contact and on the right hand side the hypoplastic contact model

7.3.2 Offshore geotechnical: Toroid penetrometer simulation

The stability and integrity of offshore pipelines is important for the safe and secure transport of gas and oil— especially in deep waters. Cathie et al. (2005) reviewed the state of the art for offshore pipeline geotechnical engineering.

In the case of pipelines embedded at the seabed, characterising the soil at the offshore mud-line is a challenging task. Several new testing devices have therefore been developed. One of these devices is the toriod penetrometer for seabed characterisation (Yan 2013). For instance, the shallow penetrometer was developed by Boscardin and Degroot (2015) to conduct model pipeline tests in fresh box core samples in order to get high-quality test data for preliminary pipeline design.

For the preliminary design of such penetrometers, Yan et al. (2010) used a simple tresca undrained soil model in a finite element analysis. The boundary value problem is described and simulated with the new hypoplastic fine-grained interface model. This demonstrates the influence of realistic modelling on frictional behaviour when considering a hypoplastic fine-grained interface model (Chapter 6).

Geometry and finite element model

The geometry of such toroidal penetrometers was described by the relationship between the lever arm length L and the diameter of the spherical ring D . The vertical load V , the torsional load T_t , and the embedment w are depicted in Figure 7.14. Typical dimensions of such devices are $D_0 = 500$ mm and $L = 200$ mm; a ratio of $L/D = 2$ is typical used. The boundary value problem was modelled with these geometrical relations. The intention was measure the

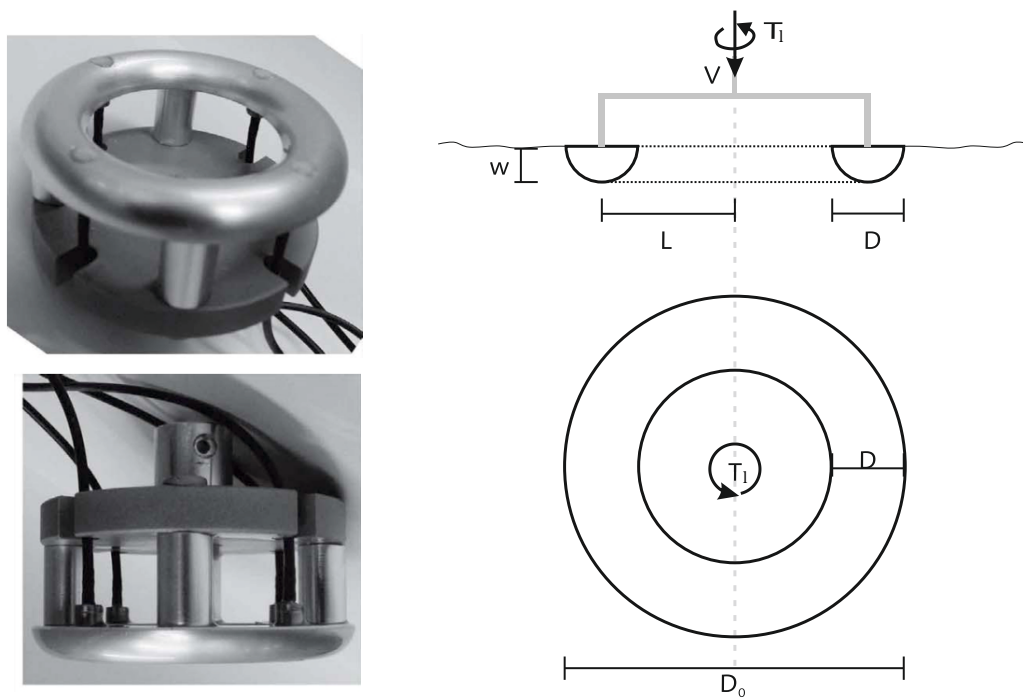


Figure 7.14: Shallow toriodal penetrometer side-view and top-view (left) and the geometrical properties (right) modified of Yan et al. (2010)

penetration resistance and the soil-structure interface friction by pushing the device into the seabed (penetration resistance) followed by the application of a torsional load to measure the axial-pipeline resistance. The boundary value problem uses the axial symmetry, taking into consideration the cyclic symmetry options in ABAQUS 6.14 (Hibbit et al. 2015a). The mesh used in the boundary value problem is shown in Figure 7.15. The model consisted of 8 noded elements with linear interpolation functions (ABAQUS keyword C3D8). The penetrometer was modelled with the same type of elements using a linear elastic model with a high stiffness (Table 7.3). The contact between the penetrometer and the soil was modelled in normal direction by an augmented Lagrange approach. For tangential contact, the hypoplastic clay model introduced in Chapter 6 was implemented with the algorithm proposed in Section 7.1.

The lateral boundaries of the model are fixed in horizontal displacement and rotations in the x and y directions. The bottom of the soil sample is constrained in all directions. The circular boundaries are constrained by the cyclic symmetry option. Yan et al. (2010) showed that the use of cyclic symmetry model led to a slight underestimation. These small discrepancies in the result are negligible compared with the computational efficiency used to analyse the full 3D model.

The soil was modelled with the hypoplastic fine-grained soil model of Mašín (2013) and the frictional constitutive model presented in Chapter 6. The soil modelled for the penetration resistance of the toriodal penetrometer was a carbonate silty clay (Ragni et al. 2016). The carbonate silty clay parameters specified by Ragni et al. (2016) were used to model an offshore sediment instead of artificial parameters. This carbonate silty clay was characterised as challenging soil

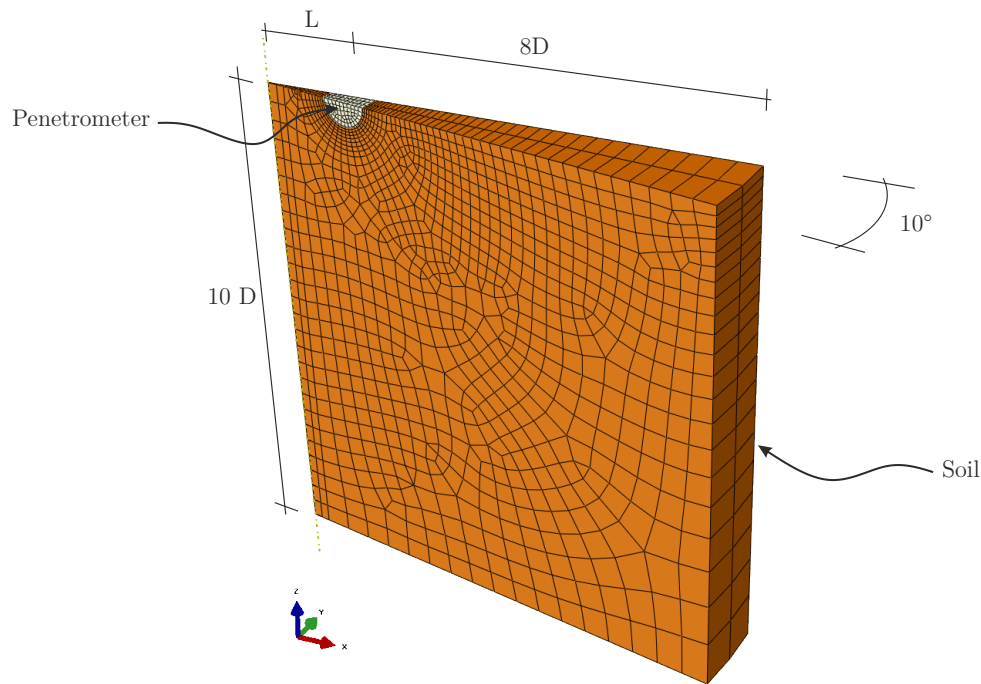


Figure 7.15: Boundary value problem: Shallow penetrometer modelled considering cyclic symmetry as 10° section

(Ragni et al. 2016). The model of Mašín (2013) and the extension were used for a meta-stable structure (Mašín 2007). By employing this hypoplastic model, the effects of remoulding and softening due to the sensitivity of the carbonate silty clay were modelled. The parameters are given in Table 7.3. It is important to mention that the meta-stable extension of the model was used only for the soil. More information about the meta-stable extension to the hypoplastic clay model can be found in Mašín (2007; 2009).

For comparison of the results, a Tresca soil model was used (Yan et al. 2010). The parameters for this model are also given in Table 7.3. To model the undrained behaviour of the soil, the frictional parameters ψ and φ were 0. An undrained shear strength s_u of 2.2 kPa was used as described by Ragni et al. (2016). This value was specified in the simulations and parameter calibration done by Ragni et al. (2016). The hole model was calculated by neglecting the unit weight. Yan et al. (2010) found that the effect of neglecting the unit weight was small compared with the practical importance and can be incorporated by Archimedes' principal. The penetrometer was modelled wish-in-place (Figure 7.15). This simplification of the analysis was justified; as shown by Stanier and White (2015), a large deformation finite element analysis gives approximately the same results. The simulation carried out in this thesis neglected the heave that can be developed around a pipeline with increasing penetration depth. In the following, the results were focussed on the penetration behaviour of this novel penetrometer.

Results

The results of the different simulations were compared. The different simulations are abbreviated as follows:

Table 7.3: Parameters for toroidal penetrometer, soil and frictional constitutive model (Ragni et al. 2016)

Soil parameters								
φ_c [°]	λ^*	κ^*	N	ν	k	A	s_f	s_{ini}
34	0.114	0.013	1.697	0.1	0.05	0.2	1.0	2.9
Interface parameters								
φ_c [°]	λ^*	κ^*	N	ν	κ_r	d_{sv}		
34	0.114	0.013	1.697	0.1	1.0/0.05	0.95		
Penetrometer linear elastic parameters								
E [kPa]	Possion's ratio ν_p							
10^{10}	0.25							
Tresca soil model								
E (kPa)	Possion's ratio ν_p	s_u (kPa)	ψ (°)	φ (°)				
1103.4	0.495	2.2	0	0				

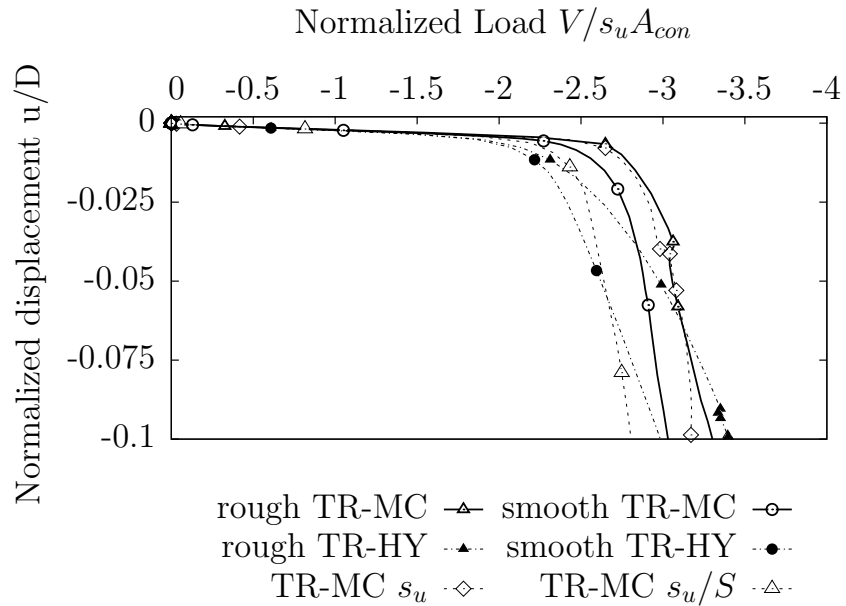
- Tresca soil model with Mohr-Coulomb interface model (TR-MC)
- Tresca soil model with hypoplastic fine-grained model (TR-HY)
- Hypoplastic model with extension for sensitivity and Mohr-Coulomb interface model (HY-MC)
- Hypoplastic model with extension for sensitivity and hypoplastic fine-grained interface model (HY-HY)

At a normalized displacement of 0.1, the normalized penetration load reached a constant value (Figures 7.16a and 7.16b). The results are given as normalized displacement on the y-axis as u/D and on the x-axis the normalized vertical load $V/s_u A_{con}$ (Figures 7.16a and 7.16b). A_{con} is the contact area of the penetrometer and is calculated as:

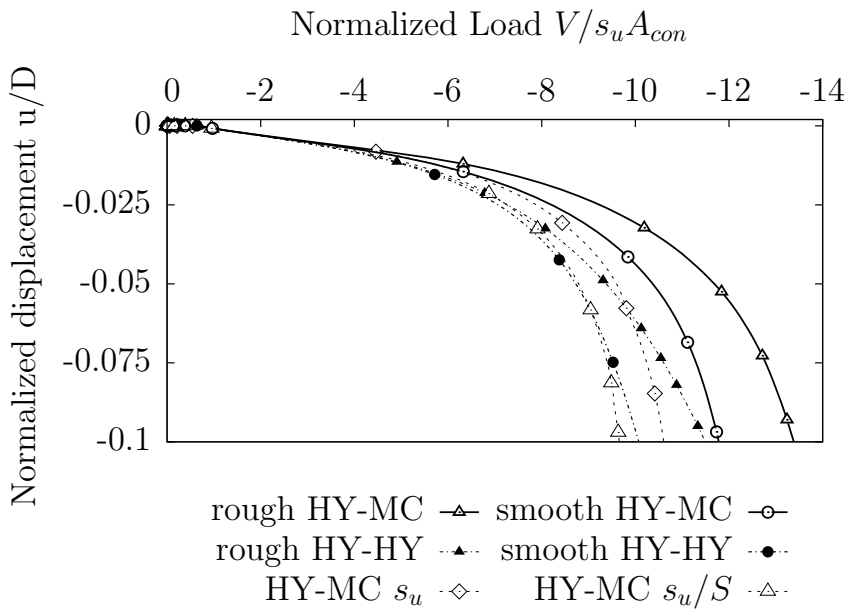
$$A_{con} = 2LD\pi. \quad (7.6)$$

Figure 7.16a shows the results for ratio of $L/D = 2$ using the Tresca soil model. The interface behaviour was modelled with the Mohr-Coulomb interface model and the hypoplastic interface model for fine-grained soils (Chapter 6). The simulations were done for six different cases. Fully rough ($\kappa_r = 1.0$) and smooth ($\kappa_r = 0.05$) conditions were utilized with both interface models. In addition, the interface conditions based on the assumptions of Stanier and White (2015) were used. They used the limiting shear stress condition $\tau_{max} = s_u$ and $\tau_{max} = s_u/S$. The undrained shear strength s_u at the mudline and S as soil initial sensitivity S_{ini} were used.

The results in Figure 7.16a indicate the importance of choosing the correct modelling with respect to the interface constitutive model. The hypoplastic interface model resulted in a lower normalized load than the Mohr-Coulomb friction model. Considering the different undrained shear stress conditions as limiting shear stress τ_{max} , the model tends to simulate intermediate



(a) Tresca soil model



(b) Hypoplastic soil model

Figure 7.16: Comparison of the different model combinations for calculated normalized load-deformation results

roughness conditions. These are more realistic than the fully rough or fully smooth conditions. As expected, the models showed higher normalized penetration load with fully rough conditions.

In conclusion the Tresca soil model combined with the hypoplastic interface model did not have any advantages. There are several possible reasons for this. For example, the parameter calibration between the interface and soil model should be improved, or the effects that can be modelled influenced the soil behaviour and vice versa. Nevertheless, both cases produced plausible results and demonstrated the upper and lower bound behaviour of the smooth and rough friction conditions as indicated by Stanier and White (2015).

When investigating the effect of remoulding and softening in a sensitive clay, the hypoplastic soil model with the Mohr-Coulomb friction model resulted in a higher load. The results of this combination were generally higher than those from the hypoplastic models for the soil and interface. The model using HY-MC s_u/S produced results that were close to the results for the HY-HY smooth conditions. A possible explanation for this behaviour is that modelling the soil and interface using a sophisticated modelling approach is more reliable than a simpler modelling frameworks. In the finite element analysis, a soil with the sensitivity of 2.9 kPa was considered. However, this behaviour could not be modelled, and the asymptotic state of the interface was not taken into consideration using the simple Mohr-Coulomb interface model. The advantage of the improved model was that the modelling of the soil and the interface was conclusive and led to a more accurate prediction than different modelling approaches. This hypothesis was proven by means of a visual comparison (Figure 7.17). At a penetration depth of $u/D = 0.1$, under consideration of different model combinations (HY-MC/HY) with different maximal shear stresses, $\tau_{max} = s_u$ and $\tau_{max} = s_u/S$ conditions led to improved model predictions.

The HY-HY models showed a good agreement with the HY-MC models using limited shear stress conditions (s_u , s_u/S). However, the results from the HY-MC models calculated sensitivities that were unexpected.

These results suggest that for penetration problems, it is beneficial to use interface models more sophisticated than the Mohr-Coulomb model friction model. The results presented are in accordance with the general importance of the accurate consideration of interface behaviour in finite element analysis.

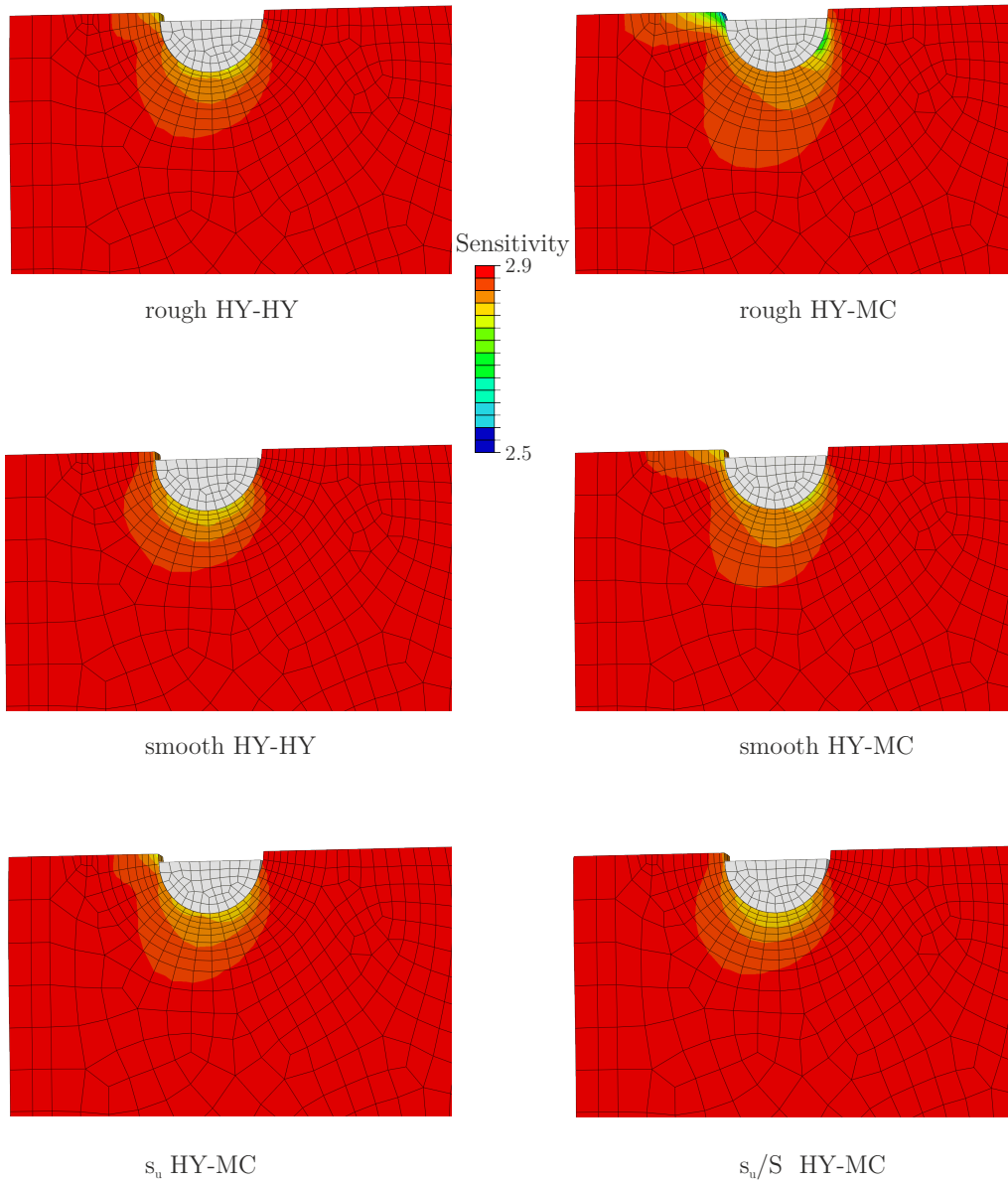


Figure 7.17: Detail in the z - x axis for the calculated sensitivity considering different model combinations (hypoplastic soil model with Mohr-Coulomb and hypoplastic interface models) at a normalized displacement of $u/D = 0.1$

7.4 Summary of Chapter 7

This chapter described a newly developed concept for using UMAT implementations for 3D soil behaviour to model interfaces. The UMAT was used as a constitutive driver under given boundary conditions. These simple shear conditions can be utilized by the UMAT, taken into consideration the special format of the stress tensor. In addition to the UMAT, the FRIC subroutine needs inputs and outputs, which are different than to the UMAT. To overcome the limitations of the surface-to-surface approach for the modelling of the normal strain, a Newton-Raphson scheme was used.

This new implementation concept was used together with the constitutive interface models developed in this thesis. The proposed concept was tested against the Gauss-point results from the granular- and fine-grained interface models in Chapters 5 and 6. In the verification of these models it was shown that mesh size has only a small influence. The prediction capability was robust and stable with the proposed implementation concept.

Two different boundary value problems were modelled, and the importance of using an advanced constitutive model for the interface was addressed. This was highlighted by simulations of a large scale shear device as well as a novel penetrometer for pipeline penetration resistance. In both simulations, different aspects were discussed with respect to modelling using an improved interface model.

Chapter 8

Beyond hypoplasticity constitutive interface models

8.1 Introduction

Chapters 5, 6, and 7, proposed new hypoplastic models and an efficient method to implement these models was presented. These models were based on the hypoplasticity framework, whereas the majority of the models developed in the last centuries are elasto-plastic models.

The aim of this chapter is to demonstrate that the new defined tensorial operators (Section 5.4) can be used with any other constitutive frameworks in addition to the hypoplastic models. Two different 3D soil models are therefore used as interface models by the redefined tensorial operators and reduced stress and strain rate tensors.

These constitutive models are the classical modified Cam-clay model (Roscoe and Burland 1968) and the Barodesy model for clay (Medicus et al. 2012). To demonstrate the applicability of the novel method for reformulating existing constitutive models, these are used for constant-volume simulations. Before the results are discussed, a brief introduction to the different used models will be given.

8.2 Barodesy model for clay

The Barodesy constitutive framework was proposed by Kolymbas (2012b). This novel framework is based on rational mechanics (Truesdell and Noll 2004). Barodesy uses the asymptotic behaviour of soils as basis. In soil mechanics, it is well known that critical states and the power law dependence on stress (Barodesy) are important. These features are inherently considered in barodetic models. Barodesy is derived from the Golderscheider rules (Goldscheider 1976). Detailed information can be found in Kolymbas (2012a; 2015), Medicus et al. (2012), Fellin (2013), and Fellin and Ostermann (2013).

The barodetic model for clay is briefly presented below. The notation of the barodetic model is given accordingly to the definition of Medicus (2014). The reference stress σ_{BC}^* is equal to 1

kPa. The following definitions are used $\epsilon = \text{tr}\mathbf{D}^0$, $\dot{\epsilon} = \|\mathbf{D}\|$, $\sigma = \|\mathbf{T}\|$. The superscript 0 refers to the normalised tensor as $\mathbf{X}^0 = \mathbf{X}/\|\mathbf{X}\|$. The model uses the constants c_1 – c_6 and the typical Cam-clay parameters λ^* , κ^* , and N . The constants used in Barodesy are defined in Equations 8.10–8.15.

The stress rate is defined as:

$$\dot{\mathbf{T}} = c_3 \sigma_{BC}^* \left(\frac{\sigma}{\sigma_{BC}^*} \right)^{c_4} \cdot (f_{BC} \mathbf{R}^0 + g_{BC} \mathbf{T}^0). \quad (8.1)$$

According to Kolymbas (2012b), the stress-like tensor \mathbf{R} is associated, with the direction of the asymptotic stress path with the stretching tensor \mathbf{D} . This relation is expressed in the barodesy clay model as:

$$\mathbf{R} = -\exp(\alpha_{BC} \mathbf{D}^0), \quad (8.2)$$

where α_{BC} is a scalar quantity, which is included in the \mathbf{R} -function. It is defined as:

$$\alpha_{BC} = \frac{\ln K_{BC}}{\sqrt{\frac{3}{2} - \frac{\epsilon^2}{2}}}. \quad (8.3)$$

The ratio of the axial stress and the radial stress K_{BC} is defined as:

$$K_{BC} = 1 - \frac{1}{1 + c_1 (m_{BC} - c_2)^2}, \quad (8.4)$$

with $m_{BC} = \frac{-3\epsilon}{\sqrt{6 - 2\epsilon^2}}$. The scalar quantity f_{BC} is defined as:

$$f_{BC} = c_6 \beta_{BC} \epsilon - \frac{1}{2} \quad (8.5)$$

and the second scalar quantity g_{BC} as:

$$g_{BC} = (1 - c_6) \beta_{BC} \epsilon + \left(\frac{1 + e}{1 + e_c} \right)^{c_5} - \frac{1}{2}. \quad (8.6)$$

In the barodetic clay model, the critical void ratio is defined as:

$$e_c = \exp \left(N - \lambda^* \ln \frac{2p}{\sigma_{BC}^*} \right) - 1. \quad (8.7)$$

The scalar quantity β_{BC} is part of the barodetic functions f_{BC} and g_{BC} ; these are defined as:

$$\beta_{BC} = -\frac{1}{c_3 \Lambda_{BC}} + 1 \frac{1}{\sqrt{3}} 2^{c_5 \lambda^*} - \frac{1}{\sqrt{3}}. \quad (8.8)$$

The last scalar quantity required is Λ_{BC} , which is written as:

$$\Lambda_{BC} = -\frac{\lambda^* - \kappa^*}{2\sqrt{3}}\epsilon + \frac{\lambda^* - \kappa^*}{2}. \quad (8.9)$$

The material constants c_1 – c_6 are calculated using the well-established Cam clay parameters.

The material constants are expressed as:

$$c_1 = \frac{K_c}{c_2^2(1 - K_c)}, \quad (8.10)$$

where $K_c = (1 - \sin \varphi_c) / (1 + \sin \varphi_c)$. The material constant c_2 is defined with $K_0 = 1 - \sin \varphi_c$ and K_c as:

$$c_2 = \frac{3\sqrt{K_c(1 - K_c)}K_0(1 - K_0) + 3K_c(1 - K_0)}{2(K_c - 1)}. \quad (8.11)$$

The third material constant c_3 is defined as:

$$c_3 = \max \left\{ \begin{array}{l} \frac{12G\sqrt{1 + K_c^2}}{\sqrt{6}\sqrt{3}p(K_c - 1)} \\ -\sqrt{3}/\lambda^* + \sqrt{3}/\kappa^* \\ 2^{c_5\lambda^*} + \left(2\frac{p}{p_e}\right)^{c_5\lambda^*} - 2 \end{array} \right. , \quad (8.12)$$

where is the equivalent pressure $p_e = \exp((N - \ln(1 + e)) / \lambda^*)$. The fourth material constant c_4 is defined as:

$$c_4 = 1 \quad (8.13)$$

c_5 is defined as:

$$c_5 = \frac{1}{K_c} \quad (8.14)$$

and the last material constant c_6 is defined as:

$$c_6 = \frac{1}{2\beta_{BC}(\epsilon = \sqrt{3})\sqrt{3}}. \quad (8.15)$$

A detailed description of the constitutive 3D soil model is given by Medicus et al. (2012) and Medicus (2014). Before comparing all three models, the modified Cam–clay model will be introduced in the next section.

8.3 Modified Cam–clay model

The second framework is the well-known modified Cam-clay model (MCCM), which was established by Roscoe and Burland (1968). The Cam-clay model can be seen as the first hardening soil model. Models of the Cam-clay form have been successfully applied to the modelling of soft

clays and have served as a basis for many different models. The stress rate for elasto-plastic loading is given as:

$$\begin{Bmatrix} \dot{p} \\ \dot{q} \end{Bmatrix} = \mathbf{D}^{ep} \begin{Bmatrix} \dot{\epsilon}_{vol} \\ \dot{\epsilon}_q \end{Bmatrix}. \quad (8.16)$$

In the modified Cam clay model, the elasto-plastic stiffness matrix \mathbf{D}^{ep} is defined as:

$$\mathbf{D}^{ep} = \mathbf{D}^e - \frac{\mathbf{D}^e \frac{\partial g}{\partial \sigma} \frac{\partial f}{\partial \sigma}^T \mathbf{D}^e}{\frac{\partial f}{\partial \sigma}^T \mathbf{D}^e \frac{\partial g}{\partial \sigma} + H}, \quad (8.17)$$

where the yield function f is defined as:

$$f = \frac{q^2}{M^2} - p(p_0 - p) = 0. \quad (8.18)$$

The classical modified Cam clay has an associated flow rule. The yield function f coincides with the plastic potential g . The elastic stiffness \mathbf{D}^e is defined as:

$$\mathbf{D}^e = \begin{Bmatrix} \frac{p}{\kappa_{MCC}} & 0 \\ \kappa_{MCC} & 3G \end{Bmatrix}. \quad (8.19)$$

The hardening function H is defined as:

$$H = p \frac{p_0}{\lambda_{MCC} - \kappa_{MCC}} (2p - p_0). \quad (8.20)$$

A comprehensive overview of the modified Cam-clay model is given in Wood (2000). After a brief introduction of both models, the next section will discuss the modelling of constant volume conditions for Kaolin and London clay.

8.4 Constant Volume simulation with Cam clay, Barodesy, and HCE model

The previously developed model (HCE) and two previously described models were used to simulate constant volume interface behaviour. The Cam-clay and Barodesy clay model were therefore used with the redefined tensorial operators given in Section 5.4 along with the reduced stress and strain rate tensors. The HCE, Cam-clay, and Barodesy interface model were used with the London clay parameters of Mašín (2005) (Table 6.1).

The London-clay simulation of all three interface models was used with the parameters for Kaolin clay given by Mašín (2013). The parameters used for the Cam-clay interface model were calibrated through isotropic compression test simulations and undrained triaxial tests.

Table 8.1: Parameters for the different clays

Hypoplastic and Barodesy	λ^*	κ^*	φ_c	N	κ_r	G_0/p_{ini}
London clay Mašín (2005)	0.11	0.016	22.6	1.375	1.0	100
Kaolin clay Mašín (2013)	0.065	0.01	27.5	0.88	1.0	20
Modified Cam clay	λ_{MCC}	κ_{MCC}	M	ν_r	–	–
London clay Mašín (2005)	0.161	0.062	0.88	0.31	–	–
Kaolin clay Mašín (2013)	0.078	0.026	1.06	0.28	–	–

London clay

Figure 8.1a shows the shear stress development of the three different constitutive interface models. The results show interface behaviour with out an peak behaviour under continuous shear strains.

Figure 8.1b had instead of the shear stress development that the normal stresses for the BC and HCE model had a distinctive peak behaviour and the MCC model not. The BC and the HCE

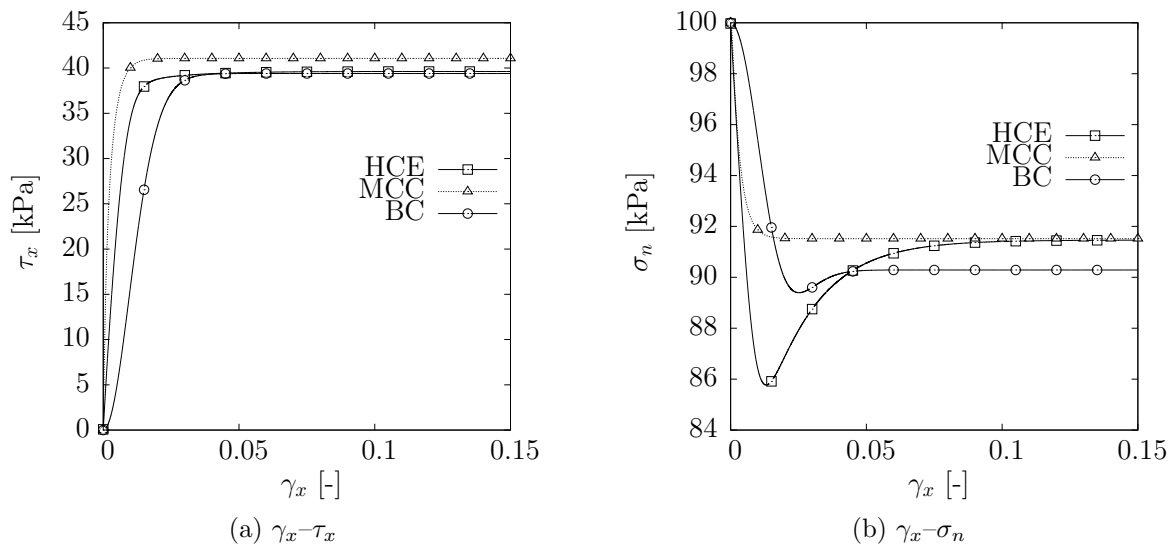


Figure 8.1: Comparison of shear and normal stress versus shear strain for CV simulation for London clay. The models are abbreviated as: Barodesy clay model as BC and modified Cam-clay model as MCC.

model reached the same stress at critical state (Figure 8.1a). The asymptotic state of the MCC model was slightly higher. The HCE model used the Matsuoka–Nakai condition, Fellin and Ostermann (2013) proved that the BC model coincides with the Matsuoka–Nakai condition.

The shear strain γ_x versus normal stress σ_n (Figure 8.1b), showed an identical trend to γ_x versus τ_x . Both results indicated that the HCE and BC model led to the same asymptotic state (Medicus 2014). The state boundary surface is well defined in both models.

The MCC model can model the interface behaviour but not at the same level of quality as the HCE and BC models. These predictions could be improved by using a different parameter set.

Kaolin clay

The results are comparable with the results for London clay, although the shear stress development showed no peak behaviour for all three different models (Figure 8.2a). The normal stress evolution showed a peak behaviour for the HCE model and no peak behaviour for the MCC and BC models (Figure 8.2b). The same trends were observed as with the London clay interface. The hypoplastic and the barodetic models reached a nearly identical asymptotic state (Medicus 2014). The modified Cam clay model did not simulate the expected behaviour; however, this could be improved by using different parameters.

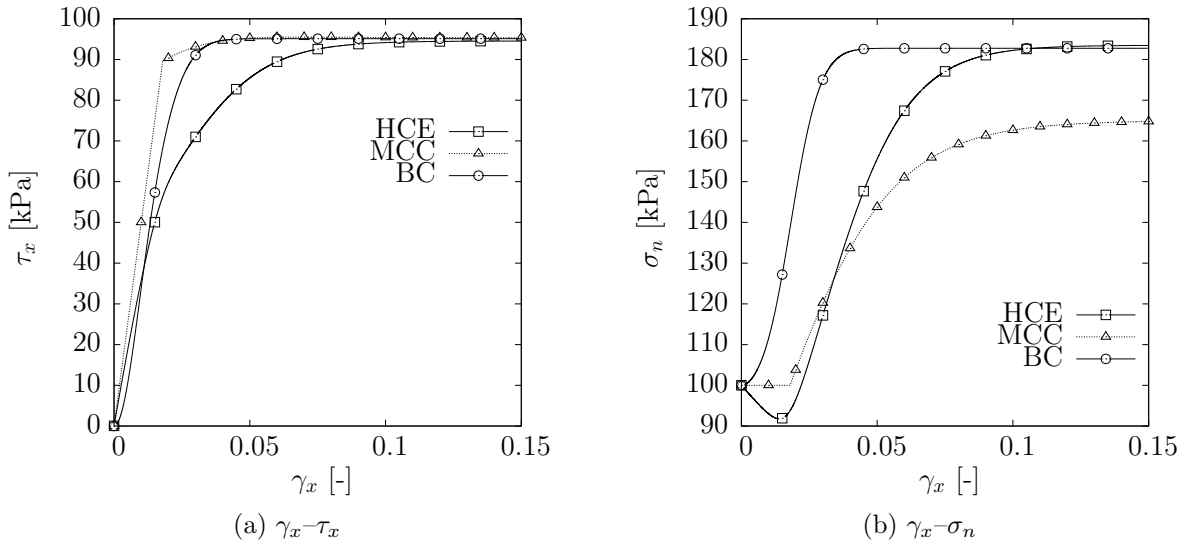


Figure 8.2: Comparison of shear and normal stress versus shear strain for CV simulation for Kaolin-clay

8.5 Summary of Chapter 8

This chapter discussed the potential for reformulating constitutive models into 2D constitutive interface models. As shown in this chapter, the innovative concept for the reformulation and the modified tensorial operators given in Section 5.4 can be used with any constitutive framework (e.g. elasto-plasticity or Barodesy). The results should not be discussed in the light of competitive comparison between the different models because the goal of this chapter was to demonstrate that the reformulation possibilities worked. However, the results indicate that the HCE and BC model have better prediction capabilities than the classical MCC model, which was to be expected. It was successfully demonstrated that the reformulation concept could also be used with other frameworks it was proven that the methods developed in Chapters 5, 6, and 7 could also be used for other advanced models.

Chapter 9

Summary, conclusions and outlook

9.1 Summary

The interface zone in soils is a narrow zone beside a structure into a soil. The physical behaviour of this zone is similar to that of soil. The modelling of this thin-zone thus becomes a challenge. In particular, the deformation behaviour in the normal direction of the interface under continuous shearing is important for accurate predictions.

At the beginning of this thesis, the different interface phenomena (e.g. deformation behaviour, influence of the surface roughness, particle size, density, confining stress and stiffness, monotonic and cyclic load paths, shear band thickness at interfaces, temperature, and partially saturation) were discussed. The different boundary conditions, experimental results, numerical modelling techniques were reviewed, and an overview of the constitutive modelling for interfaces was given. The five different models that were introduced were then studied in the model assessment.

The considerable number of constitutive interface models makes it difficult to determine the most suitable model for the constitutive description of the interface behaviour. A model assessment method that uses sensitivity as a pre-assessment tool and global model uncertainty methodology (Stutz et al. 2015, Motra et al. 2016) was therefore developed to assess the existing models. The proposed methodology is an improved version of the previous model assessment because a multi-point objective measure was used for hardening, softening, or peak states.

Motivated by the assessment of the models and the review of the state of the art, various points were identified. From a theoretical perspective, it is unclear, why the model development for soils and interfaces had been treated separately. Mathematical operators were therefore rearranged in order to use existing constitutive soil models (Stutz et al. 2016). The idea was highlighted by experimental results that were found in the literature (Boulon 1989, Boulon and Nova 1990). The implications arise from this is that the interface zone can be treated as soil medium under simple shear conditions.

After enhancing the granular hypoplastic interface model (Arnold 2005) with the theoretical concept and the newly defined operators, the model was validated with existing experimental data (Shahrour and Rezaie 1997, Gómez et al. 2003, Porcino et al. 2003) and was in good

agreement. The enhanced form of the inter-granular strain concept was also applied.

The novel approach for reformulation of the 3D constitutive models to interface constitutive models was used to propose three different clay-interfaces constitutive models based on the hypoplastic theory (Mašín and Khalili 2012, Mašín 2012; 2013). Two of these models are mechanical hypoplastic fine-grained interface models. The third is a model that was proposed for modelling temperature and unsaturated conditions at interfaces. The three models were verified and validated against different simulations and experimental data. All enhanced and newly-developed hypoplastic interface models are able to consider the effects of barotropy, pycnотropy, and surface roughness.

In addition to developing the models, it is important to highlight the new opportunities afforded by these models. To this aim, a method for the simple implementation of these models into the ABAQUS (Hibbit et al. 2015a) software package was developed. This concept uses the capabilities for user coding possibilities in ABAQUS.

The implementation scheme as well as the enhanced granular-structure and the novel fine-grained-structure interface model were verified in a finite element direct shear test analysis against the Gauss-point integration simulations used in Chapters 5, 6, and 7. The different aspects studied were the mesh sensitivity and the comparison between the Mohr-Coulomb friction model.

The models were successfully applied in boundary value problems for a large-scale shear device (Vogelsang et al. 2013) and a novel offshore penetrometer (Yan 2013). In both simulations, the global responses were improved by using the advanced interface models.

I would like to highlight the opportunities that arise through the use of redefined mathematical operators as well as reduced stress and strain rate tensors. This innovative concept of interface modelling is highlighted by the reformulation of the barodetic model for clay and the elastoplastic Cam-clay model. The different models were compared with the hypoplastic HCE model in constant volume simulations.

9.2 Conclusion

Model assessment methodology

- ✓ The model assessment developed in this thesis is suitable and can be used to assess different interface models. The expected results (i.e that the models with a high parameter uncertainty and sensitivity have a low model uncertainty) were shown. It was surprising that the simpler models (Mohr-Coulomb and Hyperbolic model) had parameter uncertainties that were only slightly better than the more complex models. Using more than one objective function quantity led to a better model assessment. The results emphasised the possibilities for estimating a quality or model assessment of interface models in particular and other kinds of models in general.

Theoretical and constitutive developments

- ✓ The enhancement of the existing hypoplastic model for 3D interface conditions (Arnold 2005) was necessary to consistently model the soil and the interface because the original model of Arnold (2005) shows differences between fully rough and simple shear conditions. To ensure consistent modelling, the enhancement of the hypoplastic model corrects the interface behaviour for fully rough conditions. This was necessary to ensure the expected interface behaviour. By enhancing this model, this goal was reached through reformulated mathematical operators and reduced stress and strain rate tensors.
- ✓ These innovative reformulation open several new possibilities for modelling soil-structure interfaces. Only the roughness of such interfaces must be embedded into the constitutive formulation. In the most cases, this can be solved without great effort. For hypoplastic models, several options for modelling surface roughness were discussed (Gutjahr 2003, Arnold and Herle 2006).
- ✓ The innovative concept was used to propose three different hypoplastic clay-structure interface models. These models are the most advanced models for clay-structure interfaces (as far as is known from the literature review). These models can handle nearly all thermo-hydro-mechanical states at fine-grained soil interfaces.
- ✓ To demonstrate the application potential of the unique concept, a barodetic and cam-clay interface model were reformulated. These models were successfully compared with the hypoplastic fine-grained model. The Barodesy framework in particular showed a huge potential for further improvements.

Numerical implementation scheme

- ✓ Theoretical and constitutive development is important. However, for the sustainable use of the proposed models and concepts, it is necessary to have an implementation scheme for numerical applications. This numerical implementation scheme uses the idea of reduced stress and strain rate vectors. By using specialized parts of the stress tensor from the 3D model in the form of a user defined material subroutine (UMAT) in conjunction with a subroutine for frictional contact (FRIC), the theoretical developed models become accessible to practical and academic users.
- ✓ The implemented Newton-Raphson scheme is used to calculate the correct modelling of volumetric behaviour. The verifications show excellent agreement between the different types of simulations by application of the Newton-Raphson scheme. The Newton-Raphson scheme shows stable and fast convergence behaviour. In addition, the results with the

Newton-Raphson scheme were accurately compared to the semi-numerical results.

- ✓ The results of the two different boundary value problems were improved with the proposed hypoplastic interface models. For example, the experimental results used for comparing the large scale shear device (Vogelsang et al. 2013) were in good agreement with the simulation results. Conversely, the Mohr-Coulomb predictions were not sufficient because of the bi-linear model formulation.
- ✓ Using penetrometer modelling, different model combinations for the soil and interface were compared. Some interesting features were revealed. If a more advanced interface model is considered, less attention must be paid to the correct initial values of limited shear stress condition at the penetrometer-soil interface (Stanier and White 2015).

Considering the achievements in this thesis, the goals to contribute to model accurate the interface behaviour without implementing additional parameters and special test conditions for interface conditions were successfully achieved. The adaptable hypoplastic model showed good possibilities to extend the models to specialized conditions (e.g. with the hypoplastic interface model under non-isothermal conditions).

The implications that develop from the above conclusions and summary are manifold with respect to using advanced interface models in the practical geotechnical engineering community. The results of this thesis are expected to contribute to the ongoing discussion on the use of simpler or more advanced models.

The proposed method is simple to use, and interface models as user-subroutines to model the behaviour of geotechnical engineering structures will become more realistic and holistic. As demonstrated, the behaviour of the interface model can contribute to a more accurate prediction parametrisation of the interface model.

9.3 Outlook

The aforementioned models can be improved, and the following research questions can be addressed. The steps required to establish the modelling frame and the research effort in conjunction with interfaces should be continued.

The following topics are of interest for future soil-structure interface research:

1. Experimental research
 - The experimental effort to characterize and develop models for fine-grained interfaces is restricted by a limited database when compared with the test data for sands.

- The dynamic and cyclic behaviour of interfaces has not been studied and will be give insights into the behaviour of interface. In particular, a high number of cycles should be studied.
- The development of a shear device that makes it possible to measure the mean in-plane stresses σ_p and their development will clarify and confirm the theoretical hypothesis.
- Studying the shear zone thickness properties in dependence of the different boundary conditions – especially for fine-grained soils – should be conducted.

2. Numerical/constitutive research

- The application of the intergranular strain (see above) as well as the development of a High Cyclic Accumulation model (Niemunis et al. 2005) could be of interest.
- The modelling of interfaces in challenging or difficult soils (e.g. sensitivity soil) or the more accurate modelling of low stress conditions at interfaces (e.g. pipeline conditions) is important because the models should predict reliable results under such conditions.
- More advanced numerical techniques for modelling the interface problems, for example the concept of third medium material, which is applied by Wriggers et al. (2013) and Nazem (2016). Would be enable the use of the in-plane terms σ_p for the modelling techniques.

3. The promotion of advanced interface models

- The subroutines should be intensively tested with varying parameters and boundary value problems in order to identify possibilities for numerical improvements of the applied scheme.
- The testing and application should be accompanied by documentation of the various modelling examples in order to demonstrate whether the assumption lead to reliable or unreliable predictions with more advanced interface models.

Bibliography

- Al-Douri, R. and H. Poulos (1992). Static and cyclic direct shear tests on carbonate sands. *Geotechnical Testing Journal* 15(2), 138–157.
- Ao, Y., J. Kodikara, and D. Robert (2014). Cyclic direct simple shear test on soft clay at low normal stress - As applicable to offshore pipeline axial walking problems. In R. Das and S. John (Eds.), *Proceedings of the 8th Australasian Congress on Applied Mechanics*, Barton, Australia, pp. 519–528.
- Arnold, M. (2004). *Zur Berechnung des Erd- und Auflastdrucks auf Winkelstützwände im Gebrauchszustand*. Ph. D. thesis, Mitteilungen - Institut für Geotechnik, Technische Universität Dresden.
- Arnold, M. (2005). Hypoplastische Beschreibung zweidimensionaler Reibungskontakte. In *Technische Universität Dresden, Mitteilungen Institut für Geotechnik, Heft 15, Ohde-Kolloquium 2005*, pp. 69–86.
- Arnold, M. (2008). Application of the Intergranular Strain Concept to the Hypoplastic Modelling of Non-Adhesive Interfaces. In *The 12th International Conference of International Association for Computer Methods and Advances in Geomechanics (IACMAG)*, pp. 747–754.
- Arnold, M. (2016). Personal communication.
- Arnold, M. and I. Herle (2006). Hypoplastic description of the frictional behaviour of contacts. In H. Schweiger (Ed.), *Numerical Methods in Geotechnical Engineering*, pp. 101–106.
- Bauer, E. (1996). Calibration of a comprehensive hypoplastic model for granular materials. *Soils and Foundations* 36(1), 13–26.
- Been, K. and M. G. Jeffries (1985). State parameter for sands. *Géotechnique* 35(2), 99–112.
- Beer, G. (1985). An isoparametric joint/interface element for finite element analysis. *International Journal for Numerical and Analytical Methods in Geomechanics* 21, 585–600.
- Belgacem, F., P. Hild, and P. Laborde (1998). The mortar finite element method for contact problems. *Mathematical and Computer Modelling* 28(4-8), 263–271.

- Boscardin, A. G. and D. J. Degroot (2015). Evaluation of a toroid for model pipeline testing of very soft offshore box core samples. In V. Meyer (Ed.), *Frontiers in Offshore Geotechnics III*, Oslo, Norway, pp. 363–368. Balkema.
- Bosscher, P. and C. Ortiz (1987). Frictional properties between sand and various construction materials. *Journal of Geotechnical Engineering* 113(9), 1035–1039.
- Boulon, M. (1989). Basic features of soil structure interface behaviour. *Computers and Geotechnics* 7, 115–131.
- Boulon, M., V. N. Ghionna, and G. Mortara (2003). A Strain-hardening elastoplastic model for sand-structure interface under monotonic and cyclic loading. *Mathematica and Computer Modelling* 37, 623–630.
- Boulon, M. and R. Nova (1990). Modelling of soil structure interface behavior a comparison between elastoplastic and rate type laws. *Computers and Geotechnics* 9, 21–46.
- Brumund, W. and G. Leonards (1973). Experimental study of static and dynamic friction between sand and typical construction materials. *Journal of Testing and Evaluation* 1(2), 162–165.
- Brumund, W. and G. Leonards (1987). Discussion. *Soils and Foundations* 27(2), 66–68.
- Burlon, S., H. Mroueh, and J. Cao (2014). Skipped cycles method for studying cyclic loading and soil–structure interface. *Computers and Geotechnics* 61, 209 – 220.
- Cathie, D., C. Jaeck, J.-C. Ballard, and J.-F. Wintgens (2005). Pipeline geotechnics - state-of-the-art. In M. F. Randolph and S. Gourvenec (Eds.), *Frontiers in Offshore Geotechnics*, Perth, pp. 95–114.
- Cerfontaine, B., A. Dieudonne, J. Radu, F. Collin, and R. Charlier (2015). 3d zero-thickness coupled interface finite element: Formulation and application. *Computers and Geotechnics* 69, 124 – 140.
- Chen, X., J. Zhang, Y. Xiao, and J. Li (2015). Effect of Roughness on shear behavior of Red clay–concrete interface in large-scale direct shear tests. *Canadian Geotechnical Journal* 52, 1122–1135.
- Cheng, Z., Z. Chunfeng, and G. Hui (2013). Elastoplastic analysis of the interface between clay and concrete incorporating the effect of the normal stress history. *Journal of Applied Mathematics* 2013, 1–12.
- Clough, G. W. and J. M. Duncan (1971). Finite Element Analyses of Retaining Wall Behaviour. *Journal of Soil Mechanics and Foundation Division* (12), 1657–1673.

- Corfdir, A., P. Lerat, and I. Vardoulakis (2004). A cylinder shear apparatus. *Geotechnical Testing Journal* 27(5), 447–455.
- Costa D Aguiar, S., A. Modaressi-Farahmand-Razavi, J. A. dos Santos, and F. Lopez-Caballero (2011). Elastoplastic constitutive modelling of soil structure interfaces under monotonic and cyclic loading. *Computers and Geotechnics* 38(4), 430–447.
- Coulomb, C. (1821). *Théorie des machines simples*.
- Coyle, H. and I. Sulaiman (1967). Skin friction for steel piles in sand. *Journal of Soil Mechanics and Foundations Division* 92(2), 261–278.
- Dafalias, Y. (1986). An anisotropic critical state soil plasticity model. *Mechanics Research Communications* 13(6), 341–347.
- Day, R. and D. M. Potts (1998). The effect of interface properties on retaining wall behaviour. *International Journal for Numerical and Analytical Methods in Geomechanics* 22(2), 1021–1033.
- De Gennaro, V. and P. Lerat (1999). Soil-structure interface behaviour under cyclic loading. In Jamiolkowski, Lancellotta, and L. Pretti (Eds.), *Pre-failure Deformation Characteristics of Geomaterials*.
- De Jong, J., M. Randolph, and D. White (2003). Interface load transfer degradation during cyclic loading: a microscale investigation. *Soils and Foundations* 43(4), 81–93.
- DeJong, J. T. and Z. J. Westgate (2009). Role of initial state, material properties, and confinement condition on local and global soil-structure interface behavior. *Journal of Geotechnical and Geoenvironmental Engineering* 135(11), 1646–1660.
- DeJong, J. T., D. J. White, and M. Randolph (2006). Microscale observation and modeling of soil-structure interface behavior using particle image velocimetry. *Soils and Foundations* 46(1), 15–28.
- Desai, C. and D. Rigby (1997). Cyclic interface and joint shear device including pore pressure effects. *Journal of Geotechnical and Geoenvironmental Engineering* 123(6), 568–579.
- Desai, C. S., E. Drumm, and M. M. Zaman (1985). Cyclic testing and modelling of interfaces. *Journal of Geotechnical Engineering* 111(6), 793–815.
- Desai, C. S. and B. K. Nagaraj (1988). Modeling for cyclic normal and shear behaviour of interfaces. *Journal of Engineering Mechanics* 114(7), 1198–1217.
- Desai, C. S. and B. K. Nagaraj (1990). Closure of the Discussion by C.S. Desai: Modelling for cyclic normal and shear behaviour of interfaces. *Journal of Engineering Mechanics* 116, 1872–1880.

- Desai, C. S., M. M. Zaman, J. G. Lightner, and H. J. Siriwardane (1984). Thin-layer element for interfaces and joints. *International Journal for Numerical and Analytical Methods in Geomechanics* 8, 19–43.
- Deuffhard, P. (2014). *Newton Methods for Nonlinear Problems* (Springer ed.). Springer Berlin Heidelberg.
- Di Donna, A., A. Ferrari, and L. Laloui (2015). Experimental investigations of the soil-concrete interface : physical mechanisms , cyclic mobilisation and behaviour at different temperatures. *Canadian Geotechnical Journal* 53(4), 659–672.
- Dietz, M. S. (2000). *Developing an holistic understanding of interface friction using sand within the direct shear apparatus*. Ph. D. thesis, University of Bristol.
- Dithinde, M., K. K. Phoon, M. De Wet, and J. V. Retief (2011). Characterization of model uncertainty in the static pile design formula. *Journal of Geotechnical and Geoenvironmental Engineering* 137(1), 70–85.
- Doherty, J. and M. Fahey (2011). Three-dimensional finite element analysis of the direct simple shear test. *Computers and Geotechnics* 38(7), 917–924.
- Dove, J., J. Frost, J. Han, and R. Bachus (1997). The influence of geomembrane surface roughness on interface strength. *Proc. Geosynthetics* 1, 863–876.
- Dumitrescu, A., A. Corfdir, and R. Frank (2009). Influence of the anisotropy of confining stress on the sand/steel interface behaviour in a cylinder shear apparatus. *Geotechnical Testing Journal* 49(2), 167–174.
- Duncan, J. M. and C. Y. Chang (1970). Nonlinear analysis of stress and strain in soils. *Journal of Soil Mechanics and Foundation Division* 56(SM5), 1625–1653.
- Dziewiecki, P., C. Weißenfels, and P. Wriggers (2015). Modelling of soil structure interaction by applying a hypoplastic material behaviour within mortar contact formulation. In Th. Triantafyllidis (Ed.), *Holistic Simulation of Geotechnical Installation Processes, Lecture Notes in Applied and Computational Mechanics*, Volume 77, pp. 59–72. Springer International Publishing Switzerland.
- Eid, H. T., R. S. Amarasinghe, K. H. Rabie, and D. Wijewickreme (2014). Residual shear strength of fine-grained soils and soil solid interfaces at low effective normal stresses. *Canadian Geotechnical Journal* 52(2), 198–210.
- Engin, H. K., H. P. Jostad, and A. Rohe (2014). On the modelling of grain crushing in hypoplasticity. In B. & R. Hicks (Ed.), *Numerical Methods in Geotechnical Engineering*, pp. 33–38.

- Evans, M. and T. Fennick (1995). Geosynthetic/soil interface friction angles using a rotation shear device. *Geotechnical Testing Journal* 18(2), 271–275.
- Evgin, E. and K. Fakharian (1996). Effect of stress paths on the behaviour of sand–steel interfaces. *Canadian Geotechnical Journal* 33, 853–865.
- Fakharian, K. and E. Evgin (2000). Elasto-plastic modelling of stress-path dependent behaviour of interfaces. *International Journal of Numerical and Analytical Methods in Geomechanics* 24, 183–199.
- Feda, J. (1976). Skin friction of piles. In *Sixth European Conference on Soil Mechanics and Foundation Engineering*, Wiesbaden, pp. 423–428.
- Feligha, M. and F. Hammoud (2015). Experimental investigation of frictional behavior between cohesive soils and solid materials using direct shear apparatus. *Geotechnical and Geological Engineering* 34, 567–578.
- Fellin, W. (2013). Extension to barodesy to model void ratio and stress dependency of the K_0 value. *Acta Geotechnica* 8(5), 561–565.
- Fellin, W. and A. Ostermann (2013). The critical state behaviour of barodesy compared with the Matsuoka-Nakai failure criterion. *International Journal for Numerical and Analytical Methods in Geomechanics* 37, 299–308.
- Fioravante, V. (2002). On the shaft friction modelling of non-displacement piles in sand. *Soils and Foundations* 42(2), 23–33.
- Fioravante, V., V. N. Ghionna, S. Pedroni, and D. Porcino (1999). A constant normal stiffness direct shear box for soil-solid interface tests. *Rivista Italiana di geotecnica* 3, 7–22.
- Fischer, K. A., D. Sheng, and A. J. Abbo (2007). Modeling of pile installation using contact mechanics and quadratic elements. *Computers and Geotechnics* 34(6), 449–461.
- Frost, J. and J. Han (1999). Behaviour of interfaces between fibre-reinforced polymers and sands. *Journal Geotechnical and Geoenvironmental Engineering* 125(8), 633–640.
- Frost, J. D., G. L. Hebler, T. M. Evans, and J. T. DeJong (2004). Interface behavior of granular soils. In *9th ASCE Aerospace Division International Conference on Engineering, Construction and Operations in Challenging Environments*, Houston, pp. 1–8.
- Ganesan, S., M. Kuo, and M. Bolton (2014). Influences on Pipeline Interface Friction Measured in Direct Shear Tests. *Geotechnical Testing Journal* 37(1), 1–13.
- Gennaro, V. and R. Frank (2002). Elasto-plastic analysis of the interface behaviour between granular media and structure. *Computers and Geotechnics* 29(7), 547–572.

- Gens, A., I. Carol, and E. Alonso (1988). An interface element formulation for the analysis of soil-reinforcement interaction. *Computers and Geotechnics* 7, 133–151.
- Ghaboussi, J., E. L. Wilson, and J. Isenberg (1973). Finite element for rock joints and interfaces. *Journal of Soil Mechanics and Foundation Division* 10, 833–848.
- Ghionna, V. N. and G. Mortara (2002). An elastoplastic model for sand - structure interface behaviour. *Géotechnique* 52(1), 41–50.
- Goldscheider, M. (1976). Grenzbedingung und Fließregel von Sand. *Mechanics Reveals and Communication* 3, 463–468.
- Gómez, J. E., G. M. Filz, and R. M. Ebeling (2003). Extended Hyperbolic Model for Sand-to-Concrete Interfaces. *Journal of Geotechnical and Geoenvironmental Engineering* 129(11), 993–1000.
- Goodman, R. E., R. L. Taylor, and T. L. Brekke (1968). A Model for the mechanics of Jointed rock. *Journal of the Soil Mechanics and Foundations Division* 94.
- Griffiths, D. (1985). Numerical modelling of interfaces using conventional finite elements. In *Fifth International Conference on Numerical Methods in Geomechanics*, Nagoya, pp. 837–843.
- Griffiths, D. (1988). Numerical studies of soil-structure interaction using a simple interface model. *Canadian Geotechnical Journal* 25(1), 158–162.
- Gudehus, G. (1996). A Comprehensive Constitutive Equation For Granular Materials. *Soils and Foundations* 36(1), 1–12.
- Gudehus, G., A. Amorosi, A. Gens, I. Herle, D. Kolymbas, D. Mašín, D. M. Wood, A. Niemunis, R. Nova, M. Pastor, C. Tamagnini, and G. Viggiani (2008). The soilmodels.info project. *International Journal for Numerical and Analytical Methods in Geomechanics* 32(12), 1571–1572.
- Gutjahr, S. (2003). *Optimierte Berechnung von nicht gestützten Baugrubenwänden in Sand*. TU Dortmund Heft 25.
- Hallquist, J. (1979). NIKE2D: An Implicit, Finite Deformation, Finite Element Code for Analysing of the Static and Dynamic Response of two-dimensional Solids. Technical report, UC-Lawrence Livermore National Laboratory.
- Hamid, T. B. and G. A. Miller (2006). Interface direct shear testing of unsaturated soil. *Geotechnical Testing Journal* 30(3), 1–10.

- Hamid, T. B. and G. A. Miller (2008). A constitutive model for unsaturated soil interfaces. *International Journal for Numerical and Analytical Methods in Geomechanics* 32(13), 1693–1714.
- Hamid, T. B. and G. A. Miller (2009). Shear strength of unsaturated soil interfaces. *Canadian Geotechnical Journal* 46(5), 595–606.
- Hansen, B. (1961). Shear box tests on sand. In *Fifth international conference of soil mechanics and foundation engineering*, pp. 127–131.
- Hanson, J. L., A. Flores, D. Manheim, and N. Yesiller (2015). Temperature effects on sand-steel interface shear and quantification of post-shear surface texture characteristics of steel. In *The International Foundations Congress and Equipment Expo 2015*, pp. 1–5.
- Haraldsson, A. (2004). *Formulierung und Simulation der Kontaktvorgänge in der Baugrund-Tragwerk-Interaktion*. Ph. D. thesis, Universität Hannover.
- Hebeler, G. L., A. Martinez, and J. D. Frost (2015). Shear zone evolution of granular soils in contact with conventional and textured CPT friction sleeves. *KSCCE Journal of Civil Engineering* 20(4).
- Helton, J. (1997). Uncertainty and sensitivity analysis in the presence of stochastic and subjective uncertainty. *Journal of Statistical Computation and Simulation* 57(1-4), 3–76.
- Herle, I. (1997). *Hypoplastizität und Granulometrie einfacher Korngerüte*. Ph. D. thesis, Institut für Bodenmechanik und Felsmechanik der Universität Fridericiana in Karlsruhe.
- Herle, I. and G. Gudehus (1999). Determination of parameters of a hypoplastic constitutive model from properties of grain assemblies. *Mechanics of cohesive -Frictional Materials* 4, 461–486.
- Herle, I. and D. Kolymbas (2004). Hypoplasticity for soils with low friction angles. *Computers and Geotechnics* 31(5), 365–373.
- Herle, I. and K. Nübel (1999). Hypoplastic description of interface behaviour. In Pande, Pietruszczak, and Schweiger (Eds.), *Numerical Models in Geomechanics- NUMOG VII*.
- Hibbit, Karlsson, and Sorensen (2015a). Abaqus version 6.14.
- Hibbit, Karlsson, and Sorensen (2015b). *ABAQUS/Standard Analysis User's Manual*. USA: Hibbit, Karlsson, Sorensen Inc.
- Ho, T., R. Jardine, and N. Anh-Minh (2011). Large-displacement interface shear between steel and granular media. *Géotechnique* 61(3), 221–234.

- Hof, C. (2003). Über das Scherverhalten von korrodierten Zementkörperoberflächen. *Bautechnik* 80(12), 896–902.
- Hof, C., T. Triantafyllidis, and F. Schmidt-Döhl (2004). Über die Abnahme der Tragfähigkeit von Verpreßankern unter Angriff von kalklösender Kohlensäure. *Bautechnik* 81(5), 357–363.
- Hohberg, J.-M. (1990). Discussion by Jörg-Martin Hohberg: Modelling for cyclic normal and shear behavior of interfaces. *Journal of Engineering Mechanics* 116, 1870–1872.
- Hohberg, J.-M. (1992). A joint element for the nonlinear dynamic analysis of arch dams. Technical Report July, Institute for Structural Engineering, ETH Zuerich, Zuerich.
- Hohberg, J.-M. and H. F. Schweiger (1992). On the penalty behaviour of thin-layer elements. In Pande & Pietruszczak (Ed.), *Numerical Models in Geomechanics*, pp. 241–248.
- Hossain, M. and J.-H. Yin (2014a). Dilatancy and strength of an unsaturated soil-cement interface in direct shear tests. *International Journal of Geomechanics* 15(5), 101–109.
- Hossain, M. A. and J.-H. Yin (2012). Influence of grouting pressure on the behavior of an unsaturated soil-cement interface. *Journal of Geotechnical and Geoenvironmental Engineering* 138(2), 193–202.
- Hossain, M. A. and J.-H. Yin (2014b). Behavior of a pressure-grouted soil-cement interface in direct shear tests. *International Journal of Geomechanics* 14(1), 101–109.
- Hu, L. and J. L. Pu (2003). Application of damage model for soil structure interface. *Computers and Geotechnics* 30(2), 165–183.
- Hu, L. and J. L. Pu (2004). Testing and modeling of soil-structure interface. *Journal of Geotechnical and Geoenvironmental Engineering* 130(8), 851–860.
- Huang, W., D. Sheng, S. Sloan, and H. Yu (2004). Finite element analysis of cone penetration in cohesionless soil. *Computers and Geotechnics* 31(7), 517–528.
- Huber, M. and H. Stutz (2013). Contribution to the quantification of model quality in geotechnical engineering. In Novák and Vorechovsky (Eds.), *International Probabilistic Workshop*, pp. 113–126.
- Jaky, J. (1948). Pressure in silos. In *2nd ICSMFE*, pp. 103–107.
- Janbu, N. (1963). Soil compressibility as determined by oedometer test and triaxial tests. In *European Conference on Soil Mechanics and Foundation Engineering, Vol. 1*, Wiesbaden, pp. 637–659.

- Jostad, H. P. and L. Andresen (2004). Modelling of shear band propagation in clays using interface elements with finite thickness. In S. Pietruszczak and G. N. Pande (Eds.), *Numerical Models in Geomechanics Proceedings of the Ninth International Symposium on Numerical Models in Geomechanics - NUMOG IX*, pp. 121–128.
- Jung, B. (2015). *Evaluation of Coupled Partial Models for the Assessment of Restraint Effects in Concrete Structures*. Ph. D. thesis, Bauhaus-Universität Weimar.
- Jung, B., H. Stutz, G. Morgenthal, and F. Wuttke (2012). Uncertainty Analysis of stiffness prediction for pile group models. In Moorman, Huber, and Proske (Eds.), *International Probabilistic Workshop*, pp. 229–241.
- Kaliakin, V. N. and J. Li (1995). Insight into deficiencies associated with commonly used zero-thickness interface elements. *Computers and Geotechnics* 17, 225–252.
- Katona, M. G. (1983). A simple contact-friction interface element with applications to buried culverts. *International Journal for Numerical and Analytical Methods in Geomechanics* 7(1982), 371–384.
- Keitel, H., B. Jung, H. Motra, and H. Stutz (2014). Quality assessment of coupled partial models considering soil structure coupling. *Engineering Structures* 59, 565 – 573.
- Keitel, H., H. Stutz, B. Jung, and H. B. Motra (2013). Prognosequalität eines Gesamtmodells Einfluss verschiedener Kopplungsszenarien auf die Interaktion Struktur–Boden. *Bautechnik* 90, 19–25.
- Khalili, N. and M. H. Khabbaz (1998). A unique relationship for χ for the determination of the shear strength of unsaturated soils. *Géotechnique* 48(5), 681–687.
- Khoury, C. N. and G. A. Miller (2012). Influence of hydraulic hysteresis on the shear strength of unsaturated soils and interfaces. *Geotechnical Testing Journal* 35(1), 1–15.
- Kim, N.-K., J.-S. Park, and S.-K. Kim (2007). Numerical simulation of ground anchors. *Computers and Geotechnics* 34(6), 498–507.
- Kishida, H. and M. Uesugi (1987). Tests of the interface between sand and steel in the simple shear apparatus. *Géotechnique* 37(1), 45–52.
- Kolymbas, D. (1977). A rate-dependent constitutive equation for soils. *Mechanics Research Communications* 4(6), 367–372.
- Kolymbas, D. (2000). *Introduction to hypoplasticity* (Advances in Geotechnical Engineering and Tunnelling ed.). San Francisco: Balkema.
- Kolymbas, D. (2012a). Barodesy: a new constitutive frame for soils. *Géotechnique Letters* 2(April-June), 17–23.

- Kolymbas, D. (2012b). Barodesy: a new hypoplastic approach. *International Journal for Numerical and Analytical Methods in Geomechanics* 36, 1220–1240.
- Kolymbas, D. (2015). Introduction to Barodesy. *Géotechnique* 65(1), 52–65.
- Kolymbas, D. and G. Medicus (2016). Genealogy of hypoplasticity and barodesy. *International Journal for Numerical and Analytical Methods in Geomechanics*.
- Koval, G., F. Chevoir, J.-N. Roux, J. Sulem, and A. Corfdir (2011). Interface roughness effect on slow cyclic annular shear of granular materials. *Granular Matter* 13(5), 525–540.
- Kuo, M.-H., C. Vincent, M. Bolton, A. Hill, and M. Rattley (2015). A new torsional shear device for pipeline interface shear testing. In Meyer (Ed.), *Frontier in Offshore Geotechnics III*, pp. 405–410.
- Lahmer, T., T. Knabe, S. Nikulla, and M. Reuter (2011). Bewertungsmethoden für Modelle des konstruktiven Ingenieurbaus. *Bautechnik Sonderdruck* 88(6), 60–64.
- Lambe, T. W. (1973). Predictions in soil engineering. *Géotechnique* 23(2), 151–202.
- Lashkari, A. (2013). Prediction of the shaft resistance of nondisplacement piles in sand. *International Journal for Numerical and Analytical Methods in Geomechanics* 37, 904–931.
- Lashkari, A. and M. Kadivar (2015). A constitutive model for unsaturated soil–structure interfaces. *International Journal for Numerical and Analytical Methods in Geomechanics*.
- Lehane, B. (1992). *Experimental investigations of pile behaviour using instrumented field piles*. Ph. D. thesis, Imperial College, University of London.
- Lemos, L. J. L. and P. R. Vaughan (2000). Clay - interface shear resistance. *Géotechnique* 50(1), 55–64.
- Li, X. S. and Y. F. Dafalias (2000). Dilatancy for cohesionless soils. *Géotechnique* 50(4), 449–460.
- Lim, J. K. and B. M. Lehane (2015). Shearing resistance during pile installation in sand. *Proceedings of the ICE - Geotechnical Engineering* 168(3), 1–9.
- Ling, H. I. and H. Liu (2009). Deformation analysis of reinforced soil retaining walls – simplistic versus sophisticated finite element analyses. *Acta Geotechnica* 4, 203–213.
- Littleton, I. (1976). An experimental study of the adhesion between clay and steel. *Journal of Terramechanics* 13(3), 141–152.
- Liu, H. and H. I. Ling (2008). Constitutive description of interface behavior including cyclic loading and particle breakage within the framework of critical state soil mechanics. *International Journal for Numerical and Analytical Methods in Geomechanics* 32(12), 1495–1514.

- Liu, H., E. Song, and H. I. Ling (2006). Constitutive modeling of soil-structure interface through the concept of critical state soil mechanics. *Mechanics Research Communications* 33(4), 515–531.
- Liu, J., D. Zou, and X. Kong (2014). A three-dimensional state-dependent model of soil-structure interface for monotonic and cyclic loadings. *Computers and Geotechnics* 61, 166–177.
- Lupini, F., A. E. Skinner, and P. R. Vaughan (1981). The drained residual strength of cohesive soils. *Géotechnique* 31(2), 181–213.
- Mara, T. and S. Tarantola (2012). Variance-based sensitivity indices for models with dependent inputs. *Reliability Engineering and System Safety* 107, 115–121.
- Martinez, A., D. Forst, and J. Su (2015). The importance of interfaces in geotechnical foundation systems. In *The International Foundations Congress and Equipment Expo*.
- Martinez, A., J. D. Frost, and G. Hebelier (2015). Experimental Study of Shear Zones Formed at Sands/Steel Interfaces in Axial and Torsional Axisymmetric Tests. *Geotechnical Testing Journal* 38(4).
- Mašín, D. (2006). *Hypoplastic models for fine-grained soils*. Ph. D. thesis, Charles University Prague.
- Mašín, D. (2007). A hypoplastic constitutive model for clays with meta-stable structure. *Canadian Geotechnical Journal* 44(3), 363–375.
- Mašín, D. (2009). Comparison of predictive capabilities of selected elastoplastic and hypoplastic models for structured clays. *Soils and Foundations* 49(3), 381–390.
- Mašín, D. and I. Herle (2005). State boundary surface of a hypoplastic model for clays. *Computers and Geotechnics* 32(6), 400–410.
- Mašín, D. and N. Khalili (2008). A hypoplastic model for mechanical response of unsaturated soils. *International Journal for Numerical and Analytical Methods in Geomechanics* 32(15), 1903–1926.
- Mašín, D. and N. Khalili (2012). A thermo-mechanical model for variably saturated soils based on hypoplasticity. *International Journal for Numerical and Analytical Methods in Geomechanics* 36, 1461–1485.
- Matsuoka, H. and T. Nakai (1974). Stress deformation and strength characteristics of soil under three different principal stresses. In *Proceedings of the Japanese Society of Civil Engineers, vol 232*, pp. 59–70.

- Mašín, D. (2005). A hypoplastic constitutive model for clays. *International Journal for Numerical and Analytical Methods in Geomechanics* 29, 311–336.
- Mašín, D. (2012). Hypoplastic Cam-clay model. *Géotechnique* 62(6), 549–553.
- Mašín, D. (2013). Clay hypoplasticity with explicitly defined asymptotic states. *Acta Geotechnica* 8(5), 481–496.
- Mašín, D. (2014). Clay hypoplasticity model including stiffness anisotropy. *Géotechnique* 2(3), 232–238.
- Mašín, D. (2015). The influence of experimental and sampling uncertainties on the probability of unsatisfactory performance in geotechnical applications. *Géotechnique* 65(11), 897–910.
- Mašín, D. (2016). Triax: element test driver for soil mechanics (personal communication).
- McKay, M., R. Beckman, and C. W. and (1979). A comparison of three methods for selecting values of input variables in the analysis of output from a computer code. *Technometrics* 21(2), 239–245.
- Medicus, G. (2014). *Barodesy and its application for clay*. Ph.d thesis, University of Innsbruck.
- Medicus, G., W. Fellin, and D. Kolymbas (2012). Barodesy for clay. *Géotechnique Letters* 2(4), 173–180.
- Miller, G. A. and T. B. Hamid (2007). Interface direct shear testing of unsaturated soil. *Geotechnical Testing Journal* 30(3), 1–10.
- Mortara, G. (2003). *An elastoplastic modelling of sand–structure interface behaviour under monotonic and cyclic loading*. Ph. D. thesis, Politecnico di Torino.
- Mortara, G., M. Boulon, and V. N. Ghionna (2002). A 2–D constitutive model for cyclic interface behaviour. *International Journal for Numerical and Analytical Methods in Geomechanics* 26(11), 1071–1096.
- Mortara, G., D. Ferrara, and G. Fotia (2010). Simple Model for the Cyclic Behavior of Smooth Sand-Steel Interfaces. *Journal of Geotechnical and Geoenvironmental Engineering* 136(July), 1004–1009.
- Mortara, G., A. Mangiola, and V. N. Ghionna (2007). Cyclic shear stress degradation and post-cyclic behaviour from sand–steel interface direct shear tests. *Canadian Geotechnical Journal* 44(7), 739–752.
- Most, T. (2011). Assessment of structural simulation models by estimating uncertainties due to model selection and model simplification. *Computers & Structures* 89(17-18), 1664–1672.

- Most, T. (2012). Variance-based sensitivity analysis in the presence of correlated input variables. In *Proceedings of the 5th International Conference on Reliable Engineering Computing*.
- Motra, H., H. Stutz, and F. Wuttke (2016). Quality assessment of soil bearing capacity factor models of shallow foundations. *Soils and Foundations* 56(2), 265–276.
- Motra, H. B. and J. Hildebrand (2013). Influence of measurement uncertainties on results of creep prediction of concrete under cyclic loading. In *VIII International Conference on Fracture Mechanics of Concrete and Concrete Structures (FraMCoS-8)*, pp. 805–814.
- Najjar, S. S., R. B. Gilbert, E. Liedtke, B. McCarron, and A. G. Young (2007). Residual Shear Strength for Interfaces between Pipelines and Clays at Low Effective Normal Stresses. *Journal of Geotechnical and Geoenvironmental Engineering* 133(6), 695–706.
- Nakai, T., H. Kawano, K. Murata, M. Banno, and T. Hashimoto (1999). Model tests and numerical Simulation of braced excavation in sandy ground: influences of construction history, wall friction, wall stiffness, strut position and strut stiffness. *Soils and Foundations* 39(3), 1–12.
- Nakayama, H. (2006). *Modelling interfaces between sand and structural elements*. Ph. D. thesis, University of Bristol.
- Navayogarajah, N., C. Desai, and P. Kioussis (1992). Hierarchical single surface model for static and cyclic behavior of interfaces. *Journal of Engineering Mechanics* 118(5), 990–1011.
- Nazem, M. (2016). On application of the third medium contact method in analysis of geotechnical problems. In *2nd Australian Geomechanics Conference*.
- Nazem, M., M. Kardani, J. P. Carter, and D. Sheng (2012). A comparative study of error assessment techniques for dynamic contact problems of geomechanics. *Computers and Geotechnics* 40, 62–73.
- Nazem, M., D. Sheng, and J. P. Carter (2006). Stress integration and mesh refinement for large deformation in geomechanics. *International Journal for Numerical Methods in Engineering* 65(7), 1002–1027.
- Neguessey, D., W. Wijewickreme, and Y. Valid (1988). Geomembrane interface friction. *Canadian Geotechnical Journal* 26, 165–169.
- Ng, K. L. A. and J. C. Small (1997). Behavior of Joints and Interfaces Subjected to Water Pressure. *Computers and Geotechnics* 20(1), 71–93.
- Niemunis, A. (2003). Extended hypoplastic models for soils.
- Niemunis, A. and I. Herle (1997). Hypoplastic model for cohesionless soils with elastic strain range. *Mechanics of Cohesive-Frictional Materials* 2(1997), 279–299.

- Niemunis, A., T. Wichtmann, and T. Triantafyllidis (2005). A high-cycle accumulation model for sand. *Computers and Geotechnics* 32(4), 245–263.
- O'Rourke, T., S. Druschal, and A. Netravali (1990). Shear strength characteristics of sand-polymer interfaces. *Journal of Geotechnical Engineering* 116(3), 451–469.
- Oumarou, T. A. and E. Evgin (2005). Cyclic behaviour of a sand–steel plate interface. *Canadian Geotechnical Journal* 42(6), 1695–1704.
- Ovando-Shelley, E. (1995). Direct shear tests on Mexico City clay with reference to friction pile behaviour. *Geotechnical and Geological Engineering* 13, 1–16.
- Paikowsky, S., C. Player, and P. Connors (1995). A dual interface apparatus for testing unrestricted friction of soil along solid surfaces. *Geotechnical Testing Journal* 18(2), 168–193.
- Pande, G. and K. Sharma (1979). On joint/interface elements and associated problems of numerical ill-conditioning. *International Journal for Numerical and Analytical Methods in Geomechanics*, 293–300.
- Pastor, M., O. C. Zienkiewicz, and A. H. C. Chan (1990). Generalized plasticity and the modelling of soil behaviour. *International Journal for Numerical and Analytical Methods in Geomechanics* 14(3), 151–190.
- Phoon, K. (2008). *Reliability-based design in geotechnical engineering: computations and applications*. CRC Press, Taylor and Francis Group.
- Porcino, D., V. Fioravante, V. N. Ghionna, and S. Pedroni (2003). Interface behavior of sands from constant normal stiffness direct shear tests. *Geotechnical Testing Journal* 26(3), 49–56.
- Potts, D. M., G. T. Dounias, and P. R. Vaughan (1987). Finite element analysis of the direct shear box test. *Géotechnique* 37(1), 11–23.
- Potyondy, J. G. (1961). Skin Friction between various soils and construction materials. *Géotechnique* 11, 339–353.
- Puso, M. A., T. A. Laursen, and J. Solberg (2008). A segment-to-segment mortar contact method for quadratic elements and large deformations. *Computer Methods in Applied Mechanics and Engineering* 197(6), 555–566.
- Qian, X.-X., H.-N. Yuan, Q.-M. Li, and B.-Y. Zhang (2013). Comparative study on interface elements, thin-Layer elements, and contact analysis methods in the analysis of high concrete-faced rockfill dams. *Journal of Applied Mathematics*, 1–11.
- Ragni, R., D. Wang, D. Mašín, B. Bienen, M. J. Cassidy, and S. A. Stanier (2016). Numerical modelling of the effects of consolidation on jack-up spudcan penetration. *Computers and Geotechnics* 78, 25–37.

- Rao, K. S. S., M. M. Allam, and R. G. Robinson (2000). Drained shear strength of fine-grained soil–solid surface interfaces. *Proceedings of the Institution of Civil Engineers – Geotechnical Engineering* 143(2), 75–81.
- Rebstock, D. (2011). *Verspannung und Entspannung von Sand entlang von Baukörpern*. Ph. D. thesis, Karlsruher Institut für Technologie.
- Roscoe, K. and J. Burland (1968). On the generalized stress-strain behavior of wet-clay. In J. Heyman and F. Leckie (Eds.), *Engineering Plasticity*, pp. 535–609.
- Rotta Loria, A. F., F. Orellana, A. Minardi, J.-M. Fürbringer, and L. Laloui (2015). Predicting the axial capacity of piles in sand. *Computers and Geotechnics* 69, 485–495.
- Rowe, P. (1962). The stress dilatancy relation for static equilibrium of an assembly of particles in contact. *Proc. Roy. Soc. A* 269, 500–527.
- Sabetamal, H., M. Nazem, J. P. Carter, and S. W. Sloan (2014). Large deformation dynamic analysis of saturated porous media with applications to penetration problems. *Computers and Geotechnics* 55, 117–131.
- Sabetamal, H., M. Nazem, S. W. Sloan, and J. P. Carter (2015). Numerical modelling of offshore pipe–seabed interaction problems. *Computer Methods and Recent Advances in Geomechanics*, 655–660.
- Said, I., V. De Gennaro, and R. Frank (2009). Axisymmetric finite element analysis of pile loading tests. *Computers and Geotechnics* 36(1–2), 6–19.
- Samtani, N. C., C. S. Desai, and L. Vulliet (1996). An interface model to describe viscoplastic behavior. *International Journal for Numerical and Analytical Methods in Geomechanics* 20(1995), 231–252.
- Satelli, A., M. Ratto, T. Andres, F. Campolongo, J. Cariboni, D. Gatelli, M. Saisana, and S. Tarantola (2008). *Global Sensitivity Analysis. The Primer*. John Wiley and Sons.
- Satelli, A., S. Tarantola, F. Campolongo, and M. Ratto (2004). *Sensitivity analysis in practice: A guide to assessing scientific models*. John Wiley and Sons.
- Schellekens, J. C. J. and R. de Borst (1993). On the numerical integration of interface elements. *International Journal for Numerical Methods in Engineering* 36, 43–66.
- Schwer, L. (2001). Constitutive model verification and validation .
- Shahrour, I. and F. Rezaie (1997). An elastoplastic constitutive relation for the soil-structure interface under cyclic loading. *Computers and Geotechnics* 21(1), 21–39.

- Shakir, R. R. and J. Zhu (2009). Behavior of compacted clay-concrete interface. *Frontiers of Architecture and Civil Engineering in China* 3(1), 85–92.
- Shao, R. C. and C. S. Desai (2000). Implementation of DSC model and application for analysis of field pile tests under cyclic loading. *International Journal for Numerical and Analytical Methods in Geomechanics* 24, 601–624.
- Sharma, K. G. and C. S. Desai (1992). Analysis and implementation of thin-layer element for interfaces and joints. *Journal of Engineering Mechanics* 118(12), 2442–2462.
- Sheng, D., K. D. Eigenbrod, and P. Wriggers (2005). Finite element analysis of pile installation using large-slip frictional contact. *Computers and Geotechnics* 32(1), 17–26.
- Sheng, D., M. Nazem, and J. P. Carter (2009). Some computational aspects for solving deep penetration problems in geomechanics. *Computational Mechanics* 44(4), 549–561.
- Stanier, S. A. and D. J. White (2015). Shallow penetrometer penetration resistance. *Journal of Geotechnical and Geoenvironmental Engineering* 141(3), 255–257.
- Stutz, H., T. Benz, and F. Wuttke (2013). A Numerical Investigation of the Artificial Stiffness Scaling in Zero Thickness Interface Elements for Soil-Structure Interaction. In *Proceedings of the Fourteenth International Conference on Civil, Structural and Environmental Engineering Computing*, Volume 197. Civil-Comp Press.
- Stutz, H., T. Benz, and F. Wuttke (2014). Extended zero-thickness interface element for accurate soil–pile interaction modelling. In *NUMGE 2014*, Delft, The Netherlands, pp. 283–288.
- Stutz, H. and D. Mašín (2016). Hypoplastic interface models for fine-grained soils. *International Journal for Numerical and Analytical Methods in Geomechanics*. (in press).
- Stutz, H., D. Mašín, and F. Wuttke (2016). Enhancement of a hypoplastic model for granular soil–structure interface behaviour. *Acta Geotechnica* 11(6), 1249–1261.
- Stutz, H., D. Mašín, Prädell, and F. Wuttke (2016). Thermo-mechanical hypoplastic interface model for fine-grained soils. In Wuttke, Bauer, and Sanchez (Eds.), *Energy geotechnics*, pp. 351–357.
- Stutz, H., G. Mortara, and F. Wuttke (2015). Simple vs advanced interface model: A comparison using a deterministic quality approach. In Rinaldi and Claria (Eds.), *Sixth International Symposium on Deformation Characteristics of Geomaterials*.
- Suchomel, R. and D. Mašín (2010). Spatial variability of soil parameters in an analysis of a strip footing using hypoplastic model. In *Numerical Methods in Geotechnical Engineering*.

- Suchomel, R. and D. Mašín (2011). Probabilistic analyses of a strip footing on horizontally stratified sandy deposit using advanced constitutive model. *Computers and Geotechnics* 38(3), 363–374.
- Sun, D., H. Matsuoka, K. Morichi, Y. Tanaka, and H. Yamamoto (2003). Frictional behaviour between clay and steel by two direct shear type apparatus. In *Deformation Characteristics of Geomaterials*, pp. 239–245.
- Swoboda, G. and X. Y. Lei (1994). Simulation of arch dam - foundation interaction with a new friction interface element. *International Journal for Numerical and Analytical Methods in Geomechanics* 17, 601–617.
- Tabucanon, J. T., D. W. Airey, and H. G. Poulos (1995). Pile Skin Friction in Sand from Constant Normal Stiffness Test. *Geotechnical Testing Journal* 18, 350–364.
- Taha, A. and M. Fall (2014). Shear behavior of sensitive marine clay-steel interfaces. *Acta Geotechnica* 9(6), 969–980.
- Tatsuoka, F. and O. Haibara (1985). Shear resistance between sand and smooth or lubricated surfaces. *Soil and Foundations* 25(1), 89–98.
- Tehrani, F. S., F. Han, R. Salgado, M. Prezzi, R. D. Tovar, and A. G. Castro (2016). Surface roughness effects on the shaft resistance of piles in dry sand. *Géotechnique* 66(5), 386–400.
- Tejchman, J. and W. Wu (1995). Experimental and numerical study of sand–steel interfaces. *International Journal for Numerical and Analytical Methods in Geomechanics* 19(1993), 513–536.
- Tika-Vassilikos, T. (1991). Clay-on-steel ring shear tests and their implications for displacement piles. *Geotechnical Testing Journal* 14(4), 457–463.
- Truesdell, C. and W. Noll (2004). *The Non-Linear Field Theories of Mechanics*.
- Tsubakihara, Y. and H. Kishida (1993). Frictional behaviour between normally consolidated clay and steel by two Direct shear type apparatuses. *Soils and Foundations* 33(2), 1–13.
- Tsubakihara, Y., H. Kishida, and T. Nishyama (1993). Friction between cohesive soils and steel. *Soils and Foundations* 33(2), 145–156.
- Uesugi, M. and H. Kishida (1986). Frictional resistance at yield between dry sand and mild steel. *Soils and Foundations* 26(4), 139–149.
- Uesugi, M., H. Kishida, and Y. Tsubakihara (1988). Behavior of sand particles in sand-steel friction. *Soils and Foundations* 28(1), 107–118.

- Uesugi, M., H. Kishida, and Y. Tsubakihara (1989). Friction between sand and steel under repeated loading. *Soils and Foundations* 29(3), 127–137.
- Uesugi, M., H. Kishida, and Y. Uchikawa (1989). Friction between dry sand and concrete under monotonic and repeated loading. *Soils and Foundations* 30(1), 115–128.
- Van Langen, H. (1991). *Numerical analysis of soil-structure interaction*. Ph. D. thesis, TU Delft.
- Vaughan, P. R., L. J. L. J. Lemos, and T. E. Tika (1996). Fast shearing of pre-existing shear zones in soil. *Géotechnique* 46(2), 197–233.
- Vermeer, P. a. and R. de Borst (1984). Non-associated plasticity for soils, concrete and rock. *Heron* 29(3), 1–64.
- Vogelsang, J., G. Huber, and T. Triantafyllidis (2013). A large-scale soil-structure interface testing device. *Geotechnical Testing Journal* 36(5), 1–13.
- Vogelsang, J., G. Huber, and T. Triantafyllidis (2015). Demonstrator Experiments on significant effects during pile installation. In Th. Triantafyllidis (Ed.), *Holistic Simulation of Geotechnical Installation Processes, Lecture Notes in Applied and Computational Mechanics*, Volume 77, pp. 1–20. Springer International Publishing Switzerland.
- Vogelsang, J., H. Zachert, G. Huber, and T. Triantafyllidis (2015). Effects of soil deposition on the initial stress state in model tests: Experimental results and FE simulation. In Th. Triantafyllidis (Ed.), *Holistic Simulation of Geotechnical Installation Processes, Lecture Notes in Applied and Computational Mechanics*, Volume 77, pp. 1–20. Springer International Publishing Switzerland.
- von Wolffersdorff, P. A. (1996). Hypoplastic relation for granular materials with a predefined limit state surface. *Mechanics of Cohesive-Frictional Materials* 1(3), 251–271.
- Weißenfels, C. and P. Wriggers (2015a). A contact layer element for large deformations. *Computational Mechanics* 55(5), 873–885.
- Weißenfels, C. and P. Wriggers (2015b). Methods to project plasticity models onto the contact surface applied to soil structure interactions. *Computers and Geotechnics* 65, 187–198.
- Wernick, E. (1978). Skin Friction of Cylindrical Anchors in Non-Cohesive Soils. In *Symposium on Soil Reinforcing and Stabilising Techniques*.
- Wood, D. M. (2000). *Soil behaviour and critical state soil mechanics*. Cambridge: Cambridge Press.
- Wriggers, P. (2007). *Computational Contact Mechanics*. Springer Berlin Heidelberg.

- Wriggers, P. and C. Miehe (1994). Contact constraints within coupled thermomechanical analysis—A finite element model. *Computer Methods in Applied Mechanics and Engineering* 113(3-4), 301–319.
- Wriggers, P., J. Schröder, and A. Schwarz (2013). A finite element method for contact using a third medium. *Computational Mechanics* 52(4), 837–847.
- Wu, W. and E. Bauer (1994). A simple hypoplastic constitutive model for sand. *International Journal for Numerical and Analytical Methods in Geomechanics* 18(12), 833–862.
- Xiao, S., M. T. Suleiman, and J. McCartney (2014). Shear Behavior of Silty Soil and Soil-Structure Interface under Temperature Effects. In *Geo-Congress*, Number GSP 234, pp. 4105–4114.
- Xu, C. and G. Z. Gertner (2008). Uncertainty and sensitivity analysis for models with correlated parameters. *Reliability Engineering and System Safety* 93, 1563–1573.
- Y B, A., H. T. Durgunoglu, and M. T. Tumay (1982). Interface properties of sand. *Journal of Geotechnical Engineering* 108(4), 648–654.
- Yan, Y. (2013). *Novel Methods For Characterising Pipe-soil Interaction Forces In Situ In Deep Water*. Ph. D. thesis, University of Western Australia.
- Yan, Y., D. White, and M. Randolph (2010). Penetration resistance and stiffness factors for hemispherical and toroidal penetrometers in uniform clay. *International Journal of Geomechanics* 11(4), 263–275.
- Yasufuku, N., H. Ochiai, and T. Kaku (2003). Internal friction of sand along steel surface up to an interfacial critical state. *Journal of Applied Mechanics* 6, 563–571.
- Yavari, N., A. M. Tang, J. M. Pereira, and G. Hassen (2016). Effect of temperature on the shear strength of soils and soil/structure interface. *Canadian Geotechnical Journal* 53(7), 1186–1194.
- Yoshimi, Y. and T. Kishida (1981). A ring torsion device for evaluating friction between soil and metal surfaces. *Geotechnical Testing Journal* 4(4), 145–152.
- Yu, Y., I. P. Damians, and R. J. Bathurst (2015). Influence of choice of FLAC and PLAXIS interface models on reinforced soil–structure interactions. *Computers and Geotechnics* 65, 164–174.
- Zhang, G., L. Wang, and J.-m. Zhang (2010). Monotonic and cyclic modeling of interface between geotextile and gravelly soil. *International Journal for Numerical and Analytical Methods in Geomechanics* 34(13), 1346–1361.

- Zhang, G. and J.-M. Zhang (2006). Monotonic and cyclic tests of interface between structure and gravelly soil. *Soils and Foundations* 46(4), 505–518.
- Zhang, G. and J.-M. Zhang (2009). Constitutive rules of cyclic behavior of interface between structure and gravelly soil. *Mechanics of Materials* 41(1), 48–59.
- Zhao, L., P. Yang, J. G. Wang, and L. C. Zhang (2014). Cyclic direct shear behaviors of frozen soil-structure interface under constant normal stiffness condition. *Cold Regions Science and Technology* 102, 52–62.

Appendix A

Statistical parameter distribution for the interface models

Table A.1: Distribution of the Mohr-Coloumb interface parameter

Parameters	Physical meaning [Unit]	Distribution	Mean value	COV
E	Youngs modulus [MPa]	log	35	0.15
ν_p	Possion ratio [-]	nor.	0.35	0.1
φ	Friction angle [°]	log	33.50	0.3
ψ	Dilatancy angle [°]	log	4	0.25
c	Cohesion [MPa]	log	4	0.15

Table A.2: Distribution of the hyperbolic model interface parameters

Parameters	Physical meaning [Unit]	Distribution	Mean value	COV
K_I	Dimensionless stiffness number [-]	nor	18500	0.2
n_{HY}	Stiffness exponent [-]	nor	0.8	0.2
R_f	Failure ratio [-]	nor	0.65	0.2
δ	Interface friction angle	log	32	0.2

Table A.3: Distribution of the EP1 model Mortara et al. (2002) parameters

Parameters	Physical meaning [Unit]	Distribution	Mean value	COV
K_n^e	Elastic normal stiffness [Pa/m]	nor	10e+10	0.1
C_k	Ratio normal and shear stiffness [-]	nor	1	0.1
α_p	Maximum value hardening function [PA ^{1-β}]	nor	2.0	0.01
α_c	Asymptotic value hardening function [PA ^{1-β}]	nor	1.75	0.01
ξ_M	w_p parameter [PA ⁻¹]	nor	8.455e-9	0.1
ζ	w_p parameter [m]	nor	5.0e-3	0.1
μ_M	d_{max} parameter [PA ⁻¹]	nor	5.04-7	0.1
ν_d	d_{max} parameter [-]	nor	0.20	0.1
ρ_M	Ratio between the stress ratios for $d = 0$ for hardening or softening condition [-]	nor	0.515	0.1
β_M	Exponent of plastic functions [-]	nor	0.92	0.1
ω	Hardening law parameter [-]	nor	220.6	0.01
ψ	Hardening law parameter [-]	nor	0.158	0.01

Table A.4: Distribution of the EP2 model (Lashkari 2013) parameters

Parameters	Physical meaning [Unit]	Distribution	Mean value	COV
K_{s0}^e	Elastic tangential stiffness constant [MPa]	nor	500e+1	0.1
K_{n0}^e	Elastic normal stiffness constant [MPa]	nor	585e+1	0.1
A_0	Dilatancy constant (initial) [-]	nor	11.0	0.1
A_{1L}	Dilatancy constant (intermediate) [-]	nor	0.85	0.1
h_0	Plastic hardening modulus constant [-]	nor	0.35	0.1
M	Critical stress ratio [-]	nor	0.638	0.1
e_0	Initial void ratio [-]	nor	1.01	0.1
λ_L	Critical state line location in $e - \ln \sigma_n$ plane [-]	nor	0.09	0.1
n^b	Influence of interface state on peak stress ratio [-]	nor	1.15	0.1
n^d	Influence of interface state on phase transformation (zero dilatancy) stress ratio [-]	nor	0.73	0.1

Table A.5: Distribution of the hypoplasticity model Gutjahr (2003) parameters

Parameters	Physical meaning [Unit]	Distribution	Mean value	COV
h_s	Granulate hardness [MPa]	log	1000.0	0.1
n	Exponent takes into account the pressure-sensitivity of the grain skeleton [-]	log	0.22	0.1
α	Exponent [-]	log	0.175	0.1
β	Exponent [-]	nor.	1.5	0.1
e_{c0}	Maximum void ratio at zero pressure [-]	nor.	0.6	0.1
φ_c	Critical friction angle [°]	log.	33	0.1

Appendix B

Results of uncertainty analysis for the model assessment

Table B.1: Results for the model uncertainty, parameter uncertainty and global model uncertainty of the interface models

Experiments	Model Uncertainty						Parameter Uncertainty						Global model uncertainty					
	MC	HY	EP1	EP2	HP		MC	HY	EP1	EP2	HP		MC	HY	EP1	EP2	HP	
Shahrour and Rezaie (1997)	loose	100	0.672	0.285	0.043	0.083	0.105	0.23	0.19	2.67	0.12	0.16	0.710	0.343	2.670	0.146	0.191	
	dense	200	0.749	0.171	0.112	0.245	0.292	0.23	0.19	2.67	0.12	0.16	0.784	0.255	2.673	0.275	0.332	
		300	0.949	0.247	0.155	0.156	0.158	0.23	0.19	2.67	0.12	0.16	0.976	0.312	2.675	0.197	0.224	
Mortara (2003)		200	0.550	0.031	0.085	0.097	0.103	0.23	0.19	2.67	0.12	0.16	0.597	0.195	2.671	0.154	0.190	
		300	0.640	0.029	0.201	0.102	0.119	0.23	0.19	2.67	0.12	0.16	0.680	0.192	2.677	0.157	0.199	
		100	0.359	0.397	0.107	0.188	0.286	0.23	0.19	2.67	0.12	0.16	0.426	0.440	2.672	0.2230	0.328	
Evgin and Fakharian (1996)		200	0.311	0.178	0.032	0.135	0.273	0.23	0.19	2.67	0.12	0.16	0.387	0.260	2.670	0.181	0.316	
		100	0.125	0.207	0.069	0.154	0.149	0.23	0.19	2.67	0.12	0.16	0.262	0.281	2.671	0.195	0.219	
		300	0.578	0.153	0.126	0.220	0.165	0.23	0.19	2.67	0.12	0.16	0.622	0.244	2.673	0.251	0.230	
	500	1.16	0.159	0.136	0.1778	0.270	0.23	0.19	2.67	0.12	0.16	1.183	0.248	2.673	0.215	0.314		

Appendix C

Solution for mixed problem of hypoplastic constitutive equation

Solving the hypoplastic constitutive equation under constant normal load and stiffness condition is a mixed control problem. Due to the fact, that the shear stress rates $\dot{\tau}_x$, $\dot{\tau}_y$ and the contact normal strain ε_n are unknown. The solution of the mixed control problem for the simple shear conditions is shown exemplary below. Further comments on the solvability of the hypoplastic equation could be found in Niemunis (2003). For hypoplastic interface models some comments can be found in Herle and Nübel (1999) and Arnold (2005).

The general hypoplastic equations is according to Gudehus (1996), defined as:

$$\dot{\boldsymbol{\sigma}} = f_s (\mathcal{L} : \dot{\boldsymbol{\varepsilon}} + f_d \mathbf{N} \|\dot{\boldsymbol{\varepsilon}}\|), \quad (\text{C.1})$$

This equation can be modified by the redefined tensors and mathematical operators (see Section 5.4) to:

$$\begin{pmatrix} \dot{\sigma}_n \\ \dot{\sigma}_p \\ \dot{\tau}_x \\ \dot{\tau}_y \end{pmatrix} = f_s \left(\begin{pmatrix} \mathcal{L}_{11} & \mathcal{L}_{12} & \mathcal{L}_{13} & \mathcal{L}_{14} \\ \mathcal{L}_{21} & \mathcal{L}_{22} & \mathcal{L}_{23} & \mathcal{L}_{24} \\ \mathcal{L}_{31} & \mathcal{L}_{32} & \mathcal{L}_{33} & \mathcal{L}_{34} \\ \mathcal{L}_{41} & \mathcal{L}_{42} & \mathcal{L}_{43} & \mathcal{L}_{44} \end{pmatrix} : \begin{pmatrix} \dot{\varepsilon}_n \\ 0 \\ \frac{\dot{\gamma}_x}{2} \\ \frac{\dot{\gamma}_y}{2} \end{pmatrix} + f_d \begin{pmatrix} N_1 \\ N_2 \\ N_3 \\ N_4 \end{pmatrix} \sqrt{\varepsilon_n^2 + 2\frac{\dot{\gamma}_x^2}{2} + 2\frac{\dot{\gamma}_y^2}{2}} \right). \quad (\text{C.2})$$

Under CNL conditions the following condition is implied $\dot{\sigma}_n = 0$. For the estimation of the normal contact strain $\dot{\varepsilon}_n$ the first line of the constitutive equation can be transform and reformulated using the mathematical operators given in Section 5.4 as:

$$0 = A_1 \dot{\varepsilon}_n^2 + B_1 \dot{\varepsilon}_n + C, \quad (\text{C.3})$$

where A_1 , B_1 and C represent the coefficient to solve the quadratic polynomial using the following equation:

$$x_{1,2} = \frac{-B_1 \pm \sqrt{B_1^2 - 4A_1C}}{2A_1} \quad (\text{C.4})$$

where:

$$A_1 = (f_s \mathcal{L}_{11})^2 - f_s^2 N_1^2 \quad (\text{C.5})$$

$$B_1 = 2f_s^2 \mathcal{L}_{11} \mathcal{L}_{13} \dot{\gamma}_x + 2f_s^2 \mathcal{L}_{11} \mathcal{L}_{14} \dot{\gamma}_y \quad (\text{C.6})$$

$$C = f_s^2 \mathcal{L}_{14}^2 \dot{\gamma}_y^2 + f_s^2 \mathcal{L}_{13}^2 \dot{\gamma}_x^2 + f_s^2 \dot{\gamma}_y \dot{\gamma}_x \mathcal{L}_{13} \mathcal{L}_{14} - f_s^2 N_1^2 \frac{\dot{\gamma}_x}{2} \dot{\gamma}_x - f_s^2 N_1^2 \frac{\dot{\gamma}_y}{2} \dot{\gamma}_y. \quad (\text{C.7})$$

It is important to mention that by inserting it can be proven that only the negative sign will give a valid solution Arnold (2004). The new $\dot{\varepsilon}_n$ is used to calculate the missing shear stress rates $\dot{\tau}_x$ and $\dot{\tau}_y$.

Statutory declaration

I hereby certify that apart from my supervisor's guidance the content and design of the essay is all my own work;
the thesis has not been submitted either partially or wholly as part of a doctoral degree to any other examining body and it has not been published or submitted for publication;
in addition, this thesis has been prepared in accordance to the Rules of Good Scientific Practice of the German Research Foundation.

Hans Henning Stutz

Kiel, 2016

